



Preclinical studies on an extracorporeal bioartificial liver

Mattia Pasqua

► To cite this version:

Mattia Pasqua. Preclinical studies on an extracorporeal bioartificial liver. Biomaterials. Université de Technologie de Compiègne, 2020. English. NNT : 2020COMP2557 . tel-03118032

HAL Id: tel-03118032

<https://theses.hal.science/tel-03118032>

Submitted on 21 Jan 2021

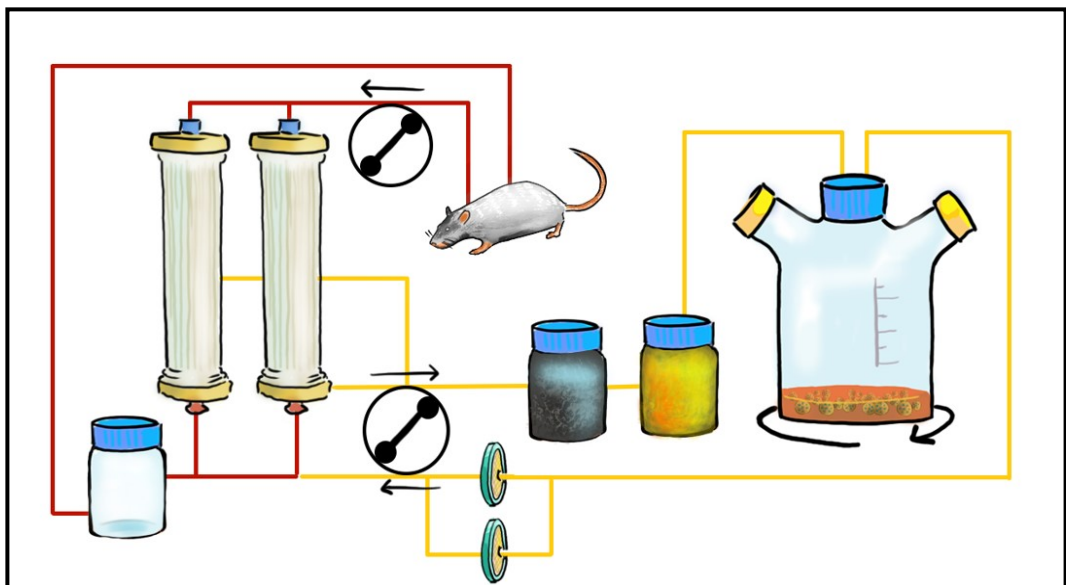
HAL is a multi-disciplinary open access archive for the deposit and dissemination of scientific research documents, whether they are published or not. The documents may come from teaching and research institutions in France or abroad, or from public or private research centers.

L'archive ouverte pluridisciplinaire **HAL**, est destinée au dépôt et à la diffusion de documents scientifiques de niveau recherche, publiés ou non, émanant des établissements d'enseignement et de recherche français ou étrangers, des laboratoires publics ou privés.

Par **Mattia PASQUA**

Preclinical studies on an extracorporeal bioartificial liver

Thèse présentée
pour l'obtention du grade
de Docteur de l'UTC



Soutenue le 19 juin 2020

Spécialité : Biomatériaux et Bio-ingénierie : Unité de
Recherche Biomécanique et Bio-ingénierie (UMR-7338)

D2557

Ecole doctorale n° 71 : Sciences pour l'ingénieur
Unité BMBI CNRS UMR 7338, équipe CBB

PRECLINICAL STUDIES ON AN EXTRACORPOREAL BIOARTIFICIAL LIVER

19 Juin 2020

Spécialité : Biomatériaux et Bioingénierie

Presented by: Mattia Pasqua

Jury referees:

- Ivan Donati, Assistant Professor, University of Trieste, Italy
- Anne Corlu, CNRS Research director, UMR 1241, Inserm - Université de Rennes 1, France

Other jury members:

- Pedro Baptista, Assistant professor, Aragon Health Sciences Institute (IACS), Spain
- Catherine Picart, Professor, UMR 5628 Laboratoire des Matériaux et du Génie Physique (LMGP), France
- Filomena Conti, Professor-Hospital practitioner, Unité de Transplantation Hépatique, Hôpital de la Pitié-Salpêtrière, France
- Christophe Egles, Professor, BMBI-CNRS UMR 7338, Université de technologie de Compiègne (UTC), France

Thesis supervisors:

- Ulysse Pereira, Research engineer, BMBI-CNRS UMR 7338, Université de technologie de Compiègne (UTC), France
- Cécile Legallais, CNRS Research director, BMBI-CNRS UMR 7338, Université de technologie de Compiègne (UTC), France

Invited members:

- Anne Dubart-Kupperschmitt, INSERM Research director, DHU Hépatinov/UMR S1193 Inserm/ Université Paris-Saclay, France
- Jean-Charles Duclos-Vallee, Hepatologist, Hôpital Paul Brousse, France

THESE PRESENTÉE POUR L'OBTENTION DU GRADE DE DOCTEUR DE
L'UNIVERSITÉ DE TECHNOLOGIE DE COMPIEGNE

List of publications and communication in link with the PhD thesis

Scientific articles

Pasqua M., Pereira U., Messina A., de Lartigue C., Nicolas J., Vigneron P., Dermigny Q., Legallais C. Preclinical characterization of alginate-Poly-L-Lysine encapsulated HepaRG for extracorporeal liver supply. Manuscript ready for submission in *Biotechnology and Bioengineering*

Pasqua M., Pereira U., Messina A., de Lartigue C., Vigneron P., Dubart-Kupperschmitt A., Legallais C. HepaRG self-assembled spheroids in alginate beads meet the clinical needs for bioartificial liver. *Tissue Eng. Part A* ahead of printing, 1–33 (2019). doi: 10.1089/ten.TEA.2019.0262

Legallais C., Kim D., Mihaila S.M., Mihajlovic M., Figliuzzi M., Bonandrini B., Salerno S., Yousef Yengej F.A., Rookmaaker M.B., Sanchez Romero N., Sainz-Arnal P., Pereira U., **Pasqua M.**, Gerritsen K.G.F., Verhaar M.C., Remuzzi A., Baptista P.M., De Bartolo L., Masereeuw R., Stamatialis D. *Bioengineering Organs for Blood Detoxification. Adv. Healthc. Mater.* 1800430, 1–32 (2018). doi:10.1002/adhm.201800430

International and national congress

Pasqua M., Pereira U., Messina A., de Lartigue C., Vigneron P., Dubart-Kupperschmitt A., Legallais C. From 3D culture to organoids, Paris, 2nd December 2019, France. Poster

de Lartigue C., **Pasqua M.**, Pereira U., Legallais C. Activity of encapsulated HepaRG in fluidized bed artificial liver. Congrès BioMat Matériaux pour la Santé 2019, La Grande Motte, 3rd-7th June 2019, France. Poster

Pasqua M., Pereira U., Duclos-Vallee JC., Dubart-Kupperschmitt A., Legallais C. Activity of encapsulated hepatic-like cells in the fluidized bed bioreactor. The Liver meeting 2017: Walter E. Washington Convention Center, Washington DC, 20th-24th October 2018, USA. Poster presentation

Pasqua M., Pereira U., Hirsinger B., Fleury MJ., Duclos-Vallee JC., Dubart-Kupperschmitt A., Legallais C. Hepatic cell microencapsulation for bioartificial liver: metabolic activity in static culture versus perfused culture in fluidized bed bioreactor. XLV ESAO congress, New organs for life, Madrid, 12th-15th September 2018, Spain. Oral presentation

Pasqua M., Pereira U., Hirsinger B., Fleury MJ., Duclos-Vallee JC., Dubart-Kupperschmitt A., Legallais C. Hepatic cell microencapsulation for bioartificial liver: metabolic activity in static culture versus perfused culture in fluidized bed bioreactor. 8th World congress of biomechanics, Dublin, 8th-12th July 2018, Ireland. Poster presentation

Pasqua M., Pereira U., Fleury M.J., Dermigny Q., Legallais C. Spheroids versus isolated cells encapsulation for bioartificial liver. Conference on Bioencapsulation, Nantes, 6th June 2017, France. Oral presentation (Award: best student contribution)

Summary

| | |
|---|----|
| List of publications and communication in link with the PhD thesis..... | 3 |
| List of figures..... | 9 |
| List of tables | 13 |
| List of abbreviations..... | 15 |
| General introduction..... | 17 |
| Chapter 1. Research context | 19 |
| 1. Definition of Acute Liver Failure (ALF) | 21 |
| 2. Etiology and treatments..... | 22 |
| 2.1. Presentation..... | 22 |
| 2.2. Treatment of ALF: state of the art and new approaches | 23 |
| 2.3. Acute on chronic liver failure (ACLF)..... | 25 |
| 3. Extracorporeal liver support systems | 25 |
| 3.1. Artificial and bioartificial liver devices: operating principle and examples | 25 |
| 3.2. Important physiological functions for a BAL | 29 |
| 3.3. Challenges concerning BALs | 36 |
| 3.4. Bioreactors for BAL: principle and designs | 44 |
| 4. Hepatocytes alginate microencapsulation: a tool for liver tissue engineering | 47 |
| 5. Animal models for BAL preclinical studies | 48 |
| 5.1. Choice of the animal model..... | 49 |
| 5.2. Choice of the pathological model..... | 49 |
| 5.3. Choice of the induction method for ALF | 49 |
| 5.4. Other essential criteria specific to ALF | 51 |
| 6. Objectives of this thesis..... | 52 |
| Chapter 2. Materials and methods..... | 55 |
| 1. 2D cell culture..... | 57 |
| 2. 3D cell culture..... | 57 |
| 3. Alginate microencapsulation..... | 57 |
| 4. External poly-L-Lysine coating of alginate beads..... | 58 |
| 5. Metabolic and xenobiotic tests..... | 58 |
| 5.1. Albumin and urea synthesis | 58 |
| 5.2. ICG assay..... | 58 |
| 5.3. EROD assay | 58 |
| 5.4. BROD assay..... | 59 |
| 5.5. Metabolic tests on BAL function test medium | 59 |
| 5.6. Metabolic tests on pathological plasma model..... | 59 |
| 5.7. MTS test for measuring the cytotoxicity of the media used..... | 59 |
| 5.8. Data normalization..... | 59 |
| 6. Cell differentiation study | 60 |
| 7. Cell proliferation inside the beads..... | 60 |
| 8. Determination of the total number of cells and total amount of cell proteins..... | 61 |
| 9. Cell viability..... | 61 |
| 10. PLL distribution in alginate beads..... | 61 |
| 11. Mechanical characterization of beads' surface | 62 |
| 12. Beads diffusion properties | 62 |
| 13. Fluidized bed bioreactor: setup for <i>in vitro</i> testing | 62 |
| 14. Perfused dynamic bioreactor: setup for <i>in vitro</i> testing | 64 |
| 15. Circuit to tests the artificial elements..... | 64 |
| 15.1. Analysis of the markers tested on artificial elements..... | 65 |
| 16. Statistical analysis..... | 65 |
| 17. Figures representation | 65 |
| Chapter 3. Phase I: HepaRG culture in alginate beads and application to the fluidized bed bioreactor..... | 67 |

| | | |
|--|--|------------|
| 1. | Introduction | 69 |
| 2. | Results..... | 72 |
| 2.1. | Step 1: Preliminary investigations on HepaRG culture conditions for BAL application.. | 72 |
| 2.2. | Characterization of the "gold standard" HepaRG 3D culture in alginate beads | 81 |
| 2.3. | Step 2: Optimization of the biomass for fluidized bed bioreactor..... | 87 |
| 2.4. | Step 3: Culture of encapsulated cells on fluidized bed bioreactor | 93 |
| 3. | Discussion..... | 96 |
| 4. | Conclusion..... | 103 |
| 5. | Key points phase I..... | 103 |
| Chapter 4. Phase II: biomass optimization for multiple bioreactor types | | 106 |
| 1. | Introduction | 108 |
| 2. | Results..... | 109 |
| 2.1. | Step 1: Influence of PLL coating on physical/mechanical properties of the beads and on cell metabolic performance..... | 109 |
| 2.2. | Step 2: influence of cell density on cell metabolic performance | 116 |
| 2.3. | Step 3: cells and beads behaviour in fluidized bed (FB) and perfused dynamic bioreactor (PDB) | 118 |
| 2.4. | Effect of pathological plasma model on cell metabolic performance..... | 121 |
| 3. | Discussion..... | 123 |
| 4. | Conclusions | 126 |
| 5. | Key points of phase II | 127 |
| Chapter 5. Phase III: towards animal investigations | | 128 |
| 1. | Introduction | 130 |
| 2. | Design of the pathological animal model..... | 131 |
| 2.1. | Choice of the animal model..... | 131 |
| 2.2. | Choice of the pathological model..... | 131 |
| 3. | Miniaturization of the pre-existing human-scale BAL..... | 135 |
| 3.1. | Sizing process | 135 |
| 3.2. | First generation of the small-scaled BAL | 138 |
| 3.3. | Second generation of the small-scaled BAL | 139 |
| 3.4. | Third generation of the small-scaled BAL..... | 140 |
| 4. | Effects of the artificial elements of the BAL on a model of pathological ALF human plasma | 141 |
| 4.1. | Effect of activated charcoal and ionic resin on perfusion medium content..... | 141 |
| 4.2. | Effect of the whole artificial components in series on the perfusion medium content | 144 |
| 4.3. | Effect of the recirculated medium on cell viability..... | 145 |
| 5. | Setting the safety analysis on healthy rats..... | 146 |
| 5.1. | Preliminary steps for animal testing | 147 |
| 5.2. | Optimization of the sterilization process of the plasmafilter | 147 |
| 5.3. | <i>In vivo</i> testing: feasibility of the plasmapheresis step | 148 |
| 6. | Conclusions | 149 |
| 7. | Key points of phase III..... | 150 |
| General conclusions and perspectives | | 152 |
| References | | 158 |
| Annexes | | 172 |
| Annex 1. Influence of the hormone triiodothyronine (t₃) on cell metabolic performance..... | | 174 |
| 1. | Introduction | 174 |
| 1.1. | Description of triiodothyronine | 174 |
| 1.2. | Mechanism of action | 174 |
| 1.3. | Catabolism..... | 175 |
| 1.4. | Interests in using hormone T ₃ on HepaRG..... | 175 |
| 2. | Materials and methods | 177 |
| 2.1. | 2D cell culture | 177 |

| | | |
|--|--------------------------|------------|
| 2.2. | Material..... | 177 |
| 2.3. | Conditions tested..... | 177 |
| 2.4. | Experimental design..... | 178 |
| 3. | Results..... | 179 |
| 3.1. | Metabolic tests | 179 |
| 3.2. | Xenobiotic tests | 180 |
| 3.3. | Cell viability | 180 |
| 4. | Discussion..... | 181 |
| 5. | Conclusions | 182 |
| Annex 2. Overview of proliferative human cell sources applied in bioartificial livers | | 184 |
| Annex 3. Other cell densities tested | | 191 |
| Annex 4. Summary of the metabolic activities measured during this thesis | | 195 |

List of figures

| | |
|---|----|
| Fig. 1: Research axes of the project RHU iLite, WP = work packages..... | 17 |
| Fig. 2: Sub-classification of ALF. HA/E/BV: hepatitis A/E/V virus. Sources: ⁷ | 21 |
| Fig. 3: Aetiology of ALF varies with geography. Source: ⁷ | 22 |
| Fig. 4: Ratio between number of liver transplanted patients and patients in waiting list for an available organ from 2007 to 2017 in France..... | 24 |
| Fig. 5: Adsorption of molecules in activated charcoal..... | 26 |
| Fig. 6: BAL setup..... | 28 |
| Fig. 7: Major liver functions in the body..... | 30 |
| Fig. 8: Organization of the liver lobule. Blood flows from the portal triad, formed by the portal vein, hepatic artery and bile duct, through the sinusoids to the central vein. Bile flows through bile canaliculi in counterflow to the bile ducts. The gradients underneath the acinus represent functional variation across the acinus. HSC: hepatic stellate cell, LSEC: liver sinusoidal endothelial cell, KC: Kupffer cell. Adapted from ref: ⁶⁶ (request permission pending)..... | 31 |
| Fig. 9: Scheme of production, metabolism, and excretion of bilirubin..... | 33 |
| Fig. 10: Sequential steps of drug elimination by metabolism and membrane transport in hepatocyte ⁸² | 35 |
| Fig. 11: Processing of cells derived from different sources for the generation of human <i>in vitro</i> liver cell culture models. Major cell types include primary human hepatocytes (PHH), hepatoma cell lines, adult stem cells, human embryonic stem cells (hESC), and induced pluripotent stem cells (iPSC). Whereas PHH can be used for <i>in vitro</i> cultivation immediately after isolation, liver cell lines or stem cells need to be expanded and/or differentiated prior to their use in experiments. Source: Zeilinger et al. 2016 ⁸⁸ | 37 |
| Fig. 12: HepaRG differentiation and dedifferentiation..... | 39 |
| Fig. 13: Portal triad anatomy (left) and bile formation process (right). Hepatocytes initiate bile formation by secreting primary bile, composed primarily of water, solutes, and ions, into canaliculi. As canalicular bile flows along the biliary tree, it is subjected to cholangiocyte secretory and absorptive processes, thus resulting in modified ductal bile. Secretion of Cl^- , HCO_3^- , and water and absorption of bile acids (BAs), glucose, amino acids (AAs), and water are the major transport processes determining the chemical composition of ductal bile. Source: ¹⁰⁶ (request permission pending). | 41 |
| Fig. 14: Derivation, cultivation and differentiation of hESCs..... | 42 |
| Fig. 15: Derivation and differentiation of iPSCs..... | 43 |
| Fig. 16: FB concept ¹²⁶ | 46 |
| Fig. 17: Concept SUPPLIVER, the patient's plasma is separated from the formed elements of blood through a plasmafilter. Then, the plasma is treated by the bioreactor hosting encapsulated hepatic cells. The alginate matrix protects hepatic cells from shear stress (perfusion), and from the immune system of the patient, favouring at the same time the mass transfer between cells and fluid. Once the plasma has been treated (detoxified and enriched with molecules produced by hepatocytes), it enters once again the patient. Source: thesis of S. Figaro ¹²⁹ | 46 |
| Fig. 18: Alginate structure (left) and gel formation (egg-box structure) (right)..... | 48 |
| Fig. 19: Role of alginate beads..... | 48 |
| Fig. 20: Objectives of this thesis..... | 53 |
| Fig. 21: Singular components of a FB (A) and FB setup for <i>in vitro</i> testing (B)..... | 63 |
| Fig. 22: Perfused dynamic bioreactor (PDB) setup..... | 64 |
| Fig. 23: Circuit to test artificial elements..... | 65 |
| Fig. 24: Concept of fluidized bed bioreactor (FB) and mass transfer..... | 69 |
| Fig. 25: Optimization of the biomass, from shaken to FB culture..... | 72 |
| Fig. 26: Experimental setup phase I, preliminary studies on culture conditions..... | 73 |
| Fig. 27: Metabolic activities measured on day 7 between SPHs 1.5% and DCs 1.5%. Albumin secretion rate (A, significance analysed by Mann-Whitney test) and ICG releasing rate (B). * indicates outliers. $N \geq 3$ | 74 |
| Fig. 28: Observation on bright field microscopy of SPHs (A) and DCs after encapsulation (B). Scale bar: 500 μm | 74 |
| Fig. 29: Mean diameter of SPHs and DCs after encapsulation on day 7..... | 74 |
| Fig. 30: Albumin secretion rate (A, significance analysed by Mann-Whitney test), ICG releasing (B). * indicates outliers. $N \geq 3$ | 75 |

| | |
|---|----|
| Fig. 31: Pictures in bright field microscope of DCs 1% (left) and DCs 1.5% (right) on day 7 post-encapsulation. Scale bar: 500 μ m..... | 75 |
| Fig. 32: Elastic modulus (in kPa) between empty alginate beads 1% and 1.5% on day 7. * indicates outliers. Significance analysed by Mann-Whitney test. N = 10 per batch of empty beads..... | 76 |
| Fig. 33: Metabolic activities of encapsulated cells on day 7 and day 14. Albumin secretion rate (A, significance analysed by Wilcoxon matched-pairs signed-ranks test), ICG releasing rate (B), CYP1A1/2 activity (C), CYP3A4 activity (D). * indicates outliers. N \geq 3..... | 78 |
| Fig. 34: CYP1A1/2 activity after induction by β naphthoflavone 100 μ M on day 7 (A) and 14 (B, significance analysed by Mann-Whitney Test). N \geq 3..... | 78 |
| Fig. 35: Elastic modulus (in kPa) of empty alginate beads at day 7 and 14. N \geq 3..... | 78 |
| Fig. 36: Albumin synthesis rate (A), ammonia (B) and lactate (C) detoxification rate on day 7 and 14. * indicated outliers. N \geq 3..... | 79 |
| Fig. 37: DCs 1.5% viability after exposition to BAL function test medium on day 7 and 14 (confocal microscopy). In green (Calcein AM): viable cells, in red (ethidium homodimer-1): dead cells, in blue (Hoechst 33342 dye): cell nuclei. Scale bar: 100 μ m..... | 79 |
| Fig. 38: Cell viability for all the conditions tested (confocal microscopy). In green (Calcein AM): viable cells, in red (ethidium homodimer-1): dead cells, in blue (Hoechst 33342 dye): cell nuclei. Scale bar: 100 μ m..... | 80 |
| Fig. 39: Cell viability after metabolic and xenobiotic tests on DCs 1.5% on day 14. (confocal microscopy). In green (Calcein AM): viable cells, in red (ethidium homodimer-1): dead cells, in blue (Hoechst 33342 dye): cell nuclei. Scale bar: 100 μ m..... | 80 |
| Fig. 40: Beads diameter over-time. N = 15 beads per day..... | 81 |
| Fig. 41: Beads morphology (bright field microscopy, scale bar: 500 μ m) and cell viability (confocal microscopy, scale bar: 100 μ m). In green (Calcein AM): viable cells, in red (ethidium homodimer-1): dead cells, in blue (Hoechst 33342 dye): cell nuclei..... | 82 |
| Fig. 42: Albumin synthesis rate over-time. N \geq 3..... | 82 |
| Fig. 43: Cells self-rearranged in aggregates: diameters over time (A). F-actin (phalloidin, in green) and nuclei (DAPI, in blue) staining on day 14 (B) (confocal microscopy). Scale bar: 20 μ m..... | 82 |
| Fig. 44: Cell proliferation inside the beads. In green: new formed cells/nuclei, in blue: cell nuclei (DAPI). Scale bar: 250 μ m..... | 83 |
| Fig. 45: Proliferation profile between the days of culture..... | 83 |
| Fig. 46: Immunofluorescence staining over time (confocal microscopy). Hepatoblast markers (Hb): HNF 6 in red, CK-19 in green, AFP in green, nuclei in blue. Mature hepatocyte markers (MH): ALB in green, HNF 4 α in red and in sand colour, CYP 3A4 in green, A1AT in red, UGT1A1 in green, SR-B1 in red, BSEP in red. Cholangiocyte markers: SOX 9 in sand colour, ASBT in red, CK-7 in green, nuclei in blue. Scale bar: 20 μ m..... | 86 |
| Fig. 47: Immunofluorescence staining of ZO-1 on day 10 (epifluorescence microscopy). In red: ZO-1; in green: hepatocytes auto-fluorescence; in blue: cell nuclei. Scale bar: 100 μ m..... | 87 |
| Fig. 48: Experimental setup, phase I step 2..... | 88 |
| Fig. 49: Metabolic performance between encapsulated cells with (+ GM) and without glass microparticles (- GM) in proliferation HepaRG medium on day 14. Albumin synthesis (A), ICG releasing rate (B), EROD activity (C). Significance analysed by Mann-Whitney test. * indicated outliers. N \geq 3..... | 89 |
| Fig. 50: Metabolic performance between encapsulated cells with (+ GM) and without glass microparticles (- GM) in BAL function test medium on day 14. Albumin secretion rate (A), ammonia (B) and lactate (C) detoxification rate. * indicated outliers. N \geq 3..... | 90 |
| Fig. 51: cell viability (confocal microscopy) of cells in beads containing (+ GM) or not glass microparticles (- GM). In green (Calcein AM): viable cells, in red (ethidium homodimer-1): dead cells, in blue (Hoechst 33342 dye): cell nuclei. Scale bar: 100 μ m..... | 90 |
| Fig. 52: Metabolic performance on day 14 between cell densities 5M/mL and 10 M/mL in proliferation HepaRG medium. Albumin synthesis (A), ICG releasing rate (B), EROD activity (C). Significance analysed by Mann-Whitney test. * indicated outliers. N \geq 3..... | 91 |
| Fig. 53: Metabolic performance on day 14 between cell densities 5M/mL and 10 M/mL in proliferation BAL function test medium. Albumin synthesis (A), ICG releasing rate (B), EROD activity (C). Significance analysed by Mann-Whitney test. * indicated outliers. N \geq 3..... | 92 |
| Fig. 54: Metabolic performance "per bioreactor" on day 14 between cell densities 5M/mL and 10 M/mL in proliferation HepaRG medium. Albumin synthesis (A), ICG releasing rate (B), EROD activity (C). Significance analysed by Mann-Whitney test. * indicated outliers. N \geq 3..... | 92 |

| | |
|--|-----|
| Fig. 55: Metabolic activities on day 14 in BAL function test medium between 5 million cells/mL and 10 million cells/mL of alginate 1.5%. Albumin secretion rate (A), ammonia (B) and lactate (C) detoxification rate. * indicated outliers. N ≥ 3..... | 93 |
| Fig. 56: Cell viability (confocal microscopy) between cell density 5 M/mL and 10 M/mL on day 14. In green (Calcein AM): viable cells, in red (ethidium homodimer-1): dead cells, in blue (Hoechst 33342 dye): cell nuclei. Scale bar: 250 µm..... | 93 |
| Fig. 57: Experimental setup, phase I step 3..... | 94 |
| Fig. 58: Albumin secretion rate over time. N ≥ 3..... | 95 |
| Fig. 59: Albumin secretion (A), ammonia (B) and lactate (C) detoxification in shaken and perfused (FB) after a 6h therapy in pathological plasma model. Significance analysed by Mann-Whitney test. * indicated outliers. N ≥ 3..... | 95 |
| Fig. 60: Cell viability shaken versus perfused culture. In green (Calcein AM): viable cells, in red (ethidium homodimer-1): dead cells, in blue (Hoechst 33342 dye): cell nuclei. Scale bar: 250 µm..... | 96 |
| Fig. 61: steps of phase II..... | 109 |
| Fig. 62: Electrostatic interactions between alginate (core of the bead) and PLL (shell)..... | 109 |
| Fig. 63: Distribution of PLL-rhodamine (red staining) in empty beads in comparison with the negative control (without PLL coating). Images taken in confocal microscopy (left images), phase contrast (central) and merging the two (right)..... | 110 |
| Fig. 64: Elastic modulus of the outer surface of empty beads with and without a PLL coating on day 14. With an indentation of 3 µm, the sensor penetrated only on the PLL layer, when present. Significance was analysed using a Mann-Whitney Test. *** indicates p < 0.001. N = 10 per batch of beads..... | 111 |
| Fig. 65: Permeability of empty beads (coated or not with PLL) to fluorescent markers (albumin, IgG, nanoparticles of different diameters). DH indicates the hydrodynamic diameter without the fluorophore; Ø indicates the diameter of the nanoparticles (NPs). Incubation lasted 24 hours. Pictures taken after washing the beads in WE. Scale bar: 100 µm..... | 111 |
| Fig. 66: Experimental setup phase II, step 1..... | 112 |
| Fig. 67: Observation of beads without and with PLL coating morphology by bright field microscopy (scale bar: 500 µm) and cell viability of alginate-PLL encapsulated cells (live/dead assay) by confocal microscopy. In green (Calcein AM): viable cells, in red (ethidium homodimer-1): dead cells, in blue (Hoechst 33342 dye): cell nuclei (scale bar 100 µm)..... | 113 |
| Fig. 68: Albumin secretion rate over time (overnight between days 0-1, 6-7, 9-10, 13-14) of encapsulated cells in alginate beads with and without PLL coating. For the condition with PLL, the increasing between day 1 and da14 was significant (* indicates p < 0.01, significance analysed by Dunn's Multiple Comparisons Test). N ≥ 3..... | 114 |
| Fig. 69: Metabolic activities of cells in alginate beads with and without PLL coating, measured on day 14 in HepaRG proliferation medium. A: Albumin secretion rate; B: ICG releasing rate by the transporters MDR3 and MRP2; C: CYP1A1/2 activity (significance analysed by Wilcoxon matched-pairs signed-ranks test). * indicated outliers. N ≥ 3..... | 115 |
| Fig. 70: Metabolic activities of cells in alginate beads with and without PLL coating, measured on day 14 in BAL test medium. A: albumin synthesis rate; B: ammonia detoxification rate; C: lactate detoxification rate. * indicated outliers. N ≥ 3..... | 115 |
| Fig. 71: Cell viability (live/dead assay) of cells in alginate beads with and without PLL coating, by confocal microscopy. In green (Calcein AM): viable cells, in red (ethidium homodimer-1): dead cells, in blue (Hoechst 33342 dye): cell nuclei. Scale bar: 100 µm..... | 116 |
| Fig. 72: Experimental plan, phase II step 2..... | 116 |
| Fig. 73: Albumin secretion rate over 14 days. N ≥ 3..... | 117 |
| Fig. 74: Cell viability (live/dead assay) of cells in alginate-PLL beads at 5M/mL and 10M/mL, by confocal microscopy. In green (Calcein AM): viable cells, in red (ethidium homodimer-1): dead cells, in blue (Hoechst 33342 dye): cell nuclei. Scale bar: 100 µm..... | 118 |
| Fig. 75: Experimental plan for phase II, step 3..... | 119 |
| Fig. 76: Culture conditions tested for next biomass metabolic characterization. A: Shaken condition. B: PDB condition..... | 120 |
| Fig. 77: Metabolic activities of cells in alginate-PLL beads, measured on day 14 in pathological plasma model, in shaken and perfused dynamic bioreactor (PDB). A: albumin synthesis rate; B: ammonia detoxification rate; C: lactate detoxification rate..... | 121 |
| Fig. 78: Cell viability (live/dead assay) of cells in alginate-PLL beads, by confocal microscopy, after exposition to pathological plasma model. In green (Calcein AM): viable cells, in red (ethidium homodimer-1): dead cells, in blue (Hoechst 33342 dye): cell nuclei. Scale bar: 100 µm..... | 121 |

| | |
|---|-----|
| Fig. 79: Cell viability via MTS test in 2D configuration. Significance analysed by Mann Whitney test. | 122 |
| Fig. 80: Miniaturization from the human-scale (A) to small-scale BAL (B) | 130 |
| Fig. 81: Human scale BAL circuit developed by S. Figaro ¹²⁹ | 136 |
| Fig. 82: First generation BAL prototype | 138 |
| Fig. 83: Second generation BAL design | 139 |
| Fig. 84: BAL circuit (top) implementing the PDB bioreactor. BAL device (down) | 140 |
| Fig. 85: Closed circuits for testing the artificial elements. Experimental setup. N = 2 | 142 |
| Fig. 86: Effect of charcoal and ionic resin (connected in series) on specific markers contained in pathological medium. Y-axis represents the concentration of the marker while X-axis the time-point of sampling (T0, time zero, means sampling after a complete pathological medium recirculation in the circuit while T6 is the sampling after 6 hours of medium recirculation in the circuit). N = 3 | 143 |
| Fig. 87: Experimental plan with all the artificial elements connected in series. N = 1 | 144 |
| Fig. 88: Cell viability (expressed in %) in relation to the control: cells treated with HepaRG medium. Significance analysed by Mann-Whitney test. | 146 |
| Fig. 89: Catheter harness and tethering mount | 147 |
| Fig. 90: Extracorporeal circulation setup | 149 |
| Fig. 91: <i>In vivo</i> experiments | 149 |
| Fig. 92: Mechanism of action of T3 | 175 |
| Fig. 93: Experimental method | 178 |
| Fig. 94: Experimental design | 178 |
| Fig. 95: Albumin synthesis rate normalised by the number of cell seeded (A). Global albumin quantity produced in each condition tested (B) | 191 |
| Fig. 96: Cell viability (confocal microscopy) between cell density at 1, 5, 10, 20 and 40 million cells/mL (M/mL) of alginate 1.5% on day 14. In green (Calcein AM): viable cells, in red (ethidium homodimer-1): dead cells, in blue (Hoechst 33342 dye): cell nuclei. Scale bar: 250 µm | 192 |
| Fig. 97: Condition 40 M/mL (bright field microscopy) | 192 |

List of tables

| | |
|---|-----|
| Tab. 1: Alternatives therapies to liver transplantation..... | 24 |
| Tab. 2: Methods of blood purification..... | 26 |
| Tab. 3: Use of activated charcoal in hemoperfusion therapy | 26 |
| Tab. 4: Most widely used artificial liver supports..... | 28 |
| Tab. 5: Bioartificial liver supports in clinical trials | 29 |
| Tab. 6: Cell sources used in BALs: pros and cons..... | 38 |
| Tab. 7: Published results on HepaRG metabolic performance..... | 40 |
| Tab. 8: Bioreactor designs. Sources: ^{62,67} | 45 |
| Tab. 9: Surgical methods for inducing ALF in animal models ¹⁵¹ | 50 |
| Tab. 10: Chemical methods for inducing ALF in animal models ¹⁵¹ | 51 |
| Tab. 11: List of antibodies used for immunofluorescence staining..... | 60 |
| Tab. 12: Qualitative evolution of cell differentiation over time..... | 84 |
| Tab. 13: Overview of a comparison between our results and other published results on various cell models in different culture conditions. | 99 |
| Tab. 14: Overview of a comparison between our results and other published results on various cell models in different culture conditions. | 100 |
| Tab. 15: Media for metabolic characterization at day 14 post-encapsulation and tests performed | 114 |
| Tab. 16: Metabolic performance of cells in pathological plasma medium. N ≥ 3 if not differently specified..... | 117 |
| Tab. 17: Effect of pathological plasma model on cell metabolic performance. HPM: HepaRG proliferation medium | 122 |
| Tab. 18: Validity of the criteria for the choice of the animal model | 131 |
| Tab. 19: BALs tested on rats, methods and outcomes | 134 |
| Tab. 20: Legend human-scale BAL components (SUPPLIVER project)..... | 137 |
| Tab. 21: Sizing of the device's components, from human to rat scale | 137 |
| Tab. 22: Summary of the activities analysed on artificial elements connected in series | 145 |
| Tab. 23: Basal production of albumin in ng/h/well and in ng/h/10 ⁶ (cell counted by DNA quantification). N = 3. Results are expressed in mean ± standard deviation..... | 179 |
| Tab. 24: Metabolic activity on day 15 in BAL function tests medium, during 2 hours of incubation. N = 3. Results are expressed in mean ± standard deviation..... | 180 |
| Tab. 25: Effect of T3 on 4-MU biotransformation by UGT enzyme. . N = 3. Results are expressed in mean ± standard deviation | 180 |
| Tab. 26: Cell viability (%) on the different conditions at the end of the experiment. N = 3. Results are expressed in mean ± standard deviation..... | 181 |
| Tab. 27: Overview of proliferative human cells sources applied in BAL..... | 189 |
| Tab. 28: Summary of the metabolic activities measured in all conditions tested. N ≥ 3 if not differently specified..... | 197 |

List of abbreviations

| | | |
|---|--|---|
| 2D : two dimensions (or dimensional) | DAMPs : damage associated molecular patterns | HPM : HepaRG proliferation medium |
| 3D : three dimensions (or dimensional) | DAPI : 4,6-diamidino-2-phenylindole | hESC : human embryonic stem cells |
| 4-MU : 4-methylumbelliferone | DCs : dissociated cells | hiPSC : induced pluripotent stem cells |
| A1AT : Alpha-1 antitrypsin | D_H = hydrodynamic diameter | HNF 4 : : hepatocyte nuclear factor 4 |
| ACLF : acute on chronic liver failure | DHU Hepatinov : Département Hospitalo-Universitaire Hepatinov | HNF 6 : hepatocyte nuclear factor 6 |
| AFP : alpha-fetoprotein | DMSO : dimethyl sulfoxide | HNF4 : hepatic nuclear factor 4 |
| AL : artificial liver | DNA : deoxyribonucleic acid | ICG : indocyanine cardio-green |
| ALB : albumin | DPBS : Dulbecco's phosphate-buffered saline | ICP : intracranial pressure |
| ALF : acute liver failure | EDTA : Ethylenediaminetetraacetic acid | IgG : immunoglobulins G |
| AMC-BAL : Amsterdam medical center-bioartificial liver | EdU : 5-ethynyl-2'-deoxyuridine | IL-1 : : interleukin -1 |
| APAP : acetaminophen | ELISA : enzyme-linked immunosorbent assay | IL-6 : interleukin -6 |
| ASBT : apical sodium-dependent bile acid transporter | ELSS : extracorporeal liver support systems | INR : international normalized ratio |
| BAL : bioartificial liver | EROD : ethoxyresorufin-O-deethylase | INRIA : institut national de recherche en informatique et en automatique |
| BROD : 7-Benzyloxyresorufin-O-dealkylase activity | ESC s: embryonic stem cells | iPSCs : induced pluripotent stem cells |
| BSA : bovine serum albumin | F-actin : filamentous actin | LDH : lactate dehydrogenase |
| BSEP : bile salt Export pump | FITC : fluorescein isothiocyanate | LDL : low-density lipoprotein |
| CBB : Cellules Biomatériaux Bioréacteurs | FB : fluidized bed bioreactor | LT : liver transplantation |
| CEA : Commissariat à l'énergie atomique Paris/Saclay | FB-BAL : fluidized bed-bioartificial liver | M/mL : millions of cells/millilitre |
| CK-19 : cytokeratin 19 | FHH : fetal human hepatocytes | MDR3 : multidrug resistance protein 3 |
| CK-7 : cytokeratin 7 | GM : glass microparticles | MELD : Model End-Stage Liver Disease |
| CNRS : Centre national de la recherche scientifique | HE : hepatic encephalopathy | mESCs : mouse embryonic stem cells |
| CTRL : control | | MHH : mature human hepatocytes |
| CYP : cytochrome | | MOF : multiple organ failure |

MPH: mature porcine hepatocytes

MRP2: multidrug resistance-associated protein 2

N: number of observations

NAD(P)H: reduced form of NADP⁺, Nicotinamide adenine dinucleotide phosphate

NPs: nanoparticles

NTCP: sodium/taurocholate co-transporting polypeptide

Ø: diameter

OATP1B3: solute carrier organic anion transporter family member 1B3

OLT: orthotopic liver transplantation

p: p-value

PAMPs: pathogen associated molecular patterns

PBS: Phosphate-buffered saline

PDB: perfused dynamic bioreactor

PERVs: porcine endogenous retroviruses

PFA: paraformaldehyde

PHH: primary human hepatocytes

PLL: poly-L-lysine

PPH: primary porcine hepatocytes

Q: flow rate

RHU iLite: Recherche Hospitalo-Universitaire, Innovations for Liver Tissue Engineering

RNA: ribonucleic acid

scBAL: small-scaled bioartificial liver

SIRS: of systemic inflammatory response syndrome

SOX 9: SRY-box 9

SPHs: spheroids (also pre-formed spheroids)

SR-B1: scavenger receptor class B type 1

T3: 3,5,3' triiodothyronine

TGF-1: transforming growth factor 1

TNF: tumour necrosis factor alpha

TR: thyroid hormone receptors

UGT: UDP-glucuronosyltransferases

UTC: Université de technologie de Compiègne

WE: William's E culture medium

WP: work package

ZO-1: zonula occludens 1

General introduction

The RHU iLite project -for Recherche Hospitalo-Universitaire Innovations for Liver Tissue Engineering (2016-2021), has the main objective of designing mini liver organs by the assembly of elementary bricks - hepatic organoids, vascular networks and bile networks - initially built separately.

In view of a clinical and industrial translation of these "hepatic bio-constructs", the project will lead to the development of an external bio-artificial liver (BAL) for patients with acute failure, waiting for a transplantation, and a liver-on-a-chip model for *in vitro* toxicology studies in microfluidic systems.

These objectives can be achieved through the collaboration of doctors, cell biologists, physicists and engineers from several universities, research institutes and companies mastering the innovative techniques required for this bioconstruction. This multidisciplinary consortium, led by Jean-Charles Duclos-Vallée and the DHU Hepatinov, brings together laboratory teams from the Universités Paris-Sud and Paris Diderot, the Université de technologie de Compiègne (UTC), the CellSpace association, the CEA, Inserm, the CNRS and INRIA, as well as four companies, around 8 research axes (or work packages), summarized in figure 1:

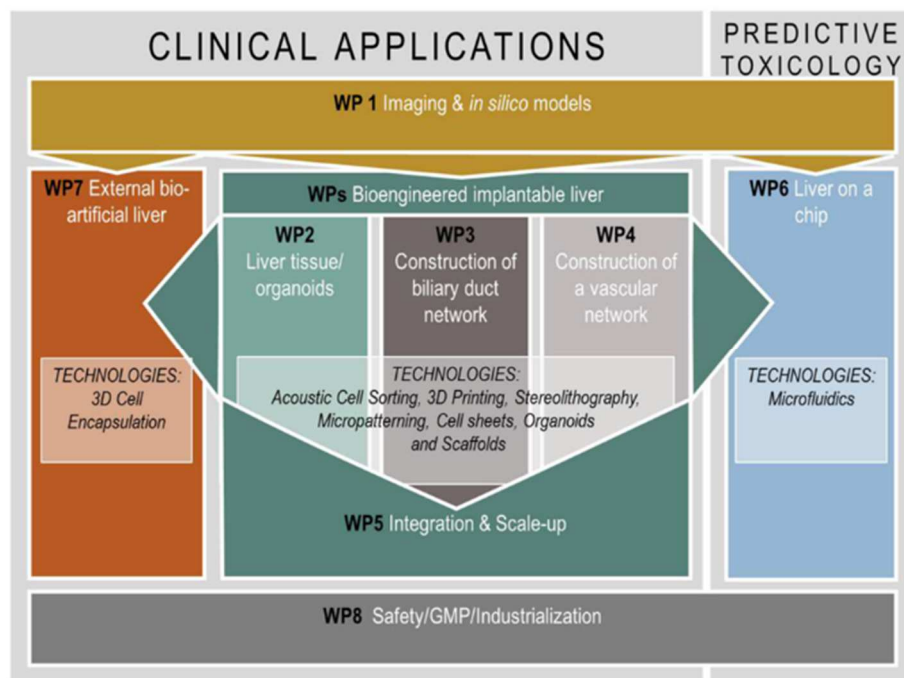


Fig. 1: Research axes of the project RHU iLite, WP = work packages

My PhD thesis is part of the work package 7 and consists in the development of an extracorporeal bioartificial liver based on a 3D microencapsulation technology and perfused bioreactor. A human size complete system classified as a combined advanced therapy medicinal product (cATMP), had already been developed during the Ph.D. of Sara Figaro at UTC ¹, using C3A cell line as biological component. In WP7, the aim is to perform the preclinical studies that will pave the way to future clinical trials. The object of my PhD was to design and evaluate a small-scale prototype for

preclinical testing in an acute liver failure (ALF)-rat model. Ultimately, induced pluripotent stem cells (iPSC)- or embryonic stem cells (ESc)-derived hepatocytes should be employed, but this requested parallel research in WP2 at Inserm U1193 (group of A. Dubart Kupperschmitt) and the company GoLiver. Therefore, HepaRG provided by the company Biopredic, partner in ILite, was the cell type chosen during my Ph.D. project.

HepaRG has extensively been characterized in both 2D and 3D (spheroids and encapsulated cells) configurations, mostly in toxicology or pharmacology studies. However, the potential of micro-encapsulated HepaRG in fluidized bed bioartificial liver (FB-BAL) remained to be investigated and it represented one of the main objective of this thesis. In particular, specific attention was paid to the characterization of the metabolic performance of the cell line HepaRG encapsulated in alginate microbeads, as well as on the beads stability for its further application in perfused bioreactor.

In the bibliographical part of the present manuscript, we propose a description of ALF and its available and advanced treatments. Then, the focus will be put on the concept of BALs, and more specifically the one developed at the University of technology of Compiègne (UTC), in terms of operating principle, main problematics, and expectations on their use in patients suffering of ALF. The preclinical models that can be implemented before the clinical studies will also be discussed.

The core of this thesis will show the scientific path followed to optimize the aforementioned cell line culture for BAL applications. The first phase deals with the optimization of the biomass production for BAL application and, in particular, for fluidized bed bioreactor (chapter 3). The second phase revolves around the optimization of the encapsulation scaffold for other types of bioreactors (chapter 4). In the third phase, we describe the pathological animal model, the miniaturization of the human-scale BAL, characterization of its artificial components and the preliminary steps for *in vivo* investigation (chapter 5).

Chapter 1. Research context

1. Definition of Acute Liver Failure (ALF)

Fulminant liver failure is a life-threatening critical illness with an extremely high mortality rate, even if intensive care is provided ^{2,3}. In particular, acute liver failure (ALF) is a devastating multi-organ syndrome occurring in a previously healthy patient. It is characterized by severe hepatocellular dysfunction, leading to death (mortality between 40-50% in the most severe cases). When damage to the hepatic parenchyma is so severe that liver is not able anymore to satisfy the metabolic needs of the body, ALF develops. The mechanism by which hepatocytes death occurs as well as the process favouring liver regeneration remains unclear. However, there are evidences that the process leading to hepatocytes death occurs via necrosis or other mechanism, depending on the type of liver failure ⁴. The original term "fulminant hepatic failure", coined by Trey and Davidson in 1970, is defined as "a severe liver injury, potentially reversible in nature and with onset of hepatic encephalopathy (HE) within 8 weeks of the first symptoms in the absence of pre-existing liver disease" ⁵ and it is still relevant today. However, nowadays there are new definitions that classify the disease phenotypes based on the onset of symptoms and the development of HE. This classification allows the comprehension of the disease type, its cause and prognosis. The sub-classification of ALF, according to O'Grady classification⁶, is summarized in figure 2.

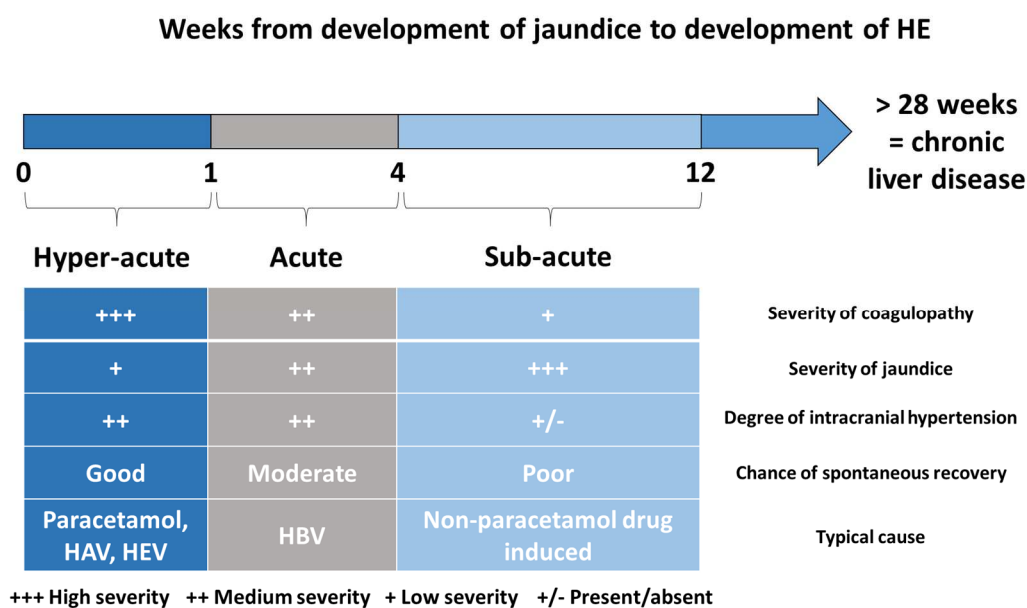


Fig. 2: Sub-classification of ALF. HA/E/BV: hepatitis A/E/V virus. Sources: ⁷

The eligibility of a patient in ALF for liver transplantation relies on prognostic models for ALF. Those models are able to classify the severity of liver disease and estimate the prognosis for ALF. An example of these models is the one developed by O'Grady and colleagues ⁸, known as King's College Criteria for acetaminophen (APAP)-induced liver toxicity and non-APAP induced liver toxicity. It takes in consideration the cause of ALF (APAP or non-APAP induced), clinical information (HE, age...), and laboratory parameters (INR, creatinine...), in order to determine which patient should be eligible for transplantation. Other known prognostic models are the Clichy criterion or the Model

End-Stage Liver Disease (MELD) score. These models can be explored in the literature and will not be further described in this manuscript ⁹.

2. Etiology and treatments

The causes of ALF are distributed in a geographic and socioeconomic manner (Figure 3). Hepatitis viruses (with infection by hepatitis A, B, and E viruses) are the most common cause in the developing world, whereas drug-induced ALF (often paracetamol) predominates in the United States and Europe. Less common causes include disorders such as Wilson's disease, Budd-Chiari syndrome, acute fatty liver of pregnancy, and chronic autoimmune hepatitis ³. A cause cannot be found (indeterminate) in as many as 19%.

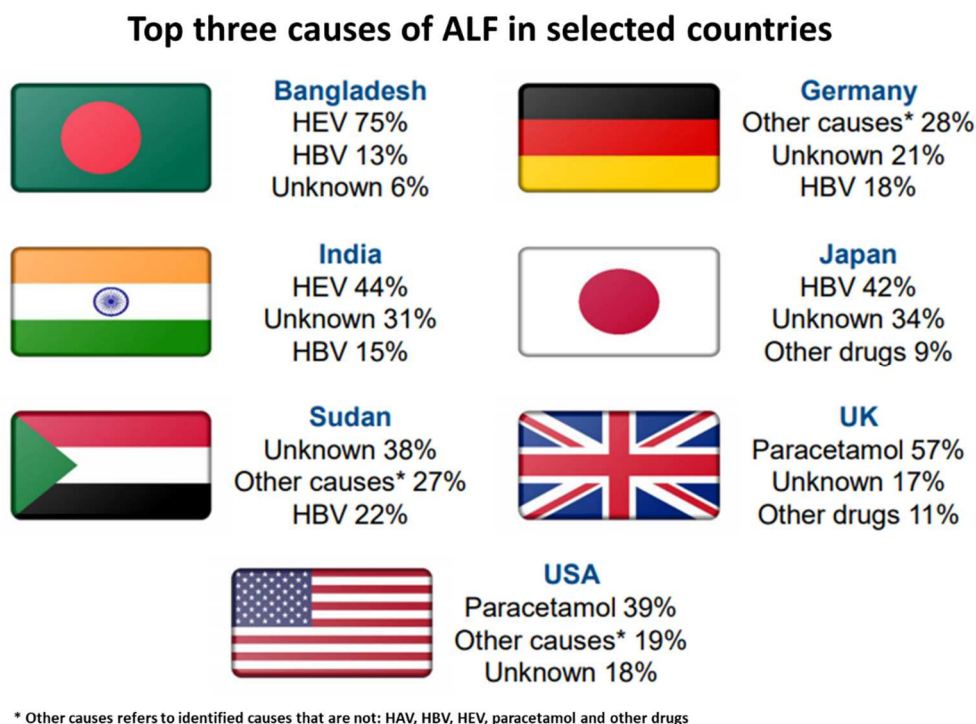


Fig. 3: Aetiology of ALF varies with geography. Source: ⁷

2.1. Presentation

ALF is associated firstly with loss of liver metabolic capacity, development of coagulopathy (International Normalised Ratio > 1.5), high level of transaminases (marker of liver damage), jaundice (due to high level of bilirubin), hypoglycaemia, hyperlactatemia, accumulation of toxins such as ammonia leading to hepatic encephalopathy often associated with cerebral oedema, hemodynamic changes, and electrolyte disturbance in a patient without a pre-existing liver disease. In patients with liver disease, changes in serum bile acids is a marker of liver damage and correlate with the severity of the disease. Hydrophobic bile acids presence in the blood can contribute to the pathogenesis of ALF ¹⁰. In a more advanced stage, multi-organ failure appears. This process may be mediated by the release of damage associated molecular patterns (DAMPs) from necrotic liver cells, pathogen associated molecular patterns (PAMPs) and virulence factors from secondary

infections and bacterial translocation, leading to a self-reinforcing cytokine cascade ¹¹. It has been observed that ALF is associated with high plasma levels of several proinflammatory cytokines, such as tumour necrosis factor alpha (TNF α) and pro-inflammatory interleukins (IL-1 and IL-6), which contribute to the development of systemic inflammatory response syndrome (SIRS), and eventually will lead to multi-organ failure and death ¹². Another key element of ALF clinical manifestation is cerebral metabolism alteration. It includes increases of cerebral blood flow, decreases of the cerebral metabolic rate for oxygen and failure of cerebrovascular autoregulation ¹³. Those features are related to diverse factors such as ammonia, lactate, glutamine, oxidative stress and pro-inflammatory factors aforementioned ^{14,15}.

2.2. Treatment of ALF: state of the art and new approaches

The aetiology of ALF is an important indicator for prognosis and the treatment strategy, especially in the necessity for emergency liver transplantation (LT). The clinical strategies of treatment that must be used in ALF patients are well described in the literature ¹⁶⁻¹⁸ and will not be further discussed in this manuscript. ALF is potentially reversible if diagnosed in time but, for patients with end-stage liver disease, to date orthotopic liver transplantation (OLT) is the only available treatment ¹⁹.

The first-line therapy consists in metabolic and nutritional support in order to improve the metabolic and hemodynamic stability, favour liver regeneration and avoid risk of complications. Patients in ALF are at increased risk of hypoglycaemia and show high protein catabolism, that compromise muscle bulk and immune functions. Therefore, glucose injection and nutritional support is required ^{3,18}. Moreover, lactate, triglycerides and ammonia plasma levels must be monitored closely to decrease the risk of intracranial hypertension. In the case where the metabolic support therapy is not sufficient, patients can be candidates for liver transplantation (LT). Before the era of LT, the mortality rate for patients with ALF ranged from 80% to 85% in one week. However, with the improvement in the field of critical care management and LT, survival for ALF patients has dramatically improved from 16% to 62% ^{20,21}. Since ALF is characterized by multiorgan failure, the early identification of ALF patients who will not survive with medical therapy alone and need LT is crucial. Different prognostic evaluation systems, such as King's College criteria ⁶, the Clichy criteria ²², the Japanese criteria ²³, and the Model End-Stage Liver Disease (MELD) ⁹ are available to identify candidates for LT but the selection of these patients remains challenging. Even if LT is often necessary for ALF patients considered to have a very poor prognosis without transplantation, it is not universally available, and less than 10% of liver transplantations are performed in patients with acute liver failure. Moreover, for patients undergoing OLT, intra- and post-operative complications are high (especially due to infection during the first three post-operative months) and the survival rate is overall lower if compared with elective liver transplantations. In addition, after LT, patients must take immunosuppressive drugs for the rest of their lives to keep the immune system from attacking transplanted organs, which leads to an increased risk of infections and cancer

development. However, outcomes are improving over year, registering a survival rate of 72% and 75% at 5 and 10 years post-OLT in Europe ²¹.

The limited availability of liver transplantation, showed in figure 4 taking the France as example (data extracted from Agence de la biomédecine, <https://www.agence-biomedecine.fr/?lang=fr>), and consequently, the growing gap between the number of patients on waiting list and the number of donor organs available, has highlighted the need for alternative therapies as a bridge to transplantation or liver regeneration ²⁴.

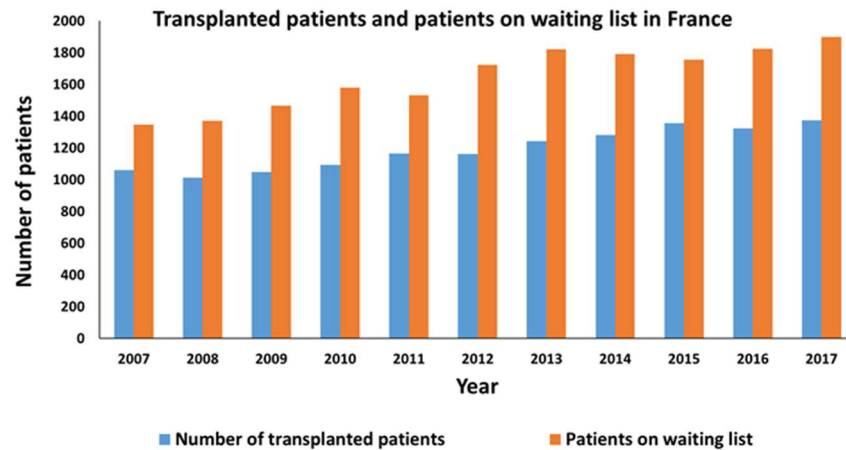


Fig. 4: Ratio between number of liver transplanted patients and patients in waiting list for an available organ from 2007 to 2017 in France

In case of ALF, a LT is needed between the 24 and 48 hours after diagnosis. In this limited time frame, it is not easy to find a compatible organ available for transplantation. In addition, there are cases where LT is not needed because of the potential of alternative therapies. These include approaches aimed to maximize the number of available grafts and these are summarized in table 1 (rearranged by the review article proposed by Cardoso et al. ²⁴).

| Alternatives to orthotopic liver transplantation | Method | References |
|--|---|------------|
| Living donor liver transplantation (LDLT) | Using liver fragments from living donor to the patient | 25–29 |
| Split liver transplant (SLT) | Obtaining two grafts from a single deceased donor, one for an adult and one for a child | 30–32 |
| Domino transplantation (DLT) | A patient with liver metabolic diseases receives a transplant; the explanted ill liver sometimes can be transplanted to another patient in situations whose livers remain structurally normal with preserved function and in which liver transplantation is expected to be curative | 24,33,34 |
| Hepatocytes transplantation (HT) | Freshly human hepatocytes injected in liver, without replacing the whole organ | 35–37 |
| Domino hepatocyte transplantation (DHT) | Hepatocytes from a donor with a certain metabolic liver disease are used to cure a different metabolic liver condition | 38,39 |
| Extracorporeal liver support systems (ELSS) | Artificial Livers (ALs) and BioArtificial Livers (BALs) | 40–42 |

Tab. 1: Alternatives therapies to liver transplantation

Among them, the focus will be put on extracorporeal liver support systems.

2.3. Acute on chronic liver failure (ACLF)

A different form of liver failure is the Acute on Chronic Liver Failure (ACLF). It is a syndrome characterized by an acute decompensation of chronic liver disease associated with multi-organ failure and short-term mortality. Alcohol and viral hepatitis are the most common causes leading to ACLF and a very strong SIRS plays a crucial role in its progression ⁴³. However, what emerges from the literature is that there is not uniformity on the definition of ACLF between research groups of different part of the world. Because of the lack of a universal definition, other features of this disease, such as prevalence, frequency of precipitating factors, and pathogenic mechanisms, remain unknown. It is very important to define properly the ACLF in order to identify patients with high risk of death for end-organ failure that require specific treatments. The European Association for the Study of the Liver-chronic liver failure (EASL-CLIF) Consortium designed a study called EASL-CLIF Acute-on-Chronic Liver Failure in Cirrhosis (CANONIC), aimed to give a definition of ACLF, able to identify cirrhotic patients with high risk of short-term mortality ⁴⁴. They defined the disease as decompensated liver cirrhosis in the presence of at least one organ failure. In the case of single-organ failure, serum creatinine level must be ≥ 1.5 mg/dL, or hepatic encephalopathy present. Based on the serial organ failure (SOFA) score, the European Association for the Study of the Liver Chronic Liver Failure (CLIF) Consortium score was developed and validated by an external cohort ⁴⁵. With this score, patients can be stratified from no ACLF to grade 3 ACLF with associated 180 days mortality rates ranging from 38% to 96%. This is currently the best-defined scoring system available, with the restriction that it is based on European data and may not be fully applicable to other geographic regions.

ACLF is usually triggered by infections or alcohol leading the patients to a critical state where liver transplantation is nearly impossible forthwith. In absence of any therapy, this critical condition leads easily to the death of the patient. However, a BAL therapy could help the patient to survive during this acute phase and potentially make the patient once again candidate for liver transplantation.

3. Extracorporeal liver support systems

3.1. Artificial and bioartificial liver devices: operating principle and examples

Extracorporeal liver support systems (ELSS) are devices for extracorporeal blood treatment that support any functions of the liver. The goal of ELSS therapy is to prolong the survival time of patients with ALF by preventing the progression of secondary organ failure ⁴⁶, bridge patients to liver transplantation or allow the native liver to recover from injury ⁴⁷. This approach could prevent liver transplantation and its associated complications. Two types of ELSS have been developed: artificial Livers (ALs) and Bio-Artificial Livers (BALs). ALs are non-biological liver support aiming at removing some potential harmful toxins involved in the progression ALF, from blood or plasma. Removal is based on physical/chemical gradients and adsorption. Those toxins are present in the blood of a patient with ALF and include ammonia, fatty acids, tryptophan, mercaptans, endogenous inhibitory neurotransmitters (such as γ -aminobutyric acid) ⁴⁸.

Early attempts at improving survival in liver failure patients consisted in trying to filter the ALF toxins via methods reported in table 2 (rearranged by the review article by Court et al. 2003 ⁴⁸).

| Method | Principle | Main outcomes |
|------------------------|---|------------------------------------|
| Hemofiltration | Haemodialysis | No long-term survival was observed |
| Hemoperfusion | Blood filtration via charcoal or membranes | |
| Plasma exchange | Replacement of plasma patient with fresh plasma | |

Tab. 2: Methods of blood purification

Some of these approaches are based on the use of sorbents, such as activated charcoal and ionic resins. Activated charcoal (Figure 5) is a high porous material essentially composed of coal material that has been carbonized at high temperature. Complex physical forces (Van der Waals) trap the solutes in its pores. It is particularly suitable for the removal of low weight non-polar molecules, such as polycyclic aromatic hydrocarbons or fatty acids and in general it is able to remove the albumin-bound toxins (e.g. tryptophan, involved in the aetiology of hepatic coma during ALF ⁴⁹).

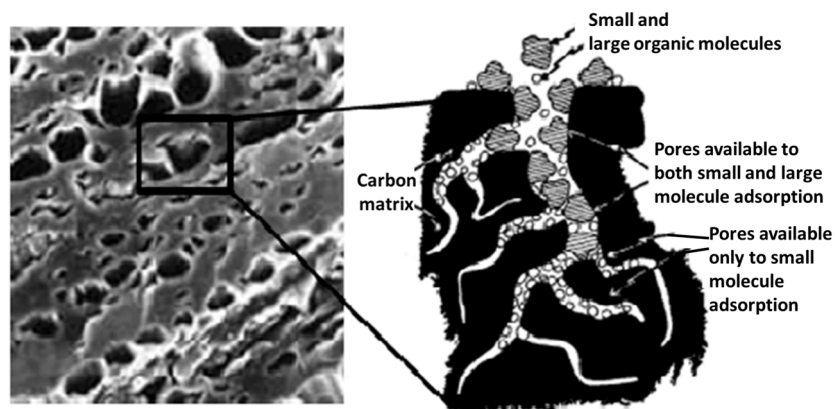


Fig. 5: Adsorption of molecules in activated charcoal Readapted from ⁵⁰.

The use of activated charcoal in hemoperfusion treatments is longstanding. The table 3 summarizes a brief history of their use in therapy.

| Date | Event |
|-------------|--|
| 1948 | Therapy introduced for adsorption of urea |
| 1964 | Yatzidis demonstrated that other substances (creatinine, uric acid, guanidine, indoles, phenolic compounds and organic acids) could be removed more efficiently with uncoated activated charcoal than existing dialysis equipment. |
| 1966 | Chang confirmed the removal of substances described by Yatzidis, but also polyamino acids, and medium molecules, with greater creatinine clearances compared to conventional haemodialysis. |
| 1971 | Chang confirmed the removal of substances described by Yatzidis, but also polyamino acids, and medium molecules, with greater creatinine clearances compared to conventional haemodialysis. |

Tab. 3: Use of activated charcoal in hemoperfusion therapy

Source: ⁵¹

During the '70, after the first observation that coated charcoal hemoperfusion improved the consciousness in a grade IV hepatic coma patient, extensive studies have been carried out in a large number of centres to assess its possible use for the treatment of patients with ALF ⁵². In addition, it has been observed that in galactosamine-induced fulminant hepatic coma rat models, charcoal hemoperfusion increased both survival time and survival rate. Nonetheless, due to the great variability of the disease in terms of survival rate, aetiology, degree of coma and other factors, it is not yet possible to establish with certainty the benefits of ALF treatment with activated charcoal. These results suggest that the use of activated charcoal in ELSS therapy, such as BAL, can be advantageous. Taking cue from previously used charcoal hemoperfusion systems for treatment of ALF patients, some BAL devices are connected to a separate adsorbent column (typically activated charcoal) to remove some toxins in the plasma before it passes through a cell-loaded bioreactor ^{53,54}. In recent years, hybrid BAL devices have been explored that combine the detoxifying capacity of an adsorbent column with the synthetic function of a cell-loaded bioreactor ^{55,56} with positive outcomes in terms of both safety and efficiency.

Ionic (or neutral) resins have also been explored as tool to remove toxins from plasma during ELSS therapy. Blood compatible resins have been used in patients to treat ALF. In a study conducted in 1979, four patients in ALF were treated with hemoperfusion over albumin-coated amberlite XAD-7. The study shows that the resin is capable of removing protein-bound and middle molecular weight substances from the blood of the patients such as bilirubin and phenols. No positive effect on patient survival was observed ⁵⁷. Another example is the anionic exchanger resin present in the system MARS (Baxter GAMBRO), an albumin-dialysis based system used to support patients in liver failure. The resin of this device is in form of microbeads made of cholestyramine, used to regenerate the albumin of the secondary dialysate circuit. In the case of liver failure, this resin is particularly suitable for the removal of molecules such as ammonia, phenols, mercaptans, fatty acids, bile acids, aromatic amino acids, and, in general, of the albumin-bound toxins (such as bilirubin). This resin was also used for the treatment of hypercholesterolemia, pruritus during liver failure, diarrhoea, *Clostridium difficile* infections by absorbing toxins A and B, and reducing the diarrhoea and the other symptoms these toxins cause.

However, the risk in using artificial sorbents such as activated charcoal and ion exchanger resins, is that, in addition to toxins, also substances essential for the normal functioning of the organism (vitamins, ions, hormones ...) can be removed in a non-specific way ⁵⁸

However, artificial liver devices started to evolve and were assessed in clinical trials. The most widely used ALs are summarized in table 4 ^{59,60}.

| System | Principle | Main outcomes |
|---|--|---|
| Molecular adsorbent recycling system (Baxter GAMBRO MARS®) | Filtration of albumin-bound and water-soluble toxins | No improvement in survival. Neurological and haemodynamic improvement ⁶¹ |
| Single-Pass Albumin dialysis (SPAD⁶²) | Albumin dialysis | Similar outcomes of MARS® treatment ⁶¹ |
| Prometheus (Fresenius Medical Care) | Fractionated plasma separation and adsorption system | No improvement in survival. Haemodynamic and biochemical improvements ⁶¹ |

Tab. 4: Most widely used artificial liver supports

What emerges from the literature is that the use of ALs brings to a general improvement of systemic hemodynamic, renal function, and HE⁶³ of patients in ALF. Nonetheless, even if results on clinical trials are encouraging, it is still uncertain if those improvements could be translated into survival benefit.

The second type of ELSS available are the BALs. They were originally developed to treat patients suffering from severe liver failure. Currently, new *in vitro* BAL applications are emerging, including drug toxicity testing, disease modelling and basic clinical research. Those devices contain a cell-housing bioreactor (biological component), the role of which is to replace the most important liver functions, such as detoxification, biotransformation, regulation, excretion and synthesis⁴⁷. The figure 6 summarizes the operating principle of a BAL.

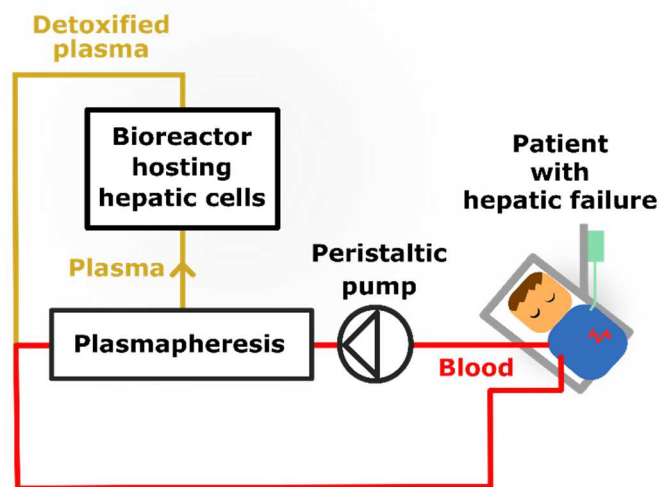


Fig. 6: BAL setup

Together with the biological component, also artificial elements (such as the aforementioned ionic resins or activated charcoals) can be included in those devices, forming systems called hybrid-bioartificial supports. The key elements of well-functioning BALs is the detoxification of harmful toxins involved in ALF, especially ammonia and other neurotoxins that act synergistically in the development of HE together with the metabolic support given by the hepatic biomass, implemented in the extracorporeal circuit. Those aspects, together with the cell sources, the bioreactor designs and the main problematic concerning BALs, will be discussed in the next paragraphs.

The general expectations of a BAL are the following:

- Provide specific liver functions, preserving cell viability and ensuring maintenance of cell metabolic activities
- Possess an adequate cell quantity to support patients in ALF
- Ensure the clinical safety, reproducible functions for a standardized quality, and avoid blood cell damage and coagulation during perfusion

Several BALs have been evaluated in clinical trials for ALF treatment and the most important examples are presented in table 5 (source: Sakiyama et al. 2017⁶⁴). However, the promising role of BALs in supplying patients in ALF still need to be demonstrated: none of the tested designs evidenced significant effects on patients' survival, probably due to limited efficiency of the biological components.

| System | Cell source | Bioreactor design | Clinical phase (year) | Main outcomes |
|---|-----------------------------------|-------------------|-----------------------|---|
| HepatAssist | Cryopreserved porcine hepatocytes | Hollow fibers | III (2004) | No improvement in survival |
| Liver Support System (LSS) | Primary porcine hepatocytes | | I/II (2002) | 8 patients bridged to OLT |
| Modular Extracorporeal Liver Support (MELS) | Primary human hepatocytes | | I (2002) | 6 patients bridged to OLT, 1 survival without OLT, 1 died without OLT |
| Extracorporeal Liver Assist Device (ELAD) | HepG2/C3A | | III (2015) | No difference 90-d overall survival (51.0% vs 49.5%) |
| The Amsterdam Medical Center Bioartificial Liver (AMC-BAL) | Primary porcine hepatocytes | Nonwoven | I (2002) | 11 patients bridged to OLT, 1 survival without OLT |

Tab. 5: Bioartificial liver supports in clinical trials

In both ALs and BALs, plasma separation (conducted via plasma filtration) is preferred to whole blood perfusion in the extracorporeal circulation, in order to reduce problems associated with bio-incompatibility, clot formation, circuit clotting, immunologic reactions between whole blood and the hepatocytes, and potential haemolysis in the blood stream. Plasma circulation is preferred in order to run the circuit at higher rates and increase the efficiency of the therapy⁴⁸ and when hepatocytes are directly perfused without an immune-isolation membrane⁶⁵, because the immune system cells present in the blood could recognize and attack the external biomass. The inconvenient is that plasma has low oxygen-carrying capacity and therefore an oxygenator is needed in the circuit, and that the circuit is more complex, since a plasma separator is necessary.

3.2. Important physiological functions for a BAL

3.2.1. The liver: structure and main functions

The liver is a gland weighing about 1.5 kg, which performs vital functions for the body. An alteration of the liver can disturb the entire organism and lead to the appearance of other diseases. According

to physiologists and clinicians, the human liver possesses more than 500 physiological functions that can be classified in three major classes: biotransformation, storage and synthesis ⁶⁶ (Figure 7).

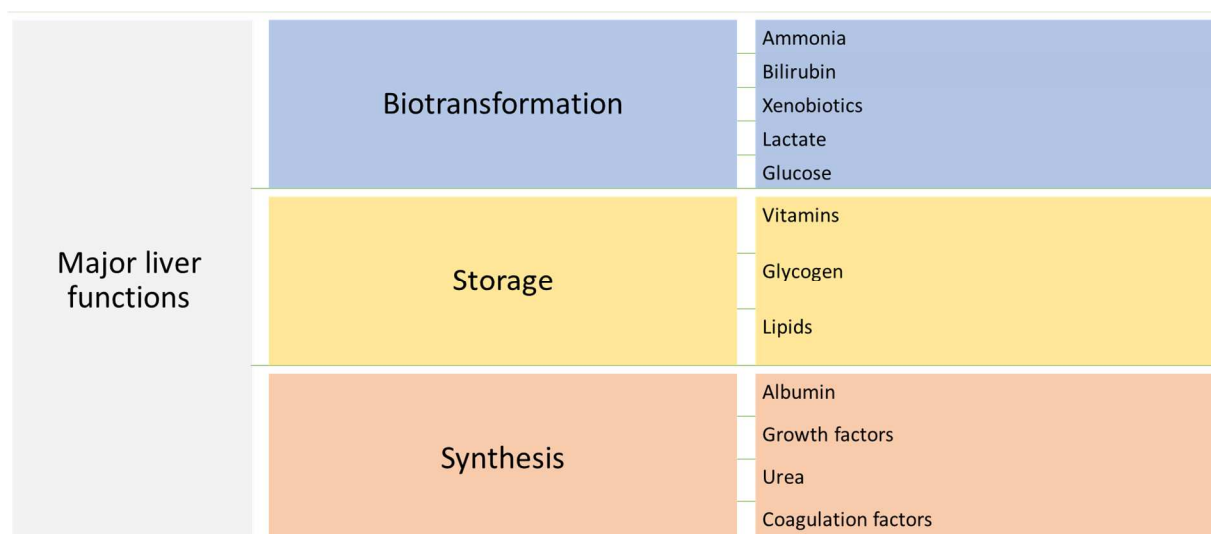


Fig. 7: Major liver functions in the body

Microscopically, liver is organized in hexagonal structures defined as hepatic lobules that contain parenchymal cells (hepatocytes) and non-parenchymal cells such as endothelial cells, biliary epithelial cells, Kupffer cells, and hepatic stellate cells (HSCs). Each lobule comprises a central vein surrounded by six hepatic portal veins at each of its six corners. Each portal vein is combined with a hepatic artery and a hepatic bile duct, forming a structure known as the portal triad (Figure 8). The lobule receives blood from the portal vein, rich in nutrients, and the hepatic artery, rich in oxygen. The sinusoids, with a capillary like structure, extend from the portal vein and arteries to the central vein. Liver sinusoidal endothelial cells (LSECs) form the wall of these sinusoids and create a barrier for the exchange of solutes between blood and space of Disse. The hepatocytes alongside such sinusoidal capillaries show remarkable heterogeneity with respect to the biochemical and physiological functions they perform, a liver feature known as metabolic zonation (Figure 8). This characteristic of the hepatic acinus is highly regulated by specific morphogen signalling pathways such as Wnt/ β -catenin signalling and TGF- ⁶⁷. Moreover, those hepatocytes form the functional unit of the liver, defined as acinus ⁶⁸. Structural and functional heterogeneity along the porto-central axis of the acinus is observed in hepatocytes and is grouped in three zones (1, 2, 3). Zone 1 (periportal area) includes hepatocytes in contact with the portal triad, where there is a high concentration of oxygen and nutrients. Zone 3 (pericentral area) includes hepatocytes near the central vein, which is poor in oxygen and nutrients. Zone 2 (central lobular area) is intermediate between the two. The oxygen and nutrient gradient observed from zone 1 to 3 leads to a different cell metabolism, for example while gluconeogenesis, urea cycle and ammonia detoxification activity occur at the periportal side of the acinus, glycolysis and lipogenesis occur mainly in hepatocytes at the pericentral area⁶⁷. In addition, also LSEC differ depending on their localization in the acinus. In fact, the fenestrae (open pores typical of this cell type) size and number depend on the localization in

the lobule, with a few large fenestrae per sieve plate (cluster of fenestrae) at the periportal region and many small fenestrae per sieve plate at the centrilobular region.

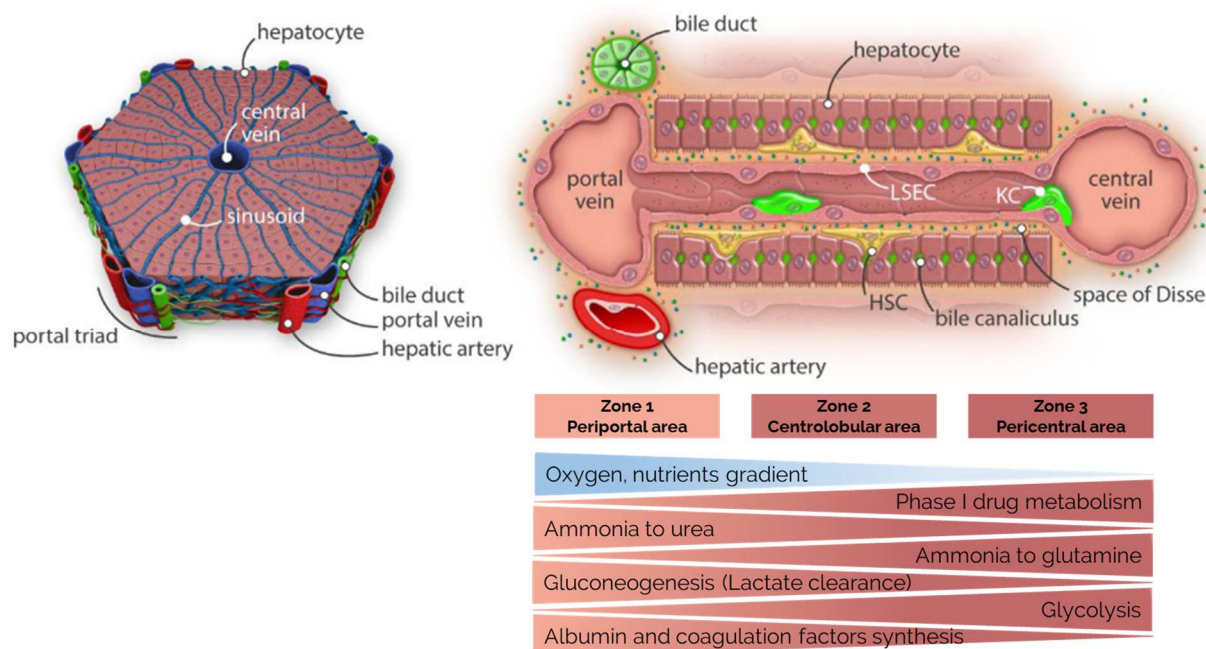


Fig. 8: Organization of the liver lobule. Blood flows from the portal triad, formed by the portal vein, hepatic artery and bile duct, through the sinusoids to the central vein. Bile flows through bile canaliculi in counterflow to the bile ducts. The gradients underneath the acinus represent functional variation across the acinus. HSC: hepatic stellate cell, LSEC: liver sinusoidal endothelial cell, KC: Kupffer cell. Adapted from ref: ⁶⁸ (request permission pending).

The hepatic cellular models used in laboratory try to mimic this structure and this kind of differential metabolism in order to better reproduce the functioning of the liver. However, returning to the main theme of BAL, it is not known which of the metabolic functions mentioned above is the most relevant for the proper functioning of a liver extracorporeal device in the treatment of liver failure. However, some of these functions can be tested *in vitro* in order to characterize hepatocyte cell models for BAL applications. The assumption is that if cells are able to perform those known functions (summarized in figure 7), they might express those that are unknown (but central in liver metabolism) ⁶⁹.

The necessary functions for clinical BALs have been recently proposed by van Wenum et al. 2014 ⁷⁰ and include: ammonia and lactate detoxification, protein synthesis, carbohydrate and lipid metabolism, xenobiotic detoxification, immunomodulation. We added other activities that, in our opinion, should be considered in BAL context.

3.2.2. Ammonia detoxification

Liver, together with other organs, is involved in the homeostasis of ammonia in the human body. The biotransformation of ammonia occurs in the hepatocytes of the periportal zone. In liver failure, ammonium homeostasis is profoundly altered resulting in hyperammonemia due to the deficient ammonium clearance by the diseased liver. Hyperammonemia consists in an imbalance between the ammonium produced and the body capacity to metabolize and remove it. There are cues that hyperammonemia is implicated in the development of HE. The concentration of ammonium in

normal human plasma ranges between 11 and 50 $\mu\text{mol/L}$ while in hyperammonemia the level of ammonia is 4 to 150 times the normal concentration. Free ammonium ions are continually produced and consumed during cell metabolism in human body tissues. They arise during the breakdown of purine and pyrimidine derivatives, polyamines, and deamination of several amino acids, including glutamine, asparagine, serine, threonine, glycine, histidine, lysine, proline, hydroxyproline, homocysteine, and cystathionine ⁷¹. Physiologically, the ammonia elimination occurs via the urea cycle or via fixation into amino acids, most notably glutamine ⁷². In the first case, ammonia is irreversibly converted in urea by hepatocytes. Then, it travels through the blood stream to the kidney and is excreted in the urine. In the second case, ammonia is fixed in glutamine, considered to be a temporary and reversible ammonia sink, since the glutaminase expressed in various cell types generates glutamate and ammonia from glutamine ($\text{glutamine} + \text{H}_2\text{O} \rightarrow \text{glutamate} + \text{NH}_3$). Moreover, glutamine in high blood concentrations compromises astrocyte functions, contributing to the progression of HE ⁷³. Consequently, a clinical BAL must eliminate ammonia at the same extent as *in vivo* PHHs, preferably via the urea cycle.

3.2.3. Lactate clearance

Lactate is the conjugate base of lactic acid produced by the activity of lactate dehydrogenase (LDH) during glucose metabolism, mainly in muscle tissue. In aerobic conditions, pyruvate coming from glycolysis enters the Krebs cycle, bypassing the production of lactate. In anaerobic conditions, pyruvate is transformed in lactate that enters the Cori cycle as substrate for gluconeogenesis. Elevated lactate is not clearly and universally defined but most studies use cut-offs between 2.0 and 2.5 mmol/L whereas "high" lactate has been defined as a lactate level $> 4 \text{ mmol/L}$ ⁷⁴. The lactate clearance via gluconeogenesis occur in periportal hepatocytes. In a general clinical picture, lactate is used by clinicians as a marker of the severity of a critically ill patient (patient in shock, i.e. with compromised oxygenation delivery). In fact, increasing in plasmatic lactate levels is a sign of unbalanced oxygen supply to organs. As consequence, the lack of adequate oxygenation leads to lactate production as source of energy. In particular, during liver failure, it can be observed increased lactate levels due to a synergic effect of increased lactate production and decreased clearance (physiologically carried out by hepatocytes), since the organ functionality is compromised. Lactate can cross the blood-brain barrier and, in high level, it correlates with high intracranial pressure (ICP), phenomenon that damages the brain ⁷⁵. However, it has to be noticed that lactate is a source of energy for the brain in physiological and pathological conditions. For this reason, a clinical BAL should favour lactate clearance at the same extend that PHHs.

3.2.1. Bilirubin metabolism

Bilirubin is a product of the metabolism of heme, a molecular complex that coordinate iron in various proteins, present in hemoglobin, myoglobin, cytochromes, catalase, peroxidase, and tryptophan pyrrolase. About the 80% of bilirubin derives from the metabolism of hemoglobin of senescent red blood cells and premature destroyed erythroid cells. Bilirubin is very poorly soluble in water at physiologic pH. Water-insoluble unconjugated bilirubin (also called indirect bilirubin) is

associated with all known toxic effects of bilirubin ⁷⁶. However, the body has developed mechanisms for its safe detoxification. Once bilirubin is released into the plasma, it is taken up by albumin, which serves as its transporter throughout the body. Then the albumin-bilirubin complex reaches the liver, where the highly permeable hepatic circulation allows the complex to reach the sinusoidal surface of the hepatocytes. This allows the pigment to disassociate from the albumin and enter the hepatocytes. Here, bilirubin is conjugated with glucuronic acid, by UDP-glucuronyl transferase enzymes. This kind of metabolism is more active in the pericentral area of the sinusoid. Bilirubin glucuronides (also called direct bilirubin) are water-soluble and are readily excreted in bile, passing across the bile canalicular membrane of hepatocytes (Figure 9).

The physiological levels of total bilirubin is < 20 mM, with < 18 mM for unconjugated and < 4 mM for conjugated bilirubin. Jaundice, a typical trait of ALF, is visible when total bilirubin is > to 40 mM. It has been described that hyperbilirubinemia (> 20 mM) has severe consequences on the body, since unconjugated bilirubin crosses the blood-brain barrier causing bilirubin-induced neurologic dysfunction⁷⁷. In addition, it has been observed that conjugated bilirubin accumulation can cause severe kidney injury described as the bile cast nephropathy ⁷⁸.

In ALF context, total bilirubin (indirect + direct bilirubin) increases due to liver dysfunction, leading to jaundice, pruritus and potentially neuro- and renal-toxicity. For BAL application, a decrease in total bilirubin levels to physiological levels would be appropriate. This can be achieved either through the biomass performance or through the incorporation of artificial elements (activated charcoal and ionic resins) specialized in the removal of these toxins into the BAL device.

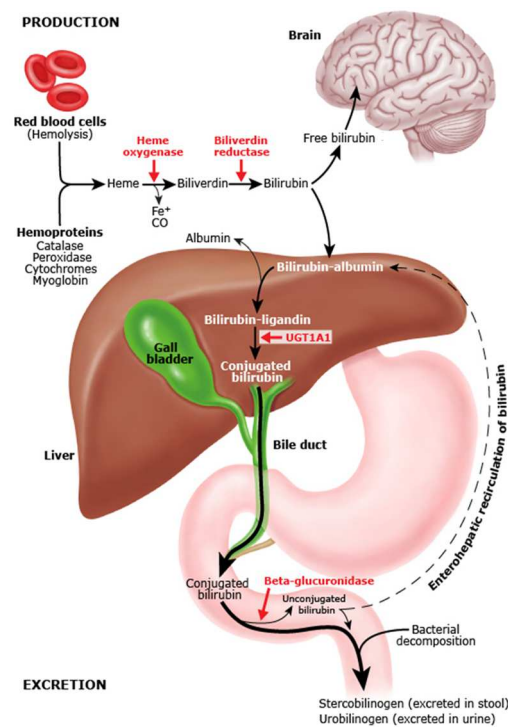


Fig. 9: Scheme of production, metabolism, and excretion of bilirubin
Source (request permission pending): ⁷⁹

3.2.2. Bile acids metabolism

Bile acids are steroid acids found predominantly in the bile, synthesized in the liver by the hepatocytes. Those molecules accumulate in the body during ALF and are known to be toxic for hepatocytes, bile duct epithelium and other organs. Moreover, those compounds can inhibit DNA synthesis and liver regeneration⁸⁰. It has been observed that certain types of bile acids, at concentration similar to those observed in ACLF, induce necrosis in cultured hepatocytes¹⁰. Thus, in patients with liver failure, the serum bile acid levels could further aggravate the disease, leading to damages observed in cholestasis. Consequently, the reduction of bile salts in blood after BAL therapy can lead to the clinical improvement of the patient in ALF.

3.2.3. Protein synthesis

The liver is implicated in the production of vital proteins such as plasma proteins including albumin, fibrinogen, complement proteins, coagulation factors, carrier proteins, hormones and apolipoproteins. One of the most studied proteins in the context of BAL is albumin, the main protein of human blood plasma, with serum concentration of 3.5–5.0 g/dL. It is expressed in the periportal area of the acinus. Its main function is the regulation of the oncotic pressure of blood and it is a transporter of endogenous (such as bilirubin, ions, fatty acids) and exogenous (i.e. drugs) ligands. However, albumin (or other proteins such as apolipoprotein A1 (Apo-A1)) can be administered exogenously in intensive care unit, thus protein synthesis is rather considered as a “quality parameter” for clinical BAL.

3.2.3.1. Coagulation factors

Coagulopathy is one of the major complications in ALF, since the liver is implicated in the production of specific coagulation factors, such as I, II, V, VII, IX, and X. It is reported that those factors are mainly expressed by the hepatocytes of the periportal zone⁸¹. The coagulation factor V is particularly important in the evaluation of the degree of ALF because it is the only one that is not influenced by the administration of drugs such as anti-vitamin K, when other conditions are concomitant. For example, a patient suffering of atrial fibrillation is normally treated with anti-vitamin K. If the same patient develops an ALF, his International Normalised Ratio (INR), that is measured on the activity of all those coagulation factors cited, will be influenced and over-estimated by his drug treatment. This is why it would be advantageous to evaluate the level of the coagulation factor V as diagnosis marker of ALF. However, for clinical BAL, the production of the coagulation factors by the hepatic external biomass is desirable. It would be pertinent to dose the level of coagulation factor V for its hepatic specificity and to omit the influence of anticoagulants used for the preparation of the extracorporeal device.

3.2.4. Carbohydrate and lipid metabolism

Among carbohydrate, only lactate elimination has been described as an important indicator for BAL. Concerning lipid metabolism, one of the most considered markers for BAL are the high density lipoproteins (HDL). Those lipoproteins are mainly implicated in the transport of cholesterol and play

a role in the modulation of infection process. High density lipoprotein levels are low in patients with liver failure and reflect its severity⁸². However, it is unclear if carbohydrate and lipid metabolism (other than lactate elimination) is a specific target for clinical BAL.

3.2.5. Xenobiotic metabolism

The term xenobiotic metabolism describes the set of metabolic pathways that modify the chemical structure of xenobiotics, which are compounds foreign to an organism's normal biochemistry (such as drugs). Those same pathways are implicated in the metabolism of toxins accumulating in ALF such as unconjugated bilirubin and endogenous benzodiazepines⁸³. Drug metabolism often converts lipophilic compounds into hydrophilic products that are more readily excreted. The metabolism of xenobiotic is predominantly associated to the periportal zone. The xenobiotic pathway is divided in four phases (Figure 10):

- **Phase 0 (Uptake):** water soluble or charged drugs need specific transporters to overcome the cell membrane and enter into the cells. Those drug transporters belong to two families: the solute carrier (SLC) families and the ATP binding cassette (ABC) carriers.
- **Phase I (Modification):** different enzymes introduce reactive and polar groups into the substrate. Those reactions may occur via oxidation, reduction, hydrolysis, cyclization, decyclization, and addition of oxygen or removal of hydrogen. A common example is the reaction mediated by the cytochrome P-450 that incorporates an atom of oxygen into the aliphatic position of an organic substrate (RH) while the other oxygen atom is reduced to water ($RH + O_2 + NADPH + H^+ \rightarrow ROH + H_2O + NADP^+$).
- **Phase II (Conjugation):** the activated metabolites from phase I are conjugated with charged species such as glutathione (GSH), sulfate, glycine, or glucuronic acid. Two important classes of this group are that of the glutathione S-transferases (GSTs) that catalyze the introduction of glutathione to the substrate, and the UDP-glucuronosyltransferases (UGT) that catalyzes the conjugation of glucuronic acid.
- **Phase III (Export):** operated by transporters of the class ABC carriers, such as multidrug resistance-associated protein 2 (MRP2) and others.

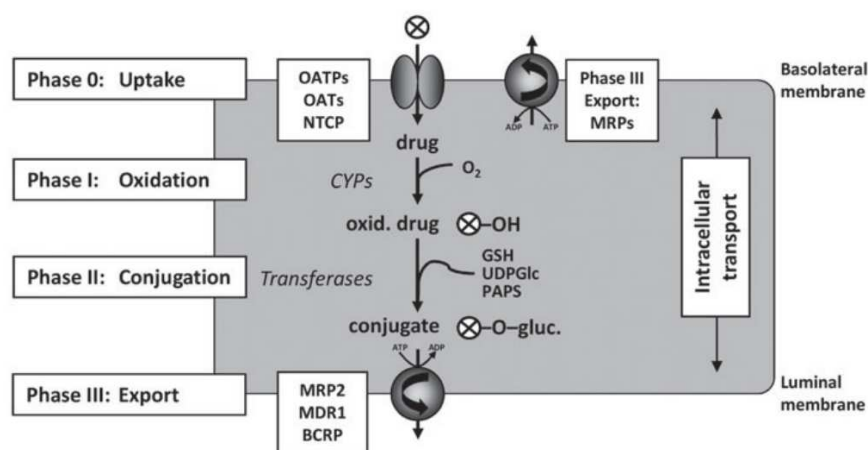


Fig. 10: Sequential steps of drug elimination by metabolism and membrane transport in hepatocyte⁸⁴

It has been observed that in rodents, accumulation of endogenous neurotoxins normally eliminated by the liver, contribute to the development of HE during ALF ⁸⁵. The effect of the accumulation of those toxins in human is still unclear. However, since there is evidence that those toxins can contribute to the progression of ALF, the xenobiotic metabolism is required for clinical BAL.

3.2.6. Immunomodulation

It has been reported that BAL therapy in rats can favour liver regeneration probably due to the decrease in the expression of transforming growth factor- (TGF-) plasma levels, a potent inhibitor of hepatocytes proliferation) ⁸⁶. It means that BAL treatment can influence the level of cytokines that control the process of inflammation and liver regeneration and the process of SIRS that characterizes the pathophysiology of acute liver failure. Immunomodulation in liver remains not clear but it can represent a benefit for clinical BAL, through attenuation of SIRS and stimulation of liver regeneration.

3.3. Challenges concerning BALs

The most relevant challenges about BALs concern the cell source and the quantity of bioactive mass (quantity of hepatic cells or liver tissue) in the bioreactor, as this element has the potential to cure the patient.

3.3.1. Cell quantity/biomass

Based on studies of liver regeneration after partial hepatectomy, it is assumed that between 15 and 20×10^9 functional hepatocytes (corresponding to 150-200g, about the 20% of liver mass), working at same extent of *in vivo* primary hepatocytes, are needed to keep an ALF human patient alive until transplantation ^{87,88} but this assumption is not yet confirmed. It means that, when using a different cell source (i.e. primary porcine hepatocytes, hepatoma cell line etc.), the equivalent of the activity of 15 - 20×10^9 functional hepatocytes is needed for a successful therapy. In order to reach this goal, two strategies can be adopted:

- Increase the number of cells in the BAL ($>10^9$ - 10^{11} and not less)
- Improve the cellular activity (spheroids/hepatospheres culture, tissue engineering approach, co-culture and so on, rather than 2D cultures)

Very often, reference is made to a minimum number of cells necessary to ensure BAL therapy, assuming that 20% of the liver mass is needed to elicit *in vivo* liver regeneration. In this regard, it would be more correct to take into account the functionality of the biomass used for therapy. Starting from the functionality of the latter, it would be appropriate to express an equivalence with the minimal biomass assumed for therapy (i.e. that 20% mentioned), in terms of number of cells. Therefore, the right question to consider is: given the hepatic function registered in *in vitro* experiments (among those required for a BAL listed above), what amount of biomass is needed to correspond to 20 % of an *in vivo* liver mass?

By answering this question, we would obtain a more correct order of the biomass needed (presumably different for each cell model used) for a successful BAL therapy.

3.3.2. Cell sources

Generally, the cell sources used for BAL applications are the following: primary cells, either human or of xenogeneic derivation, cell lines (hepatoma cell lines or immortalized cell lines) or developing expandable progenitor cell populations ⁸⁹. An overview of the available cell model for *in vitro* liver cell culture (and BAL application) is presented in figure 11 ⁹⁰. Each of those cell sources, presents advantages and disadvantages, summarized in table 6 (rearranged from the review of Zeilinger et al 2016 ⁹⁰)

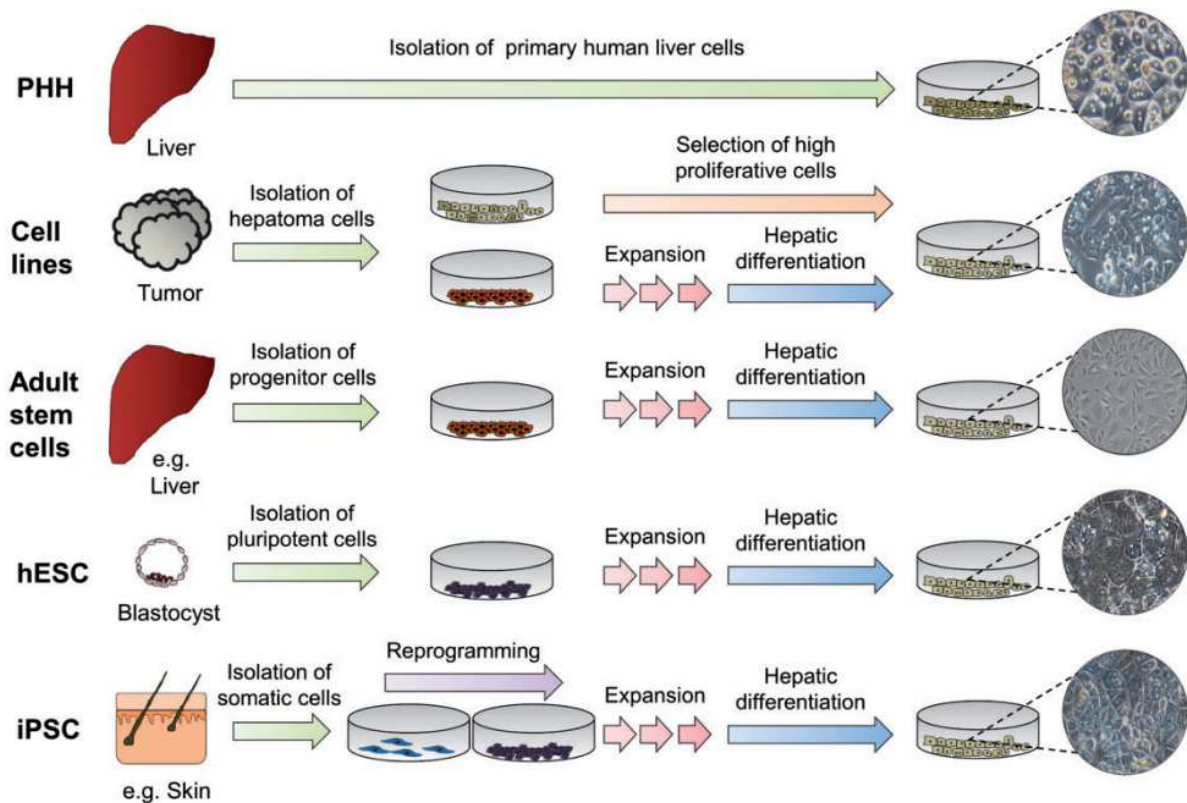


Fig. 11: Processing of cells derived from different sources for the generation of human *in vitro* liver cell culture models. Major cell types include primary human hepatocytes (PHH), hepatoma cell lines, adult stem cells, human embryonic stem cells (hESC), and induced pluripotent stem cells (iPSC). Whereas PHH can be used for *in vitro* cultivation immediately after isolation, liver cell lines or stem cells need to be expanded and/or differentiated prior to their use in experiments. Source: Zeilinger et al. 2016 ⁹⁰.

| Cell type | Pros | Cons |
|---|---|---|
| Primary human hepatocytes | <ul style="list-style-type: none"> • High functionality • Reflect human metabolism | <ul style="list-style-type: none"> • Limited availability • Inter-donor variability • Rapid de-differentiation <i>in vitro</i> • No proliferation <i>in vitro</i> |
| Primary porcine hepatocytes | <ul style="list-style-type: none"> • High functionality • Close to human physiology • Availability | <ul style="list-style-type: none"> • Possible immune responses • Possible zoonotic diseases • Inter-donor variability • Rapid de-differentiation <i>in vitro</i> • No proliferation <i>in vitro</i> |
| Hepatoma cell lines (e.g. HepG2, HepaRG) | <ul style="list-style-type: none"> • High proliferation activity • Good availability • Stable metabolic performance | <ul style="list-style-type: none"> • Alteration in liver specific functions (e.g. reduced activity of drug metabolizing enzymes) • Tumorigenicity (not for HepaRG⁹¹) |
| Adult stem cells (e.g. liver progenitor cells, mesenchymal stem cells) | <ul style="list-style-type: none"> • Option for patient specific derivation • Committed to hepatic lineage (liver progenitor cells) • Good availability (from bone marrow, placenta, umbilical cord) and unlimited growth (mesenchymal stem cells) | <ul style="list-style-type: none"> • Limited proliferation capacity • Scarce tissue availability (liver progenitor cells) • Low frequency in tissue (liver progenitor cells) • Incomplete hepatic differentiation with current protocols (mesenchymal stem cells) |
| Pluripotent stem cells (e.g. hESC, hiPSC) | <ul style="list-style-type: none"> • Unlimited growth • Differentiation not affected by epigenetic memory (hESC) • Good availability and no ethical restrictions (hiPSC) | <ul style="list-style-type: none"> • Fetal phenotype of differentiated cells with current protocols • Lack of standardized methods for cell differentiation and characterization • Ethical consideration restrict research on hESC • Epigenetic memory may impair hepatic differentiation (hiPSC) |

Tab. 6: Cell sources used in BALs: pros and cons

3.3.2.1. Primary cells

Among primary cells used for BAL applications, it is possible to distinguish human hepatocytes (PHH) and porcine hepatocytes (PPH). PHH represent the ideal source of cells for BALs. However, their limited availability (the high demand for donor organs makes it unlikely that sufficient excess tissues would be available for non-transplantation application), the phenotypic instability ⁷⁰, the inter-donor variability, as well as logistical issues, hampers their use in BALs. Consequently, chances of a BALs based on PHH eventually reaching the clinic are negligible ⁹². However, PHH have been used in BALs and there is a Phase I study describing their safe use in ALF patients ⁹³.

Subsequently, most of the BALs in clinical or preclinical studies had relied in the past on PPH, due to their easy availability and high functional activities ⁹⁴⁻⁹⁶. However, transfer of zoonotic diseases (for example due to porcine endogenous retroviruses -PERVs- transmission) ⁹⁷, protein-protein incompatibility between species and possible immune responses generated during treatment remain challenges for the use of xenogeneic hepatocytes ⁹⁸. However, xenotransplantation legislation in many European countries prohibits the use of porcine hepatocytes in clinically applied BAL systems ⁹⁹.

3.3.2.2. Cell lines – Focus on HepaRG cell line

The main advantages of hepatocyte cell lines are their almost unlimited proliferative capacity, the relatively cheap culture process, and the reproducibility in metabolic performance between

different batches (the latter is one of the main problematics in using primary human hepatocytes). On the other side, they must demonstrate metabolic functionalities comparable to that of human hepatocytes and also to be safe and non-tumorigenic ⁸⁸. The cell lines today available or under characterization have been largely reviewed ^{64,69,70,92} are reported in annex 3 (source: M. van Wenum et al. 2014 ⁷⁰). Overall, so far, no proliferative human cell source show metabolic performances at the same extent as PHH.

Among several established cell lines, HepaRG cells have emerged as the most appropriate surrogate to PHH ¹⁰⁰. The HepaRG cell line was established from tumour of a female patient suffering from chronic hepatitis C infection and hepatocarcinoma ¹⁰¹. A whole genome expression profile analysis revealed that HepaRG cells transcribe genes at levels more similar to PHH and human liver tissue than other liver cell lines ¹⁰². Importantly, the profiles of drug processing genes in HepaRG cells and PHH were found to be similar. More detailed examination of the expression of 115 genes involved in xenobiotic metabolism and disposition demonstrated similar levels in HepaRG cells and PHH with a few exceptions (e.g. cytochrome P450 (CYP)1A2, CYP2A6 and CYP2D6 had a significantly lower level of expression in HepaRG cells than in primary human hepatocytes ^{103,104}).

HepaRG cells display a great plasticity and are bi-potent progenitor cells. During the earlier stage of cell culture, they exhibit an epithelial phenotype. Along the culture period, they engage a differentiation program that involves their specialization towards either biliary (cholangiocyte-like) or hepatocyte-like lineages and resulting in differential expression patterns of many liver-specific genes. In addition, differentiated HepaRG cells are capable of dedifferentiation after enzymatic detachment followed by low-density seeding ¹⁰⁵ (Figure 12).

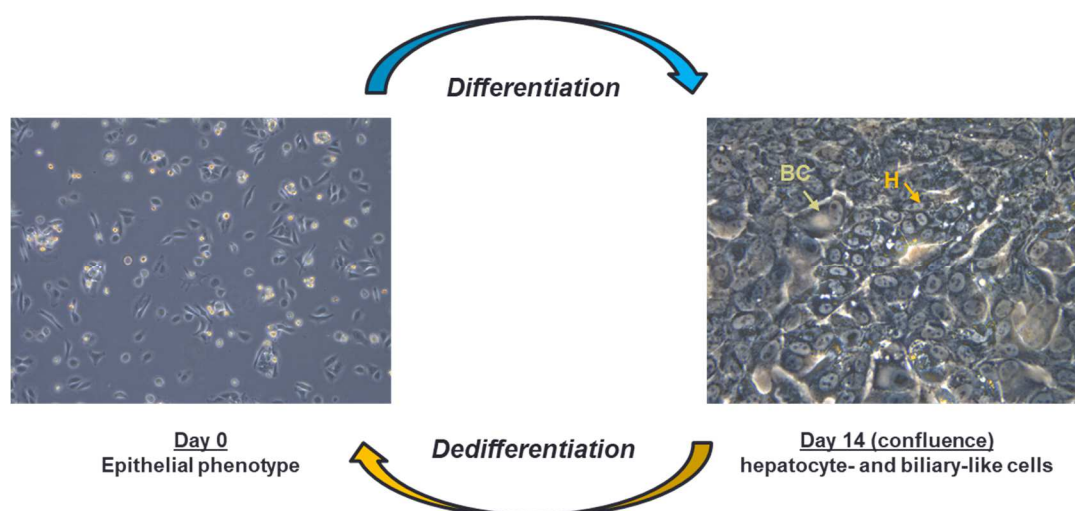


Fig. 12: HepaRG differentiation and dedifferentiation
H indicates hepatocytes, BC indicates biliary cells

If cells are detached and re-seeded at high density, they maintain the hepatocyte-like phenotype. When HepaRG are seeded at low density, they proliferate until reaching confluence on day 10. After that, cells start to differentiate towards the two cell types, with a maximum peak on day 14 post-seeding. Cell differentiation can be maximized adding dimethyl sulfoxide (DMSO), a modulator of chromatin structure, for 2 weeks more. In this condition, hepatocyte-like cells represents about 50%

of the cell population, presenting a phenotype similar to PHH (expression of hepatic nuclear factor 4 (HNF4) or bile canaliculus-like structures)^{100,104}. The removal of DMSO from culture media results in significant reduction in the levels of expression of the CYP enzymes (especially CYP3A4), although their expression remains stable at a lower level in differentiated HepaRG cell cultures for up to 2 weeks¹⁰⁰.

On the other side, it has been observed that DMSO treatment promotes cell death¹⁰⁶. Therefore, the decision of adding (or not) DMSO to complete the cell differentiation program is a choice that should depend on the final application. If HepaRG are intended to toxicology studies, where the enzymes of the xenobiotic pathways (involved in detoxification processes) are needed, then the choice to add DMSO is justified. In a context of BAL application, where an important cell mass is needed, and where it is not clear which is the key function that hepatocytes should possess, then it can be preferred to work without DMSO and not affect cell viability.

HepaRG have been tested in three-dimensional (3D) configuration (spheroids or BAL models) for both toxicology applications and ALF-treatment. Overall, what emerges is that the 3D models better recapitulate liver physiology and show improved metabolic performance *in vitro* when compared to two-dimensional (2D) culture models. The following table (Table 7) recapitulates some recent published results of metabolic performance of HepaRG in 2D and 3D configuration. The metabolic activities presented are the most important for BAL applications (as explained at §3.2 of the present chapter).

| Author | Culture condition | Albumin prod. (µg/h/10 ⁶) | Urea prod. (µg/h/10 ⁶) | Ammonia detox (nmol/h/10 ⁶) | Lactate detox (nmol/h/10 ⁶) | CYP 1A2 (pmol/h/10 ⁶) | CYP 3A4 (pmol/h/10 ⁶) |
|---|--|---------------------------------------|------------------------------------|---|---|-----------------------------------|-----------------------------------|
| Lübberstedt et al., 2011 ¹⁰¹ | 2D | 0.2 | - | - | - | 180 | 10.5 |
| Nibourg et al., 2013 ¹⁰² | AMC-BAL - DMSO | - | - | 27 | 10 | - | - |
| Leite et al., 2012 ¹⁰³ | Spheroid culture in spinner flask + DMSO | 0.48 | - | - | - | - | - |
| Gunnness et al., 2013 ¹⁰⁴ | 2D (collagen coated culture plate) | 0.33 | 0.06 | - | - | - | - |
| | Spheroid culture | 1 | 1.8 | - | - | - | - |
| Rebello et al., 2015 ¹⁰⁵ | 2D-DMSO | 0.125 | 1.25 | - | - | 2 × 10 ⁶ | 3 × 10 ⁶ |
| | 2D+DMSO | 0.125 | 2 | - | - | 3 × 10 ⁶ | 10 × 10 ⁶ |
| | Spheroids. encaps in alg. beads 1% | 0.33 | 3 | - | - | 3.5 × 10 ⁶ | 13 × 10 ⁶ |

Tab. 7: Published results on HepaRG metabolic performance

One of the most relevant works about the use of HepaRG cell line in BAL for pre-clinical test, has been realized by the group of Prof. Chamuleau with AMC-BAL¹⁰⁶. Firstly, the authors proved that HepaRG cell line is suitable for BAL application for its proliferation capacity and its high metabolic and synthetic properties in the absence of DMSO¹⁰⁷. Then, they characterized the *in vitro* hepatic functionality of HepaRG differentiated in their bioreactor, testing also its effectiveness (HepaRG-AMC-BAL) in a rat model of ALF. They observed that the HepaRG-AMC-BAL displayed a broad and a high level of hepatic functionalities *in vitro* (elimination of ammonia, production of urea, production of 6 -hydroxytestosterone, consumption of lactate, and synthesis of apolipoprotein A-1). In addition, they demonstrated that the HepaRG-AMC-BAL increased survival time of acute liver failure rats about 50% compared to acellular-BAL treatment¹⁰⁶.

While the presence of hepatocytes is clearly necessary for BAL, the one of cholangiocytes (the other cell type of HepaRG differentiation) has to be better investigated. Physiologically, cholangiocytes are the epithelial cells of the bile duct and their main function is the modification of hepatocyte-derived bile (primary bile), an intricate process regulated by hormones, peptides and other molecules. The following figures (Figure 13), by Tabibian et al. 2013¹⁰⁸, gives an overview of bile formation and modification that allows a simple comprehension of cholangiocytes function.

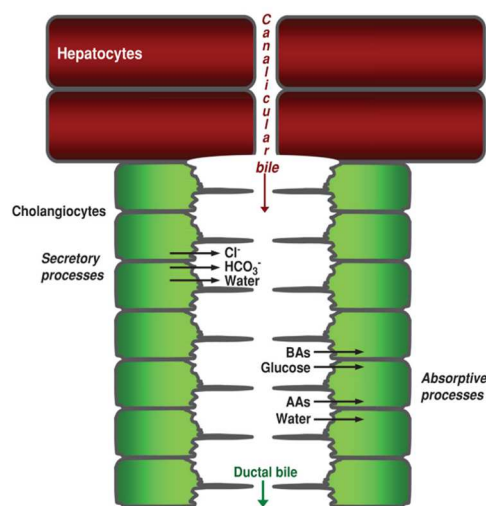


Fig. 13: Portal triad anatomy (left) and bile formation process (right). Hepatocytes initiate bile formation by secreting primary bile, composed primarily of water, solutes, and ions, into canaliculi. As canalicular bile flows along the biliary tree, it is subjected to cholangiocyte secretory and absorptive processes, thus resulting in modified ductal bile. Secretion of Cl^- , HCO_3^- , and water and absorption of bile acids (BAs), glucose, amino acids (AAs), and water are the major transport processes determining the chemical composition of ductal bile. Source: ¹⁰⁸ (request permission pending).

The secreted bile moves via the biliary tree and then is stored and concentrated into the gallbladder, before being released into the small intestine during the process of digestion. Bile is an aqueous solution that contains a variety of solutes (electrolytes, bile acids, bilirubin, lipids, proteins, peptides, vitamins etc.). It has been observed that HepaRG cell line has the capacity to secrete certain solutes of bile such as bile acids^{109,110}. In the context of fundamental biology, toxicology, and in the study of certain diseases, this characteristic is advantageous in order to recapitulate most of liver functions. In contrast, in the context of BAL applications, the components of the bile secreted by cells, is injected to the patient' systemic circulation and it could lead to

adverse effects. It remains an open question whether the presence of these molecules produced by the biomass may have undesirable effects on the patient undergoing BAL therapy.

3.3.2.3. Embryonic stem cells (ESCs)

Human embryonic stem cells (hESCs) are pluripotent cells which give rise to all somatic cell types in the embryo. These characteristics also make them tumorigenic, and therefore, hinder their clinical application. To date, hundreds of hESC lines are generated from donated embryos produced by *in vitro* fertilization (IVF). Isolation of the embryoblast (also known as the inner cell mass) from the trophectoderm at the blastocyst stage is achieved by immunosurgery or mechanical dissection ¹¹¹ (Figure 14).

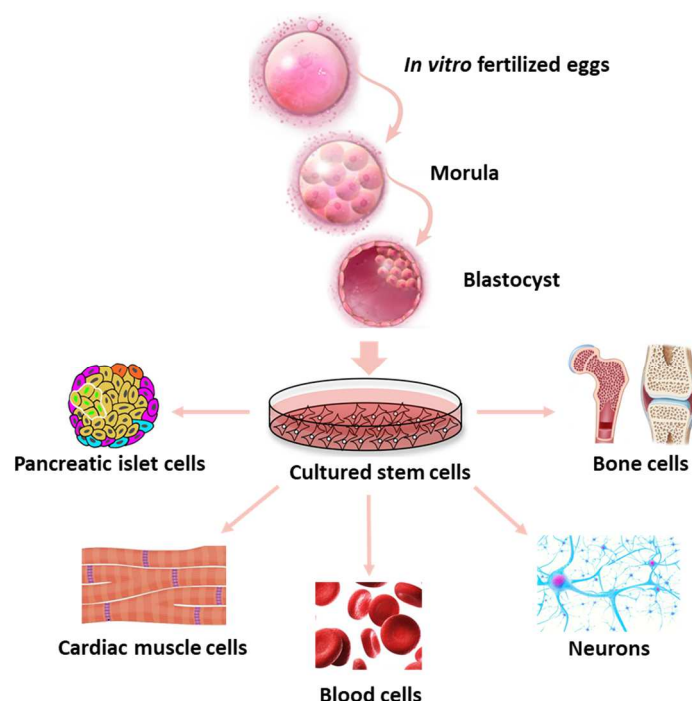


Fig. 14: Derivation, cultivation and differentiation of hESCs

Even if there are not standardized protocols for differentiating hESCs in hepatocytes like cells, most of the known procedures are based on a 3-step strategies, which mimics ontogenic liver development. The first step uses as inducers activin A, FGF2, WNT3A, BMP4 and LY294002 to generate definitive endoderm cells. The second step is hepatic specification to produce hepatoblast cells (using FGF2, FGF4, BMP). The last step tries to induce differentiation into hepatocytes using HGF, oncostatin M, dexamethasone and follistatin. New approaches of differentiation are based on the use of small molecules or miRNAs. Nonetheless, to date, hepatocyte-like cells obtained from hESCs are not sufficiently differentiated and are closer to a fetal phenotype ¹¹².

Overall, what emerges is that there are common limitations (such as high costs) and risks that hamper their use in clinical applications. They are the following: lack of standardized protocols, for obtaining scalable amounts of differentiated cells, poor understanding of differentiation process,

functional stability over time and safety not proven¹¹³. hESCs cannot be used in context of transplantation into humans, since formation of teratoma and teratocarcinoma has been observed¹¹⁴. While the use of hESCs-derived hepatocytes for certain clinical applications (such as hepatocytes transplantation) is not yet possible due to the risk of tumorigenicity, their application is suitable for BALs. In fact, in these devices, the risk of tumorigenicity is minimized since the cells are physically isolated from the patients' circulation by filter membranes⁶⁴.

To our knowledge, there are very few studies about BAL based on ESCs. In one study, mouse ESCs (mESCs) were used in ALF-model rats. Overall, the authors showed that, even if cells were not fully differentiated in hepatocyte-like cells, their bioreactor containing mESCs-derived hepatocytes had a good potential to support liver function¹¹⁵. In another study, the authors used mESCs in a hollow-fibre based BAL. After an *in vitro* characterization of cells, ALF-induced Wistar rats were connected to the BAL containing mESCs. After one hour of extracorporeal circulation, two rats out of three connected to the BAL containing cells survived and recovered after the operation. The control rats connected to BAL without cells, died 10 hours after the operation¹¹⁶.

So far, no studies of hESCs in BAL devices for the treatment of ALF in animal models have been realized

3.3.2.4. Induced pluripotent stem cells (iPSCs)

Recent advancements in stem cells research, demonstrated that hepatocyte-like cells can be obtained from patients' own cells by introducing specific transcription factors (Figure 15). Those cells are called induced pluripotent stem cells (iPSCs). Their unique ability to self-renew (capacity to proliferate indefinitely while maintaining their cellular identity) and to differentiate into cells of the three germ layers makes them an invaluable tool for the future of regenerative medicine.

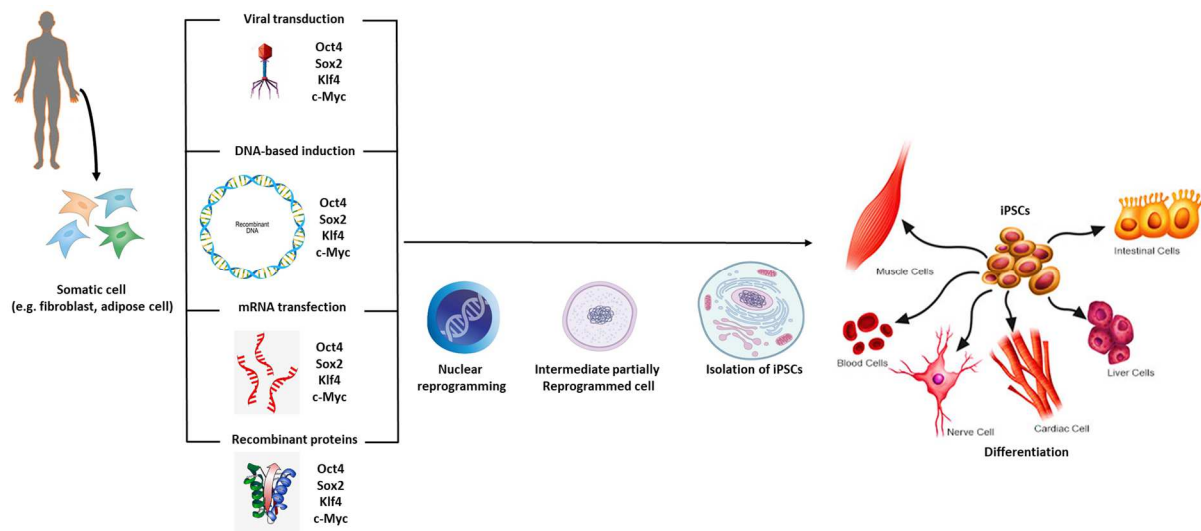


Fig. 15: Derivation and differentiation of iPSCs

However, the same properties also make them tumorigenic (due to genetic and epigenetic aberrations), and therefore hinder their clinical application¹¹⁴. Recent works have demonstrated that iPSCs-derived hepatocytes are able to express typical hepatocytes markers (genes and proteins)

and functions, such as albumin secretion, urea synthesis, glycogen storage and CYP450 activity^{117,118}. Nonetheless, despite the huge efforts in order to obtain protocols for hepatocytes differentiation from iPSCs, the resulting functions of the iPSCs-derived hepatocytes remain relatively immature, being more comparable to fetal/neonates than to adult hepatocytes¹¹⁹. The review article by Hannoun et al. 2016¹¹⁹ discusses the potential applications and existing limitations of human iPSC-derived hepatocytes in regenerative medicine, drug screening, *in vitro* disease modelling and bioartificial livers. It focuses also on relevant protocols used for obtaining human iPSC-derived hepatocytes.

Like for hESCs, the use of iPSC-derived hepatocytes for certain clinical applications (such as hepatocytes transplantation) is not yet possible due to the risk of tumorigenicity, but they can be suitable for BALs.

To our knowledge, there is only few studies about iPSC-derived hepatocytes on BAL. Ren et al. 2016¹²⁰, seeded human iPSC-derived hepatocytes in a hollow fibre system and characterized their *in vitro* functionality. Shi et al.¹²¹ used human functional hepatocytes (hiHep) derived from human fetal fibroblasts in a BAL in D-galactosamine ALF-induced pigs. The hiHep-based BAL treatment could attenuate liver damage, resolve inflammation, enhance liver regeneration and prolong survival; however, it is cumbersome and time-consuming to prepare adequate and high-quality cells for emergent patient demands.


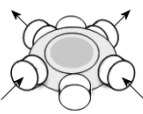

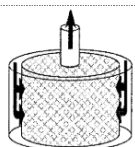

3.4. Bioreactors for BAL: principle and designs

3.4.1. General considerations

Bioreactor is defined as a volume (or vessel) in which one or more biochemical or biological processes take place¹²². This term is used to define culture systems such as static supports (Petri dishes, T-flasks, and culture well plates for 2D culture) and dynamic supports (spinner flasks, rotating wall bioreactors, perfusion bioreactors, hollow fibre bioreactors, fluidized bed bioreactors). For hepatic cell culture, the goal is to create, into the bioreactor, an environment that supports cell viability and that favours metabolic functions typical of the liver. The main expectations of a bioreactor used for culturing hepatic cells in BAL context has important expectations:

- Host a large number of cells
- Provide cells with adequate amounts of oxygen and nutrients to survive and proliferate
- Favour mass transfer between cells and blood/plasma of the patient in ALF
- Protect the cells from the immunological system of the patient in ALF
- Be easily scaled-up to therapeutic levels
- Allow cryopreservation of the biomass (in order to have cells ready to use for clinical application)

The table 8 summarizes the bioreactor designs that have already been proposed in the literature, with their advantages and disadvantages (rearranged from the review articles proposed by Allen et al. 2001 ⁶⁹ and Sakiyama 2017 ⁶⁴).

| Bioreactor type | | Pros | Cons |
|---|---|--|--|
| Hollow fibre (tubular) |  | Simple design, immunoisolation, well characterized, minimal shear stress | Non-uniform cell distribution, low mass exchange, no intrinsic oxygen supply |
| Hollow fibre (interwoven) |  | Ease of scale-up, efficient and uniform mass transport, minimal shear stress, immunoisolation, good oxygen and nutrient supply | Complex design |
| Flat plate and mono/multilayer membrane |  | Uniform cell distribution and microenvironment | Complex scale-up, potential large dead volume, cells exposed to shear stress, no intrinsic oxygen supply |
| Perfused beds/scaffolds/sponges |  | Ease of scale-up, minimal barrier to nutrient/metabolite transport | Non-uniform cell distribution, cells exposed to shear stress, no intrinsic oxygen supply |
| Encapsulation and suspension/fluidized - bed |  | Ease of scale-up, uniform microenvironment, enhanced mass transfer | Poor cell stability, barrier to nutrient/metabolite transport due to encapsulation, degradation of microcapsules over time, no intrinsic oxygen supply |

Tab. 8: Bioreactor designs. Sources: ^{64,69}

3.4.2. Fluidized bed bioreactor developed at UTC

The team of C. Legallais has been focusing on BALs for the last 20 years. The team proposed an innovative BAL system based on a fluidized bed bioreactor (FB), hosting hepatocytes encapsulated in alginate microbeads. In FB, beads are pushed upwards by the blood/plasma flow and they start to move up and down therefore maximizing the mass transfer with the fluid and limiting the damage provoked by the perfusion (shear stress) (Figure 16). The role of the alginate matrix is discussed in the next paragraph. Bioreactors hosting alginate beads have been tested also in fixed bed setup ¹²³, where the beads are fixed and exposed to the plasma flow. In this setup, the most relevant disadvantage is that the blood/plasma entering in contact with the beads, takes preferential paths limiting therefore the mass transfer between fluid and cells. Moreover, if compared with hollow fibre design, alginate beads provide short diffusion length, best surface/volume ratio, possibility of cryopreservation of encapsulated cells (since alginate microbeads protect hepatocytes from physical damage caused by the growth of extracellular ice crystals) ^{124,125}. Also other investigators rely on the technology of the fluidised bed, such as Selden's group ^{126,127}.

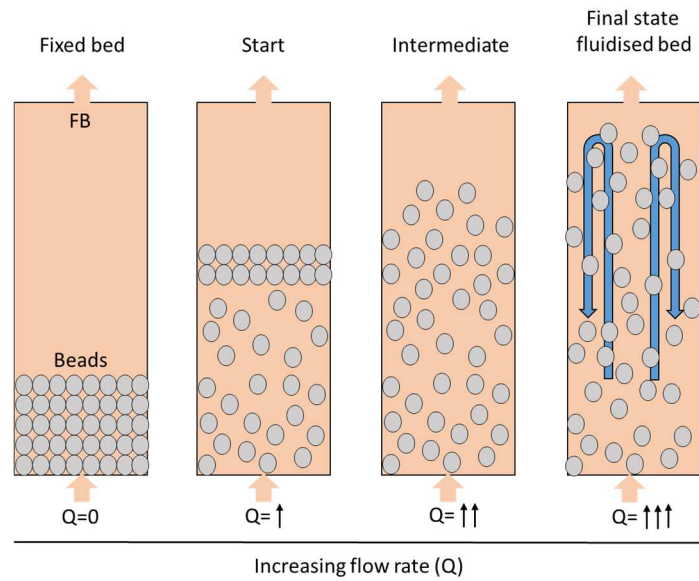


Fig. 16: FB concept ¹²⁸

Previously, other Ph.D. students under the direction of Dr. C. Legallais, have investigated and characterized the design of the BAL device and the role of its components. In particular, B. David developed the system and characterized the metabolic performance of cell line HepG2/C3A over short perfusion periods ¹²⁹. A. Gautier analysed the performance of the same cell line over longer periods. S. Capone focused on the functionalization of alginate with collagen and fibrinogen, in order to optimize the metabolic activity of primary human hepatocytes ¹³⁰. S. Figaro, involved in the SUPPLIVER project, developed the human-scale BAL, hosting in the bioreactor HepG2/C3A cells ¹ (Figure 17). Finally, V. Pandolfi investigated the possibility to improve cell functionalities through co-cultures between hepatocytes and non-parenchymal hepatic cells.

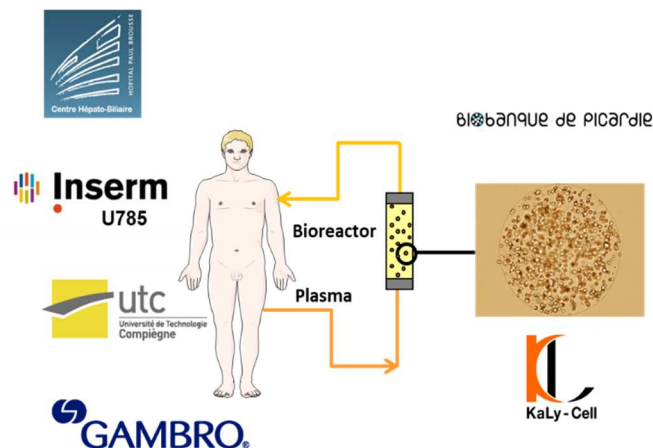


Fig. 17: Concept SUPPLIVER, the patient's plasma is separated from the formed elements of blood through a plasmafilter. Then, the plasma is treated by the bioreactor hosting encapsulated hepatic cells. The alginate matrix protects hepatic cells from shear stress (perfusion), and from the immune system of the patient, favouring at the same time the mass transfer between cells and fluid. Once the plasma has been treated (detoxified and enriched with molecules produced by hepatocytes), it enters once again the patient. Source: thesis of S. Figaro ⁵⁰

4. Hepatocytes alginate microencapsulation: a tool for liver tissue engineering

Microencapsulation consists in forming beads or capsules in which hepatic cells are entrapped. The most common natural hydrogel-forming polymer for biomedical applications is alginate, a linear copolymer containing blocks of (1,4)-linked β -D-mannuronate (M) and α -L-guluronate (G) residues, obtained from brown seaweed (Figure 18). The monomers occur in a block-like fashion, where the G-blocks are responsible for the specific ion binding and hence also the gelling properties of alginate. This material is quite inert and not toxic regarding cells, ensuring adequate biocompatibility. Alginate has therefore been used to produce biomedical scaffolds for the cultivation of various types of cells. Applications include *in vitro* toxicology and regenerative medicine. In addition, its relatively low cost and gelation capacity by divalent cations such as Ca^{2+} (Figure 18) makes the process suitable for cell encapsulation. The most relevant feature of alginate is its capacity to form gels. In fact, G-residues are capable of chelating divalent ions (Ba^{2+} , Ca^{2+} , Mg^{2+} , etc.) according to the so-called egg-box model, promoting the sol-gel transition¹³¹.

This cells immobilization technique was originally developed by Lim and Sun¹³². Later, various techniques have been reported⁶⁶ mainly using a two-step procedure: i) formation of droplets containing the cells mixed with the material achieved via extrusion through a needle ii) droplet solidification (gel formation) in the gelation bath composed of divalent cations (such as Ca^{2+}). In this manuscript, this two-steps procedure was part of the co-axial airflow extrusion method used as technique of cell encapsulation.

The beads size is an important parameter and can be tailored (micro to macroscale) depending on specific demands. It depends on the diameter of pipette or syringe, the generation of additional forces to push the droplets to fall down (coaxial airflow, electrostatic generator, jet-cutter, etc.), the viscosity of the alginate solution and the rate of alginate flow. Generally, for biomedical applications, beads with a diameter of 200–1000 μm are preferred to promote exchanges¹³³. The smaller the beads, the larger the ration surface/volume, leading to better nutritional and oxygen exchange between encapsulated cells and surrounding medium.

As-manufactured-alginate matrix has tunable porosity (nano to micro scale¹³⁴, mainly depending on encapsulation technique, M/G ratio, and divalent ions concentration¹³⁵) which allows oxygen and nutrients (such as proteins, glucose, vitamins, etc.) bi-directional diffusion. The porosity range has the advantage of preventing immune cells and antibodies, which might destroy the enclosed cells, from entering the capsule. The manufacturing process also allows the tuning of some mechanical properties such as Young's modulus (ranging from 0.5 kPa to 2 kPa in our case). Young modulus is well known to affect cell behaviour¹³⁶. For certain type of cells such as hepatocytes, the hydrophilic polymer characteristic of alginate limits cell adhesion and therefore promotes cellular interaction and spheroids formation, enhancing cell-cell interaction and hepatocyte functionality^{137–140}. It is recognized that culturing cells as spheroids enhances and prolongs hepatic-specific functions for primary hepatocyte cultures¹⁴¹, hepatic cell lines¹⁴² and iPSCs¹⁴³. If cell adhesion is needed, alginate functionalities can be modified by the addition of cell attachment peptides or

other biologically active molecules (chitosan, fibrin gels, Matrigel, collagen)^{144,145}. The 3D architecture of the spheroid provides a biological environment that resembles the *in vivo* structure of the hepatic lobule, which results on correct assembly of polarity proteins and transporters¹⁴⁶. In addition, the alginate matrix offers protection to the hepatic biomass from hydrodynamic shear stress in specific bioreactors type (e.g. stirred bioreactors¹⁴⁷), while creating an extracellular environment that enables diffusion of nutrients and soluble factors through the hydrogel structure¹⁴⁷ (Figure 19). The technique of alginate microencapsulation of hepatocytes is therefore used by many authors with different purposes, from toxicology¹⁴⁷, to transplantation¹⁴⁸, and BAL applications^{126,149}.

To conclude, an overview on alginate and its application in liver tissue engineering is presented in the review article "Bioengineering Organs for Blood Detoxification" (DOI: 10.1002/adhm.201800430) by Legallais et al. 2018⁶⁶, that contains a paragraph (§4.2.4) written by me and reported in Annex 5, section 3 of this manuscript..

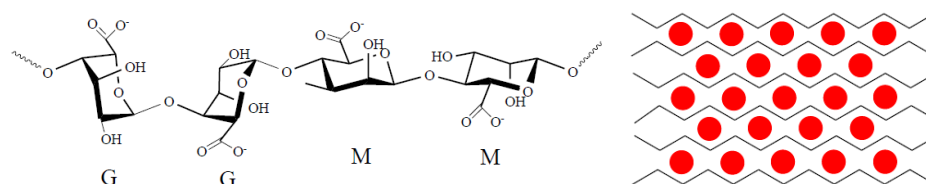


Fig. 18: Alginate structure (left) and gel formation (egg-box structure) (right)

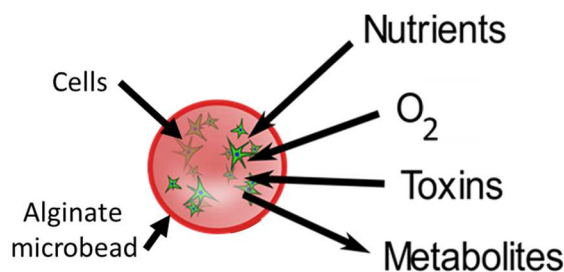


Fig. 19: Role of alginate beads

5. Animal models for BAL preclinical studies

Using a BAL in clinical application requires meeting the regulations for combined advanced therapy medicinal products (cATMP) established through preclinical and clinical testing, to ensure its safety and effectiveness. For these reasons, it is necessary to go through the stages of preclinical studies on animal models, in respect of the European legislation on animal models for research (EU Directive 2010/63/EU). According to the literature³ there is a lack of standard clinically relevant animal models capable of reproducing the pattern of symptoms typical of ALF, since the numerous etiologies and complications of ALF contribute to the complexity of this condition and render the development of an ideal experimental model more difficult than expected.

5.1. Choice of the animal model

In general, the choice of animal models for studying diseases depends on the construct validity criterion. It describes how well the mechanism used to induce the disease phenotype in animals reflects the currently understood disease etiology in humans (similarity in the biological function/dysfunctions between the human and animal model). It requires an adequate species with high degree of genetic, anatomical, and functional similarity to human, such as pigs or rodents.

5.2. Choice of the pathological model

After this first restriction criterion, the pathological animal models must be examined. They are mainly divided in two types:

- **Spontaneous models:** utilize naturally occurring genetic variants (mutants). Many hundreds of strains/stocks with inherited disorders, modelling similar conditions in humans, have been characterized and conserved ¹⁵⁰
- **Induced models:** involve healthy animals in which the condition to be investigated is experimentally induced, e.g. acute liver failure, partial hepatectomy to study liver regeneration, etc. The induced model group is the only category that theoretically allows a free choice of species ¹⁵⁰

5.3. Choice of the induction method for ALF

5.3.1. Induction methods criteria

In order to choose the optimal method of induction to obtain the pathological animal model, the following two criteria are mainly used:

- **Predictive validity:** is defined as the measure of how well a animal model can be used to predict features of the disease in humans
- **Face validity:** is defined as how well an animal model replicates the symptoms of the disease in humans

The most used ALF induction methods are based on surgical techniques or hepatotoxic drugs. The use of methods based on viral infection have been reported ¹⁵¹ but this procedure is less spread. In any case, none of these procedures is able to reflect the global typical pattern of human ALF and each method presents pros and cons that are discussed in the next paragraphs.

5.3.2. Surgical methods

Among the surgical methods, two different procedures are distinguished (Table 9).

| ALF induction method | Animal model | Advantages | Disadvantages |
|----------------------------------|------------------------------|--------------------------------------|---|
| Surgical methods | | | |
| Total/partial hepatectomy | Pig, dog, rabbit, rat, mouse | Hepatic encephalopathy; reproducible | No reversibility; no long-term survival |

| | | | |
|--|-----------------------|--------------------------------------|---|
| Total/partial devascularisation | Pig, dog, rabbit, rat | Hepatic encephalopathy; reproducible | No reversibility; no long-term survival |
|--|-----------------------|--------------------------------------|---|

Tab. 9: Surgical methods for inducing ALF in animal models ¹⁵²

- **Partial/total hepatectomy:** partial hepatectomy consists in the surgical resection of a certain volume of liver. This procedure has been successfully applied to rats, dogs and pigs to induce ALF or to generate models of liver regeneration. It has been observed that the resection of 95% of a rat liver provides a good model for ALF ¹⁵³. In pigs, the resection of 70% of the liver mass leads to death from ALF after an interval that allows the study of hepatic support therapies¹⁵². Total hepatectomy cannot reflect properly the pattern of human ALF: without remnant liver, toxic molecules and inflammatory factors that play an important role in ALF, are absent.
- **Devascularization:** this method consists in performing a portocaval shunt followed by occlusion (clamping) of the hepatic artery and of the bile common bile duct. The reversibility of the model depends on the time of temporary occlusion. This technique has been tested on pigs, provoking a reproducible model of ALF and to test artificial and bioartificial liver devices ¹⁵⁴.

According to the literature, the best choice among the surgical procedures for studying liver deficiency status and ALF treatment with bioartificial liver devices is the partial hepatectomy ¹⁵⁵, especially on large animal models such as pigs. However, it is not fully representative of human ALF, which never results from a surgical act.

5.3.3. Chemical methods

Chemical methods are based on the action of hepatotoxic molecules (Table 10). The most frequently used hepatotoxic drugs for inducing ALF are acetaminophen, D-galactosamine and thioacetamide. Relying on hepatotoxic drugs makes possible to observe some ALF clinical characteristics, such as hypoglycaemia, encephalopathy, and increased blood levels of hepatic enzymes. For this reason, chemical methods are frequently used as a model for ALF. The main disadvantage in using hepatotoxic drugs is the reproducibility and the extrahepatic toxicity.

| ALF induction method | Animal model | Advantages | Disadvantages |
|-----------------------------|------------------------------|--|---|
| Chemical methods | | | |
| Acetaminophen | Pig, dog, rabbit, rat, mouse | Hepatic encephalopathy; no hazard | Non-reproducible; variable interval between damage and death; species and age variability |
| Amanitin | Pig | Hepatic encephalopathy; specific toxic effects; large animal | Adapted laboratory animal house; hazard |
| Azoxymethane | Mouse | Hepatic encephalopathy; reproducible | Small size; hazard |
| Carbon tetrachloride | Pig, rabbit, rat, mouse | Hepatic encephalopathy | Non reproducible; extrahepatic toxicity; small time window before death |

| | | | |
|---------------------------|------------------------------|--|---|
| Concanavalin A | Rat, mouse | Hepatic encephalopathy | Small size |
| Galactosamine | Pig, dog, rabbit, rat, mouse | Hepatic encephalopathy; biochemical markers | Non-reproducible; hazard; variable interval between damage and death; species differences |
| Lipopolysaccharide | Rat, mouse | Hepatic encephalopathy | Non-reproducible; small size; hazard; small time window before death |
| Thioacetamide | Rabbit, rat, mouse | Hepatic encephalopathy; reproducible; large time window before death | Hazard |

Tab. 10: Chemical methods for inducing ALF in animal models ¹⁵²

As example of chemical agent, the mechanism of action of D-galactosamine is discussed here. D-galactosamine is an amino sugar that is metabolized by the galactose pathway in the liver. The latter transforms the galactose in glucose-6-phosphate (first intermediate in glycolysis) and UDP-glucose (precursor of glycogen, sucrose, lipopolysaccharides and glycosphingolipids formation). The metabolism of D-galactosamine leads to depletion of intracellular uridine moieties, which disturbs hepatocytes RNA metabolism. This process leads to hepatocytes necrosis. Importantly, D-galactosamine appears to have fewer extrahepatic effects than other toxic agents ¹⁵⁶. This drug has been used on different animal models. In experiments carried out on anesthetized dogs, it has been observed that the drug caused the typical effects of human ALF (such as an increase in blood levels of liver enzymes, bilirubin, ammonium or lactate and the associated coagulopathy, hypoglycaemia, and increase in intracranial pressure) ¹⁵⁷. Reproducible models of ALF induced by D-galactosamine have been obtained with pigs and applied for testing the effect of BAL devices for treating ALF ¹⁵⁸. The effect of BAL treatment in D-galactosamine-induced ALF in rats has also been explored ^{159,160}. Importantly, the characteristics of ALF induced by D-galactosamine are different across species. Noticeably, the window between the ALF induction and death is not uniform, the drug is expensive especially for large animal modes (such as pigs) and it presents health risks.

5.4. Other essential criteria specific to ALF

Regarding ALF, Terblanche and Hickman ¹⁶¹ added other criteria for satisfactory animal models, here resumed:

- **Reversibility:** the ALF induced in the animal model should be potentially reversible so that animals can respond and survive if a suitable treatment is utilized (e.g. BAL therapy).
- **Reproducibility:** without treatment, there should be nearly universal mortality of the animal models.
- **Death from liver failure:** it should reflect the same biochemical and histological course as in the clinic scenario.
- **Adequate animal size:** to allow blood and tissue analysis.
- **Therapeutic window:** this should be long enough after the insult is administered to enable the treatment to be initiated and its effects to be assessed.
- **Minimal hazard to personnel:** any methods used should present minimal risks to the laboratory personnel involved.

Later other authors ^{156,162} also added other important features required for an appropriate ALF animal model:

- **Appropriate metabolism/physiology:** the species utilized should have metabolic and physiological properties similar to humans (i.e. construct validity).
- **Conscious animal model:** assessment of hepatic encephalopathy should be possible.
- **Compliance with ethical standards:** protocols must respect ethical and animal welfare standards.

Overall, animal models used in research for ALF and for BAL applications are still limited. As a result, investigators adapt the animal model to their own needs, such as the design of their BAL and the ease of manipulation in the laboratory.

6. Objectives of this thesis

Our own approach for external BAL relies on the microencapsulation of hepatic cells in alginate beads located in a perfused bioreactor placed in series with artificial components. In the framework of the Ilite program, and considering the concomitant progresses in several fields of tissue engineering reported in the previous parts, this PhD thesis aims at paving the way to the clinical application of our system.

In agreement with the consortium, we chose to perform the preclinical evaluation, i.e. safety and performances of our device both *in vitro* and in a relevant small animal model, so as to limit the amount of biomass and thus the cost of the experiments. One of the novelty in the project relies on the choice of HepaRG as cell source, this progenitor cell line being considered as a relevant model before further use of differentiated iPSCs or ESCs that are studied by other groups. Our own experience, combined with others, outlined the need for revisiting the 3D culture conditions once cell type is changed. More specifically, we hypothesized that the reorganization of cells in clusters or spheroid would trigger their differentiation and functions. Another key point is the reduction of the size of the whole system, which was initially designed for human application, and the evaluation of the effects of its different components.

To achieve these goals, the thesis is divided into three complementary phases that reflect our objectives, summarized in figure 20.

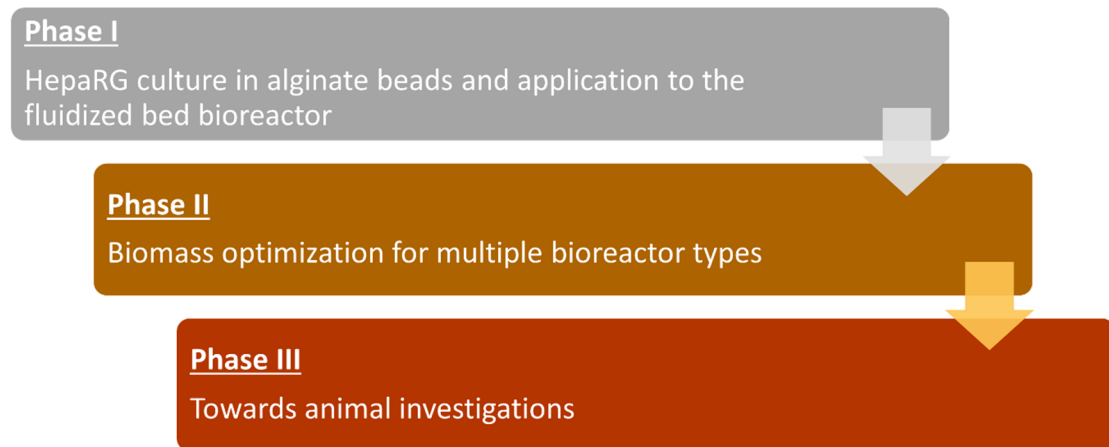


Fig. 20: Objectives of this thesis

- **Phase I: HepaRG culture in alginate beads and application to the fluidized bed bioreactor (chapter 3)**

We firstly characterized the metabolic performance of a biomass of alginate encapsulated HepaRG, investigating several culture parameters (such as spheroid culture, different polymer concentrations and so on). Then, this biomass was optimized for fluidized bed-bioreactor.

- **Phase II: biomass optimization for multiple bioreactor types (chapter 4)**

The culture of the biomass in fluidized bed bioreactor raised some problems regarding the mechanical stability of the biomaterial. In this chapter we tried to solve this problem realizing an external polymeric coating. This chapter revolves around the characterization of the new biomass in terms of metabolic activities and physical/chemical properties of the biomaterial. This biomass is finally implemented in bioreactors dedicated to BAL application.

- **Phase III: towards the animal investigations (chapter 5)**

In this chapter, we describe the steps that led to the choice of the pathological animal model for *in vivo* testing and the implementation of the BAL device adapted to this model. In a first phase, the device was scaled down, starting from the pre-existing BAL at human scale. In parallel, the effect of activated charcoal and ionic resin was evaluated studying their ability to detoxify a medium containing the toxins present in the blood during ALF (such as ammonia). The first steps of the safety of the device are finally described.

Chapter 2. Materials and methods

1. 2D cell culture

HepaRG from Biopredic (Rennes, France) cells were expanded in two-dimensional (2D) monolayers following the indications reported by the supplier. Cells were passaged every 2 weeks until passage 18, with proliferation culture medium (William's E -WE-, with sodium bicarbonate, without L-glutamine and phenol red, Sigma-Aldrich, with added Biopredic 710 proliferation media) replenishment three times per week. The cultures were maintained in a humidified environment at 37°C, 5 % CO₂. After that, cells were detached by trypsin-ethylenediaminetetraacetic acid (EDTA) 0.25% (ThermoFisher scientific) from the culture flasks and used for the cell encapsulation process (explained in §3).

2. 3D cell culture

For the dissociated cells (DCs) condition, after cell amplification in 2D monolayers, cells at passage 18 were detached, mixed with the alginate solution at density of 5×10^6 cells per mL and encapsulated. The same protocol was also used for cell encapsulation at higher cell densities.

For the pre-formed spheroids (SPHs) condition, 5×10^6 cells were inoculated as dissociated cells in glass culture dishes (50 mm x 15mm), coated with an anti-adhesive coating (Sigmacote®, SL2 Sigma-Aldrich). Cells were subject to continuous orbital agitation at 60 rpm with oscillation amplitude of 16 mm (SSL1 orbital shaker, Stuart) in a humidified environment at 37°C and 5% CO₂. Proliferation culture medium was replaced one time during the spheroids formation. After 3 days of aggregation, spheroids were encapsulated. Cell aggregates and beads size was determined by measuring their diameter using ImageJ software version 1.52h.

3. Alginate microencapsulation

DCs or pre-formed SPHs were encapsulated in alginate (Manucol LKX from FMC BioPolymer, Guluronic/Mannuronic ratio 30-70, viscosity Cps (1%) 60-170) at 1% (w/v) or 1.5% (w/v), sterilized by successive filtrations (0.8, 0.45, and 0.22 µm pore size membrane filters). The encapsulation was performed with a home-made system based on a coaxial air flow extrusion method¹³⁰. Briefly, the alginate solution (1 mL) containing cells (5 million) was rapidly extruded through a 24 G nozzle and the droplets fell into a gelation bath (NaCl 154 mM, HEPES 10 mM and CaCl₂ 115 mM, pH 7.4). Droplets produced were allowed to settle for 15 min in the gelation bath to ensure gel formation. After that, the microbeads were washed three times in WE medium and then resuspended in proliferation culture medium. Finally, the encapsulated DCs or SPHs were transferred in culture dishes with 8 mL of proliferation medium, and maintained along 7 or 14 days in continuous orbital shaking (60 rpm) in a humidified environment at 37 °C, 5 % CO₂ (condition named "shaken culture"). Proliferation culture medium was replaced each 2 days. 1 mL of empty microbeads (without cells) was also produced as control for the following metabolic tests. The same protocol was also used for cell encapsulation at higher cell densities. In the experiments where we added glass

microparticles at different concentrations (see results section), they were mixed with the alginate-cell solution before encapsulation process.

4. External poly-L-Lysine coating of alginate beads

To avoid alginate beads deterioration, an external coating was realized using Poly-L-Lysine -named PLL- (Poly-L-lysine hydrobromide, molecular weight 30,000-70,000, Sigma-Aldrich), at day 1 post-encapsulation. The coating protocol is inspired to Khanna et al. 2012 ¹⁶³ but adapted to our needs. Briefly, alginate beads (with and without cells) in proliferation medium, were transferred in a 15 mL tube and washed 3 times in WE medium. At the same time, a solution of 0.1%(w/v) PLL in WE medium was prepared and sterilized by filtration (0.22 µm filters). Therefore, beads were incubated with this solution and transferred in Petri dish in continuous orbital shaking (60 rpm) in a humidified environment at 37 °C, 5 % CO₂, for 30 minutes. After that, beads were transferred in 15 mL tube and washed 3 times with WE medium. Finally, beads were incubated with HepaRG proliferation medium and transferred in Petri dish in continuous orbital shaking (60 rpm) in a humidified environment at 37 °C, 5 % CO₂ along the days of culture. The metabolic performance was tested on day 14 post encapsulation, following the previous setup.

5. Metabolic and xenobiotic tests

5.1. Albumin and urea synthesis

Albumin synthesis was quantified by ELISA test (Human Albumin ELISA kit, Bethyl Laboratories, Inc.), whereas urea secretion was determined by colorimetric assay (QuantiChrom TM Urea Assay Kit, BioAssay Systems). Analyses were performed in conformity with the manufacturer's instructions.

5.2. ICG assay

As described by Gabriel et al. 2012 ¹⁶⁴, indocyanine green (ICG, Sigma-Aldrich) was dissolved in DMSO at 25 mg/mL. Then, the solution was added to microbeads to obtain a total concentration of 1 mg/mL in proliferation medium. Microbeads were incubated 30 minutes at 37°C and 5% CO₂ to favour the uptake of ICG by the transporters OATP1B3 (solute carrier organic anion transporter family member 1B3) and NTCP (sodium/taurocholate co-transporting polypeptide) ¹⁶⁵. ICG was then removed by washing with medium WE five times and the microbeads were incubated with proliferation culture medium for 1 hour to study the releasing of ICG by the transporters MDR3 (multidrug resistance protein 3) and MRP2 (multidrug resistance-associated protein 2) ¹⁶⁶. The quantity of ICG released was obtained by measuring its absorbance (at 820 nm) based on a linear standard curve generated from a known solution containing ICG 1 mg/mL.

5.3. EROD assay

The activity of the cytochrome P450 1A1/2 (CYP1A1/2) was studied with the ethoxyresorufin-O-deethylase (EROD) assay ¹⁶⁷. Microbeads were incubated in ethoxyresorufin (10 µM), prepared in

WE, for 1 hour at 37°C. The substrate included salicylamide (3 mM) + dicumarol (40 µM) in order to inhibit phase II enzymes. The substrate is converted in resorufin then measured in the supernatant by spectrometry (excitation wavelength of 535 nm and emission wavelength of 595 nm, Spectafluor Plus, TECAN). The standard curve was generated with a solution containing exogenous resorufin (10 µM).

In addition, the inducibility of the cytochrome was studied by adding -Naphthoflavone 100 µM (Sigma Aldrich) to the medium 72 hours before the test.

5.4. BROD assay

The activity of the cytochrome P450 3A4 (CYP3A4) was studied with the 7-Benzyloxyresorufin-O-dealkylase activity (BROD) assay ¹⁶⁷. Microbeads were incubated in 7-benzyloxyresorufin (10 µM), prepared in WE, for 1 hour at 37°C. The protocol is then the same as for the EROD assay.

5.5. Metabolic tests on BAL function test medium

Cultures on day 7 and 14, were incubated with "BAL function test medium", containing proliferation culture medium supplemented with 1.5 mM NH₄Cl (Sigma Aldrich) + 2 mM L-Lactate (Sigma Aldrich) described elsewhere ¹⁰⁶. After 2 hours of incubation, the supernatants were collected and analysed by Indiko™ (Thermofisher) to determine the concentration of ammonia, by Lactate Assay Kit (Sigma-Aldrich) to measure the concentration of lactate, following the indications reported by the supplier, and by ELISA kit for albumin concentration.

5.6. Metabolic tests on pathological plasma model

Cultures on day 14 were incubated in "pathological plasma model", just after 2 hours of exposure to an equivalent plasma model. The pathological plasma model reproduces an ALF-human patient plasma and contains proliferation culture medium with 70 g/L bovine serum albumin (BSA, Sigma Aldrich), 1.5 mM NH₄Cl + 2 mM L-Lactate. After 6 hours of incubation, the supernatants were collected and analysed with Indiko™ (Thermofisher) to determine the concentration of ammonia, using the Lactate Assay Kit (Sigma-Aldrich) to measure the concentration of lactate, following the indications reported by the supplier, and with an ELISA kit for albumin concentration.

5.7. MTS test for measuring the cytotoxicity of the media used

Cell viability was tested by CellTiter 96® AQueous One Solution Cell Proliferation Assay (MTS) following the manufacturer instructions. The test was realized in a 12 multiwells culture dish with HepaRG monolayers on day 14.

5.8. Data normalization

The metabolic activities are normalised by the quantity of metabolite produced or consumed/hours of incubation/millions of cells seeded. This way of normalizing data evidences a global cell activity starting from a given initial hepatic biomass.

6. Cell differentiation study

Cell differentiation was studied via immunofluorescence staining on days 0, 7, 10 and 14 post-encapsulation and metabolic test (albumin synthesis) on days 0-1, 6-7, 9-10, 13-14 post-encapsulation. For cell differentiation, aliquots of encapsulated HepaRG were degelified in a sodium citrate-EDTA solution (NaCl 154 mM, sodium citrate 50 mM, EDTA 55 mM, pH 7.4), fixed in 4% paraformaldehyde (PFA) in PBS for 4 hours at 4°, then cytocentrifuged (Shandon Cytospin®) and stored at -80 °C. For detection of intracellular epitopes, cells were permealized with PFS solution (0.7% gelatine, 0.025% Saponin, 0.02% NaN₃). Primary antibodies (Table 11) were incubated for 2 h at 37°C. Alexa Fluor 488-conjugated and Alexa Fluor 568-conjugated second antibodies were added and incubated for 1h at room temperature. Cell nuclei were stained with DAPI (DAPI Fluoromount-G®) and phalloidin (Alexa Fluor™ 488 Phalloidin, Thermofisher) staining was used for F-actin visualization. Samples were visualized by confocal microscopy (Zeiss LSM 710).

| Protein | Reference | Type |
|---|----------------------------------|-----------------------|
| AFP (alpha-fetoprotein) | SC 8399 | mouse monoclonal IgG |
| ALB (albumin) | Sigma A6684 | mouse monoclonal IgG |
| CK-19 (cytokeratin 19) | DAKO Mo888 | mouse monoclonal IgG |
| CYP3A4 (cytochrome P450 3A4) | SC 53850 | mouse monoclonal IgG |
| HNF 4α (hepatocyte nuclear factor 4α) | SC 8987 | rabbit polyclonal IgG |
| HNF 6 (hepatocyte nuclear factor 6) | SC 13050 | rabbit polyclonal IgG |
| A1AT (Alpha-1 antitrypsin) | DAKO A0012 | rabbit polyclonal IgG |
| ASBT (apical sodium-dependent bile acid transporter) | SC- 27493 | goat polyclonal IgG |
| BSEP (Bile Salt Export Pump) | Sigma HPA019035 | rabbit polyclonal IgG |
| CK-7 (cytokeratin 7) | DAKO M7018 | mouse monoclonal IgG |
| SOX 9 (SRY-box 9) | SC-20095 | rabbit polyclonal IgG |
| SR-B1 (Scavenger receptor class B type 1) | (Novus Biologicals) NB400-131 | goat polyclonal IgG |
| UGT1A1 (UDP glucuronosyltransferase 1A1) | SC-271268 | mouse monoclonal IgG |
| ZO-1 (Zonula Occludens 1) | NBP1-85047 | rabbit polyclonal IgG |

Tab. 11: List of antibodies used for immunofluorescence staining

7. Cell proliferation inside the beads

To determine if cells are able to proliferate within the beads, it was used the Click-iT® Plus EdU Proliferation Kit (Thermofisher), following the manufacturer's instruction. For the essay, encapsulated cells cultured in proliferation culture media, were incubated between days 0-1, 6-7, 9-10, 13-14 post-encapsulation, with the alkyne-containing thymidine analog EdU (5-ethynyl-2'-deoxyuridine), during 20 hours. This compound is incorporated into DNA during active DNA synthesis. After incubation, cells were fixed in PFA 4%, the beads degelified in a sodium citrate-EDTA solution and then cells were cytocentrifuged (Shandon Cytospin®). The incorporated EdU is then detected by a click reaction copper-catalysed azide-alkyne cycloaddition using a fluorescent

Alexa Fluor® or Pacific Blue™ dye containing a picolyl azide moiety. Newly DNA is detected using confocal microscopy.

The number of new-formed cells (or nuclei) was calculated counting, in the pictures acquired via confocal imaging, the number of new formed cells or nuclei (stained in green) divided by the total number of nuclei (DAPI, stained in blue). The results were expressed in percentage.

8. Determination of the total number of cells and total amount of cell proteins

To determine the total number of cells at the end of the experiments, alginate microbeads were degelified in a sodium citrate-EDTA solution. Then, cells were collected by centrifugation at 300 g for 10 minutes. The pellet was washed 3 times in PBS and then resuspended in 2 mL of milli-Q water. Cell lysis were performed via freeze-thaw lysis method and the quantification of total DNA via FluoReporter™ Blue Fluorometric dsDNA Quantitation Kit (Thermofisher). The total number of cells was obtained by measuring the fluorescence based on a linear standard curve generated from a known solution of cells (total DNA content).

To determine the total amount of cell proteins, it was used the same protocol of cell lysis and the quantification was done by Bicinchoninic Acid Kit (Sigma-Aldrich). The total amount of cell proteins was obtained by measuring the absorbance based on a linear standard curve generated from a known solution of proteins (bovine serum albumin in Milli-Q H₂O at 4 mg/mL) and cells.

9. Cell viability

In order to observe cell viability, at the end of each experiment, aliquots of encapsulated cells were collected and a Live/Dead assay was performed following the manufacturer instructions (Invitrogen™LIVE/DEAD™ Viability/Cytotoxicity Kit, for mammalian cells, ThermoFisher). Nuclei were stained by Hoechst 33342 dye (3 µM). Encapsulated cells were visualized by confocal microscopy.

10. PLL distribution in alginate beads

In order to visualize the distribution of the PLL in the empty alginate beads (i.e. without cells, produced using the same protocol previously presented), a staining of PLL with rhodamine was realized. Firstly, we prepared a NHS-Rhodamine (Thermofisher) solution in DMSO at concentration 50 mg/mL and a solution of sodium bicarbonate at 8.3 mg/mL in double distilled H₂O, pH 8.2. PLL was solubilized in the sodium bicarbonate solution at final concentration 0.1% w/v, containing NHS-Rhodamine solution at final concentration 500 µg/mL. In order to favour the conjugation between NHS-Rhodamine and epsilon-NH₂ of lysine residues, the solution were incubated in the dark for 3 hours at room temperature. The control solution did not contain PLL. After that, the PLL coating was realized putting the beads in contact with this solution, according to the protocol already described. The beads were finally washed 3 times in DPBS and visualized by confocal microscopy. The thickness of the external coating was measured using ImageJ 1.52h software.

11. Mechanical characterization of beads' surface

The elastic modulus of the outer surface of the empty beads was measured by microindentation (system ChiaroOptics 11, Amsterdam, NL) mounted on a microscope. The probes used for surface indentation had a radius of around 25 μm and a spring constant of 0.5 N/m and 5 N/m, for pure alginate beads and PLL coated ones, respectively. Indentations of the beads were performed at 1.12 $\mu\text{m/s}$. Before testing, the optical sensitivity and the geometrical factor were calibrated by indenting a hard surface (e.g. glass slide). Alginate beads were deposited on a glass slide and then immersed in HepaRG proliferation culture medium. The probe was placed in contact with a single bead and a maximal indentation of 3 μm was applied. All experiments were performed at room temperature. For each condition, about 15-20 curves (load vs indentation depth) were acquired. Data were analysed with the DataViewer 2.2 software (Optics 11, Amsterdam, NL) using the Hertzian theory, which provided the elastic modulus of the indented area.

12. Beads diffusion properties

The permeability of the empty alginate with and without PLL coating beads was studied by putting them in contact with fluorescent molecules of different molecular weights and sizes, on day 14. The permeability to these molecules was examined by confocal microscopy, exploring them inside along the Z-axis. In order to study the permeability of the alginate beads to albumin-fluorescein isothiocyanate (FITC) conjugate (Sigma Aldrich), empty alginate beads 1.5% were incubated with WE medium containing 100 $\mu\text{g/mL}$ of this molecule for about 24 hours in orbital agitation, at 37°C. Then, the beads were rapidly washed once in William E and visualized at the confocal microscope. This molecule has a molecular weight of about 66 kDa and hydrodynamic diameter of 7.3 nm, without the fluorophore ¹⁶⁸. The same protocol was used for Alexa Fluor 488 conjugate IgG (Thermofisher), inspired to Wang et al. ¹⁶⁹. This molecule has a molecular weight of about 160 kDa and hydrodynamic diameter of 11.5 nm, without the fluorophore ¹⁷⁰. The permeability was also investigated using fluorescent polystyrene nanoparticles (NPs) of different diameters (41, 103, 249 nm) (Estapor, Merk Chimie), as previously described ¹⁷¹. Each type of NP, at concentration 1 mg/mL, was incubated with empty alginate beads at a ratio of 1:2 (bead volume/nanoparticles solution volume) under orbital agitation for 24 hours at room temperature. Beads were then rapidly washed once in William E medium and visualized by confocal microscopy.

13. Fluidized bed bioreactor: setup for *in vitro* testing

For the experiments in fluidized bed bioreactor (FB), we used the following components:

- A glass bioreactor with double entry, total volume of 19.4 mL, internal diameter of 1.83 cm outer diameter of 2 cm, inner diameter of the screw pitch of 0.8 cm, height of 12 cm. At the two inlets, a plastic screw cap with aperture is screwed in the pinch, in order to connect the bioreactor to the silicone tubing of the circuit. Inside each cap, it has to be inserted in the order: a glass funnel adapter (that connects the bioreactor to the silicon tubing), a silicone-

sealing ring, a piece of filter membrane (SEFAR NITEX 03-100/44) with mesh opening of 100 μm , another silicone-sealing ring to block the latter. Those pieces are then screwed to the bioreactor screw pitches. The filter membrane is essential to prevent the release of alginate debris and cells from the bioreactor. Plastic and silicone supports were purchased from DURAN®. The biomass present is at cell density 10×10^6 , 5 mL of beads, 50 million cells total. The different components are described in figure 21.

- The tubing of the circuit consists of silicone tubes with an internal diameter of 1 mm and an external diameter of 3 mm. Tubing were purchased from VWR™.
- These tubes connect the assembled bioreactor to a glass bottle containing the culture medium (media reservoir) through a system of needles inserted to the bottle cap. A peristaltic pump (by ISMATEC®) allows the medium to pass through the entire circuit at controlled flow rate (measured in mL/min). There are three needles connected to the bottle cup: one to pump the culture medium towards the bioreactor via the peristaltic pump, the second allows the arrival of the medium from the bioreactor, the third allows access to the medium for sampling. The total internal volume of the circuit (bioreactor + tubing) is about 20 mL (Figure 21).

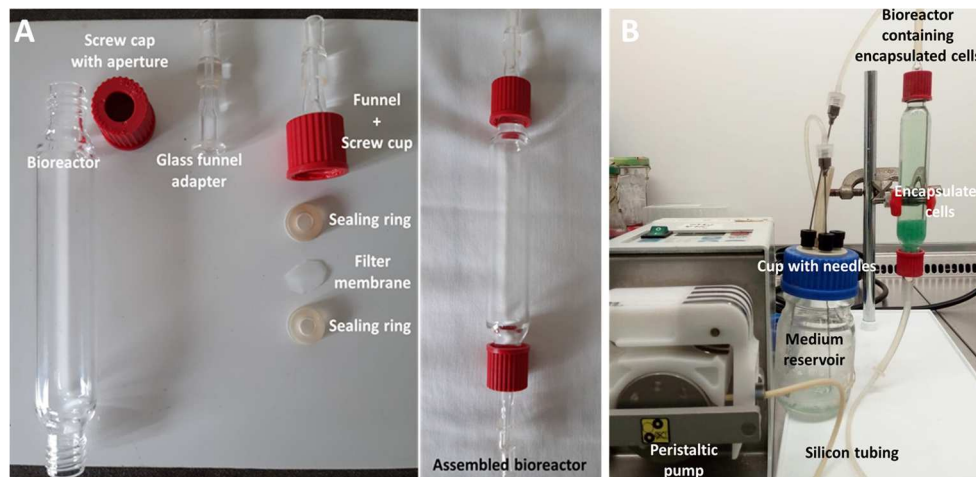


Fig. 21: Singular components of a FB (A) and FB setup for *in vitro* testing (B)
(Beads are coloured in green since the picture was taken after the ICG test. This is a fixed bed, since the pump was switched off)

- All these materials must be autoclaved before use.

To insert the encapsulated cells into the bioreactor it is necessary to work under a sterile hood to maintain sterility. Firstly, it is necessary to prime (removing the air) the tube that connects the media reservoir to the bioreactor using culture medium. Afterwards, the upper cap of the bioreactor is opened and the beads are inserted by means of a serological pipette. The cap is then closed and, at low flow rate, the circuit is primed to purge the air in the remaining tubes and needles. Depending on the condition, the circuit is normally filled with a volume of culture medium of 37.5 mL or 40 mL. The system is now ready and is inserted into the incubator (37°C and 5% CO₂) to perform the desired metabolic tests. The flow rate (mL/min) that allows the formation of a fluidized bed is variable for each experiments and it is superior to 7 mL/min.

14. Perfused dynamic bioreactor: setup for *in vitro* testing

The alternative bioreactor tested in this thesis is the perfused dynamic bioreactor (PDB). It is a double arm glass flask adapted to media perfusion from a reservoir. It is kept in continuous orbital shaking (80 rpm). Perfusion is conducted by peristaltic pump at flow rate 0.4 mL/min, with a system of tubes connecting medium reservoir and PDB. The needles for media recirculation are protected with filter membrane to avoid biomaterial debris and biomass escaping from the PDB. In the latter, some outlets are dedicated to filtered air intake to preserve sterility and guarantee gas exchanges. Encapsulated biomass (cell density 10×10^6 , 5mL of beads, 50 million cells total) remained in shaken condition until day 14, when it was transferred into the PDB for subsequent metabolic characterization.

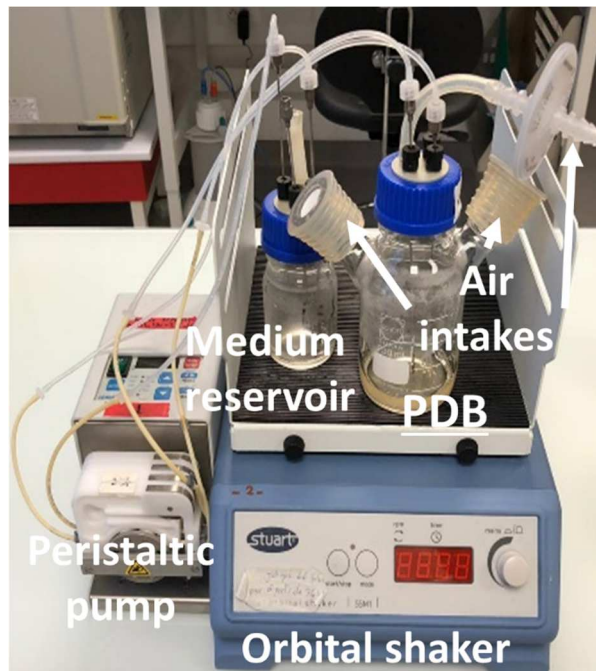


Fig. 22: Perfused dynamic bioreactor (PDB) setup

15. Circuit to tests the artificial elements

The circuits tested in this campaign are composed of:

- A glass bottle containing the culture medium (media reservoir). It has a cap with 3 needle inlets. One entrance is dedicated to the medium's inflow, one for the outflow and another one for the sampling
- The tubing of the circuit consists of silicone tubes with an internal diameter of 1 mm and an external diameter of 3 mm. Tubing were purchased from VWR™
- A peristaltic pump allows the medium to pass through the entire circuit at controlled flow rate (measured in mL/min)
- Glass containers containing activated charcoal or ionic resin. The inner surface of the bottle is covered with a filter membrane of 100 μm mesh opening, to avoid loss of particulate

matter. Each container can be filled with 2.1 g of activated charcoal and 2.4 g of ionic resin and it has an inlet for medium inflow and an outlet for medium outflow (Figure 23)

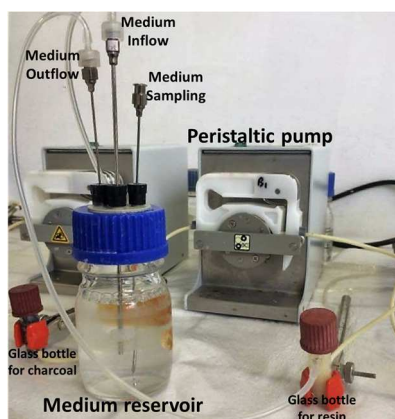


Fig. 23: Circuit to test artificial elements

15.1. Analysis of the markers tested on artificial elements

Ammonia and glucose concentrations were analysed by Indiko™ (Thermofisher), lactate by Lactate Assay Kit (Sigma-Aldrich), calcium ions by Calcium Colorimetric Assay Kit (Sigma-Aldrich) following the indications reported by the supplier. Total proteins concentration was determined by Bicinchoninic acid (BCA) assay used reagents purchased from Sigma-Aldrich.

16. Statistical analysis

All presented results were obtained from at least three independent cultures ($N \geq 3$). The statistical analysis has been realized by the software GraphPad InStat v.3.10. Unpaired data were subjected to Mann Whitney test or Dunn's Multiple Comparisons Test while paired data to Wilcoxon matched-pairs signed-ranks test, with a 95 % confidence level considered significant. P values are presented as follow: no stars: $p > 0.05$ (not significant), * $p < 0.05$, ** $p < 0.01$, *** $p < 0.001$.

17. Figures representation

For the realization of figures 26, 48, 57, 66, 75, 85, 87, 90 of this manuscript, we used images taken from Servier Medical Art (www.smart.servier.com). For the figure 2 and 3, the authors acknowledge EASL as the source.

Chapter 3. Phase I: HepaRG culture in alginate beads and application to the fluidized bed bioreactor

1. Introduction

In this introduction, some key points already discussed in the first chapter will be briefly taken up in order to give a clear background to the work done during this phase I. A part of those results has been published in Tissue Engineering (see list of publications).

In the context of BAL, hepatic cell microencapsulation in alginate porous beads has been recognized as an interesting alternative to classical cell immobilization in hollow fibre membranes. This material is quite inert, not toxic regarding cells and ensures an adequate biocompatibility. In addition, its relatively low cost and gelation capacity by divalent cations such as Ca^{2+} makes the process suitable for hepatocyte encapsulation ⁶⁶. *In vitro* liver models combined with tissue engineering approaches provide a 3D microenvironment which can be expected to mimic *in vivo* conditions. In the process of encapsulation, cells are entrapped within spherical alginate microbeads that protect them from mechanical stress while ensuring exchanges of nutrients or waste molecules within the surrounding medium. The immuno-isolation supposed to be ensured by alginate encapsulation is undoubtedly the major advantage of this technology ¹⁷¹. Since 2000, our lab works on this concept, and designed a fluidized bed bioreactor easy to scale up or down according the number of cells to mobilize. In this configuration, alginate beads motion represents a regular loop from the bottom to a maximal height in the bioreactor (called fluidization maximal height). This behaviour results from the combined effect of the lift due to plasma/culture medium perfusion and the gravity due to beads density greater than that of plasma/culture medium ¹²⁸, therefore maximizing the mass transfer (i.e. exchanges of oxygen, nutrients, metabolites and toxins) with the fluid and limiting the damage provoked by the perfusion ¹⁷². Figure 24 recapitulates the concept of beads fluidization and mass transfer between fluid and encapsulated cells. The advantages and disadvantages of using this type of bioreactor were discussed in the first chapter of this thesis.

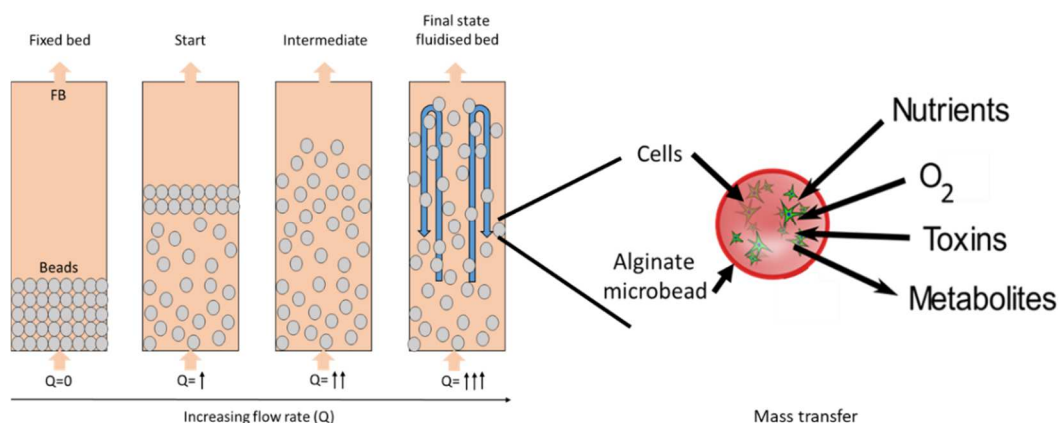


Fig. 24: Concept of fluidized bed bioreactor (FB) and mass transfer

Previous Ph.D. students have extensively investigated the concept of fluidized bed bioreactor in our laboratory. In particular, B. David developed the system and characterized the metabolic performance of cell line HepG2/C3A over short perfusion periods ¹²⁹. A. Gautier analysed the

performance of the same cell line over longer periods. S. Figaro, involved in the SUPPLIVER project, developed the human-scale BAL, hosting in the bioreactor HepG2/C3A cells ¹. This configuration has also been object of preclinical studies by other authors. With a similar bioreactor hosting HepG2 grown in alginate beads, Selden's group observed the improvement of clinical parameters in a surgical porcine model of liver failure ¹²⁶. Zhou et al. ¹⁷³ also obtained prolonged survival time for pigs with D-galactosamine induced ALF using a fluidized bed BAL hosting porcine primary hepatocytes encapsulated in alginate-chitosan beads. Overall, *in vitro* characterization on cellular models and preclinical studies on different animal models suggest that this technology is suitable as biological component of a BAL.

Access to a bioactive mass (or biomass) is the main challenge in the context of human BALs, and thus in our case of fluidised bed BAL hosting hepatic cells encapsulated in alginate beads. Although primary human hepatocytes are still considered the gold standard, their limited availability, the phenotypic instability ⁷⁰, as well as logistical issues, hamper their use in BALs. In a previous project (ANR SUPPLIVER, 2011-2015), our group and collaborators had to face the scarcity and the donor's variability with these cells (either freshly collected from donors or resection or cryopreserved). To improve their stability as differentiated cells, we proposed to cultivate them as spheroid before performing the encapsulation in alginate beads ¹.

In the past, most of the BALs in clinical or preclinical studies relied on primary porcine hepatocytes, due to their easy availability and high functional activities ⁹⁴⁻⁹⁶. However, transfer of zoonotic diseases ⁹⁷, protein-protein incompatibility between species and possible immune responses generated during treatment remain challenges for the use of xenogeneic hepatocytes ⁹⁸.

Recently, the focus has been put on the use of induced pluripotent stem cells and embryonic stem cells as innovative cell source for BAL, especially for their great proliferative capacity and their potential to show metabolic functions close to those of human hepatocytes. However, today these cell types are not able yet to exhibit full functions of mature hepatocytes in terms of metabolic performance and efforts have still to be made to allow their clinical use ¹⁷⁴. In the framework of iLite project, this research activity is led by the group of Dr A. Dubart Kupperschmitt at Inserm U1193.

Therefore, human cell lines keep a great potential for BAL application. The main advantages of hepatocyte cell lines are their almost unlimited proliferative capacity and the relatively easy and cheap culture process. They demonstrate some metabolic functionalities comparable to human hepatocytes and also to be safe and non-tumorigenic ⁸⁸. On the one hand, HepG2 and its sub-clone C3A present limited metabolic functions ⁷⁰ for BAL applications, although encouraging results were recently presented by the group of Selden on a pig model of ALF. On the other hand, HepaRG is a hepatic progenitor cell line able to differentiate into hepatocyte-like and cholangiocyte-like cells after 14 days of specific culture ¹⁰¹. Investigators already demonstrated that HepaRG cell line was suitable for BAL application for their proliferation capacity and their enhanced hepatic metabolism in three-dimensional (3D) configuration ¹⁰⁷. HepaRG can be cultivated adding dimethyl sulfoxide

(DMSO) that acts as inducer of the enzymes involved in the xenobiotic pathway but reducing cell viability ¹⁰⁶.

In our case, considering that:

- a highly viable biomass is essential for BAL application
- there is not clear evidence that xenobiotic functionalities at its highest level is crucial for BAL ⁷⁰
- microencapsulation of HepaRG evidenced high hepatic cell metabolism without the use of DMSO ^{106,147}

we made the choice to cultivate our cells without this inducer.

For BAL application, the challenge is to induce/maintain the hepatic functions over time starting from an initial biomass, taking into account parameters such as costs, manipulation ease for the operator, and scaling-up feasibility. Recently, some authors successfully enhanced biosynthetic and xenobiotic performance of HepaRG functions, cultivating cells as spheroids (SPHs) before encapsulation, without the use of DMSO ¹⁴⁷. Nevertheless, the technologies available nowadays for the production of large amounts of spheroids (such as rotating or shaking reactors) may lead to an unacceptable loss of cells that reduces considerably the initial biomass. Indeed, the majority of these studies are focused on toxicology approaches in which it is important to evaluate the metabolic activity "per cell". In the context of BAL, the challenge is not to determine the best activity "per cell" but rather "per bioreactor", taking into account logistic hurdles or costs due to additional manipulation.

The aim of the phase I was firstly to gradually optimize the hepatic biomass for the activities required for ALF treatment in bioartificial liver context. The term "optimization" refers to the set of processes that allowed us to make the most of an initial biomass of hepatic cells, in terms of cellular metabolic performance and logistic. Secondly, this hepatic biomass was adapted for fluidized bed bioreactor, the component of our small-scaled BAL developed during this thesis.

The phase I is divided in 3 steps (Figure 25). The first step revolved around the preliminary investigations of different HepaRG culture setups for BAL applications. In particular, we firstly evaluated the best encapsulation option between pre-formed spheroids (SPHs) and dissociated cells (DCs), in terms of logistic and metabolic performance. Then, we wanted to offer the best microenvironment to cells in terms of biomaterial mechanical properties by comparing two concentrations of alginate. Finally, we evaluated the best temporal window in terms of cell activity. Therefore, a characterization of encapsulated cells differentiation over-time was carried out in order to evaluate when the cell model displays the full set of hepatic features necessary for the treatment of a patient in ALF. Once established the most suitable culture condition, the next second step was to further optimize the biomass for its use in fluidized bed bioreactor (FB) and, finally, the third step regarded the characterization of the cell metabolic performance in the latter culture setup.

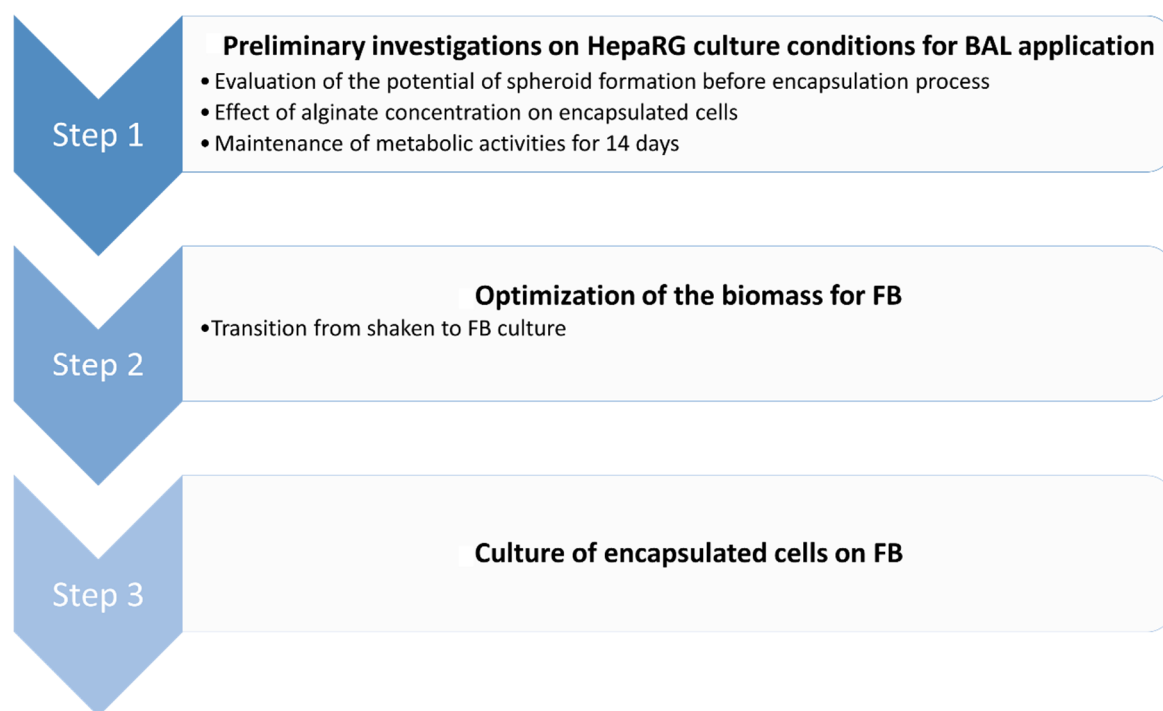


Fig. 25: Optimization of the biomass, from shaken to FB culture

2. Results

2.1. Step 1: Preliminary investigations on HepaRG culture conditions for BAL application

The experimental design for the step 1 is presented in figure 26. After 2D amplification in culture flasks, cells were recovered by trypsinization and a part of them (so-called "dissociated cells") was encapsulated in alginate (either 1% or 1.5%). With the remaining part, spheroids formation was started. After 3 days of cell aggregation, pre-formed spheroids were encapsulated in alginate 1.5%. On day 7 and/or 14 post-encapsulation, the cell performance was assessed through metabolic and xenobiotic tests, as described in the Materials and Methods chapter. At the end of each experiment, microbeads were collected and assessed for cell viability. The quantity of marker analysed was calculated and normalised by the number of hours of incubation and the number of cells seeded. Moreover, in order to avoid artefacts, all the metabolic activities tested were normalised by the quantity present at time zero and by carrying out controls with empty microbeads. Therefore, any influence of the empty beads on the cellular activities assessed was corrected during the analysis of the results. These controls were also used for the experiments of the other steps.

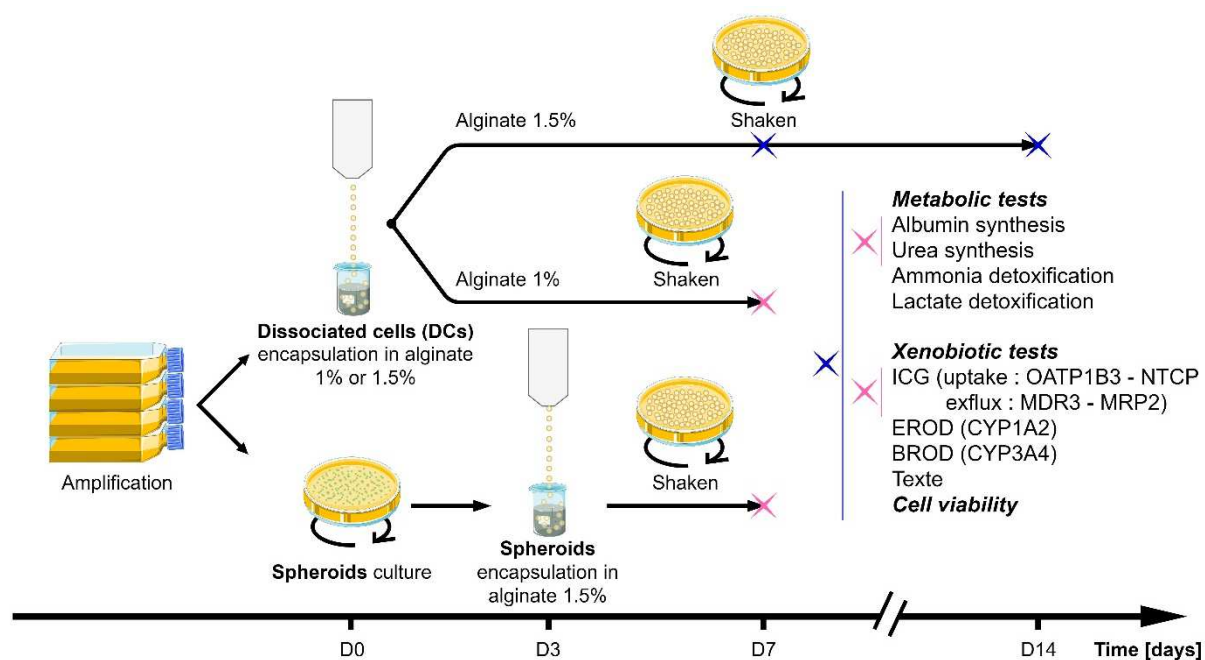


Fig. 26: Experimental setup phase I, preliminary studies on culture conditions.

2.1.1. Is it necessary to form spheroids before the encapsulation process?

Firstly, we wanted to understand if it is better to encapsulate pre-formed HepaRG spheroids or dissociated cells (DCs), in terms of cell metabolic performance and logistic (ease of manipulation, costs, large-scale production).

As preliminary experiments, we performed these experiments at day 7 post-encapsulation. On this day, the cellular activity was already present for the assays we were investigating. This allowed us to avoid longer cell culture periods and thus additional costs. In addition, based on the literature, we decided to set the cell density at 5×10^6 cells/mL of alginate. As already explained, no DMSO was used for cell culture.

The metabolic activity of SPHs 1.5% and DCs 1.5% was investigated analysing the synthesis of albumin, urea, and ICG releasing rates (performed by the enzymes involved in the xenobiotic metabolism pathway MDR3 and MRP2). In both conditions, no urea production could be detected. DCs 1.5% showed a 2.5X higher secretion of albumin (Figure 27A) and higher ICG releasing activity (Figure 27B).

Of note, qualitative observations to the bright field microscope showed that the cells, in the condition DCs 1.5%, seemed to aggregate to form spheroids in an autonomous way (Figure 28). This phenomenon was also observed by other authors working with alginate encapsulated HepG2/C3A^{138,139} and Huh-7¹⁴⁰. The diameter of the spheroids, both for SPHs 1.5% and DCs 1.5%, remained comparable between the two conditions as shown in figure 29.

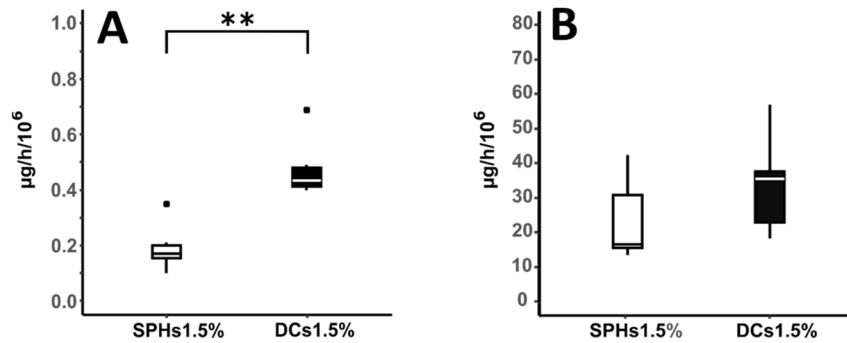


Fig. 27: Metabolic activities measured on day 7 between SPHs 1.5% and DCs 1.5%. Albumin secretion rate (A, significance analysed by Mann-Whitney test) and ICG releasing rate (B). * indicates outliers. $N \geq 3$

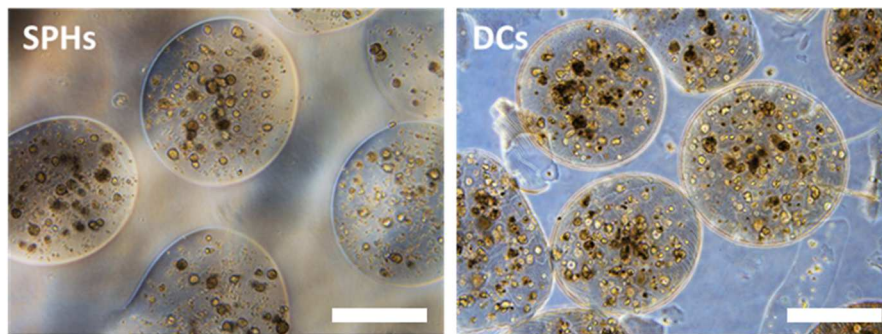


Fig. 28: Observation on bright field microscopy of SPHs (A) and DCs after encapsulation (B). Scale bar: 500 μm

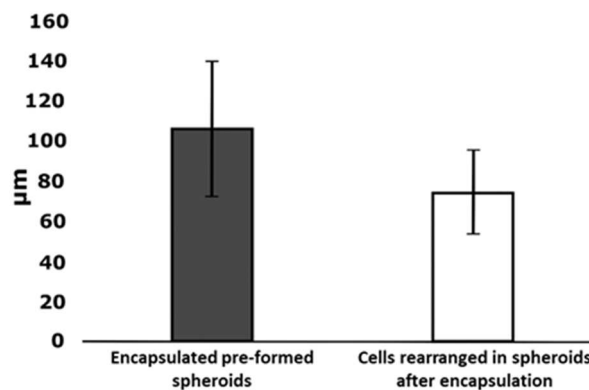


Fig. 29: Mean diameter of SPHs and DCs after encapsulation on day 7

The results showed that DCs produced significantly more albumin than pre-formed spheroids while the transporters activity (ICG releasing) was comparable. These observations could be due to two different aspects. First, the DCs, rearranged in spheroid-like structures, could have a comparable metabolic activity to pre-formed encapsulated spheroids. Second, a different total number of cells is present in the two cultures. In fact, despite the use of an anti-adherent dish to form spheroids, many cells anchored to the surface (and so did not form aggregates) and were lost before encapsulation. Indeed, figure 28 shows a slight difference in cell density between the two conditions, that justifies the lower results compared to DCs (to remind, the results are normalised by the number of cells encapsulated, i.e. 5 million). However, our interest is not to measure an activity "per cell" but rather a global activity per "bioreactor" (a Petri culture dish in our case), starting from a given biomass and considering all the necessary manipulations until the end of the

experiment. Rebelo et al.¹⁴⁷ also entrapped HepaRG in alginate beads, with high performances regarding biotransformation, interesting in toxicological issues. However, they encapsulated pre-formed spheroids and not dissociated cells, as proposed in the present work. When encapsulating a biomass for long time cultures, it is important to consider different logistical parameters influencing the whole process of manipulation for a future scaling-up for clinical BAL application. From our own experience, we observed a loss of cells when preparing aggregates/spheroids before encapsulation, especially using processes that can be up scaled such as rotating or shaking reactors. This loss is limited with hanging drop or microfluidic techniques¹⁷⁵, but these latter cannot treat billions of cells as requested for a human BAL size. In addition, aggregates pre-formation request at least 3 days of specific culture, before encapsulation, and additional handling that make the GMP production more complex and not cost-effective. As our results did not show any evidence of better performances of encapsulated pre-formed HepaRG spheroids, we conclude that their self-reorganization into alginate beads with appropriate density should be preferred in a clinical application strategy. Therefore, we decided to use DCs for the next characterization.

2.1.2. What is the impact of alginate concentration on cell activity?

In this section, we wanted to offer the best microenvironment to cells, comparing the conditions DCs in alginate 1% (DCs 1%) versus DCs in alginate 1.5% (DCs 1.5%) to evaluate the influence of the matrix stiffness on the cell metabolic performance, on day 7. Albumin and urea secretion, and ICG releasing rates were tested. Once again, no urea synthesis was detected. DCs 1.5% showed a twice higher secretion of albumin (Figure 30A) and higher ICG releasing activity (Figure 30B).

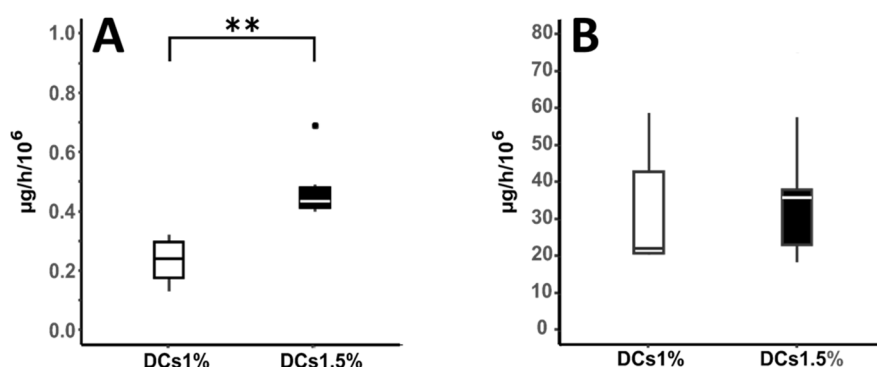


Fig. 30: Albumin secretion rate (A, significance analysed by Mann-Whitney test), ICG releasing (B). * indicates outliers. N ≥ 3

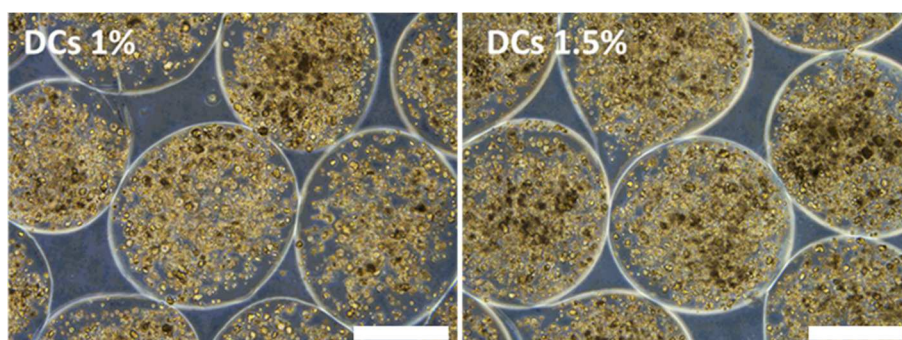


Fig. 31: Pictures in bright field microscope of DCs 1% (left) and DCs 1.5% (right) on day 7 post-encapsulation. Scale bar: 500 µm

In parallel, a mechanical characterization of the empty beads was performed via micro indentation. The elastic modulus (E) showed significant difference between empty beads at 1% and 1.5% (Figure 32). The latter presented E 2.6X stronger than the other condition, although they were quite low in both cases. Combining this observation with the metabolic behaviour, it seemed that the different stiffness of the biomaterial had an influence on cell metabolic activities, stronger in stiffer alginate.

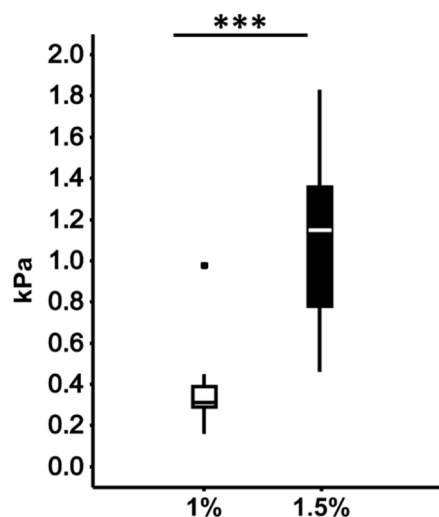


Fig. 32: Elastic modulus (in kPa) between empty alginate beads 1% and 1.5% on day 7. * indicates outliers. Significance analysed by Mann-Whitney test. N = 10 per batch of empty beads

Overall, DCs 1.5% produced significantly more albumin than DCs 1% while the xenobiotic transporters activity was comparable. Apparently, a higher stiffness of the alginate matrix better favoured cell activity. Several investigators focused on hepatocytes behaviour when cultured on biomaterials at different rigidity. Chen et al.¹⁷⁶ cultured rat hepatocytes on polyelectrolyte multilayers and found that albumin production and CYP450 1A activity decreased with increasing substrate stiffness. You et al.¹⁷⁷ cultured rat primary hepatocytes on heparin-based hydrogels at increasing elastic moduli (ranging from 11 to 110 kPa) observing that albumin production is higher in soft gels. Our observation highlighted a different behaviour. According to Nemir et al., liver has a rigidity between 0.6 – 1.2 kPa¹⁷⁸. Our results showed an elastic modulus of around 0.5 kPa for the 1% polymer concentration and about 1 kPa for 1.5%. Therefore, we hypothesized that the concentration 1% has too low rigidity compared to the physiological condition, affecting cellular activity.

It is important to notice that the mechanical properties obtained with our device Chiaro, are local and measured at the surface of the bead, with an indentation of 3 μ m depth. Those properties do not reflect the properties of the bulk material. They remain however indicators of a different biological cell behaviour.

Bead mechanical stiffness has been previously investigated by measuring the bulk properties typically using a texture analyser. Bulk properties are determined by measurement of the mechanical properties at the millimetre scale or greater. However, cells feel the matrix they are attached to in the micron and nanometre scales and receive exogenous forces from the surface

environment at those scales — which is an important effector of cell behaviour. Measurements at the micron and nanoscale scale can be achieved by application of local micro/nano Newton (nN) forces via indentation techniques (using our method or AFM approach). In addition, indentation measurements can be performed in liquid condition mimicking the cell culture environment ¹⁷⁹.

Clearly, our data have to be improved, for example using different depths of indentation, and compared with other techniques. However, we decided to use DCs 1.5% for the further step.

2.1.3. How long should last the culture of the biomass?

In this last section, we compared the metabolic performance of DCs 1.5% at two different days of differentiation, day 7 and day 14, to evaluate the best temporal window in terms of cell activity. We analysed the following metabolic activities: albumin synthesis rate (Figure 33A), ICG releasing rate (Figure 33B), CYP1A1/2 (EROD assay, Figure 33C) and CYP3A4 (BROD assay, figure 33D) activity. The results showed that cells had stronger metabolic activities on day 14 (except for ICG), with statistical significance for albumin synthesis (1.35X higher). The basal activity of the cytochrome CYP1A1/2 was not detectable on day 7 but it was on day 14. Of note, the CYP1A1/2 remains inducible via prototypical inducers on day 7 (Figure 34A) and 14 (40X stronger, figure 34B).

In addition, we measured the elastic modulus of the empty alginate beads at day 7 and 14 (Figure 35), registering lower values at day 14. The decrease in the mechanical properties of alginate is due to a loss of mechanical stability during the long culture period. This phenomenon has already been described by other authors and is due to presence of Ca^{2+} chelators or anti-gelling cations (Na^+ and Mg^{2+}) in the culture media¹⁸⁰. The decreasing in local beads mechanical properties over time was also reported by Chui et al. (2019) ¹⁷⁹ using a very similar experimental design. They kept their 1% alginate beads in culture medium along 14 days. During this period, they measured the surface stiffness of the beads by indentation technique (AFM). The test was conducted in culture media, and they obtained a Young's modulus of about 3 kPa at day 0 and about 2.1 kPa at day 14.

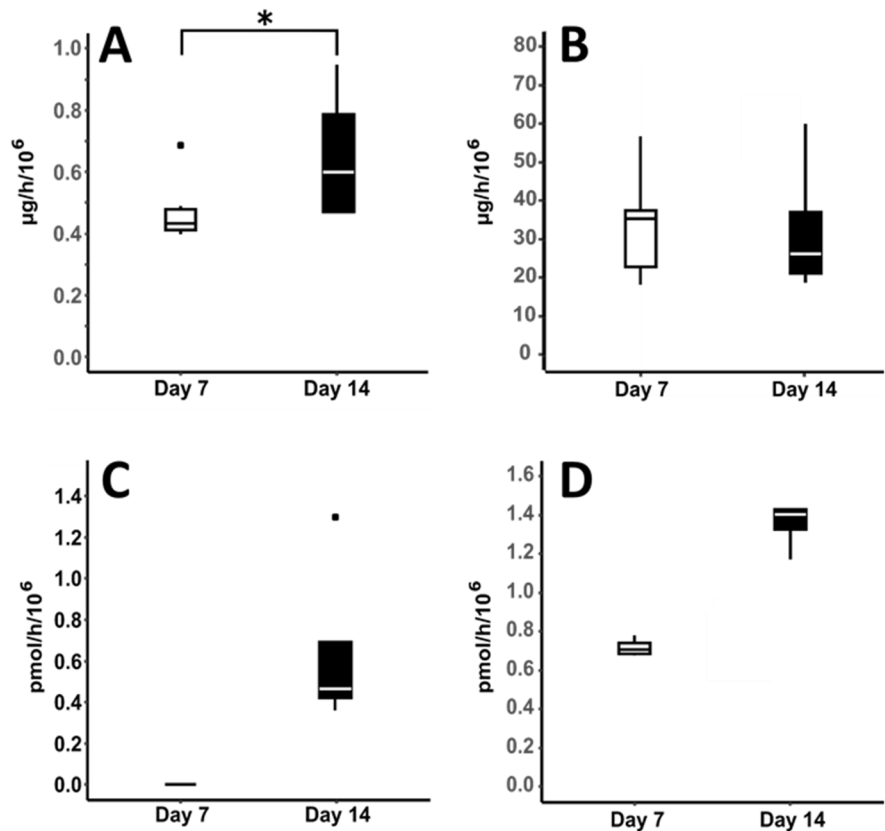


Fig. 33: Metabolic activities of encapsulated cells on day 7 and day 14. Albumin secretion rate (A, significance analysed by Wilcoxon matched-pairs signed-ranks test), ICG releasing rate (B), CYP1A1/2 activity (C), CYP3A4 activity (D). * indicates outliers. $N \geq 3$

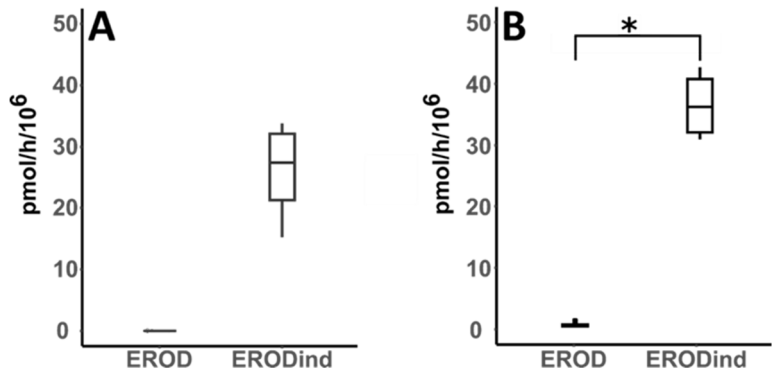


Fig. 34: CYP1A1/2 activity after induction by naphthoflavone 100 μM on day 7 (A) and 14 (B, significance analysed by Mann-Whitney Test). $N \geq 3$

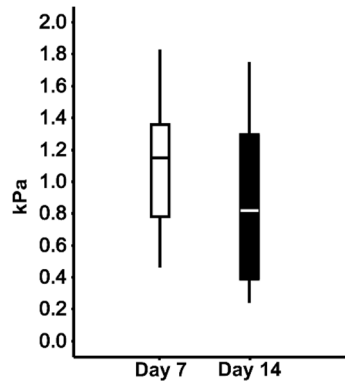


Fig. 35: Elastic modulus (in kPa) of empty alginate beads at day 7 and 14. $N \geq 3$

Finally, we studied the ability of cells to detoxify typical ALF toxins, in view of a future application of these cultures for a BAL. Cells were incubated for 2 hours in BAL function test medium containing ammonia and lactate. The ability of cells to produce albumin and detoxify these toxins is shown in figure 36. Again, the metabolic activities measured tended to be stronger on day 14. Importantly, the same samples tested on day 7 were tested again on day 14. After the exposition to the BAL function test medium, the cell viability remained overall high and stable (Figure 37).

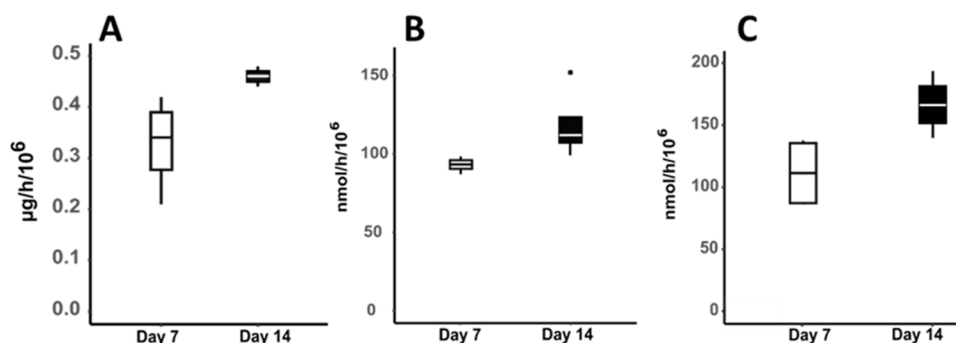


Fig. 36: Albumin synthesis rate (A), ammonia (B) and lactate (C) detoxification rate on day 7 and 14. * indicated outliers. N ≥ 3

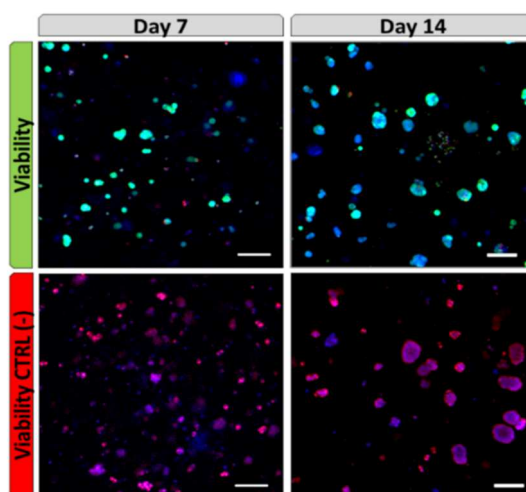


Fig. 37: DCs 15% viability after exposition to BAL function test medium on day 7 and 14 (confocal microscopy). In green (Calcein AM): viable cells, in red (ethidium homodimer-1): dead cells, in blue (Hoechst 33342 dye): cell nuclei. Scale bar: 100 µm

It has to be noticed that the albumin synthesis rates in proliferation medium ($0.64 \pm 0.21 \mu\text{g/h}/10^6$, mean and standard deviation, figure 33A) and in BAL function test medium ($0.51 \pm 0.08 \mu\text{g/h}/10^6$, figure 36A) was not significantly different. Therefore, the presence of typical ALF toxins (ammonia and lactate) in the medium did not seem to affect the activity of protein synthesis.

Importantly, the number of viable hepatocytes within the microbeads remained high over time (Figure 38) as very few dead cells (red stained nuclei) were observed, in comparison with the negative control where cells were killed by ethanol exposure. Therefore, qualitatively the long-time culture did not affect cell viability. Cells showed high viability even after each xenobiotic test (ICG, EROD and BROD assay) performed on day 14 (Figure 39).

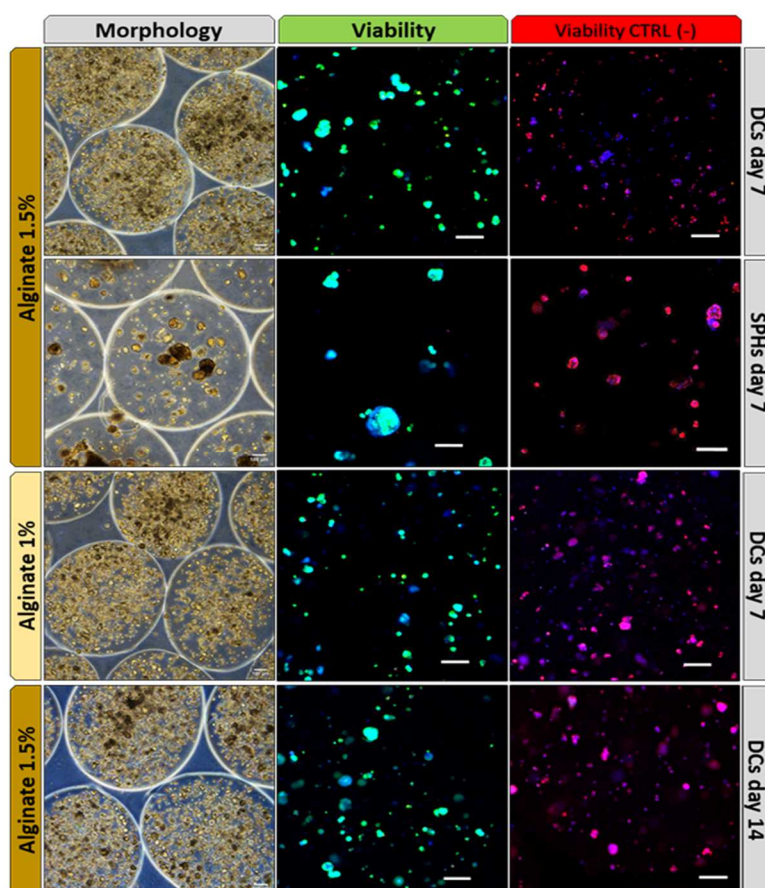


Fig. 38: Cell viability for all the conditions tested (confocal microscopy). In green (Calcein AM): viable cells, in red (ethidium homodimer-1): dead cells, in blue (Hoechst 33342 dye): cell nuclei. Scale bar: 100 μ m

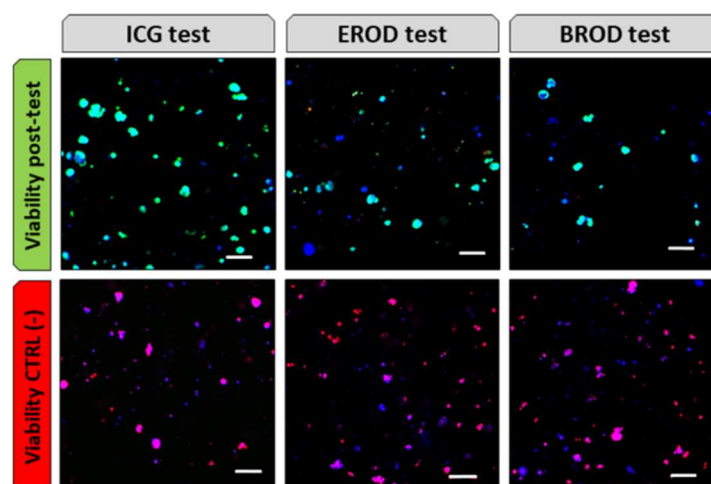


Fig. 39: Cell viability after metabolic and xenobiotic tests on DCs 1.5% on day 14. (confocal microscopy). In green (Calcein AM): viable cells, in red (ethidium homodimer-1): dead cells, in blue (Hoechst 33342 dye): cell nuclei. Scale bar: 100 μ m

Overall, among the several conditions analysed, DCs 1.5% on day 14 seemed the most promising in terms of cell metabolism, for future fluidized bed based BAL application. Therefore, we decided to better characterize this condition (considered as our gold standard), studying cell differentiation into the beads. For reminder, HepaRG is a cell line able to differentiate in hepatocyte-like and cholangiocyte-like cells during 14 days of cultivation in 2D configuration. It was worth understanding whether even in alginate beads, cells needed the same timing for complete differentiation.

2.2. Characterization of the “gold standard” HepaRG 3D culture in alginate beads

2.2.1. Beads morphology and cell viability

The following series of experiments concern a deeper characterization of the condition DCs 1.5%. We started with the characterization of beads morphology, in terms of diameter and deterioration, and cell viability over-time. The beads did not undergo any significant change in diameter (Figure 40) or structural integrity (Figure 41).

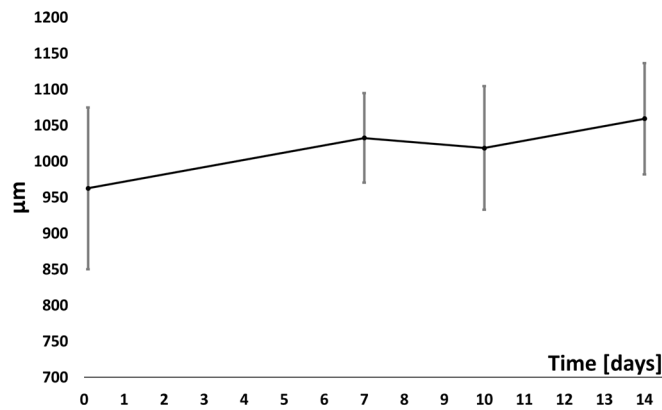


Fig. 40: Beads diameter over-time. N = 15 beads per day

Qualitative observations using bright field microscopy showed homogeneous cell distribution among the beads without any visible empty beads. We counted approximately 1100 beads per encapsulation batch (1 mL of alginate solution). As the initial biomass was 5 million cells/mL of alginate, cell density was approximately 4500 per bead. The number of viable hepatocytes (in green) within the microbeads remained high over time as very few dead cells (red stained nuclei) were observed, in comparison with the negative control where cells were killed by ethanol 70% exposure (Figure 41). Therefore, as previously observed, the long-time culture did not affect cell viability. According to Van Wenum et al. ⁷⁰, albumin production should be considered as a quality marker of the hepatic biomass in a bioreactor. In this sense, we evaluated the secretion rate of albumin in order to determine quantitatively the biomass functionality over the 14 days of culture (Figure 42).

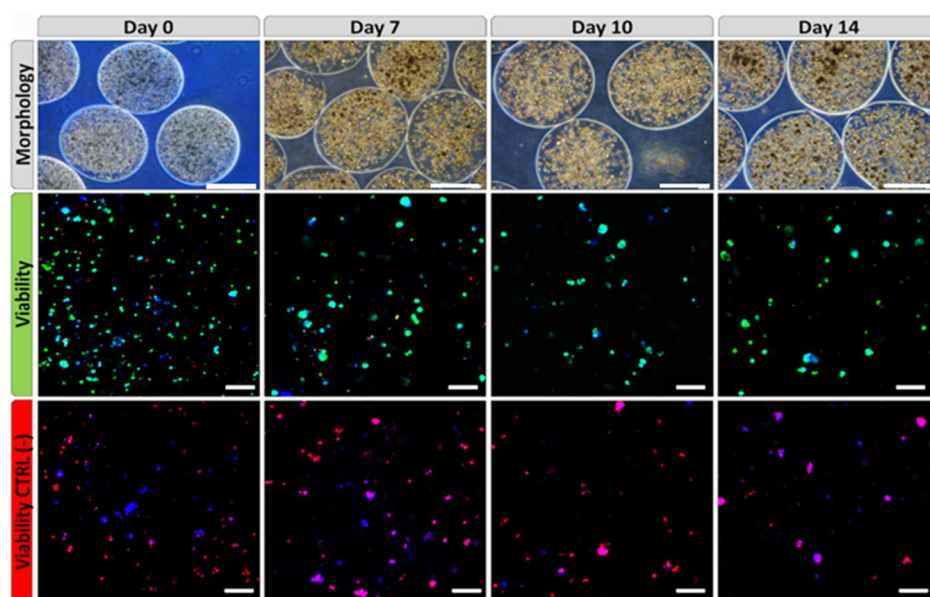


Fig. 41: Beads morphology (bright field microscopy, scale bar: 500 μm) and cell viability (confocal microscopy, scale bar: 100 μm). In green (Calcein AM): viable cells, in red (ethidium homodimer-1): dead cells, in blue (Hoechst 33342 dye): cell nuclei.

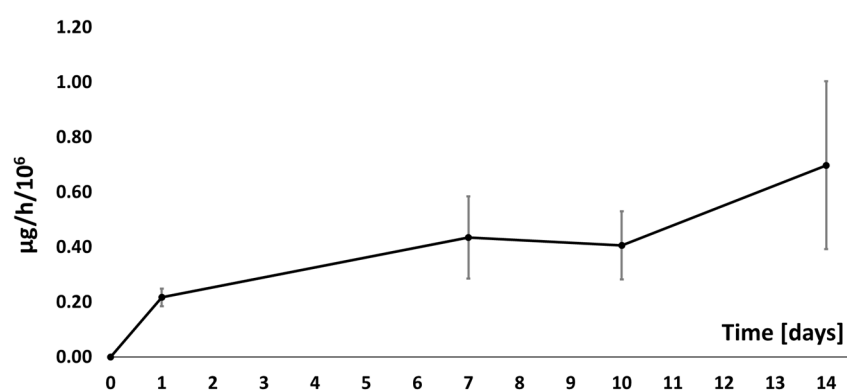


Fig. 42: Albumin synthesis rate over-time. $N \geq 3$

Interestingly, after a few days of culture, cells self-rearranged within the beads forming compact aggregates, as previously observed. The evolution of their diameter over time is presented in figure 43A while the morphology of an aggregate, stained with phalloidin (F-actin staining), on day 14 is showed in figure 43B.

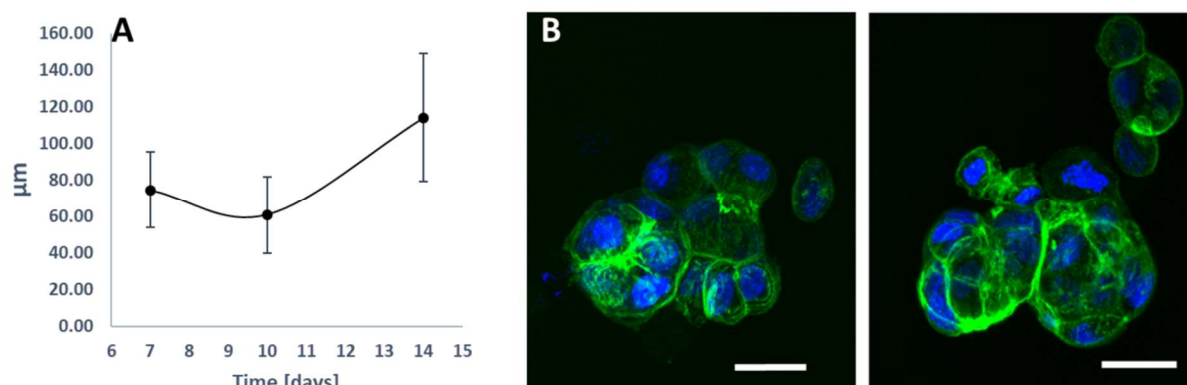


Fig. 43: Cells self-rearranged in aggregates: diameters over time (A). F-actin (phalloidin, in green) and nuclei (DAPI, in blue) staining on day 14 (B) (confocal microscopy). Scale bar: 20 μm

2.2.2. Cell proliferation within the beads

It was interesting to evaluate if cells inside the alginate matrix were able to proliferate over the two weeks of culture. The results showed that there is neo-synthesis of DNA (green spots in figure 44). However, it must be remembered that hepatocytes are polynuclear cells. Consequently, the green fluorescence may be due to the formation of either new cells or new nuclei. In any case, there was a phenomenon of new DNA synthesis that seemed to decrease over time (Figure 45).

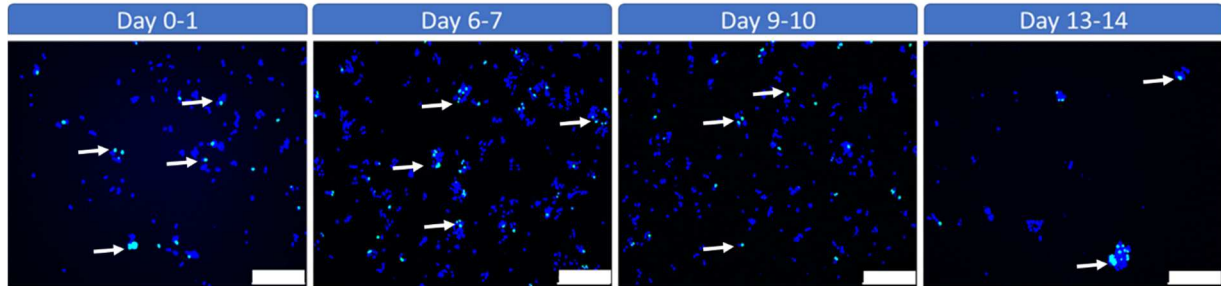


Fig. 44: Cell proliferation inside the beads. In green: new formed cells/nuclei, in blue: cell nuclei (DAPI). Scale bar: 250 μ m

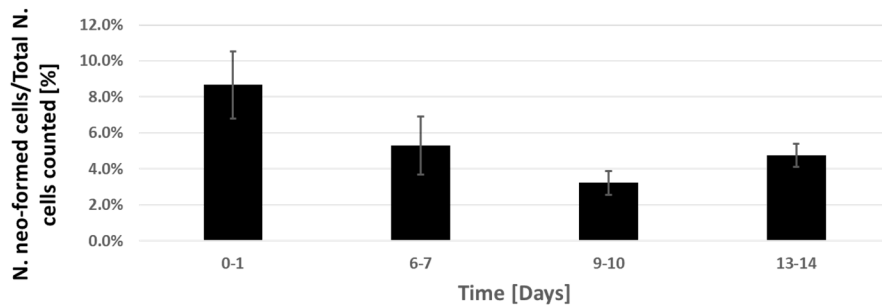


Fig. 45: Proliferation profile between the days of culture.














X-axis: number of neo-formed cells or nuclei/number of cells counted in percentage. Y-axis: days of observation (20 hours incubation)

Overall, the cells scarcely proliferated within the beads, probably as a result of the gel structure itself and minimal interactions with the matrix. These observations were in agreement with those obtained by David et al.¹²⁹ on HepG2/C3A encapsulated in alginate beads and Glicklis et al.¹⁸¹ using rat hepatocytes on alginate sponges. The consequence of this is relevant: for an application as a BAL, the beads should thus be seeded with the required amount of cells, in contrast with other systems where cells were expected to proliferate before offering a required extracorporeal supply (e.g. AMC-BAL).




2.2.3. Cell differentiation study

In order to study the differentiation of cells, on day 0, 7, 10, and 14 post-encapsulation the subcellular localization of proteins typically expressed by hepatoblasts and mature hepatocytes was assessed by immunofluorescence (Figure 46) (experiments realized in collaboration with Dr Antonietta Messina and Dr Anne Dubart-Kupperschmitt (INSERM U1193)). On day 0 post-encapsulation, hepatoblasts were present since we observed their typical markers such as AFP, HNF 6 and CK-19. During the differentiation process, the level of hepatoblasts markers decreased while the mature hepatocytes markers showed up (ALB, HNF 4, CYP 3A4, A1AT, UGT1A1, SR-B1,

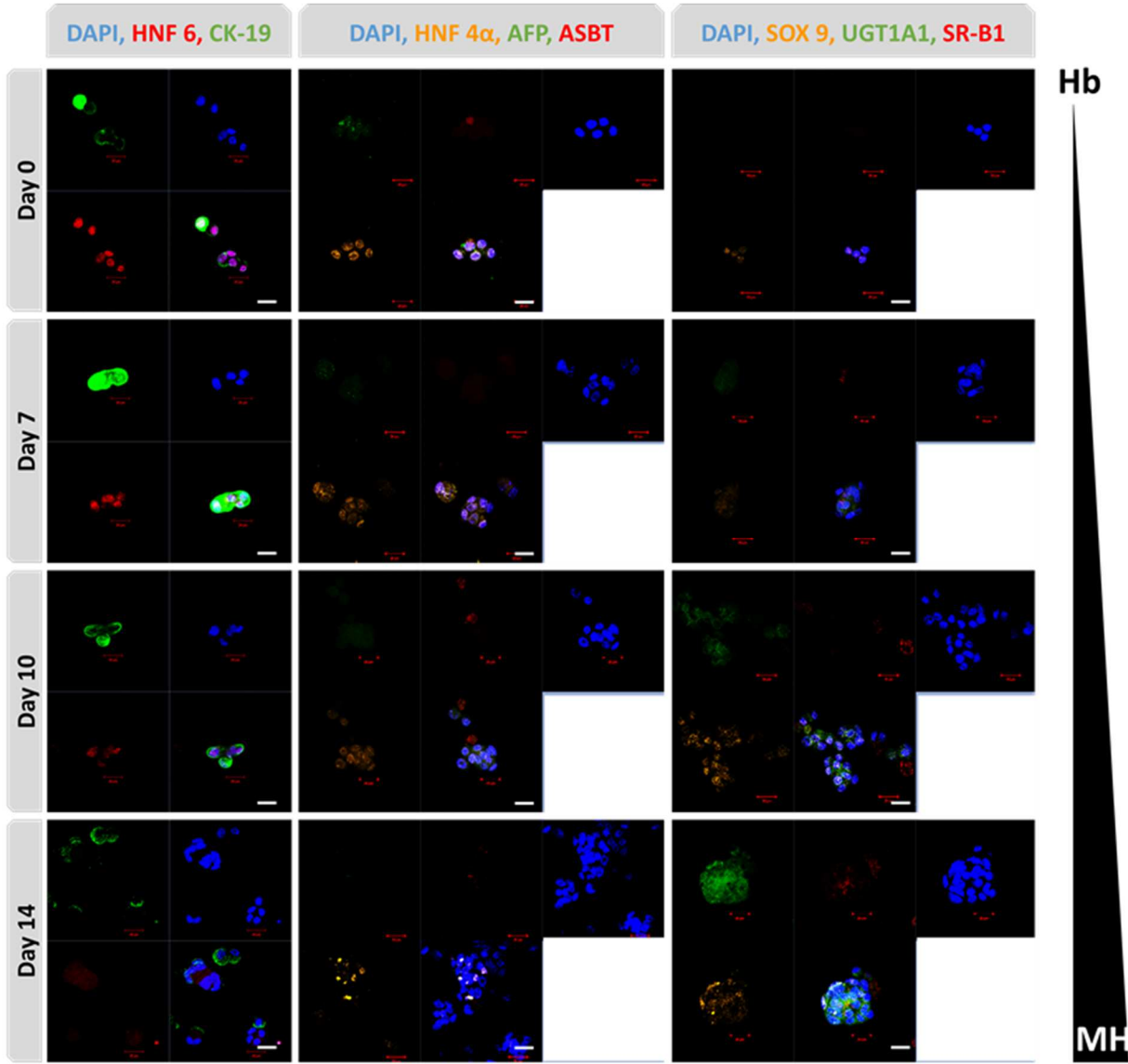
BSEP). Those qualitative observations are summarized in table 12. In addition, the increasing in albumin secretion rate (Figure 42) previously mentioned, correlated with hepatocytes differentiation.

| Cell state | Marker | Localization | Day 0 | Day 7 | Day 10 | Day 14 |
|---------------------------|----------------|--------------|--|-------|--------|--------|
| Hepatoblasts | HNF 6 | N |  | | | |
| | CK-19 | PM, IFs, C |  | | | |
| | AFP | C |  | | | |
| Mature Hepatocytes | HNF 4 α | N |  | | | |
| | ALB | C |  | | | |
| | CYP 3A4 | ER |  | | | |
| | A1AT | ER, C |  | | | |
| | UGT1A1 | ER |  | | | |
| | SR-B1 | PM |  | | | |
| | BSEP | BC |  | | | |
| Cholangiocytes | SOX9 | N |  | | | |
| | ASBT | PM |  | | | |
| | CK-7 | C |  | | | |

Tab. 12: Qualitative evolution of cell differentiation over time

Legend: C = cytosol; PM = plasma membrane; N = nucleus; IFs = Intermediate filaments; ER = endoplasmic reticulum; BC bile canaliculi;  (increasing expression),  (decreasing expression),  (constant expression)

In addition, some markers typical of cholangiocytes were analysed by immunofluorescence staining, such as the apical sodium dependent bile acid transporter (ASBT, protein involved in the enterohepatic recirculation of bile acids), the transcription factor SOX9 (involved in the bile duct morphogenesis¹⁸²), and the cytokeratin CK7 (cytokeratin specifically expressed by cholangiocytes). We observed that ASBT, CK-7, and SOX9 started to show up after day 10.



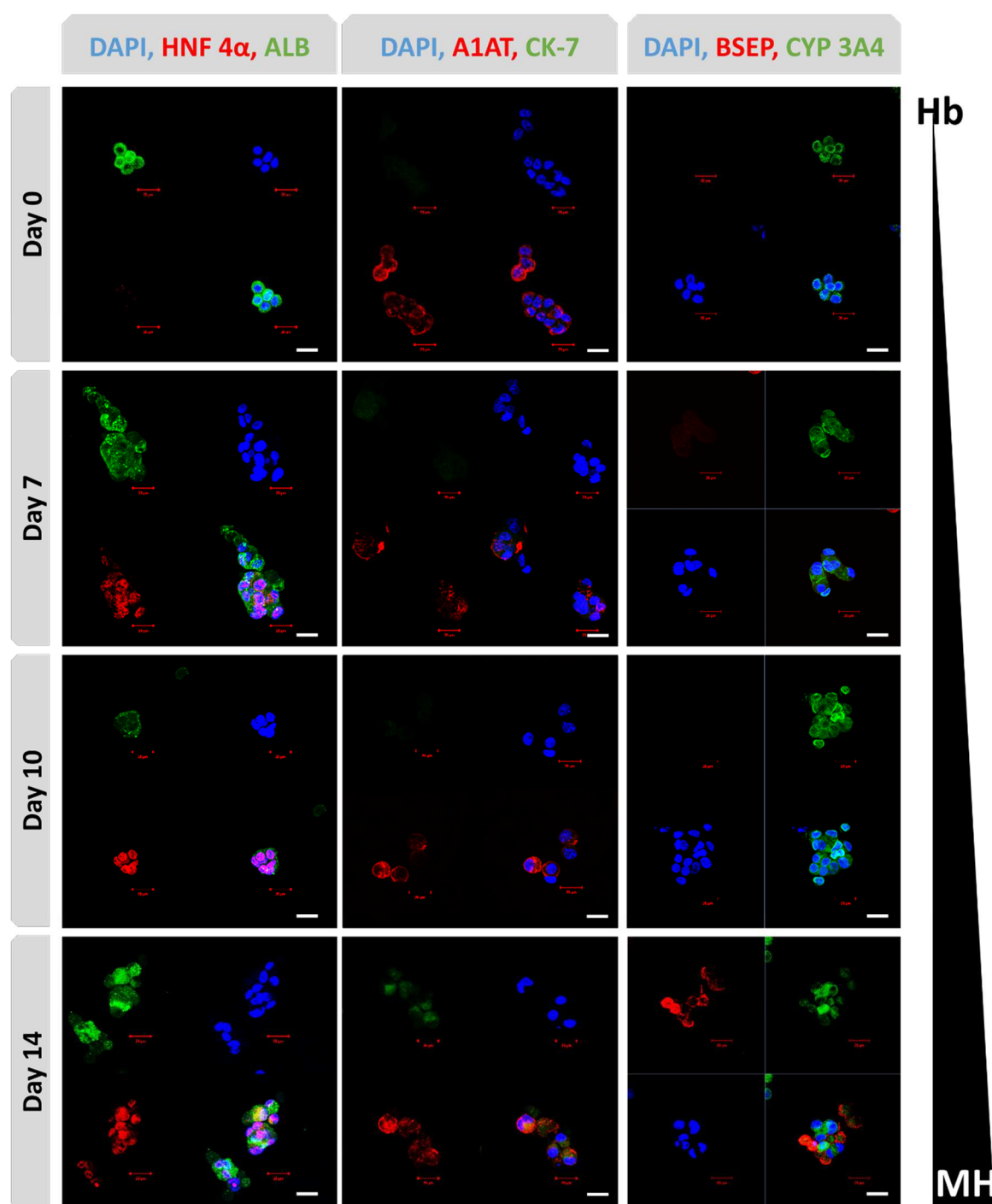


Fig. 46: Immunofluorescence staining over time (confocal microscopy). Hepatoblast markers (Hb): HNF 6 in red, CK-19 in green, AFP in green, nuclei in blue. Mature hepatocyte markers (MH): ALB in green, HNF 4 in red and in sand colour, CYP 3A4 in green, A1AT in red, UGT1A1 in green, SR-B1 in red, BSEP in red. Cholangiocyte markers: SOX 9 in sand colour, ASBT in red, CK-7 in green, nuclei in blue. Scale bar: 20 μm

A staining for the tight junction Zonula Occludens protein 1 (ZO-1) (Figure 47), a protein localized in the sub-apical membrane of hepatocytes, was also realized. This staining was performed on day 10, since we had no more samples on day 14, and it confirmed the presence of these junctions between cells. We supposed that if the protein was present on day 10 then it was also present on day 14. The auto fluorescence measured (Figure 47 in green) is linked with the presence of mature hepatocytes containing endogenous fluorophores, such as proteins, bound and free NAD(P)H, flavins, vitamin A, arachidonic acid.

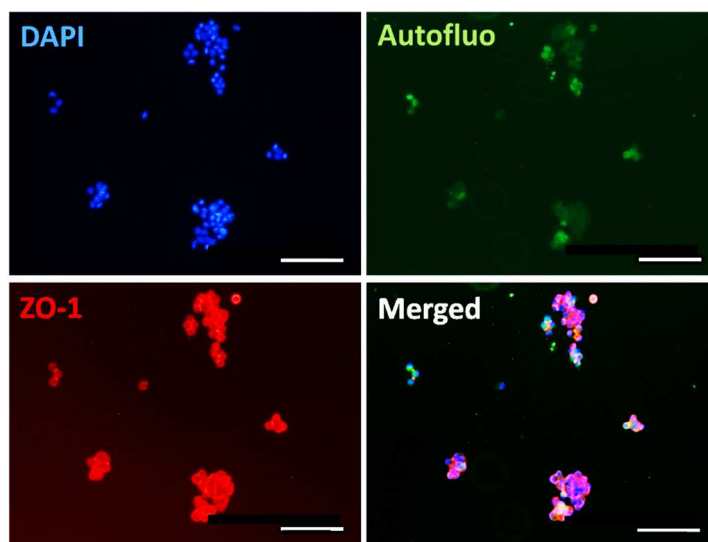


Fig. 47: Immunofluorescence staining of ZO-1 on day 10 (epifluorescence microscopy). In red: ZO-1; in green: hepatocytes auto-fluorescence; in blue: cell nuclei. Scale bar: 100 μ m

To conclude the step 1, we demonstrated that HepaRG cells were able to freely form spheroids when entrapped in 1.5% alginate beads. After 14 days of culture, these encapsulated cells presented a wide range of hepatic functions (protein synthesis, enzymatic activities and biotransformation of toxins) that are necessary for bioartificial liver application. Parts of those results were valorised with our article entitled "HepaRG selfassembled spheroids in alginate beads meet the clinical needs for bioartificial liver" (DOI: 10.1089/ten.TEA.2019.0262), published on Tissue Engineering Part A on 20th February 2020 ¹³⁷.

Based on these promising results, we decided to use this biomass for fluidized bed setup. However, a transition phase was necessary to adapt the biomass (until now characterized in shaken culture) to the new type of culture. The next step elucidates the details of this transition phase.

2.3. Step 2: Optimization of the biomass for fluidized bed bioreactor

After the previous characterizations, we carried out a new optimization campaign to implement this biomass to a fluidized bed bioreactor (FB). This characterization is a paramount for our final application since in the small-scale BAL device that we developed during this thesis (later presented in chapter 5), the biological component is a bioreactor where encapsulated cells will be subjected to perfusion. The transition from stirred culture to FB setup involved an optimization phase. In fact, we needed to add glass microparticles (GM) into the beads, in order to increase their

density and obtain a homogeneous fluidization in the specific culture medium used for the experiments in FB (later explained). In addition, we decided to increase cell concentration from 5 million cells/mL alginate (5 M/mL) to 10 M/mL, in order to benefit from a more consistent biomass for the future preclinical trials. In particular, we investigated if GM and the new cell concentration had an impact on the metabolic performance and viability of cells.

The experimental design for step 2 is shown in figure 48. After 2D amplification in culture flasks, cells were encapsulated in the different conditions:

- DCs 1.5%, cell density 5M/mL, the gold standard, used as control
- DCs 1.5% 5M/mL + 1.25% w/v glass microparticles (GM) with diameter between 1-50 μm (PGB-05 Kisker). GM were mixed to the alginate-cell solution before encapsulation
- DCs 1.5% 10M/mL

The culture conditions were kept in shaken culture in a humidified environment at 37 °C, 5 % CO₂. The metabolic performance was tested on day 14.

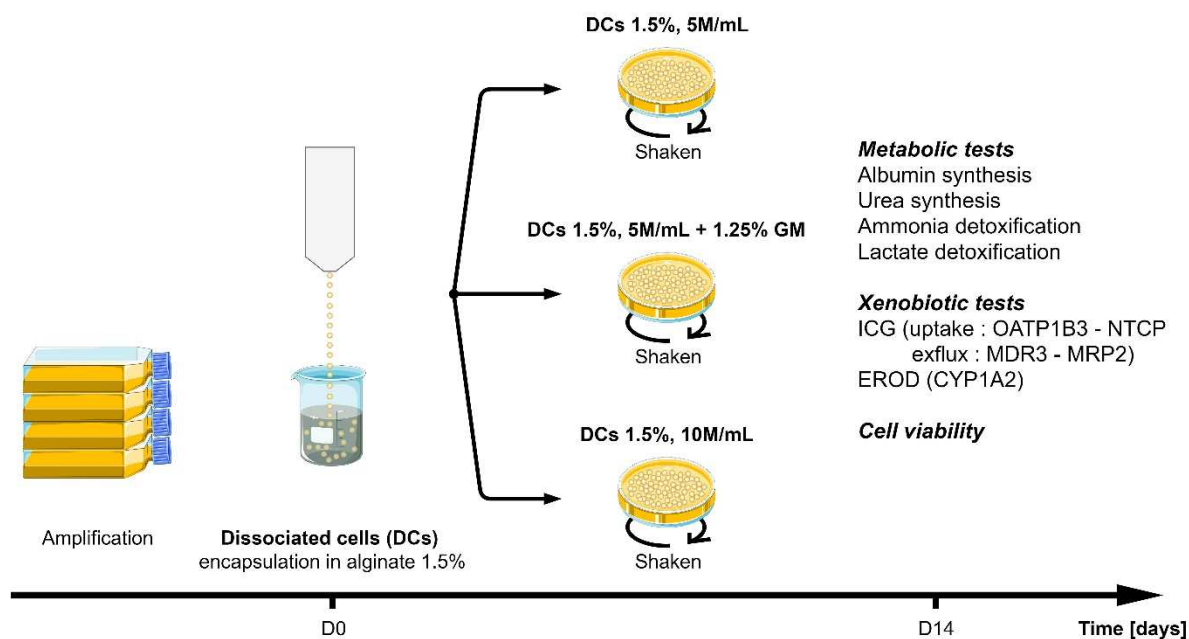


Fig. 48: Experimental setup, phase I step 2

2.3.1. Effect of the presence of glass microparticles in the alginate beads

For subsequent experiments conducted in fluidized bed bioreactors (step 3), we decided to use a supernatant that could mimic human plasma in terms of volumetric mass density and viscosity in view of a human clinical application. Therefore, we supplemented the HepaRG proliferation medium with bovine serum albumin (BSA) up to the concentration of 70 g/L, corresponding to the average total protein concentration in human plasma. This new medium was defined "equivalent plasma". Preliminary tests showed that the alginate beads, when put in contact with this medium, floated and did not fall. This would not allow obtaining a homogenous fluidized bed. Fluidization process is in fact governed the Archimedes number (Ar), in which the density difference between the solid phase (the beads) and the liquid one plays a key role. This relation is described by the

following equation (Eq. (1)). Alginate beads and fluid present very close density, since alginate beads are mostly composed of fluid.

$$Ar = [d_b^3 * g * \rho_f * (\rho_b - \rho_f)] / \mu_f^2 \quad [\text{Eq. 1}]$$

with d_b : bead diameter, g : gravity constant, ρ_f fluid density, ρ_b : bead density, μ_f : fluid viscosity.

Therefore, based on the investigation by Figaro et al. 2017¹⁷², we decided to add glass microparticles (GM) to the alginate solution, before the encapsulation process, in order to increase the density of the alginate beads. They measured that a similar medium to ours presented a density of 1.016 kg.m⁻³. In order to obtain beads more dense than this medium, they added glass microparticles (density 2.5 kg.m⁻³) to the alginate solution at a concentration of 1.25% w/v. In this way, the beads stopped floating and they obtained homogeneous fluidization in the bioreactor.

We evaluated then their effect on the metabolic properties and viability of encapsulated HepaRG cells. For simplicity reasons, we tested these elements on regular HepaRG proliferation medium, without excess of BSA. We compared alginate beads with versus without glass microparticles at concentration 1.25%w/v, at cell density 5 million/mL. On day 14 post encapsulation, we tested albumin (Figure 49A) and urea synthesis rate, ICG releasing rate (Figure 49B), EROD activity (Figure 49C). These activities were comparable between both conditions. The activity of the CYP 1A1/2 was 10 times stronger when GM were present.

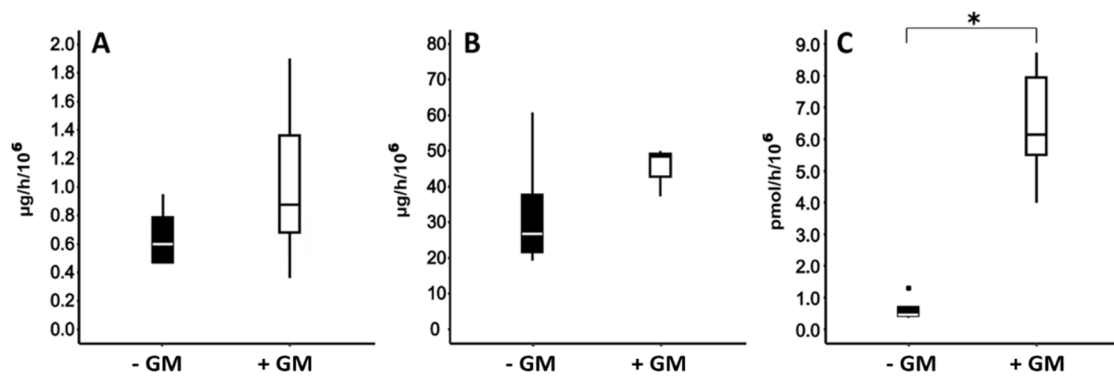


Fig. 49: Metabolic performance between encapsulated cells with (+ GM) and without glass microparticles (- GM) in proliferation HepaRG medium on day 14. Albumin synthesis (A), ICG releasing rate (B), EROD activity (C). Significance analysed by Mann-Whitney test. * indicated outliers. N ≥ 3

In parallel, we studied the ability of cells to detoxify typical ALF toxins, in view of a future application of these cultures for a BAL. Cells were incubated for 2 hours in BAL function test medium containing ammonia and lactate. The ability of cells to detoxify these toxins is respectively shown in figure 50B and 50C, while the albumin synthesis rate in figure 50A. The metabolic activities measured were comparable between the two conditions. No urea secretion was detected.

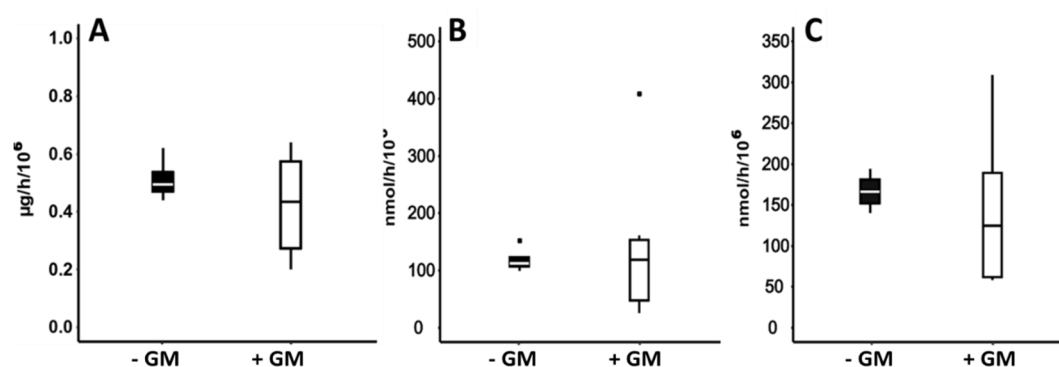


Fig. 50: Metabolic performance between encapsulated cells with (+ GM) and without glass microparticles (- GM) in BAL function test medium on day 14. Albumin secretion rate (A), ammonia (B) and lactate (C) detoxification rate. * indicated outliers. N ≥ 3

Overall, the presence of glass microparticles did reduce neither the metabolic performance nor the cell viability, as qualitatively observed through live/dead test in the figure 51. Therefore, our observations are similar to those by Figaro et al.¹⁷², where the presence of glass microparticles had not deleterious effects on HepG2/C3A cells viability and metabolism.

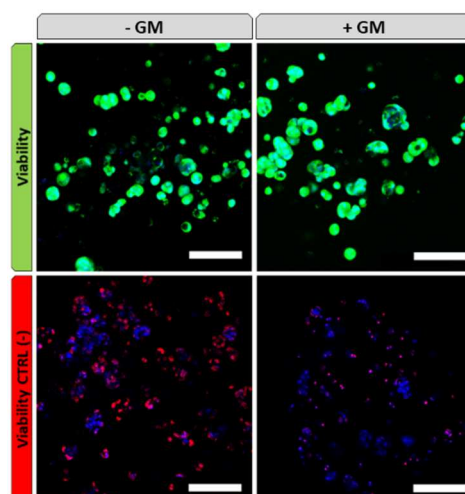


Fig. 51: cell viability (confocal microscopy) of cells in beads containing (+ GM) or not glass microparticles (- GM). In green (Calcein AM): viable cells, in red (ethidium homodimer-1): dead cells, in blue (Hoechst 33342 dye): cell nuclei. Scale bar: 100 µm

Unfortunately, we were not able to measure the mechanical properties of beads with GM due to technical problems. However, according to the literature, these properties should not vary in the presence of GM¹⁷².

2.3.2. Effect of increasing cell concentration in the alginate beads

In the context of BAL, one of the most important problems is the accessibility of large quantities of cells. In our case, the use of the cell line HepaRG ensures an almost infinite cell availability at affordable costs. The main challenge is the number of cells content to be placed into the bioreactor, capable of ensuring a therapy with beneficial effects. Indeed, as highlighted in chapter 1, in addition to the number of cells, it would be important to consider their functionality *in vitro*. Starting from the functionality of the cell model used (HepaRG in our case), it is possible to calculate the number of

cells needed for BAL therapy, referring to the functionality of primary hepatocytes (or the true liver function). This observation will be taken up in the discussion section of this chapter.

The fluidized bed bioreactor that will be implemented in our small-scaled BAL device has an internal volume of 19 mL. In order to ensure a proper fluidized bed, it can be filled up to a maximum of 60% of its internal volume, corresponding to a volume of alginate beads of around 11 mL. This volume of beads is therefore a fixed parameter. Consequently, what can be varied is the number of total cells in the alginate solution (or cell density). In order to have a higher cell availability, we decided to increase the cell density in the alginate beads to 10 million cells/mL. Since it is known that cell concentration in the beads significantly influences cell activity and viability¹⁸³, we decided to investigate the metabolic performance between the two cell densities mentioned above.

At day 14, we tested albumin (Figure 52A) and urea synthesis rate, ICG releasing rate (Figure 52B), and EROD activity (Figure 52C). When reported to the number of encapsulated cells, albumin synthesis was found 2.5X stronger for the gold standard, ICG releasing rate seemed higher for 10M/mL, and EROD activity was 5.5X stronger for the condition 10M/mL.

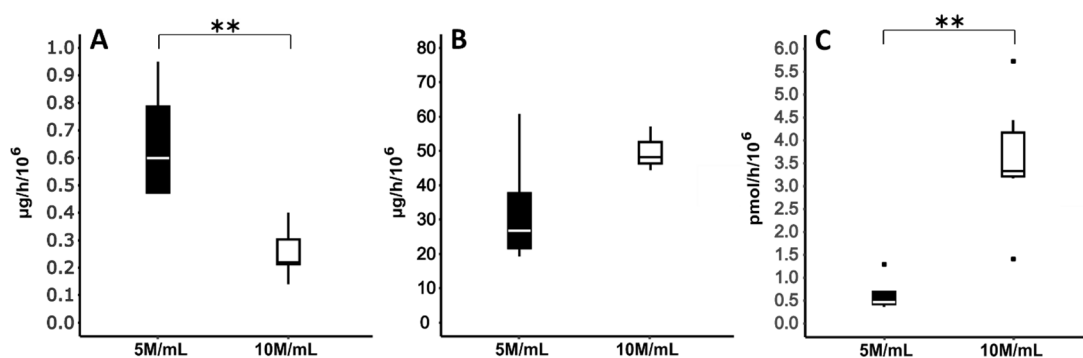


Fig. 52: Metabolic performance on day 14 between cell densities 5M/mL and 10 M/mL in proliferation HepaRG medium. Albumin synthesis (A), ICG releasing rate (B), EROD activity (C). Significance analysed by Mann-Whitney test. * indicated outliers. N ≥ 3

In parallel, we studied the ability of cells to detoxify typical ALF toxins, in view of a future application of these cultures for a BAL. Cells were incubated for 2 hours in BAL function test medium containing ammonia and lactate. The ability of cells to detoxify these toxins is respectively shown in figure 53B and 53C, while the albumin synthetic rate in figure 53A. The metabolic activities measured tended to be stronger for the condition 5M/mL. Ammonia detoxification and lactate clearance rates were significantly stronger for the condition 5M/mL. For cell density 10M/mL production of lactate was observable. No urea secretion was detected.

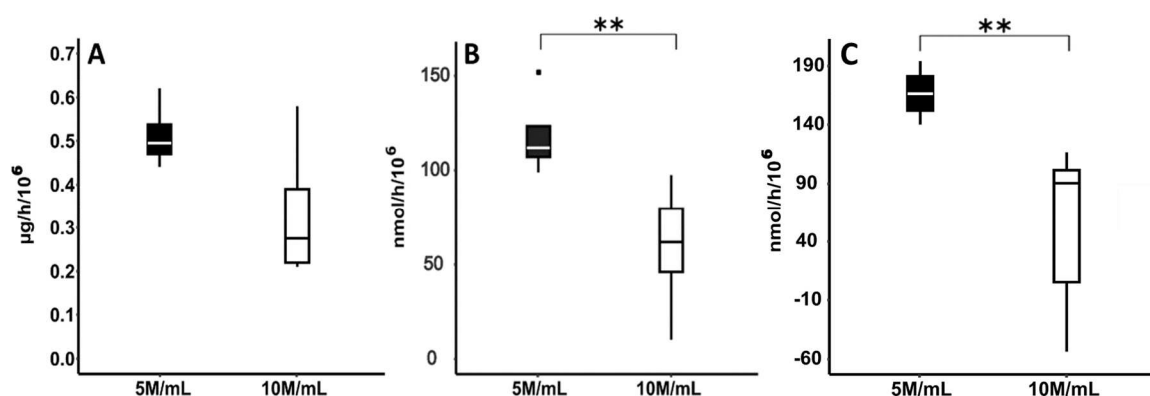


Fig. 53: Metabolic performance on day 14 between cell densities 5M/mL and 10 M/mL in proliferation BAL function test medium. Albumin synthesis (A), ICG releasing rate (B), EROD activity (C). Significance analysed by Mann-Whitney test. * indicated outliers. N ≥ 3

According to these results, it appears that the concentration of 5 M/mL demonstrated better performance “per cell” than the concentration of 10 M/mL.

However, when results are considered as net activity “per bioreactor” (i.e. a Petri dish in this preliminary analysis), without normalising by the number of cells seeded, the condition 10M/mL showed higher global activities, especially for the xenobiotic metabolism. In HepaRG proliferation medium, albumin synthesis rate was comparable between the two conditions (Figure 54A), ICG releasing rate was about 3.4X stronger for 10M/mL (Figure 54B), and EROD activity was 11X stronger for 10M/mL (Figure 54C).

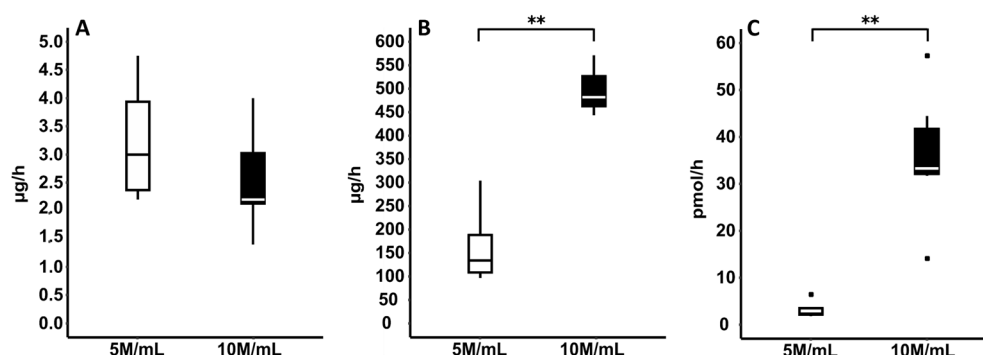


Fig. 54: Metabolic performance “per bioreactor” on day 14 between cell densities 5M/mL and 10 M/mL in proliferation HepaRG medium. Albumin synthesis (A), ICG releasing rate (B), EROD activity (C). Significance analysed by Mann-Whitney test. * indicated outliers. N ≥ 3

In BAL function test medium, albumin synthesis, ammonia detoxification, and lactate clearance rates remained comparable between the two conditions tested, with slight tendency to be stronger for 10M/mL (Figure 55).

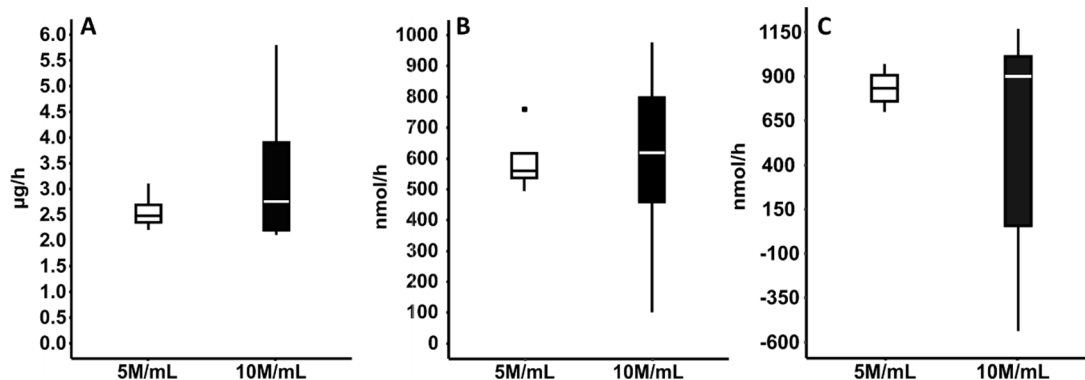


Fig. 55: Metabolic activities on day 14 in BAL function test medium between 5 million cells/mL and 10 million cells/mL of alginate 1.5%. Albumin secretion rate (A), ammonia (B) and lactate (C) detoxification rate. * indicated outliers. N ≥ 3

Cell viability was qualitatively evaluated by live/dead assay at the end of the experiments, exploring different sections of the beads, from the outer part to its core (Figure 56). No difference in cell viability is observable. Therefore, cell concentration did not affect cell viability.

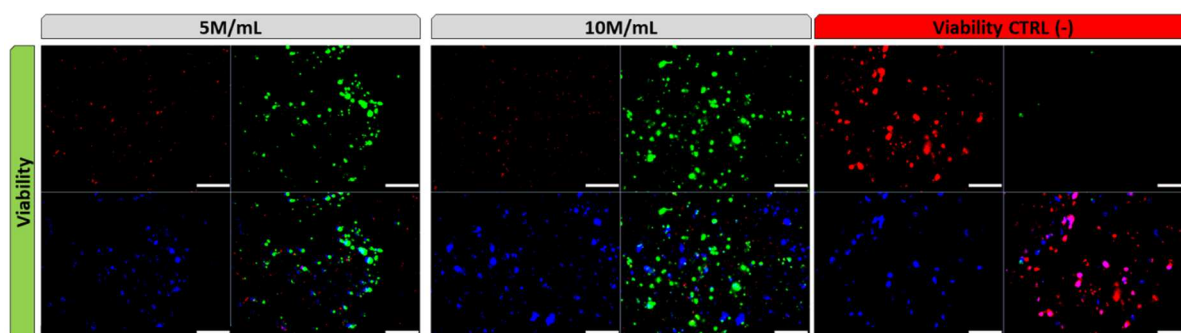


Fig. 56: Cell viability (confocal microscopy) between cell density 5 M/mL and 10 M/mL on day 14. In green (Calcein AM): viable cells, in red (ethidium homodimer-1): dead cells, in blue (Hoechst 33342 dye): cell nuclei. Scale bar: 250 µm

Overall, based on these observations, we decided to proceed with the experiments on fluidized bed bioreactor using the cell density 10M/mL + 1.25% w/v glass microparticles.

2.4. Step 3: Culture of encapsulated cells on fluidized bed bioreactor

Once optimized the biomass, we carried out experiments in order to study the cell behaviour in fluidized bed bioreactor (FB). Our previous experiments showed that glass microparticles did not affect the metabolic properties and viability of cells and that the cell density of 10 M/mL results in better global cell activity. As a result, experiments on FB were performed on cell density of 10 M/mL of alginate 1.5% + 1.25% w/v glass microparticles.

In order to investigate the role of fluidization on cell behaviour, the following experimental setup was used (Figure 57). After 2D amplification in culture flasks, cells were recovered by trypsinization and mixed with a solution of alginate 1.5% containing 1.25% of GM at cell density 10 M/mL. Encapsulated cells were cultured in petri dishes with 8 mL of proliferation medium, in continuous orbital shaking (60 rpm) and in a humidified environment at 37 °C, 5 % CO₂ (i.e. "shaken culture"), for 14 days. On day 14, beads were divided between the two conditions:

- Shaken culture: total biomass content of 1 mL of beads equivalent to 10 million of cell seeded.
- Perfused culture (FB): total biomass content of 5 mL of beads equivalent to 50 million of cell seeded.

At this point, cells were incubated for 2 hours with a homemade medium, containing proliferation medium + 70 g/L of bovine serum albumin (BSA) ("equivalent plasma"). For the condition shaken culture, beads were incubated in 8 mL of this medium while for the perfused culture in 40 mL (5X higher, so as to maintain a linearity between total biomass content and culture medium, in the two culture conditions). The aim was to mimic a human healthy plasma in terms of density and viscosity and allow cells to adapt at this new medium (i.e. during the priming of the circuit, before BAL therapy). This was done because the ultimate goal of this device will be the human application.

After 2 hours of cell adaptation, beads were transferred in another homemade medium, called pathological plasma model. It has the same composition of the previous, but it contains also 1.5 mM ammonium chloride and 2 mM L-lactate, toxins accumulating in human plasma during ALF. For the condition shaken culture, beads were incubated in 7.5 mL of this medium while for the perfused culture in 37.5 mL. In this new environment, the following activities were investigated along 6 hours of incubation: albumin and urea synthesis, ammonia detoxification and lactate clearance. Aliquots of supernatant were taken on time 0, 2 and 6 hours. The latter is the estimated time interval for the future BAL therapy. At the end of each experiment, microbeads were collected and assessed for cell viability.

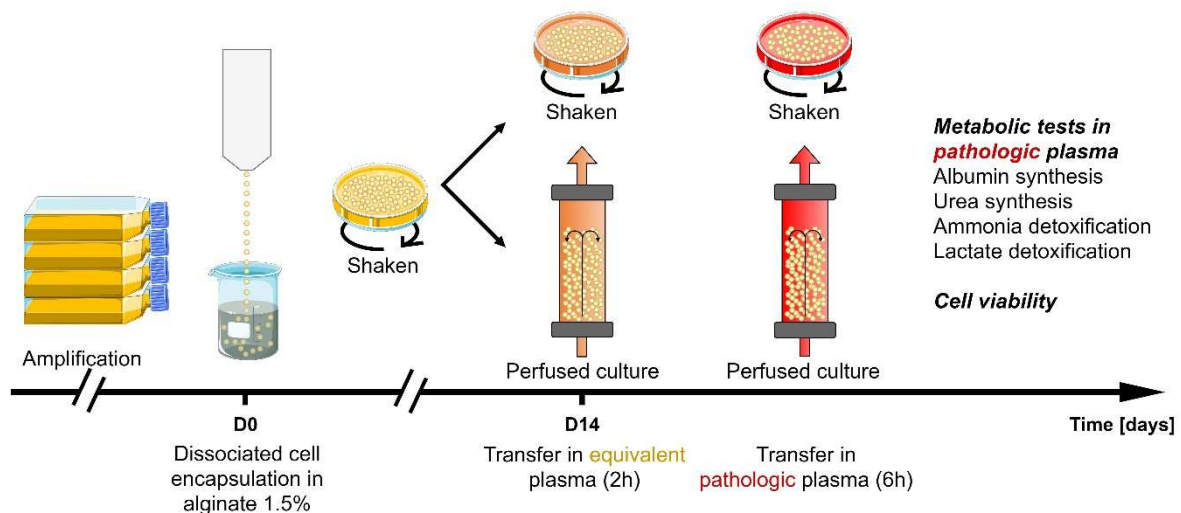


Fig. 57: Experimental setup, phase I step 3

The aim of these experiments was to evaluate if the cell metabolic activity in the bioreactor is similar or higher in comparison to the shaken condition, since the bioreactor is what we will use for our small-scaled bioartificial liver.

During the 14 days of shaken culture, we evaluated albumin secretion on different days in order to verify the functionality of cells. Albumin secretion rate increased over time, with a pick at day 10 (Figure 58) and overall on day 14 the cells were metabolically active.

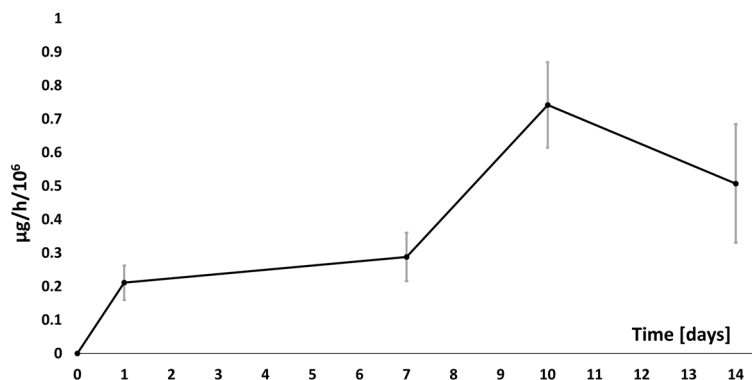


Fig. 58: Albumin secretion rate over time. $N \geq 3$

On day 14, part of the biomass was transferred in the fluidized bed bioreactor (5 mL of beads, corresponding to 50 million cells) and another part kept in shaken culture as control (1 mL of beads, 10 million cells). In this way, it was possible to compare the metabolic activities in the two systems of culture. After 2 hours of adaptation in equivalent plasma, cells were incubated with the pathological plasma model for 6 hours. In this medium, the cell metabolic performance and viability were tested. This long time of incubation mimicked a future BAL therapy.

The metabolic performance was tested evaluating the synthesis of albumin (Figure 59A) and urea rate, the detoxification of ammonia (59B) and clearance of lactate (59C) in pathological plasma model. No urea was detectable. Overall, FB setup seemed to favour cells activities. Albumin secretion and ammonia detoxification rates are comparable. Of note, while lactate is produced in shaken culture, it is consumed in FB setup.

The results obtained were normalised by the quantity of marker analysed/6 hours of incubation/cell seeded. This normalization was necessary to compare the two cultivation methods, since the quantity of biomass as well as the volume of medium (7.5 mL of beads for shaken and 37.5 mL for perfused culture), was not the same.

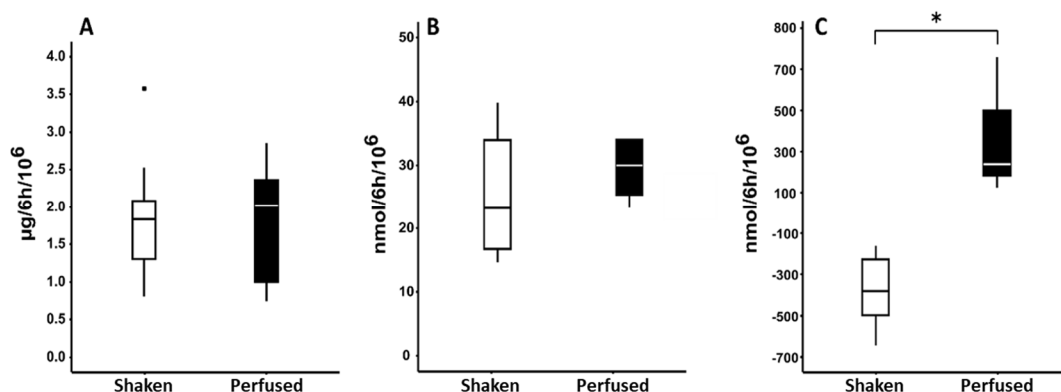


Fig. 59: Albumin secretion (A), ammonia (B) and lactate (C) detoxification in shaken and perfused (FB) after a 6h therapy in pathological plasma model. Significance analysed by Mann-Whitney test. * indicated outliers. $N \geq 3$

Cell viability was evaluated after the metabolic tests performed and cells remained highly viable for both conditions, in comparison with the negative control where cells were killed by ethanol exposure (Figure 60).

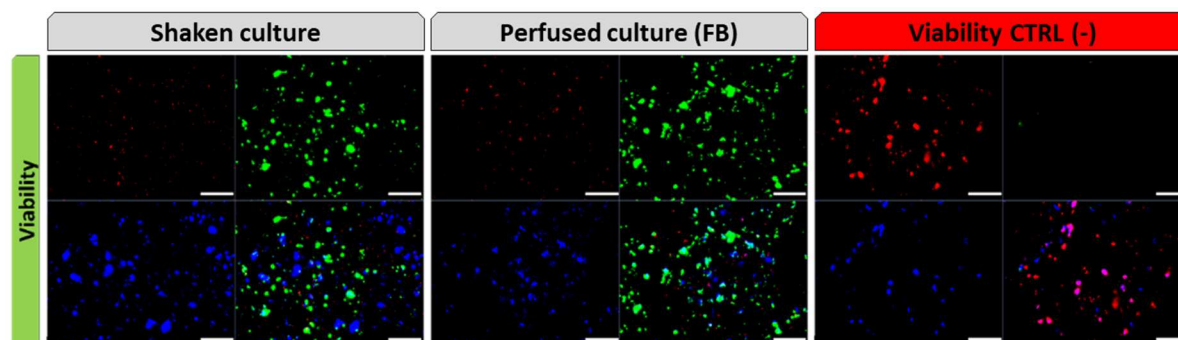


Fig. 60: Cell viability shaken versus perfused culture. In green (Calcein AM): viable cells, in red (ethidium homodimer-1): dead cells, in blue (Hoechst 33342 dye): cell nuclei. Scale bar: 250 μ m

Overall, we showed that the biomass in FB setup maintained the metabolic capacities registered for shaken culture and, of note, had a positive effect on lactate clearance. These results are very promising for future application of this FB on the small-scaled BAL developed in our laboratory.

However, during the experiments conducted with the pathological plasma model, we observed a phenomenon of alginate beads deterioration, which was more pronounced in FB setup due to perfusion and hydrodynamic shear stress. This phenomenon is in line with the mechanical investigation carried out, which showed a loss of mechanical stability of the beads during the long culture period (Figure 35). For this reason, many experiments conducted on FB failed and others were of poor reproducibility. The need to reinforce the mechanical stability of alginate beads through a polymeric coating progressively emerged. This led to a new campaign of experiments and characterizations that will be presented in the next chapter 4.

3. Discussion

In phase I, we optimized the hepatic biomass for fluidized bed bioreactor, the component of our small-scaled BAL, exploring different culture setups. The choice of this type of bioreactor, developed in our laboratory and in others¹⁸⁴, was supported by the promising results obtained in our previous works^{1,149,172} and by other investigators cited in the introduction of this chapter. However, further clinical applications require the production of large quantities of encapsulated cells in order to obtain a functional and costeffective biomass at the human scale. The hepatic cell functions required are mainly protein synthesis (albumin and clotting factors), ammonia and lactate elimination (both implicated in hepatic encephalopathy and cerebral oedema), xenobiotic detoxification (enzyme machinery involved in cleaning toxins accumulating during ALF)⁷⁰. In this chapter, we demonstrated that the biomass here developed showed those important features.

Preliminary investigations allowed us to optimize the cell culture setup, leading to choose dissociated cells cultivated into a 1.5% alginate beads. During the days of culture, these cells freely formed spheroids with polarized structure. On day 14, cells showed higher metabolic performance

(and higher degree of differentiation) for those functions required for BAL. Starting from this biomass, we performed other optimizations required for its use in fluidized bed bioreactor, such as the addition of glass microparticles, and the increasing in cell density. Finally, the optimized biomass was tested in fluidized bed bioreactor using a pathological plasma model to mimic a clinical therapy, demonstrating important functions required for BAL, such as ammonia detoxification and lactate clearance. Importantly, this culture setup can easily be scaled-up for production of large quantities of encapsulated cells to use in clinical treatment of ALF.

In the gold standard culture developed, most of the metabolic activities were stronger on day 14 probably due to a better degree of cell aggregation and differentiation. To demonstrate it, we provided a study of DCs 1.5% differentiation over time. It is known that HepaRG cell line in 2D culture requires 14 days of culture for its differentiation in hepatocyte- and cholangiocyte-like cells. We tried to understand if it is the same case in 3D culture. Rebelo et al.¹⁴⁷ studied the 3D differentiation of encapsulated HepaRG spheroids on day 14 post-encapsulation. Therefore, our goal was to understand if the cells were ready (as biomass for future BAL clinical application) and metabolically active before 14 days of culture. According to our results, it appears that encapsulated cells, like for 2D cultures, needed 14 days to fully display the typical hepatocyte markers and those activities required for BAL application. Overall, our results show that cell viability, for all the condition tested, was affected neither by the encapsulation process nor by the long-time culture cells, nor by the exposition to a toxic culture media, containing typical ALF toxins. Inside the beads, cells were able to self-rearrange, forming aggregates. Aggregates dimension increased over the days of culture but remained in a range (maximum 120 μm) where mass transfer was not affected, and where oxygen gradient can take place¹⁸⁵. This ability of dissociated hepatocytes to assemble into spheroid-like structures can be exploited in the development of tissue substitutes. For example, the use of those self-assembled spheroids rather than isolated cells in a bioartificial liver device may provide benefit in terms of function and scaling-up considerations^{186,187}. Hepatic cells are epithelial cells that need to be anchored to a substrate. Alginate is an inert biomaterial that does not offer any site of attachment to cells. Therefore, cells are forced to interact with each other. We observed the formation of tight junctions ZO-1 (a marker of spheroid formation for cell-cell contact¹⁷⁵) between the sub-apical membranes of the cells, those anchors that maintain the union between cells and the compactness of the spheroid. It has been observed that when HepaRG in 2D configuration are cultured in orbital shaking, hepatic differentiation and metabolic functions are both positively affected due to higher mitochondrial biogenesis¹⁸⁸. Also in our experimental setup, the encapsulated cells are kept in orbital shaking. Taken together, the presence of self-assembled spheroids and this kind of shaken culture described could induce a gain of function in the whole cell metabolic performances that can explain why some of our activities are stronger in comparison with other authors. Chamuleau's group seeded HepaRG in the Amsterdam Medical Center Bioartificial Liver (AMC-BAL), a membrane-based bioreactor in which cells are in direct contact with plasma. They reported ammonia (around 27 $\text{nmol/h}/10^6$) and lactate (around 10 $\text{nmol/h}/10^6$) detoxification with lower rates in comparison with our results (respectively $119 \pm 20 \text{ nmol/h}/10^6$ and

$167 \pm 24 \text{ nmol/h/10}^6$)¹⁸⁹. These differences may be explained by the fact that in our system, the cells formed spheroids on the one hand, and were protected from hydrodynamic shear stress by the alginate structure, on the other. Compared to HepG2/C3A, we observed that albumin production was in the order of magnitude, and that all phases of enzymatic biodegradation were present, although they were lower than those of primary human hepatocytes just after their collection. Considering Selden's promising results in preclinical studies with HepG2, the same could be expected with HepaRG.

The following tables summarize a comparison of our results with some other published results, regarding both HepaRG and primary human hepatocytes. In order to be comparable to the results of other authors, our results were normalised:

- By the number of cells counted (Table 13) at the end of the experiments. Via DNA quantification we counted $4.5 \pm 0.9 \times 10^6$ cells (mean \pm standard deviation)
- By the milligrams of proteins quantified (Table 14) at the end of the experiments. Via total proteins quantification, we found about 0.12 mg of proteins per million of cells

Overall, our activities are in the order of magnitude of those measured by other authors. While our activities of detoxification of ammonia and lactate are undoubtedly superior, those related to cytochromes are often inferior. This is due to the fact that

- In many cases, the techniques for studying the activities of cytochromes are different
- Our cells are cultivated without DMSO, a stimulator of the cytochromes expression
- In most cases, the authors report the activities of cytochromes induced with prototypical inducers (not in our case)

In any case, our results are very encouraging and fall within the range of values reported in the literature.

We have previously pointed out that it is relevant to analyse functionality rather than the number of cells to be used as biomass for a BAL. In light of our results, taking albumin secretion and ammonia detoxification rates as markers, we observed that the functionality of our cells is similar to that of primary hepatocytes (see table 13, especially Poyck et al.¹⁹⁰, who cultivated primary hepatocytes in the AMC-BAL bioreactor). Consequently, we can conclude that for a BAL therapy, we can use a quantity of biomass equivalent to the minimum amount of primary hepatocytes required for a BAL (about 200 gr for human application).

| Normalization : quantity of metabolite/hours of incubation/10 ⁶ counted | | | | | | | | |
|--|---------------|---|--|---|---|---|--|--|
| Author | Cell type | Culture condition | Albumin production (μg/h/10 ⁶) | Urea production (μg/h/10 ⁶) | Ammonia detox (nmol/h/10 ⁶) | Lactate detox (nmol/h/10 ⁶) | CYP 1A2 (pmol/h/10 ⁶) (test performed) | CYP 3A4 (pmol/h/10 ⁶) (test performed) |
| Our work | HepaRG | DCs encaps. in alg. beads 1.5% | 1.26 ± 0.82 | - | 153.5 ± 26.3 | 130.7 ± 33.37 | 0.67 ± 0.24 (EROD) | 1.48 ± 0.3 (BROD) |
| Lübberstedt et al., 2011 ¹⁹¹ | | 2D | 0.2 | 0 | - | -4.2 | 150 (EROD) | 0.01x10 ⁶ (Testosterone 6β-hydroxylation) |
| Gunness et al., 2013 ¹⁹² | | 2D | 0.33 | 0.06 | - | - | - | - |
| | | Spheroid culture | 1 | 1.8 | - | - | - | - |
| Rebello et al., 2015 ¹⁴⁷ | | 2D-DMSO | 0.125 | 1.25 | - | - | 2 × 10 ⁶ (Luciferase) | 3 × 10 ⁶ (Midazolam) |
| | | 2D+DMSO | 0.125 | 2 | - | - | 3 × 10 ⁶ (Luciferase) | 10 × 10 ⁶ (Midazolam) |
| | | Spheroids encaps in alg. beads 1% | 0.33 | 3 | - | - | 3.5x 10 ⁶ (Luciferase) | 13 × 10 ⁶ (Midazolam) |
| Lübberstedt et al., 2011 ¹⁹¹ | | 2D | 0.05 | 0.4 | - | -1.04 | 264 (EROD) | 0.0018x10 ⁶ (6β-OH-Testost.) |
| Mueller et al., 2011 ¹⁹¹ | Fresh PHH | 3D hollow-fibre bioreactor | 0.004 to 0.06 | 1.87 to 6.25 | - | - | 40 (Phenacetin) | 3.6 (Midazolam) |
| Biemel et al., 2012 ¹⁹³ | | 3D hollow-fibre bioreactor | - | 8 | - | - | 344 (Acetaminophen) | 6.6 (Midazolam) |
| Hengstler et al., 2000 ¹⁹⁴ | Cryopres. PHH | 2D | 0.2 | - | - | - | - | - |
| | Fresh PHH | | 0.25 | | | | | |
| Acikgoz et al., 2013 ¹⁹⁵ | Plated PHH | 2D | 0.07 | 30 | - | - | - | - |
| Tostões et al., 2012 ¹⁴¹ | PHH | 3D-spheroids in stirred tank bioreactor | 0.004 to 0.41 | 1.25 - 33.4 | - | - | - | - |
| Poyck et al. ¹⁹⁰ | MPH | | 0.08 to 0.16 | 1.7 to 14 | 180 to 230 | | | |
| | PHH | 0.075 to 0.13 | 510 to 850 | 90 to 110 | | | | |
| | | FHM | AMC-BAL | 0.1 to 0.22 | 340 to 680 | 0 to -100 (production) | - | - |

Tab. 13: Overview of a comparison between our results and other published results on various cell models in different culture conditions.

PHH: primary human hepatocytes, MPH: mature porcine hepatocytes, FHM: fetal human hepatocytes Results normalised by the quantity of marker produced or consumed/hour of incubation/million cells counted

| Normalization: quantity of metabolite/hours of incubation/mg proteins | | | | | | | | |
|---|-------------------|--------------------------------|-----------------------------------|--------------------------------|--------------------------------|--------------------------------|---|---|
| Author | Cell type | Culture condition | Albumin production (µg/h/mg prot) | Urea production (µg/h/mg prot) | Ammonia detox (µmol/h/mg prot) | Lactate detox (µmol/h/mg prot) | CYP 1A2 (pmol/h/mg prot) (test performed) | CYP 3A4 (pmol/h/mg prot) (test performed) |
| Our work | HepaRG | DSc encaps. in alg. beads 1.5% | 18.41 ± 08.01 | - | 2.02 ± 0.09 | 2.67 ± 0.26 | 11.29 ± 5.63 (EROD) | 25.07 ± 3.84 (BROD) |
| Gripon et al., 2002 ¹⁰¹ | HepaRG | 2D | - | - | - | - | 0.33 to 0.54 (Phenacetin) | 1 (Nifedipine) |
| | HepG2 | | | | | | 0.18 to 0.11 (Phenacetin) | < 0.1 (Nifedipine) |
| | PHH | | | | | | 0.1 to 25 (Phenacetin) | 0.5 to 30 (Nifedipine) |
| Gebhardt et al., 2003 ¹⁹⁶ | Cryopreserved PHH | 2D | - | - | - | - | 32.4 (EROD) | - |
| | Fresh PHH | | | | | | 39.6 (EROD) | |
| Gómez-Lechón et al., 2008 ¹⁹⁷ | Plated PHH | 2D | - | - | - | - | 136.2 (EROD) | - |
| Wenum et al., 2017 ¹⁹⁸ | HepaRG | AMC-BAL | 68 | 0.84 | 0.08 | 0.035 | - | 600 (Testosterone 6-hydroxylation) |
| Wang et al., 2019 ¹⁹⁹ | HepaRG | 2D | 0.42 | - | 0.6 | - | - | - |
| | HepaRG | Spheroids 3D | 0.84 | - | 2.44 | - | - | - |
| | Fresh PHH | 2D | 2.29 | - | 9.66 | - | - | - |

Tab. 14: Overview of a comparison between our results and other published results on various cell models in different culture conditions. PHH: primary human hepatocytes. Results normalised by the quantity of marker produced or consumed/hour of incubation/mg proteins

It is of note that encapsulated HepaRG are responsive to the ICG tests. The uptake of this dye is carried out by the transporters OATP1B3 and NTCP that are expressed at the basolateral plasma membrane of hepatocytes ¹⁶⁵ and excretion is regulated by the transporters MDR3 and MRP2 ¹⁶⁶, expressed in the hepatocytes apical (canalicular) membrane ²⁰⁰. In addition, ZO-1 and BSEP expression, and F-actin accumulating at cellular junctional sites of the cell aggregates, resembled interconnected bile canaliculi networks, structures that physiologically are in fact rich in actin ²⁰¹. This observation has also been noticed by Rebelo et al. ¹⁴⁷ on HepaRG spheroids and Hansen et al. ¹⁸⁶ on rat hepatocytes spheroids. The set of these observations indicate a highly polarized cellular organization favouring cell maturation ²⁰².

About the xenobiotic machinery, from a metabolic point of view, the enzymes of the xenobiotic signalling pathway (including transporters OATP1B3, NTCP, MDR3, MRP2, the CYP 1A1/2 and 3A4) showed positive activity. Of note, the CYP1A1/2 activity remained inducible via prototypical inducers on day 7 and 14. In addition, immunofluorescence staining demonstrated the presence of CYP 3A4 and UDP glucuronosyltransferase family 1 member A1 (UGT1A1, implicated in glucuronidation reactions). Overall, we showed that our cellular system included a variety of enzymes involved in xenobiotic detoxification.

The immunofluorescence staining highlighted also the presence (albeit slight) on day 14 of the scavenger receptor, class B type 1 (SR-B1), physiologically expressed in mature hepatocytes and implicated in cholesterol metabolism. Its presence could represent an added value for BAL applications since high-density lipoprotein (HDL) serum levels are affected in cases of ALF ⁷⁰.

Cholangiocyte-like markers (SOX 9, ASBT, CK-7) shows up from day 10. This late cellular specialization is similar to the physiological one, in which cholangiocytes differentiate later than hepatocytes. Qualitatively, it appeared that in the cellular aggregates observed there is a cholangiocyte/hepatocyte ratio that is more shifted toward the second. Overall, our hypothesis is that this culture method favoured more the differentiation towards hepatocyte-like rather than cholangiocyte-like cells, advantageous for BAL application. As stated in the introduction, while the presence of cholangiocyte-like cells results advantageous for certain applications (such as toxicology), it is not clear if their presence in a context of BAL is a positive fact or not. It is known that HepaRG cell line has the capacity to secrete certain solutes of bile such as bile acids ^{109,110} and that some bile acids presence in the blood can contribute to the pathogenesis of ALF ¹⁰. In a BAL system, the risk is to inject toxic bile compounds directly in the circulation of the patient. This is why it is important to implement, in the BAL device, artificial elements able to block part of those toxics. However, only better *in vivo* investigation will give the good response.

It has to be noticed that, in all the cases tested, no urea synthesis was detected with the kit used for our experiences (detection limit to 13 μ M). This observation can be related to the fact that cells are differentiating over days, losing their capacity to produce urea. This is coherent with other published works. In fact, it has been described that differentiated HepaRG showed low expression of key enzymes implicated in the urea cycle (arginase 1, ornithine transcarbamylase, and carbamoyl

phosphate synthetase I) and elevated glutamine synthetase activity¹⁰⁷. In ALF patients, ammonia levels are dangerously high. Physiologically, the ammonia elimination occurs via the urea cycle or via fixation into amino acids. If HepaRG lack of the key enzymes involved in urea cycle then the ammonia is preferably fixed into amino acids (glutamine) rather than being converted into urea. This can represent a problem in the context of ALF patients, since glutamine in high concentrations, compromises astrocyte functions, contributing to the progression of hepatic encephalopathy⁷³. Therefore, this observation has to be considered when working with HepaRG for the treatment of ALF. However, preclinical tests conducted on surgically ALF-induced rats using the AMC-BAL containing HepaRG, have shown encouraging results¹⁰⁶. Only *in vivo* experiments will be able to elucidate any complications due to this phenomenon.

During the transition phase from shaken to fluidized bed culture, we added glass microparticles (without any negative effect on cell metabolism and viability) and increased the cell density, passing from 5 M/mL to 10 M/mL. The latter choice was taken since there is the need to have a higher amount of biomass for further use in BAL. Roughly speaking, for a BAL adapted to the size of a rat, at least 100 - 300 million cells (1-3 gr), working at the same extent of primary hepatocytes, are required. This value was obtained through a linear relationship that links the number of cells needed for human therapy (20 billion) with a liver weighting 1.5 kg, to the number of cells needed for rat therapy with a liver weighing 15 g. Knowing that our bioreactor can host a maximum of about 11 mL of alginate beads, working at a concentration of 5 M/mL of alginate then it would get a biomass of 55 million of cells, not enough for the purpose. Duplicating this biomass, it results in 110 million cells, a number that comes closer to the minimum amount of cells required for BAL, but which is worth testing in preclinical stages. According to these simple considerations, we therefore duplicated the cell density and studied how the cell concentration affects the metabolic activities of the encapsulated cells. The results showed that cellular concentration actually plays an important role in the metabolic functions analysed, reducing the rate of certain activities, such as the production of albumin or the detoxification of ammonia. In particular, cell density influenced the metabolism of the lactate, since at density 10M/mL, production of lactate was observable in a few samples (3 samples up to 11). This observation can be related to a more hypoxic environment due to high cell concentration. It has been observed that in hypoxic condition, HepaRG (in 2D configuration), show decreased ammonia detoxification capacity and increased lactate production, with a general maintenance of stem cell characteristics²⁰³. Lactate consumption is a hallmark of freshly isolated hepatocytes²⁰⁴. In contrast, hepatic cell cultures produce lactate under anaerobic conditions or when the cells have dedifferentiated. The latter effect, known as the Warburg effect, is also a feature of tumour cells as a means for rapid cytosolic energy production²⁰⁵. These considerations might explain our experimental observations. However, considering rather a "global activity" of the bioreactor (i.e. the raw amount produced by the total number of cells in the Petri dish), almost all the activities measured are globally stronger for the condition 10 M/mL. For this reason, subsequent experiments on bioreactors were carried out using this last cell density.

Finally, we studied the effect of fluidization on cell metabolic activity. As already mentioned, the main advantage of a fluidized bed bioreactor is to maximize the mass transfer (i.e. exchanges of oxygen, nutrients, metabolites and toxins) between beads and fluid and to minimize the cell damage provoked by the perfusion¹⁷². Moreover, fluidized bed bioreactors appeared to be the best option for perfusing large number of encapsulated cells with the patient's plasma in comparison to other options, such as fixed beds. They ensure permanent motion of the beads in a closed tank and avoid the creation of a preferential channel leading to poor mass transfer. With our experiments, we wanted to verify whether the culture of encapsulated cell in fluidized bed bioreactor showed an improvement in the activities required for BAL treatment, compared to the reference culture (shaken culture). In these experiments, we preferred to work with a plasma-like medium to be closer to a human clinical context. The results showed that the cell culture in the fluidized bed bioreactor actually maintained the metabolic activities analysed. However, an important observation was the switch in lactate metabolism. While in shaken culture we observed also lactate production, perfusion in the bioreactor favoured its consumption, important expectation of a BAL. Based on the fact that fluidized bed improves mass transfer, it can be assumed that in this condition there was a better exchange of oxygen (main molecule of aerobic metabolism) between the culture medium and cells, which promoted a metabolism of consumption of lactate. Nibourg et al. 2013 observed that lactate production in 2D monolayer cultures of HepaRG switched into lactate consumption in perfused HepaRG-AMC-BAL¹⁸⁹. The authors attributed this metabolic switch to a better degree of cell differentiation in the bioreactor rather than better oxygenation. However, they pointed that the causal relation between oxygenation, lactate metabolism and hepatic differentiation needs to be further established. Also in our case, those observation need to be better clarified. However, we think that a better differentiation of the cells in the bioreactor can be excluded, in such short perfusion times (only 8 hours of perfusion).

4. Conclusion

In conclusion, in phase I we optimized the cell culture for fluidized bed bioreactor. We demonstrated that HepaRG cells were able to self-organize as spheroids when entrapped in 1.5% alginate beads. After 14 days of shaken culture, encapsulated cells presented a wide range of functions (protein synthesis, enzymatic activities and biotransformation of toxins) that are in the range or above those presented in other studies about bioartificial liver. These activities were also preserved in fluidized bed bioreactor. Despite the promising metabolic results, beads deterioration was observed and we needed to better optimize this biomass.

5. Key points phase I

- Encapsulated dissociated cells showed stronger global metabolic activity in comparison to pre-formed spheroids
- Alginate stiffness affected cell activity. Alginate 1.5%, showing rigidity values within the range of an healthy liver, promoted better metabolic performance in comparison to 1%

- Encapsulated dissociated cells self-rearranged in compact aggregates that presented features of spheroids (round morphology and tight junctions expression)
- Those structures were able to differentiate in hepatocyte-like and cholangiocyte-like cells, along 14 days of culture
- Metabolic activities required for BAL in the clinical treatment of acute liver failure were present and stronger on day 14. Cell viability remained high until the end of cell manipulation
- Glass microparticles did not affect cell metabolic performance and viability
- Cell density in alginate beads played an important role in the metabolic performance of encapsulated cells
- The fluidized bed bioreactor demonstrated to enhance the metabolic performance of encapsulated HepaRG
- An external coating capable of enhancing alginate beads stability is necessary to avoid beads deterioration and loss of cells during a future fluidized bed based BAL therapy

Chapter 4. Phase II: biomass optimization for multiple bioreactor types

1. Introduction

In this chapter, we will describe the phase II of the thesis, regarding the optimization of the biomass for use in different types of bioreactor. A part of those results has been submitted (see list of publications).

At the end of chapter 3, we highlighted the need of a reinforcement of alginate beads stability, which showed severe deterioration during experiments in the homemade pathological plasma model under shear conditions. We can suspect that beads perfused with real plasma in a clinical context would present the same problem of deterioration, with loss of cells. For safety issues in a BAL therapy, the cells present in the bioreactor must not escape and enter the circulation of a patient. For this reason, the fluidized bed bioreactor that we developed had filter membranes at the inlet and outlet, capable to block alginate debris or cells. Nonetheless, a better protection of the biomass appeared necessary. For this reason, we decided to realize a polymeric coating of the alginate beads, in order to maintain their integrity stability and prevent cell escaping from the beads and, further, from the bioreactor.

Several types of external coatings have been proposed to date in the literature^{180,206,207}. They are often developed to formulate capsules, whose core is liquid in contrast to beads. These techniques involve either ionic or covalent^{180,208,209} interactions between the surface of the alginate gel and the coating materials. In particular, ionic cross-linking coating of the beads can be performed thanks to the alginate's ability (with a negatively charged surface) to form strong electrostatic complexes with polycations¹⁸⁰. Of the latter, the natural polymers Poly-L-lysine (PLL) and Poly-L-ornithine (PLO) are most frequently used to reinforce the mechanical stability of the alginate beads^{180,210–212}. However, to our knowledge, it has never been applied in the context of an external bioartificial liver application. On the other hand, an external coating modifies the permeability of the beads without heavily affecting the cells' metabolic performances and viability, as observed by Capone et al. (2013) using encapsulated HepG2/C3A in alginate-PLL beads¹³⁸.

Taking cues from a previous study conducted in our laboratory¹³⁸, we realized a PLL external coating and we proposed analysing its impact on alginate beads' physical and mechanical properties, and its role on encapsulated HepaRG cells' metabolic performances. For this new campaign of characterization, we started with a cell density of 5 M/mL that, in the previous chapter, demonstrated to be the most efficient. The new type of biomass was then tested in fluidized bioreactor. However, a series of problems encountered during the experiments pushed us to change the type of bioreactor, passing from the fluidized bed to a perfused dynamic setup.

Therefore, in this chapter we will describe the process that led from the optimization of the new biomass to its use in the new type of bioreactor.

The phase II is divided in 3 steps. The first step focuses on the physical/mechanical characterization of the biomaterial and on the biomass metabolic performance, when PLL coating is added. In the step 2, we studied the influence of cell density in cell metabolic performance, passing from 5 M/mL

to 10 M/mL encapsulated in alginate-PLL beads. In the third step, we used this optimized biomass in fluidized bed bioreactor (FB) and a new type of bioreactor called perfused dynamic bioreactor (PDB).

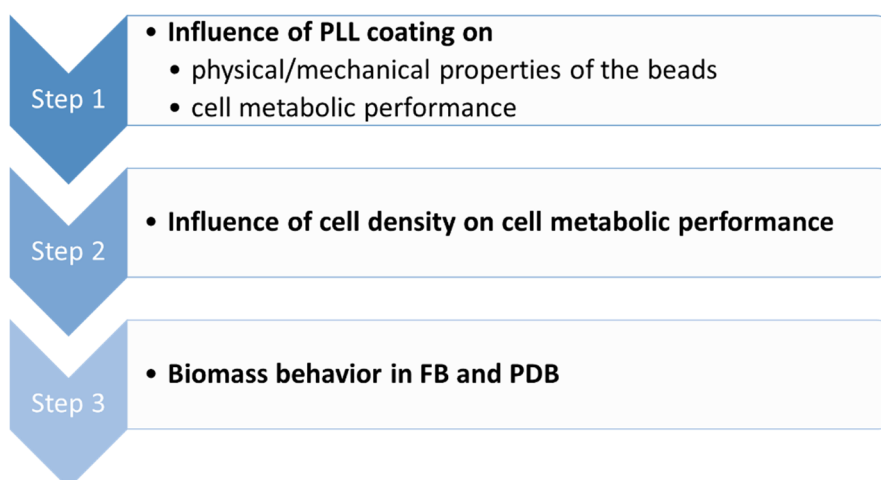


Fig. 61: steps of phase II

2. Results

2.1. Step 1: Influence of PLL coating on physical/mechanical properties of the beads and on cell metabolic performance

2.1.1. Physical/mechanical characterization of alginate beads

In order to enhance alginate resistance and avoid beads deterioration observed in homemade pathological plasma model, an external coating of 0.1% poly-L-Lysine (PLL) was realized. The interaction between the alginate surface and PLL is governed by electrostatic interactions between side chain NH_3 functional group of the polyamino acid and carboxyl group of alginate (Figure 62). After preliminary experiments, we decided to perform the external PLL coating on day 1 post encapsulation.

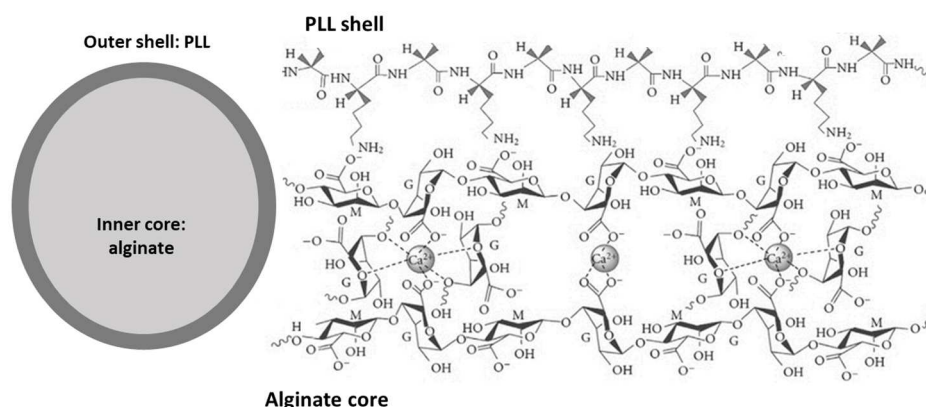


Fig. 62: Electrostatic interactions between alginate (core of the bead) and PLL (shell)

2.1.1.1. PLL coating and distribution around the alginate beads

The test was realized on empty alginate beads with and without PLL coating, at day 14 post-encapsulation. On day 1, after PLL coating, a variation in the sphericity of the beads was visible (Figure 67A), due to a shrinking effect. The diameter of the beads decreased by about 20%, from $949 \pm 49 \mu\text{m}$ post-encapsulation to $785 \pm 25 \mu\text{m}$ after PLL coating. The diameter of the beads, with or without a PLL coating, then remained stable until the end of the experiment.

Phase contrast and confocal microscopy clearly showed that PLL was distributed only on the surface of the alginate beads, causing a slight morphological variation on their periphery (Figure 63). The thickness of the external coating was around $14.4 \pm 6.4 \mu\text{m}$.

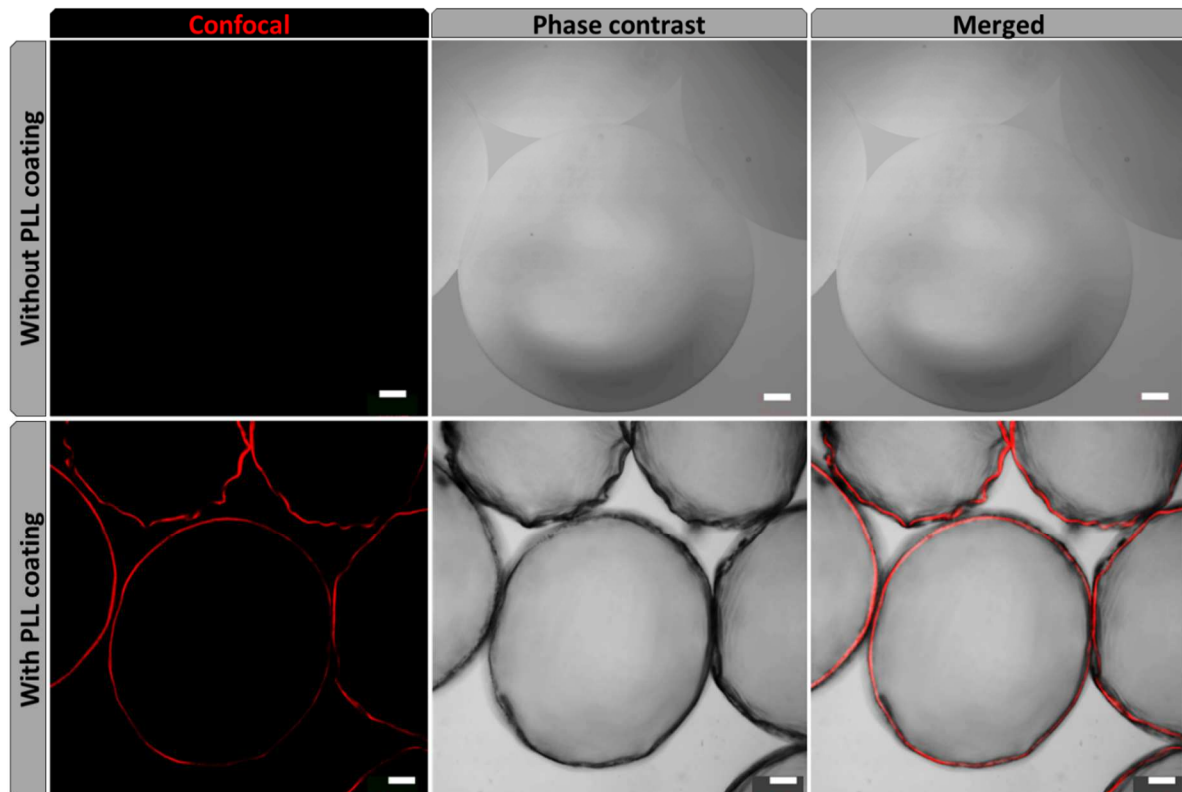


Fig. 63: Distribution of PLL-rhodamine (red staining) in empty beads in comparison with the negative control (without PLL coating). Images taken in confocal microscopy (left images), phase contrast (central) and merging the two (right)

2.1.1.2. Mechanical properties of PLL layer

The mechanical properties of the surface of single, empty beads were assessed by microindentation. The results showed a significant increase in the elastic modulus of the external area of the beads coated with PLL, 6.6 times higher in comparison with the pure alginate condition (Figure 64), ensuring surface mechanical reinforcement and thus better stability.

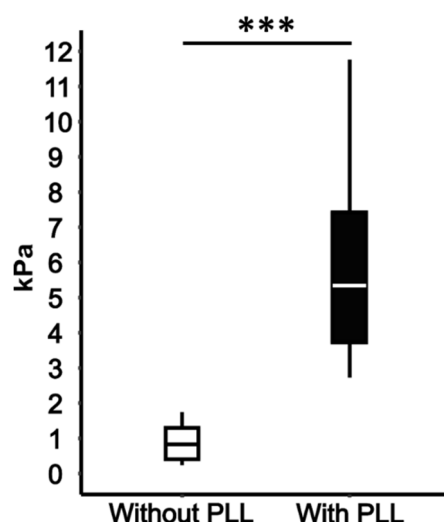


Fig. 64: Elastic modulus of the outer surface of empty beads with and without a PLL coating on day 14. With an indentation of 3 μm , the sensor penetrated only on the PLL layer, when present. Significance was analysed using a Mann-Whitney Test. *** indicates $p < 0.001$. $N = 10$ per batch of beads

2.1.1.3. Beads permeability

The porosity of empty alginate beads with or without a PLL coating was evaluated by means of exposure to different fluorescent markers of increasing size. The microscope observations (Figure 65) did not show any measurable differences between conditions. Albumin, IgG, and 41 nm diameter NPs were able to penetrate the core of the beads. Larger NPs were fully retained outside the beads, and did not color their inner part green. The cut-off threshold for both conditions was thus between 41 nm and 103 nm.

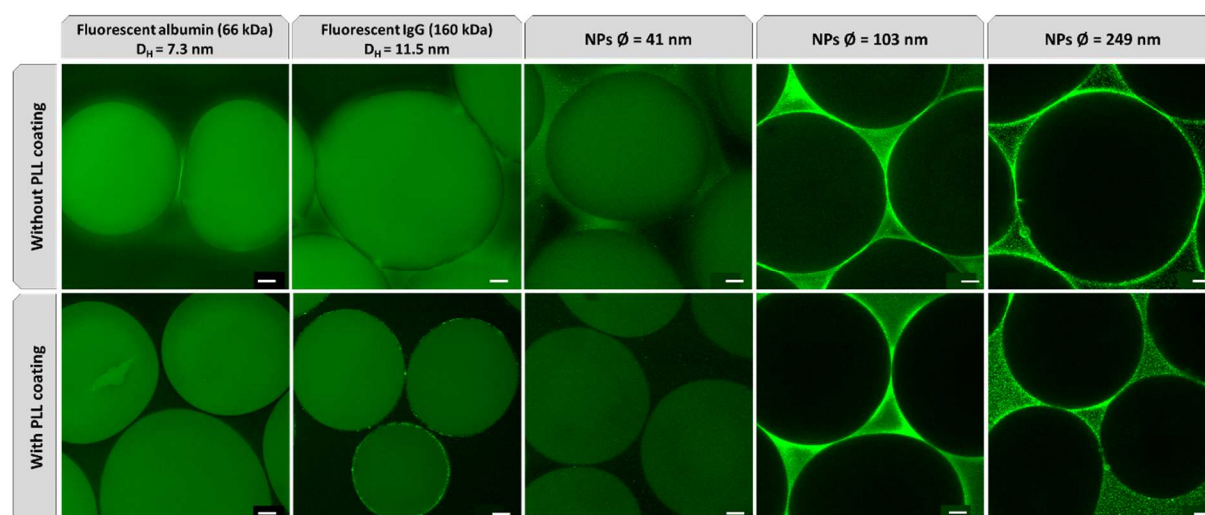


Fig. 65: Permeability of empty beads (coated or not with PLL) to fluorescent markers (albumin, IgG, nanoparticles of different diameters). DH indicates the hydrodynamic diameter without the fluorophore; \varnothing indicates the diameter of the nanoparticles (NPs). Incubation lasted 24 hours. Pictures taken after washing the beads in WE. Scale bar: 100 μm

2.1.2. Cell metabolic characterization

The experimental setup designed to assess cell metabolic performance is shown in Figure 66. On day 0, the cells were encapsulated in alginate 1.5% and kept in shaken condition until day 14. On day 1, PLL coating was realized. Cell culture evolution was studied analysing cell viability (by Live/Dead

staining on days 0, 1, 7, 14) and albumin synthesis rate (overnight between days 0-1, 6-7, 9-10, 13-14) as hepatocyte quality marker. On day 14 post-encapsulation, cell performance was tested by means of metabolic and xenobiotic tests. The latter were conducted at intervals of up to 2 hours of incubation and, at each time-point (time 0, time 2 hours), aliquots of supernatant were collected for further analysis. The samples were tested sequentially in HepaRG proliferation medium and BAL test medium. At the end of each experiment, microbeads were recovered and assessed for cell viability.

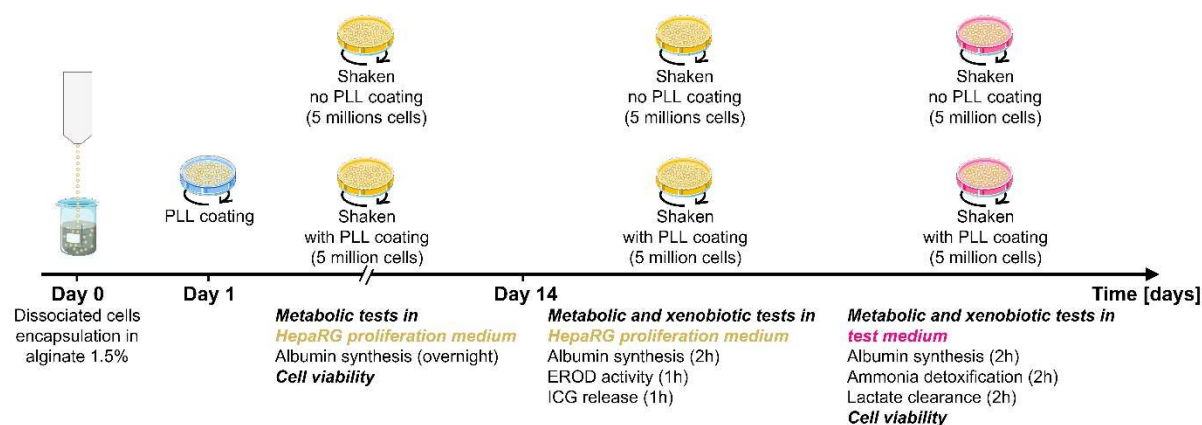


Fig. 66: Experimental setup phase II, step 1

2.1.2.1. Viability of encapsulated cells over 14 days

The production of alginate beads with homogeneous cell distribution was achieved with success and no empty beads were visible after the cell encapsulation process. We estimated approximately 1100 beads per encapsulation batch (1 mL of alginate solution) by counting them with the optical microscope. As the initial biomass was 5 million cells/mL of alginate, we calculated approximately 4500 cells per bead. As previously observed on empty beads, the PLL coating provoked a shrinking effect of about 20% in the diameter of the beads.

The number of viable hepatocytes (Figure 67, in green) within the microbeads remained high over time, as very few dead cells (Figure 67, red stained nuclei) were observed, in comparison with the negative control where cells were killed by ethanol 70% exposure. The PLL coating did not seem to affect cell viability. Therefore, neither the long-time culture nor the coating process had any significant impact on cellular viability. Qualitatively from day 1 to day 14, a phenomenon of cell-cell aggregation likely occurred, visible through the incorporation of Calcein-AM by living cells. We observed very similar results in beads without a PLL coating (data not shown). It should be noted that, once the PLL coating was present, the beads became opaque making the encapsulated cells difficult to visualize under the light microscope.

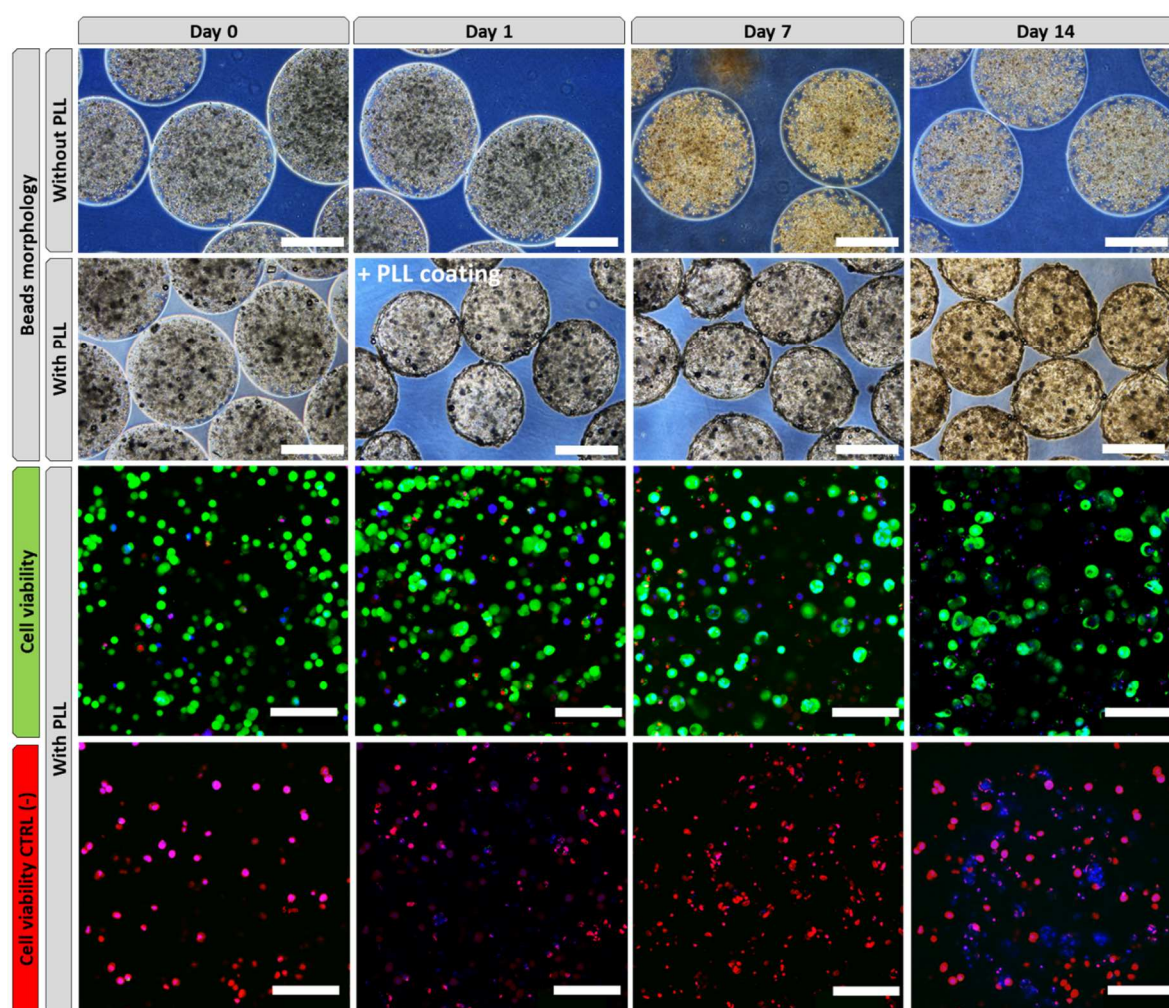


Fig. 67: Observation of beads without and with PLL coating morphology by bright field microscopy (scale bar: 500 µm) and cell viability of alginate-PLL encapsulated cells (live/dead assay) by confocal microscopy. In green (Calcein AM): viable cells, in red (ethidium homodimer-1): dead cells, in blue (Hoechst 33342 dye): cell nuclei (scale bar 100 µm)

Albumin production is considered as a quality marker for the hepatic biomass in a bioreactor⁷⁰. In this sense, we evaluated the secretion rate of albumin in order to determine quantitatively the biomass functionality over the 14 days of culture (Figure 68). Albumin secretion rate increased along the two weeks of culture for both conditions, significantly between day 1 and day 14 ($p < 0.01$) when PLL coating was present.

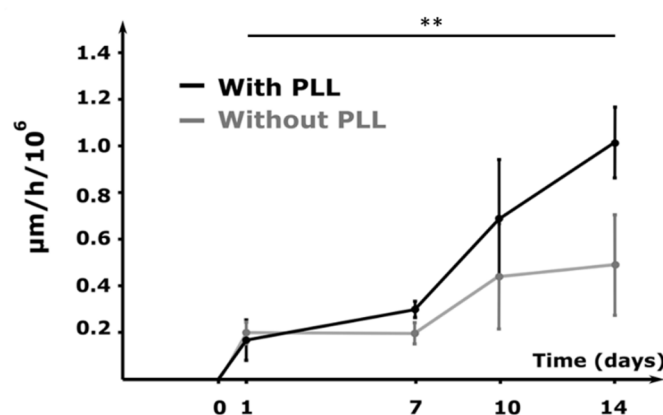


Fig. 68: Albumin secretion rate over time (overnight between days 0-1, 6-7, 9-10, 13-14) of encapsulated cells in alginate beads with and without PLL coating. For the condition with PLL, the increasing between day 1 and da14 was significant (** indicates $p < 0.01$, significance analysed by Dunn's Multiple Comparisons Test). $N \geq 3$

2.1.2.2. Metabolic activity of cells on day 14

To investigate the impact of the PLL coating on cell metabolic performance, we designed culture media with increasing complexity in their composition (Table 15), in order to progressively mimic a clinical condition of ALF human plasma.

| | HepaRG proliferation culture medium | BAL function test medium | Pathological plasma model |
|---|--|---|---|
| Medium composition | William's E medium + Biopredic 710 proliferation media | HepaRG proliferation culture medium + 1.5 mM ammonium chloride + 2 mM L-Lactate | HepaRG proliferation culture medium + 70 g/L bovine serum albumin + 1.5 mM ammonium chloride + 2 mM L-Lactate |
| Metabolic performances tested (Test duration) | Albumin synthesis rate (2 h) | Albumin synthesis rate (2 h) | Albumin synthesis rate (6 h) |
| | ICG clearance rate (1 h) | Ammonia detoxification rate (2 h) | Ammonia detoxification rate (6 h) |
| | CYP 1A1/2 activity (1 h) | Lactate clearance rate (2 h) | Lactate clearance rate (6 h) |

Tab. 15: Media for metabolic characterization at day 14 post-encapsulation and tests performed

The cell metabolic characterization on day 14 was firstly performed on HepaRG proliferation medium and BAL function test medium.

2.1.2.2.1. Metabolic tests on HepaRG proliferation medium

On day 14, we compared the metabolic performance of encapsulated cells with and without PLL. We analysed the following metabolic activities: albumin synthesis rate (Figure 6gA), ICG releasing rate (Figure 6gB), and CYP1A1/2 activity (Figure 6gC). The results showed that when PLL coating was present, there was a tendency for metabolic activities to decrease, significant for CYP1A1/2, 3.5 fold lower ($p < 0.01$). However, even in presence of a PLL coating, cells remained metabolically active.

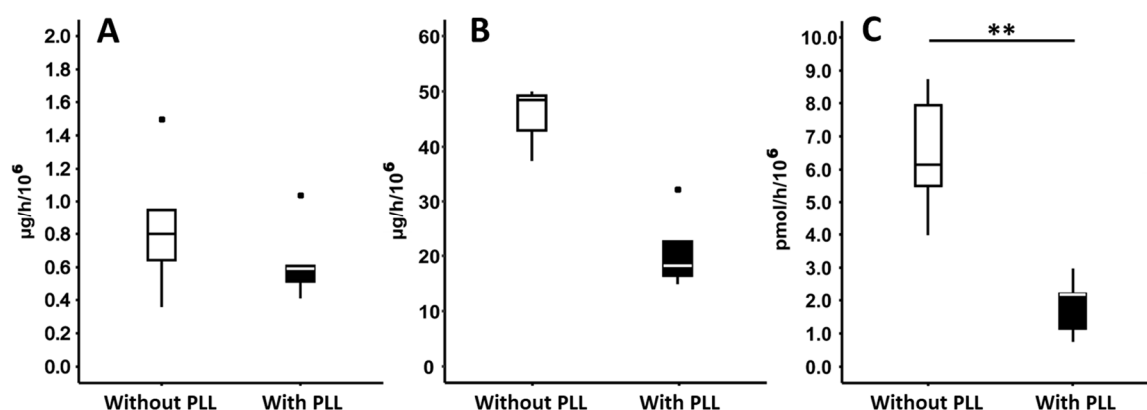


Fig. 69: Metabolic activities of cells in alginate beads with and without PLL coating, measured on day 14 in HepaRG proliferation medium. A: Albumin secretion rate; B: ICG releasing rate by the transporters MDR3 and MRP2; C: CYP1A1/2 activity (significance analysed by Wilcoxon matched-pairs signed-ranks test). * indicated outliers. N ≥ 3

2.1.2.2.1. Metabolic tests in BAL function test medium

After previous metabolic tests, the same biomass was tested to evaluate the ability of cells to detoxify typical ALF toxins. The cells were incubated for 2 hours in BAL test medium containing ammonia and lactate. The ability of the cells to produce albumin and detoxify these toxins is shown in Figure 70A, 70B and, 70C respectively. The metabolic activities measured remained equivalent between the two conditions.

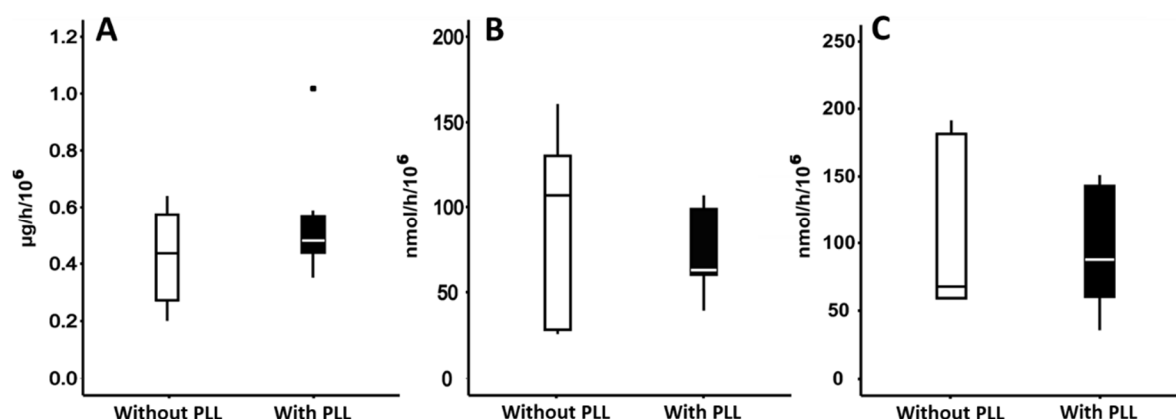


Fig. 70: Metabolic activities of cells in alginate beads with and without PLL coating, measured on day 14 in BAL test medium. A: albumin synthesis rate; B: ammonia detoxification rate; C: lactate detoxification rate. * indicated outliers. N ≥ 3

The metabolic tests presented by now (ICG clearance, EROD activity, and cell performance on BAL function test) were performed sequentially on the same samples. Therefore, at the end of this campaign of tests we evaluated the cell viability that remained high and overall stable (Figure 71). Moreover, a phenomenon of cell-cell aggregation inside the beads is observed.

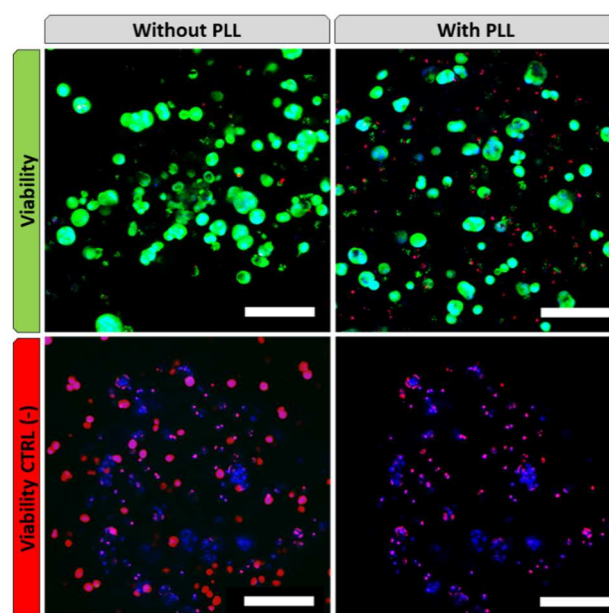


Fig. 71: Cell viability (live/dead assay) of cells in alginate beads with and without PLL coating, by confocal microscopy. In green (Calcein AM): viable cells, in red (ethidium homodimer-1): dead cells, in blue (Hoechst 33342 dye): cell nuclei. Scale bar: 100 μm

2.2. Step 2: influence of cell density on cell metabolic performance

In step 2, we investigated the influence of cell density on cell metabolic performance, comparing cell density 5 M/mL to 10 M/mL, encapsulated in alginate-PLL beads. The experimental plan is similar to the previous one but, on day 14, the biomass was tested directly on the pathological plasma model in order to approach the tests on bioreactor. In particular, on day 14, cells were incubated for 2 hours with 8 mL of equivalent plasma. After that, beads were incubated in 7.5 mL of pathological plasma model for 6 hours and the following activities were investigated: albumin and urea synthesis, ammonia detoxification and lactate clearance. Aliquots of supernatant were taken on time 0, 2 and 6 hours. At the end of each experiment, microbeads were collected and assessed for cell viability.

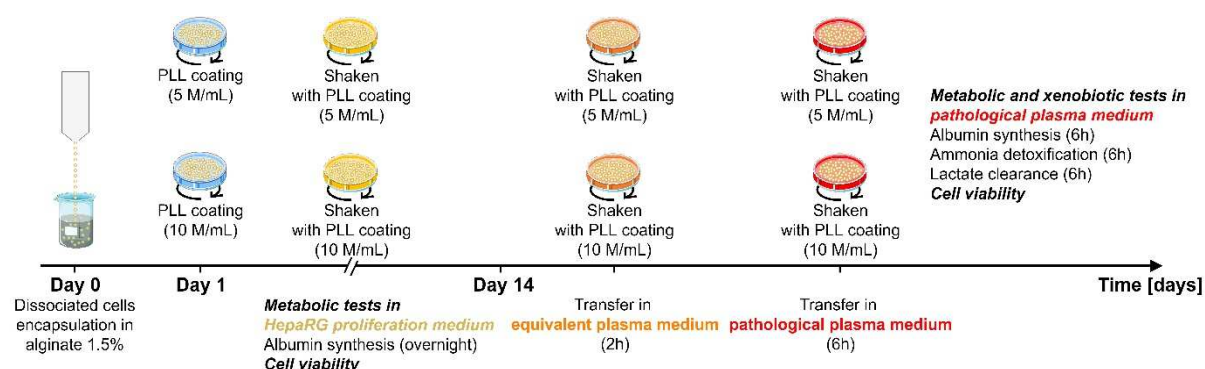


Fig. 72: Experimental plan, phase II step 2

During the two weeks of culture, the secretion of albumin was measured as quality parameter of hepatocyte functionality (Figure 73), in overnight incubations at different days. Even if the profile of the curves is not the same, at day 14, cells have comparable albumin secretion rate.

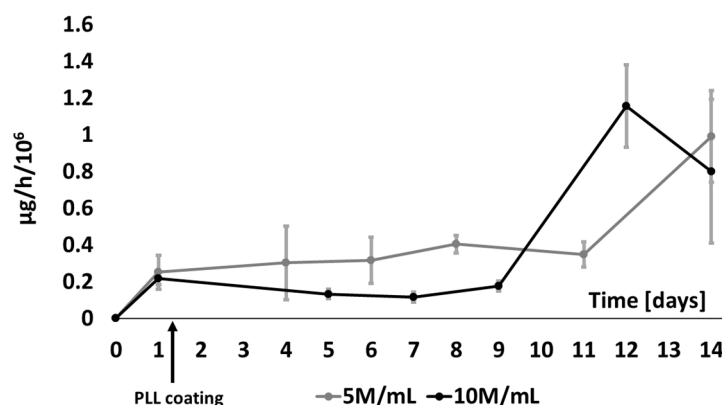


Fig. 73: Albumin secretion rate over 14 days. $N \geq 3$

At day 14, before testing in pathological plasma medium, the biomass was exposed to an equivalent plasma (HepaRG proliferation medium supplemented with 70 g/L bovine serum albumin, to mimic a healthy human plasma in total protein concentration), in order to reproduce the priming of the BAL, in vision of a clinical therapy. After that, cells were exposed to the equivalent pathological plasma medium for 6 hours. We measured albumin secretion, ammonia detoxification and lactate clearance rates. Albumin secretion rate is about 7 times stronger for 10 M/mL (significance analysed by Mann Whitney test, $p < 0.01$), while ammonia and lactate elimination remained comparable. Unfortunately, for the condition 10 M/mL, we could not have better data for lactate consumption rate due to an experimental mistake. The results are summarized in table 16 and expressed as global activity per bioreactor in 6 hours incubation.

Importantly, those experiments conducted on the pathological plasma medium showed that the PLL coating prevented beads deterioration and loss of cells, observing the supernatant on bright field microscopy. This observation is of essential importance to conduct a safe therapy for the patient, once in BAL treatment.

| Cell density in alginate-PLL beads | Albumin synthesis rate ($\mu\text{g}/6\text{h}$) | Ammonia detoxification rate ($\text{nmol}/6\text{h}$) | Lactate clearance rate ($\text{nmol}/6\text{h}$) |
|------------------------------------|--|---|--|
| 5M/mL | 6.04 ± 1.17 | 923.5 ± 233 | 518.3 ± 308.8 |
| 10M/mL | 42.7 ± 15.6 | 834.9 ± 65.8 | 691 (N=1) |

Tab. 16: Metabolic performance of cells in pathological plasma medium. $N \geq 3$ if not differently specified

Even in the condition 5M/mL appeared to be more efficient (when normalizing by number of cells seeded), in terms of global activity 10M/mL showed more interesting results. Therefore, we proceeded with the latter cell density for testing in FB and PDB.

For both condition, cell viability remained very high at the end of the experiments (Figure 74). Moreover, a phenomenon of cell-cell aggregation inside the beads was observed.

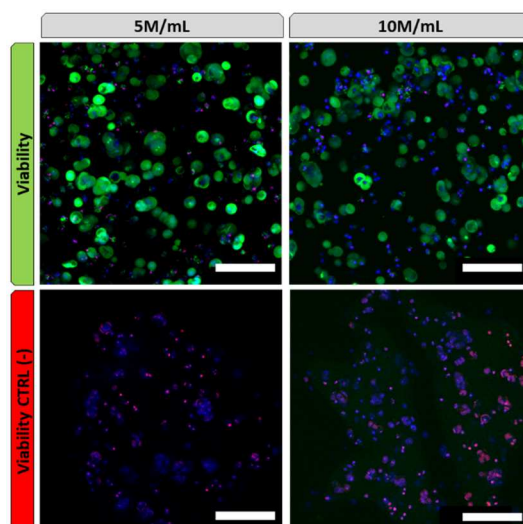


Fig. 74: Cell viability (live/dead assay) of cells in alginate-PLL beads at 5M/mL and 10M/mL, by confocal microscopy. In green (Calcein AM): viable cells, in red (ethidium homodimer-1): dead cells, in blue (Hoechst 33342 dye): cell nuclei. Scale bar: 100 μ m

2.3.Step 3: cells and beads behaviour in fluidized bed (FB) and perfused dynamic bioreactor (PDB)

In step 3, we investigated the behaviour of alginate-PLL encapsulated cells, at cell density 10M/mL, in shaken, FB and PDB setups. The experimental plan is similar to the previous one (Figure 75). At day 14, some samples were transferred in:

- FB: 5 mL of beads, 50 million cells
- PDB: 5 mL of beads, 50 million cells
- Shaken condition: 1 mL, 10 million cells

After 2 hours of exposure to a homemade equivalent plasma, cells were incubated in pathological plasma model (7.5 mL for shaken condition, 37.5 mL for FB and PDB) for 6 hours and the following activities were investigated: albumin and urea synthesis, ammonia detoxification and lactate clearance. Aliquots of supernatant were taken on time 0, 2 and 6 hours. At the end of each experiment, microbeads were collected and assessed for cell viability. Of note, the alginate-PLL beads dedicated to FB, contained 0.05% glass microparticles to favour fluidisation.

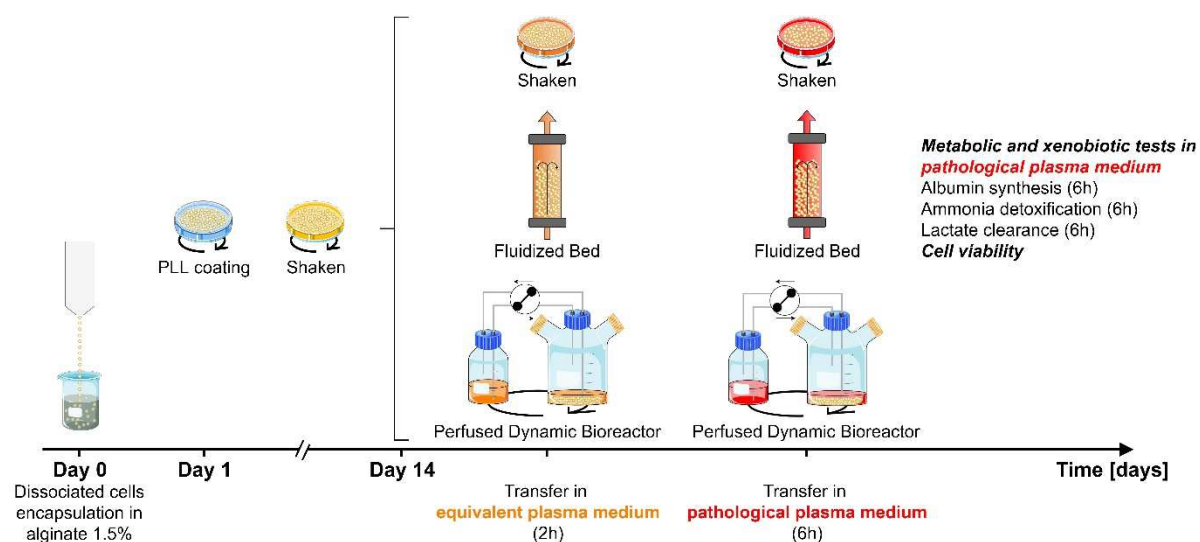


Fig. 75: Experimental plan for phase II, step 3

In a first moment, we wanted to test the FB, since it was the technology to implement in our BAL. The albumin secretion over the two weeks of shaken culture is the same previously presented in figure 73 (condition 10M/mL). On day 14, beads were divided between the 2 conditions to test (shaken, used as control, and FB), incubated in equivalent plasma for 2 hours and then in pathological plasma model for 6 hours. We measured albumin secretion, ammonia detoxification and lactate clearance rates.

Importantly, the beads dedicated to FB contained 0.05% glass microparticles, optimized to make them precipitate and have correct fluidization (density beads > density surrounding medium). Nonetheless, once the beads were transferred in FB and put in contact with the equivalent plasma, it was not possible to obtain a correct fluidisation. Other GM concentrations were assayed (0.5%, 0.75%, 1%, and 1.25%) but each experiment on FB failed. Here are summarized the reasons:

- When we tested the glass microparticles concentration of 1.25%, we observed a fixed bed of beads impossible to fluidize. Instead, at lower glass microparticles concentrations, they were not well distributed in the alginate solution, forming gradients. After encapsulation process, some beads contained glass microparticles, other beads did not
- Once alginate beads were put in contact with the equivalent plasma (and then pathological plasma), inside the bioreactor a lot of beads were floating, even if most of the other beads were precipitating
- The floating beads, once started the perfusion in FB, started to accumulate in the filter membrane at the outlet of the bioreactor, causing an augmentation of pressure and a disconnection of the tubes
- The remaining beads started to accumulate at the inlet of the bioreactor causing also in this case, an augmentation of pressure and disconnection of tubes

Those problems of fluidization were related very probably to a not homogeneous distribution of the glass microparticles in the alginate beads.

Consequently, it was not possible to continue experiments on FB. In order to successfully repeat the experiments, a bioreactor with a more pertinent design should probably be used, with flow dividers and filters to prevent the accumulation of beads at the inlet and outlet of the bioreactor. These observation were also highlighted by Lu et al.²¹³.

For these reasons, we decided to use a new type of bioreactor, based on the very promising results obtained with our standard shaken setup. This bioreactor is in fact a similar version of the shaken culture but including a perfusion system (Figure 76), and called perfused dynamic bioreactor (PDB).

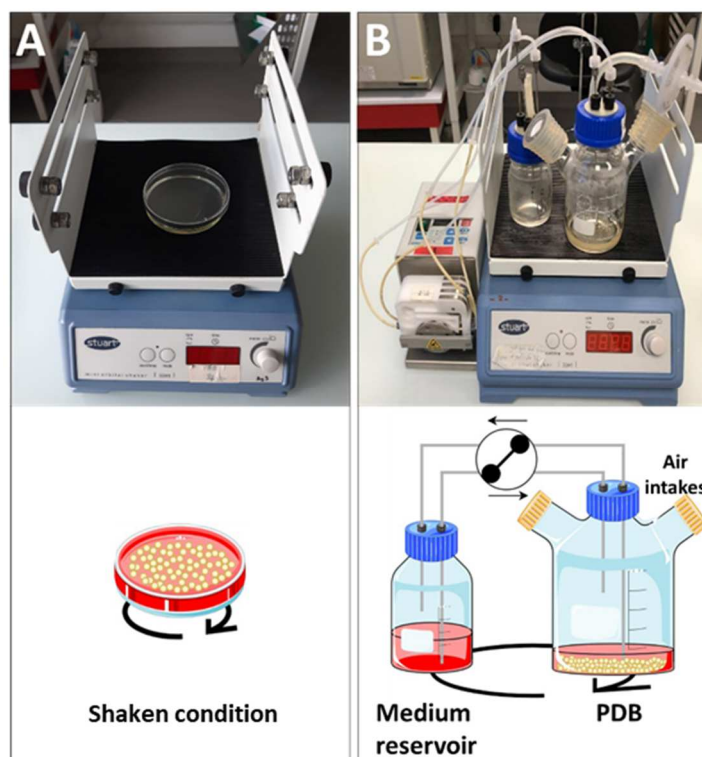


Fig. 76: Culture conditions tested for next biomass metabolic characterization. A: Shaken condition. B: PDB condition

Therefore, we used our optimized biomass for testing its activity on PDB, compared to standard shaken culture. The aim was to compare the two culture setups and especially to reproduce a BAL therapy, using an ALF-human plasma model. Importantly, before testing in equivalent pathological medium, the biomass was exposed to an equivalent plasma (HepaRG proliferation medium supplemented with 70 g/L bovine serum albumin, to mimic a healthy human plasma in total protein concentration) for 2 hours, in order to reproduce the priming of the BAL, in vision of a clinical therapy. After that, cells were exposed to the pathological plasma model for 6 hours.

The ability of the cells to produce albumin, detoxify ammonia and eliminate lactate is shown in Figure 77. While albumin secretion rate (Figure 77A) was favoured in shaken culture, ammonia detoxification (Figure 77B) and lactate clearance (Figure 77C) were stronger in PDB setup. No statistic was realized since the results in PDB have to be confirmed (N=2).

However, our main goal was to evaluate whether, qualitatively, our PDB was able to show positive metabolic performance, since this bioreactor could potentially be used in our BAL. Importantly,

those experiments conducted on the pathological plasma medium showed that the PLL coating prevented beads deterioration and loss of cells, observing the supernatant on bright field microscopy. This observation was of essential importance to conduct a safe therapy for the patient, once in BAL treatment.

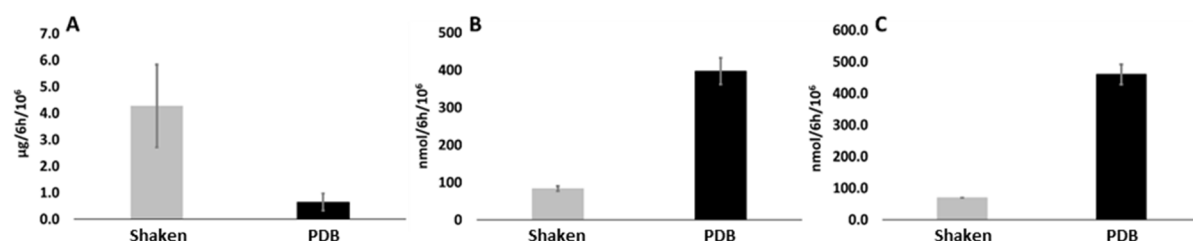


Fig. 77: Metabolic activities of cells in alginate-PLL beads, measured on day 14 in pathological plasma model, in shaken and perfused dynamic bioreactor (PDB). A: albumin synthesis rate; B: ammonia detoxification rate; C: lactate detoxification rate.

At the end of the experiments, we evaluated the cell viability that remained high and stable overall for both conditions (figure 78). Moreover, a phenomenon of cell-cell aggregation inside the beads is observed.

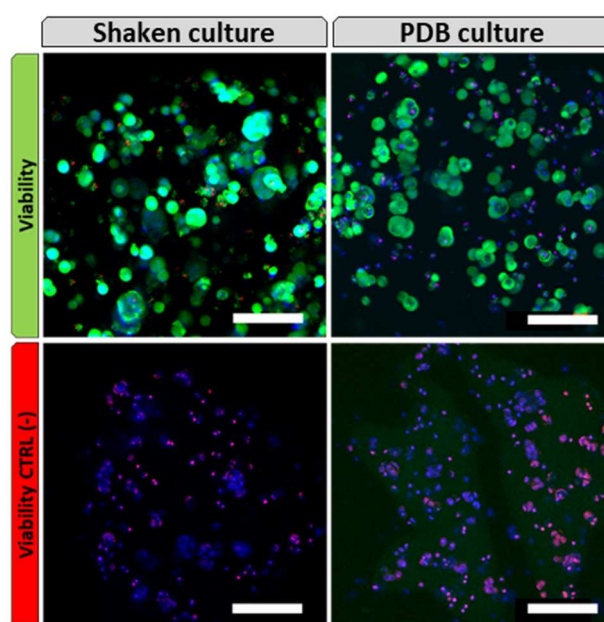


Fig. 78: Cell viability (live/dead assay) of cells in alginate-PLL beads, by confocal microscopy, after exposition to pathological plasma model. In green (Calcein AM): viable cells, in red (ethidium homodimer-1): dead cells, in blue (Hoechst 33342 dye): cell nuclei. Scale bar: 100 µm

2.4.Effect of pathological plasma model on cell metabolic performance

Importantly, we noticed that when comparing the metabolic performance of alginate-PLL coated beads in BAL test medium and pathological plasma model, there was a significant decrease in albumin secretion, ammonia detoxification and lactate clearance rate, with $p < 0.01$ for all the cases. The same trend was also observed in chapter 3, when beads were still without PLL coating.

| Biomass | Culture condition | Culture medium | Medium composition | Albumin synthesis rate ($\mu\text{g/h}/10^6$) | Ammonia detoxification rate ($\text{nmol/h}/10^6$) | Lactate clearance rate ($\text{nmol/h}/10^6$) |
|--|-------------------|---------------------------|--|---|--|---|
| Alginate beads with PLL coating (5×10^6 cells) | Shaken condition | BAL test medium | HPM + 1.5 mM ammonium chloride + 2 mM L-lactate | 0.56 ± 0.24 | 73.7 ± 28.4 | 95.6 ± 50.4 |
| | | Pathological plasma model | HPM + 70 g/L BSA + 1.5 mM ammonium chloride + 2 mM L-lactate | 0.20 ± 0.04 | 30.8 ± 7.8 | 17.3 ± 10.3 |

Tab. 17: Effect of pathological plasma model on cell metabolic performance. HPM: HepaRG proliferation medium

In order to verify if the homemade pathological plasma model could have deleterious effects on cell viability, we realized an experience in 2D, to test its cytotoxicity. In this experiment, we tested three different conditions, on day 14 post seeding:

- CTRL + (positive control of viability): cell cultured in HepaRG proliferation medium
- Eq. plasma: cells treated for 2 hours in equivalent plasma
- Pathological plasma model: cells treated for 2 hours with equivalent plasma and 6 hours with pathological plasma model (to imitate a complete therapy as for the bioreactor)

All wells were treated in the same way in terms of washings and changing of the medium, in order to avoid artefacts in the viability due to these passages. At the end of the experiment, cell viability was measured considering the condition CTRL+ as 100% viability and the viability values of the remaining conditions were compared to it. The results showed that once cells were exposed for 2 hours in equivalent plasma, there is a significant reduction in viability (i.e. decreased activity in reduction of MTS compound to formazan), but when cells are sequentially exposed to equivalent plasma and pathological plasma, the viability is not significantly affected in comparison with the control (Figure 79). Probably, the longer the exposure time to these complex media, the longer the time to adapt and regain cellular activity. However, cell viability remained greater than or equal to 90%.

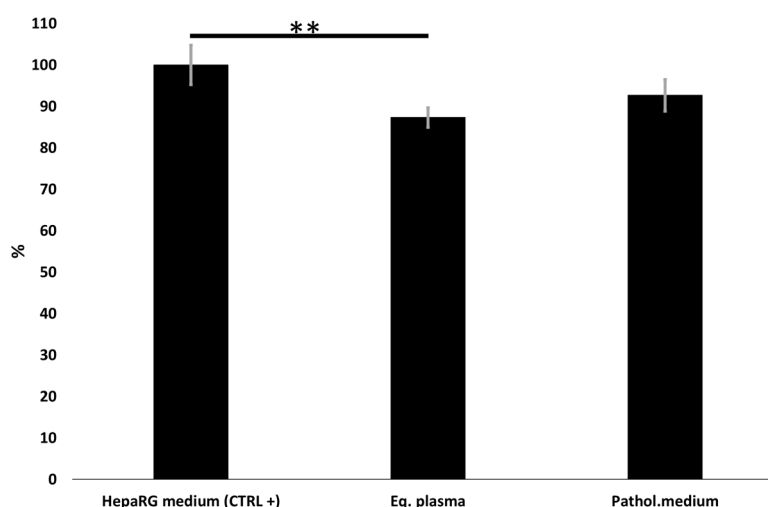


Fig. 79: Cell viability via MTS test in 2D configuration. Significance analysed by Mann Whitney test.

3. Discussion

In the previous phase I, we demonstrated the benefits of using HepaRG cells encapsulated in alginate beads as biomass for BAL ¹³⁷. Because of the risk of beads' deterioration in pathological plasma, we highlighted the need to reinforce the mechanical properties of the biomaterial. Indeed, it has been reported that a drawback of using alginate beads for long-term culture is their limited stability, because these gels can be dissolved due to release of divalent ions into the surrounding media due to exchange reactions with monovalent cations ²¹⁴. Therefore, the present phase II focused on the characterization of the biomaterial bearing a PLL coating, the metabolic performance of the new biomass, and its transfer within a bioreactor compatible with a BAL therapy.

The phenomenon of alginate beads deterioration in pathological plasma medium was observed in all the culture setups tested, but it was especially pronounced in fluidized bed and perfused dynamic bioreactors. Therefore, clearly, the perfusion played a role in this phenomenon, since it might have increased the hydrodynamic stress of the surrounding medium on the beads. Overall, we hypothesized that the deterioration was due to the synergic presence of an excess of BSA and lactate in the surrounding medium (both capable of sequestering calcium ions involved in the formation of the alginate gel), the increased hydrodynamic stress imposed by the perfusion, and a higher cell activity (if compared with the shaken condition in Petri dish).

In the first step, we wanted to investigate the physical and mechanical properties of the beads, in presence (or not) of the PLL coating. This investigation was important in order to study a direct or indirect impact of the coating on cell metabolic performance. In the literature, PLL coating has been proposed to increase the structural stability of alginate beads and to limit the access of the immune system into the beads/capsules ^{138,215,216}. For this specific application, if PLL was not additionally coated with a layer of alginate (i.e. alginate-PLL-alginate beads), it demonstrated immunogenicity ²¹⁶ and caused fibrotic overgrowth when implanted in mice ²¹⁷. If this additional layer of alginate on the PLL coating appeared essential for implantation of the encapsulated cells, this is not the case for extracorporeal circulation devices such as BAL therapy. In fact, most BAL devices, as well as the one developed in our laboratory ¹, include a plasmafilter to separate the plasma from the formed elements of the blood. As a result, the cells of the immune system are discarded upstream, before entering into contact with the therapeutic biomass, making the activation of a specific immune response unlikely.

Preliminary experiments conducted on our medium model of pathological plasma showed that PLL coating successfully prevented beads from deterioration. Looking at the morphology, we observed an immediate and stable reduction of about 20% in the beads' diameter after PLL coating without any significant impact on cell viability. The analysis of the distribution of PLL showed that it was not able to enter into the core of the alginate bead, remaining only on its shell. Therefore, a direct interaction between cells and PLL can be excluded. This phenomenon was also reported by Yahia et al. ²¹⁸. In addition, the presence of the coating increased significantly the elastic modulus of the external area of beads, making it resistant to deterioration. About the porosity, we did not notice any

measurable difference between beads with and without PLL coating. Both conditions have a cut-off between 41 and 103 nm. Indeed, fluorescent albumin, IgG, and nanoparticles of 41 nm in diameter could enter the beads, after 24 hours incubation but they were impermeable to polystyrene nanoparticles of 103 nm, as also observed by Tran et al.¹⁷¹. Of note, some large molecules physiologically produced by hepatocytes fell within this cut-off value (such as fibrinogen, about 48 nm in hydrodynamic diameter²¹⁹) and their transfer between the polymer network and the surrounding medium could be hindered. Importantly, considering that liver sinusoidal endothelial cells (the cells that delimit the space of Disse together with hepatocytes, controlling the trafficking of macromolecules), have fenestrae with diameter between 50-300 nm²²⁰, the cut-off values of our beads fitted well with this physiological range. According to our results, we concluded that a large set of molecules produced by the encapsulated hepatocytes (and those present in the medium culture) could leave (and enter) the alginate matrix, an essential factor for BAL therapy.

Importantly, we observed that fluorescent IgG could enter the beads, after 24 hours of incubation. Similar observations about fluorescent IgG permeability on alginate beads at 1% polymer concentration, were made by Wang et al.¹⁶⁹. This observation has an important implication, since many investigators claim that alginate has an immuno-protective role. The term immune protection designates the protection of the encapsulated cells against high molecular weight effector molecules of the adaptive immune system such as immunoglobulins and complement factors²²¹. We showed that IgG can enter into the beads and, therefore, any effector of the immune response of the same size can enter in contact with encapsulated cells, disproving this definition. On the contrary, if the definition was extended to the cellular level (cells of the immune system), the alginate could effectively create a protective barrier to prevent the recognition of the encapsulated cells as non-self elements. The greatest consequence of this observation would be in the context of alginate beads transplantation. On the other hand, for extracorporeal circulation devices, there should be no immune responses if plasmapheresis is carried out since the formed elements of the blood would be excluded upstream. Overall, the fact that IgG can enter our beads should not have serious implications for future BAL therapy.

Then, we evaluated if the presence of this additional polymer could affect the cell metabolic performance. According to our observations, encapsulated cell viability was affected neither by the long-term culture of cells nor by the presence of PLL. Noticeably, one of the markers of liver cell functionality is albumin production. Monitoring this secretion between the two conditions (with or without PLL) in shaken condition showed a progressive increase throughout the culture up to day 14 with an advantage for PLL coated beads, corresponding to efficient HepaRG differentiation. On day 14, we tested different metabolic activities required for BAL application, such as ammonia and lactate elimination (in BAL test medium). We were not able to measure any significant difference between both conditions with the exception of a downward trend in the xenobiotic activities and more precisely for CYP1A1/2, when coating was present. It might be due to an increase in beads core stiffness after shrinking (therefore, an indirect effect of the PLL coating). In fact, Chen et al.¹⁷⁶

cultured rat hepatocytes on polyelectrolyte multilayers and found that albumin production and CYP450 1A activity decreased with increasing substrate stiffness.

In the second step, we increased the cell density from 5 M/mL to 10 M/mL. As previously observed in chapter 3, the increasing in cell density negatively affected the cell performance. However, in terms of global activity per bioreactor, 10 M/mL demonstrated better performance and therefore we used this cell density for next testing in bioreactors. It was not easy to identify a specific cause on the lower efficiency of cells, when cell density doubled. Overall, the elements that play a determinant role on cell metabolic performance are the availability of oxygen (that plays a crucial role in HepaRG metabolism ²⁰³), the level of differentiation (possibly the cells differentiate with greater difficulty at higher cell density), the level of cell-cell aggregation within the beads (qualitatively, cells showed better cell-cell aggregation at density 5 M/mL). Those observations deserve to be better clarified. Moreover, the tests were performed in pathological plasma model, to be closer to the next experiments in fluidized bed and perfused dynamic bioreactors.

In step III, we tested the optimized biomass in two types of bioreactors. The experiments conducted in fluidized bed bioreactor failed for the reasons previously mentioned. Therefore, we focused to the perfused dynamic bioreactor. The latter is similar to the standard shaken culture in Petri dish (in which we achieved very promising results in terms of cell metabolic activity ¹³⁷), but is adapted to its connection to the BAL device developed in our lab (see chapter 5). Since, after the addition of the PLL coating, we were not able to carry out experiments on fluidized bed bioreactor, we decided to move on the new type of bioreactor and reproduce a clinical BAL therapy.

Similar bioreactor designs, such as stirred-tank bioreactors, have long been used in large-scale culture of mammalian cells to provide an environment allowing control of oxygen, pH, and continuous addition and removal of medium. They are commonly used for the production of spheroids that can be maintained for extended periods in large scale ¹⁴¹, classically employed in toxicological applications ¹⁴⁷. Moreover, the group of Dr. Nyberg, who recently investigated the role of the spheroid reservoir BAL on a pig model of ALF ²²², highlighted how an impeller-agitated bioreactor could support high volumes of hepatocyte spheroids solutions, with a simple and compact design easy to scale up for BAL clinical application ²²³. Overall, we consider that the PDB hosting alginate-PLL encapsulated HepaRG fitted those important criteria and, to our knowledge, it is the first time that this design is used for BAL applications.

HepaRG matured in PLL alginate beads were able to produce proteins, detoxify ammonia and metabolize lactate to levels comparable or superior to other published works with similar cells ¹⁸⁹ or primary porcine hepatocytes in the AMC-BAL ²⁰⁴. The latter two activities were superior in PDB compared to shaken setup in link with net cellular activity, since the results were normalized by the controls with empty alginate-PLL beads. It is difficult to assume that the perfusion of medium was the key element to the enhanced activity observed in PDB, given the very low perfusion flow in our experiments (0.4 mL/min). We thus hypothesized that such improvement was promoted by an increased oxygenation of the culture medium. The latter is associated with the synergistic role of

orbital shaking culture and the increased exchange surface between medium and external environment in PDB rather than the shaken setup. Adam et al. 2018 assumed that an improved oxygenation when cultivating HepaRG cells in shaking conditions led to a stimulation of mitochondrial biogenesis, improving hepatic differentiation and cell metabolic activity (such as ammonia detoxification and CYP 3A4 activity) ¹⁸⁸. In addition, the role of oxygen on HepaRG differentiation and functions is crucial, as observed by van Wenum et al. 2018, where the authors demonstrated that culturing HepaRG in hyperoxia (i.e. 40 % O₂) enhanced cell differentiation and improved metabolic functions (such as ammonia detoxification and CYP3A4 activity), when compared with normoxia condition (i.e. 21% O₂) ²⁰³.

In PDB, we noticed an important decrease of around 40% in initial ammonia concentration and around 30% in lactate after 6 hours of cell perfusion in the equivalent pathological plasma medium. At the end of the experiment, we did not notice any deterioration of the alginate-PLL beads or loss of cells, observing the supernatant on bright field microscopy. This feature, together with the presence of filters that avoid cell escaping from the bioreactor, is of essential importance to conduct a safe therapy for the patient.

Cell metabolic performance appeared negatively affected when alginate-PLL beads were exposed to the pathological plasma medium in comparison with the BAL function test medium, although the cellular activities remained very high. The only difference between these two media is the total protein content. In fact, the test medium contains only 5 g/L of total proteins while the equivalent pathological plasma contains 70 g/L, in order to mimic the characteristics of plasma ¹⁷² (by the addition of 65 g/L of BSA). The Chamuleau group observed that HepaRG exposed to ALF-rat plasma showed increased cell leakage, lipid droplet formation and reduced transcript levels of various hepatic genes, disrupting some metabolic activities ²²⁴. Moreover, a severe decline in drug metabolizing and ammonia eliminating activity was also observed in monolayer and in BAL cultures of primary hepatocytes after exposure to ALF plasma ²²⁴. Our homemade equivalent pathological plasma medium does not present the typical toxic background of a real ALF-plasma in terms of pro-inflammatory cytokines, bile acids and bacteria lipopolysaccharide. Therefore, our hypothesis to explain the decreasing in cell functionality is the high concentration of albumin, in synergy with the presence of ammonia and lactate, and the slight decreasing of cell viability (observed in 2D configuration). In this sense, further investigation is necessary.

4. Conclusions

During this phase, we analysed the various stages to adapt the optimized culture method developed in chapter 3 to bioreactors compatible with our BAL. We adapted the HepaRG biomass encapsulated in alginate beads to the condition of ALF therapy by adding a PLL coating. This coating covered the shell of the beads without altering the porosity or viability of cells. In terms of metabolic activity, we measured very interesting performance in line with the required for BAL in

the treatment of ALF. The next step will be to implement the PDB in the BAL in the process of optimization in our laboratory and start the preclinical experiments on ALF rodent models.

5. Key points of phase II

- The use of an equivalent human plasma model containing typical ALF toxins had deleterious effect on alginate beads stability. Same effects could be expected in a clinical setting.
- It emerged the need to improve the mechanical stability of the alginate beads
- An external coating of PLL was realized, increasing the mechanical resistance of the beads, without importantly altering the metabolic performance of encapsulated HepaRG
- Experiments on fluidized bed bioreactor failed
- As an alternative, we proposed the use of a perfused dynamic bioreactor (PDB), adapted to the BAL device realized in our laboratory (discussed in chapter 5), hosting HepaRG encapsulated in 1.5% alginate - 0.1% PLL coated beads. No glass microparticles were required, as the mass transfer occurred by orbital shaking and not by fluidization, simplifying the cell encapsulation process
- This setup demonstrated very promising results in terms of safety of therapy (no beads degradation/no loss of cells in the circuit) and cell metabolic performance
- Since the fluidized bed bioreactor need to be better designed, preclinical tests on ALF rodent models will be soon started using our PDB based BAL

Chapter 5. Phase III: towards animal investigations

1. Introduction

In this chapter, we describe the steps that led to:

1. The choice of the animal model for *in vivo* evaluation of the treatment
2. The miniaturization of the human-scale BAL to small animal model
3. Effects of the artificial elements of the BAL (activated charcoal and ionic resin) on a model of pathological ALF human plasma
4. Effects of the whole artificial component of the BAL (activated charcoal, ionic resin, and perfused dynamic bioreactor hosting empty beads, in series) on a model of pathological ALF human plasma
5. Setting the safety analysis on healthy rats

All these operations are part of a bioengineering approach that required the collaboration of engineers and clinicians from iLite programme. The device created meets the needs of the animal model but also those of the engineers involved in its creation and the clinicians who have to follow the evolution of the disease during treatment.

As described in chapter 1, the research group headed by Dr. Legallais has been working for many years on the development of a BAL based on fluidized bed technology. This technology needs to be validated on preclinical models before moving on to human experimentation. In previous work, a BAL of this type was realized on a human scale in our laboratory, and it was tested on large animal models (sheep) for its safety ²²⁵ and fully described in Sarah Figaro PhD thesis ⁵⁰.

During this thesis, it was chosen to work on small animals, for reasons explained in results §2.1, to validate the technology of fluidized bed BAL for preclinical studies. The concept of miniaturization of the pre-existing device from human to small animal models is shown in figure 80.

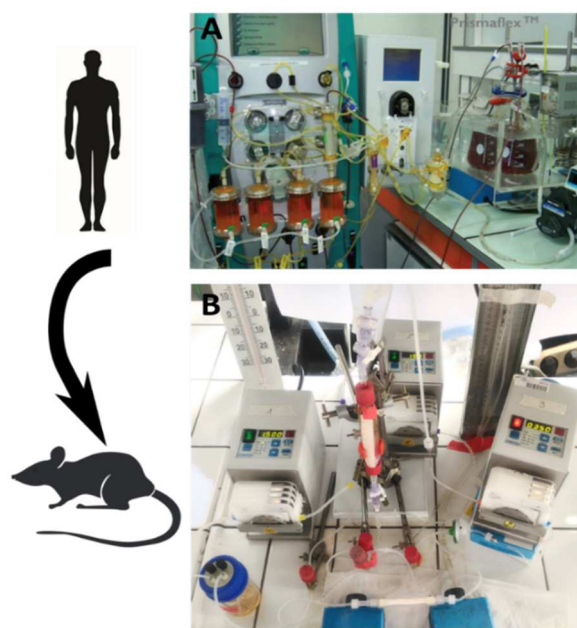


Fig. 80: Miniaturization from the human-scale (A) to small-scale BAL (B)

2. Design of the pathological animal model

In this section, we describe the choice of the animal model, the pathological model; and the method of ALF induction, following the steps previously proposed in chapter 1 section 5.

2.1. Choice of the animal model

According to the construct validity criterion, our initial choice has been limited to pig and rodent models (rat or mouse) because both share some similar anatomical and functional features with human ^{226–230}. For a first proof of concept, together with our partners (clinicians, Dr J.C. Duclos-Vallée and Dr Faouzi Saliba, and regulatory affairs, Dr V. Vanneau and Dr N. Ferry), we decided to use the rat for the scientific pertinence of the model, and also the ease of manipulation (size of the model, simple animal care unit, etc.) and its lower costs in comparison to pigs.

2.2. Choice of the pathological model

Between the spontaneous and induced animal models, we chose the second option because there are no spontaneous models of ALF ²³¹. Among the different methods, we choose the chemical induction using D-galactosamine because it reproduces a number of important ALF human features, such as hypoglycaemia, hepatic encephalopathy, increased blood levels of hepatic enzymes, and a typical inflammatory response similar to those seen in humans ²³². Moreover, since drug intoxication is one of the major causes of ALF, induced models via hepatotoxic drugs is representative of the reality. The predictive and face validities criteria are therefore respected (Terblanche and Hickman ¹⁶¹ for ALF and table 18). In particular, after a bibliographic analysis, the pathological animal model that appears most reproducible is Wistar rats weighing 180-220 gr with ALF induction through a single intraperitoneal injection of D-galactosamine at 1.2 g/kg ¹⁶⁰.

| D-galactosamine ALF-induced rat | |
|---|--|
| Criteria | Score on the validity of the criterion (* low, ++ medium, +++ high) |
| Predictive Validity | ++ |
| Face Validity | ++ |
| Construct Validity | ++ |
| Reversibility | +++ |
| Reproducibility | ++ |
| Death from liver failure | +++ |
| Adequate animal size | ++ |
| Therapeutic window | +++ |
| Minimal hazard to personnel | + |
| Conscious animal during treatment | +++ |
| Compliance with animal standards | +++ |
| Ease and cost of manipulations | ++ |
| Established methods in literature | +++ |
| Extrahepatic effects of D-galactosamine | + |
| Features of human ALF | ++ |

Tab. 18: Validity of the criteria for the choice of the animal model

Therefore, the choice of this pathological models for our research relies on scientific reasons (robustness of the model), but also economic (quantity of cells, culture medium, etc.) and practical (simpler experiments, smaller structures to accommodate animals, etc.) advantages.

Of note, several research teams have already worked on the rat as the animal model using different methods of ALF induction, for BAL application. They did not all follow our approach regarding the way to induce ALF. Their methodology and main outcomes are summarized in table 19 and will guide us in the set up and the data analysis.

| Animal model | Induction method of ALF | BAL setup | Cell source | Cell quantity (million/BAL) | Perfusion time after ALF induction (treatment time) | <i>In vitro</i> (on cells)/ <i>in vivo</i> (on animal) characterization | Main outcomes | Refs. |
|--|---|--|-----------------------------|-----------------------------|--|---|---|-------|
| Male Wistar rats, 275–325 g | Liver ischemia | Plasma separator. 3D nonwoven polyester fabric | Primary porcine hepatocytes | 440 | Until death of the animals (maximum 14 hr perfusion) | <ul style="list-style-type: none"> ➤ <i>In vitro</i>: pig alpha glutathione –S-transferase (cellular damage) ➤ <i>In vivo</i>: animal survival time, evaluation of neurological status by clinical grading (see ref.), hemodynamic (blood pressure), ammonia and lactate levels, rat alpha glutathione –S-transferase (α-GST, hepatocellular damage) | <ul style="list-style-type: none"> ➤ Significantly prolonged survival in treated group (BAL with cells) in comparison with control groups (no BAL and BAL without cells) ➤ Significantly delayed deterioration in neurological status ➤ Improved hemodynamic stability ➤ Ammonia and lactate levels lower than control groups ➤ The porcine hepatocytes can support BAL therapy along 14 hr therapy | 233 |
| Lewis rats, 350–400 g | Partial hepatectomy combined with induction of right liver lobes necrosis | Whole blood perfusion. Microcarrier-attached hepatocytes inoculated into the extrafiber compartment of a small hollow fibre module | Primary rat hepatocytes | 300 | 4 hr | <ul style="list-style-type: none"> ➤ <i>In vitro</i>: no test ➤ <i>In vivo</i>: survival time, blood chemistry (sodium, potassium, glucose, lactate, albumin, ammonia, bilirubin, blood urea nitrogen, creatinine and uric acid levels, activity of alanine and aspartate aminotransferase, lactate dehydrogenase, alkaline phosphatase, prothrombin time, and partial thromboplastin time), blood hepatocyte growth factor and TGF-β1 | <ul style="list-style-type: none"> ➤ Significantly prolonged survival in treated group (BAL with cells) in comparison with control group (BAL without cells) ➤ Improved blood chemistry especially for alkaline phosphatase, prothrombin time, partial thromboplastin time, blood urea nitrogen and uric acids level ➤ Both in the treated and in the control group, blood hepatocyte growth factor remained elevated but, in the treated group, the level of blood TGF-β1 was significantly lower than the control group | 86 |
| Male Sprague-Dawley rats, 250–350 g | D-galactosamine (1.2 g/kg intraperitoneal) | Plasma separator. Flat plate bioreactor with internal membrane oxygenator | Porcine hepatocytes | 14 | 10 hr | <ul style="list-style-type: none"> ➤ <i>In vitro</i>: no test ➤ <i>In vivo</i>: liver histology, liver function parameters (total bilirubin, aspartate aminotransferase, alanine aminotransferase, alkaline phosphatase, ammonia and prothrombin time), and animal survival | <ul style="list-style-type: none"> ➤ Massive hepatocellular necrosis with an acute inflammatory response was observed in both treatment groups (BAL with cells, BAL without cells (control)) ➤ Less severe liver injury occurred in the animal group that received treatment with the BAL containing porcine hepatocytes ➤ Ammonia level and prothrombin time significantly lower after perfusion ➤ Significantly prolonged survival in treated group (BAL with cells) in comparison with control groups (no BAL and BAL without cells) | 234 |

| | | | | | | | | |
|------------------------------------|-------------------------|---|------------------|------------------|--|--|--|-----|
| Male Wistar rats, 325-350 g | Complete liver ischemia | Third generation AMC-BAL | Cell line HepaRG | 750 | Until death of the animals (maximum 16 hr perfusion) | <ul style="list-style-type: none"> ➤ <i>In vitro</i>: ammonia, urea, 6β-hydroxytestosterone, apolipoprotein A-1, lactate ➤ <i>In vivo</i>: survival time, clinical hepatic encephalopathy grading score, blood ammonia, plasma creatinine concentrations, plasma alanine aminotransferase, aspartate aminotransferase levels, haemoglobin levels, and blood glucose levels | <ul style="list-style-type: none"> ➤ High level of hepatic functionality <i>in vitro</i>, measured by the elimination of ammonia, production of urea, production of 6β-hydroxytestosterone, consumption of lactate, and synthesis of apolipoprotein A-1. ➤ HepaRG-AMC-BAL. prolongs the life of ALF rats substantially with ~50% | 106 |
| Male Wistar rats, 250-350 g | Partial hepatectomy | Plasma separator. Hybrid cryogel (Poly(NiPAAm)-chitosan) based bioreactor hosting hepatocytes and containing activated charcoal | Cell line HepG2 | 1.5 per scaffold | 3 hr | <ul style="list-style-type: none"> ➤ <i>In vitro</i>: adsorption capacity of activated charcoal on ALF plasma (bilirubin, aspartate aminotransferase, urea ammonia and albumin). Effect of activated charcoal on cell viability and functionality (albumin secretion) ➤ <i>In vivo</i>: liver functional parameters | <ul style="list-style-type: none"> ➤ Activated carbon reduces the toxin load of ALF plasma to some extent ➤ ALF plasma affect cell viability and functionality ➤ Positive effect on cell viability when ALF plasma is pre-treated with activated charcoal ➤ Cryogel based bioreactor shows better efficacy in terms of detoxification and synthetic functions than the conventional BAL setup use as control | 235 |

Tab. 19: BALs tested on rats, methods and outcomes

3. Miniaturization of the pre-existing human-scale BAL

As previously presented in chapter 1, our system is composed of several components (Fig. 81), both artificial and tissue engineered ones. In the 70's, it has been demonstrated that in galactosamine-induced fulminant hepatic coma rat models, charcoal hemoperfusion increased both survival time and survival rate ²³⁶. Moreover, in recent years, hybrid BAL devices involving artificial and biological elements showed that combining the detoxifying capacity of an adsorbent column with the synthetic function of a cell-loaded bioreactor might lead to positive outcomes in terms of both safety and efficiency ^{55,56}. The overall results suggest that the use of activated charcoal and ionic exchanger resin in BAL can be advantageous. Therefore, under suggestion of Dr Faouzi Saliba (involved in clinical studies on MARS²³⁷), activated charcoal and ionic exchanger resin were added in our device. The activated charcoal used in our BAL is taken from the cartridge diaMARS[™] AC250 by MARS[®] system. The carbon is uncoated and especially suited for elimination of low-molecular, non-polar compounds (such as polycyclic aromatic hydrocarbons, fatty acids, urea, creatinine, uric acid ²³⁸) and in general it is able to remove the albumin-bound toxins (e.g. tryptophan and glutamine, involved in the aetiology of hepatic coma during ALF ⁴⁹). The ion exchange resin is taken from the IE250 by MARS[®] system. It is made of microbeads of cholestyramine and it is able to remove water-soluble and albumin-bound toxins (such as bile acids and bilirubin). In the MARS[®] system, those elements are used to clean and regenerate the human serum albumin dialysate. The general goal of the MARS[®] therapy is to remove water-soluble and albumin-bound toxins accumulating during ALF (such as ammonia, creatinine, urea, bilirubin, bile acids or small proteins such as cytokines ⁶¹ and small peptides ²³⁹) via an albumin dialysis, thereby helping patients recover native liver functions or help bridge them to transplantation. Those toxins in fact compromise liver function causing hepatocytes necrosis and apoptosis. This is accompanied by the release of proinflammatory cytokines (especially TNF- α and IL-6) overall creating a vicious circle of autointoxication, progressing hepatocellular damage and inflammation. It has been observed that MARS[®] therapy can not only remove toxins but also the cytokines that, in case of ALF, can favour the progression of the disease ²⁴⁰, since they are implicated in the development of HE, vasodilation, systemic inflammatory response syndrome (SIRS) and multiple organ failure (MOF)⁶¹.

3.1. Sizing process

The design of the small-scaled BAL was realized by linear miniaturization of all the components of the human-scale BAL was initiated by UTC engineering students Claire de Lartigue (now engineer in our team) and Florent Hublet, under the supervision of Dr. C. Legallais. The main objective of their internship was to reduce the size of the pre-existing human-scale BAL to the size of a rat, considered as 1/250 the human size in weight (75 kg for the human and 300 g for the rat).

Based on this ratio, the sizing of the different component of the devices was calculated (presented in figure 81, and tables 20, 21). The human-scale BAL is composed of a plasmafilter (TPE2 by Gambro), four bioreactors in parallel (hosting the biomass), an oxygenator/heater (Prismalung[™] by

Gambro), artificial detoxifying elements (an activated carbon cartridge Adsorba™ and an ion exchange cartridge IE250™, by MARS), and a syringe pump for anticoagulation ²²⁵.

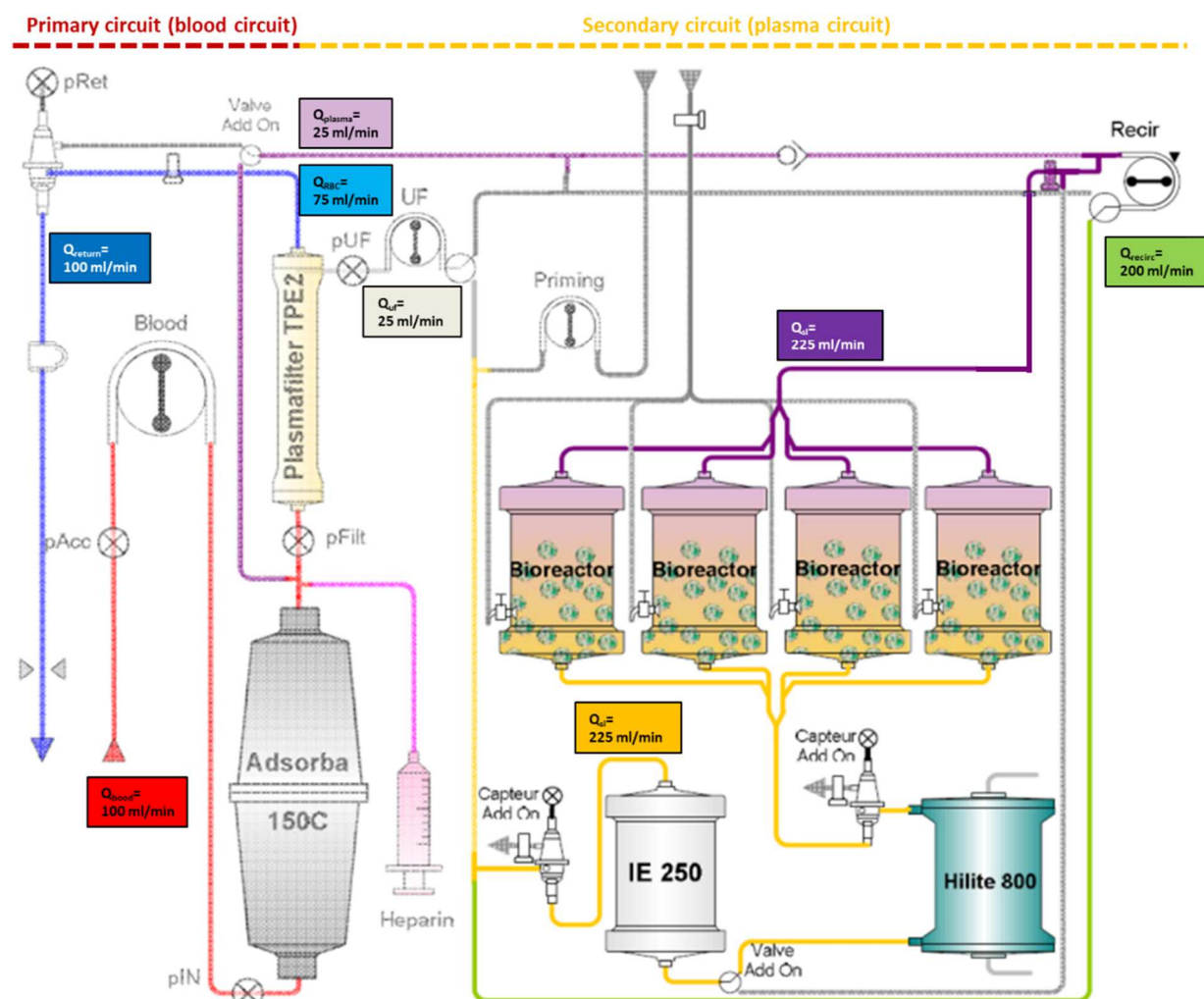


Fig. 81: Human scale BAL circuit developed by S. Figaro ⁵⁰.

| Abbreviation | Full name |
|---------------------|--|
| Flow rates | |
| Q_{blood} | Flow rate of blood in |
| Q_{RBC} | Flow rate of red blood cells |
| Q_{UF} | Flow rate of ultrafiltration |
| Q_{recirc} | Flow rate of plasma recirculation |
| Q_{sl} | Flow rate in resin, charcoal and bioreactors |
| Q_{plasma} | Flow rate of treated plasma |
| Q_{return} | Flow rate of blood out |
| Pressures | |
| p_{Acc} | Vascular pressure |

| | |
|-----------------------|-------------------------------|
| pIN | Plasmafilter in pressure |
| pUF | Ultrafiltration pressure |
| pRet | Return pressure |
| Other elements | |
| BLD | Blood Leak Detector |
| UABD | Ultrasonic Air Blood Detector |

Tab. 20: Legend human-scale BAL components (SUPPLIVER project)

The results obtained after the calculations for the scaling down are summarized in the following table 21.

| Component | Abbreviation | Human | Rat |
|-------------------------------|-------------------------------------|----------|----------|
| Flow rate | | | |
| Blood in | Q_{blood} (mL/min) | 100 | 0.55 |
| Ultrafiltration | Q_{uf} (mL/min) | 25 | 0.14 |
| Recirculation | Q_{recirc} (mL/min) | 200 | 1.10 |
| Plasma in bioreactors | Q_{sl} (mL/min) | 225 | 1.24 |
| Treated plasma | Q_{plasma} (mL/min) | 25 | 0.14 |
| Red blood cells | Q_{RBC} (mL/min) | 75 | 0.41 |
| Blood out | Q_{return} (mL/min) | 100 | 0.55 |
| Active charcoal | | | |
| Volume | V_{charc} (mL) | 140 | 0.77 |
| Plasmafilter | | | |
| Hydraulic permeability | L_p (m/min/mmHg) | 343 | 343 |
| Surface | S (m ²) | 3.50E-01 | 1.20E-03 |
| Ionic resin | | | |
| Volume | V_{resin} (mL) | 100 | 0.55 |
| Bioreactor | | | |
| Beads volume | V_{beads} (L) | 1 | 0.05 |
| Bioreactor volume | V_{bior} (L) | 2 | 0.1 |
| Bioreactor height | H_{bior} (m) | 9.40E-02 | 1.00E-01 |
| Bioreactor section | S_{bior} (m ²) | 2.64E-03 | 8.00E-04 |

Tab. 21: Sizing of the device's components, from human to rat scale

About the plasmafilter, it was decided to use a membrane of 34 cm² and not of 12 cm² as calculated, in order to guarantee a correct filtration. Note that the flow rate needed to obtain a fluidized bed in the bioreactor was determined experimentally. The results summarized in the table below have evolved during the project but they allowed having an idea of the size of the elements of the device.

It should be emphasized that in addition to the scaling down process, a more suitable design was realized for the rat. The aim was to minimize the dead volume of the device and its components. In the first design (§3.2), the activated charcoal was placed after the plasmafilter (to better treat the

plasma, rather than whole blood, where the toxins of ALF are concentrated), the oxygenator was removed (in order to reduce the volumes of the circuit), the number of fluidized bed bioreactors was reduced (one instead of four). Oxygenation is supposed to be provided by the gas-permeable silicone tubing. If the oxygenator is needed, it will be later implemented. In addition, the bioreactor will be heated at 37 °C either by a system of tubes coiled around the bioreactor in which heated water recirculates or via a double-walled bioreactor, containing recirculating heated water between the two walls. The heating system is being optimised.

3.2. First generation of the small-scaled BAL

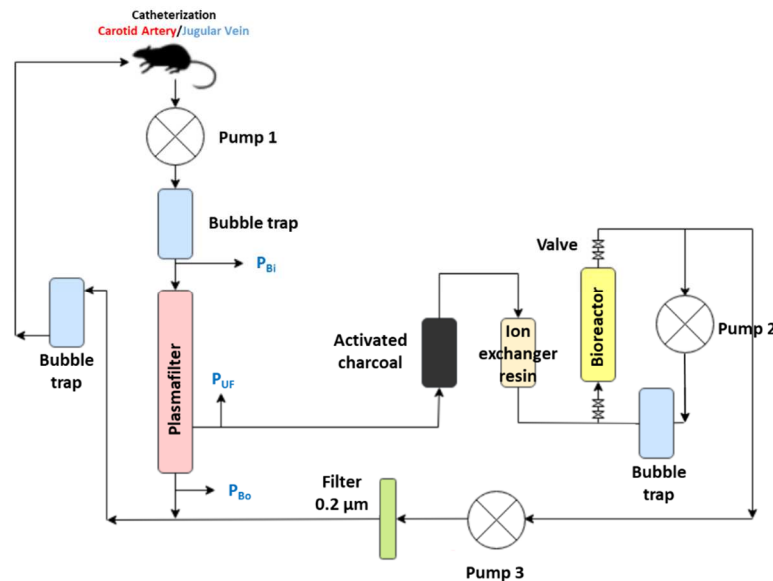


Fig. 82: First generation BAL prototype

In this setup (Figure 82), the whole blood is picked up by the carotid catheter (see §5.1) implanted in the rat, through a peristaltic pump. A bubble trap avoids the forming air bubbles to continue the path. The whole blood arrives to the plasmafilter where it is separated into formed elements (blood cells) and plasma. The blood cells continue the path and re-enter in the animal, through a catheter placed in the jugular vein (see §5.1). 20-25% of the plasma is directed towards the two artificial elements of the BAL, respectively the activated charcoal and the ion exchanger resin. Then, the plasma arrives into the fluidized bed bioreactor, the biological component of the BAL, where it enters in contact with the encapsulated HepaRG. Here, the pump 2 ensures a loop circulation that is independent by the rest of the circuit and that guarantees the fluidized bed formation in the bioreactor, and multiple fluid passages with cells. This plasma is then pushed by the pump 3 towards the animal. During this final step, the treated plasma passes through a 0.2 μm filter, that blocks alginate debris and cells escaped from the bioreactor, and can re-join the formed elements of the blood. The reformed whole blood passes through a bubble trap and then it can finally enter in the animal.

The circuit has 3 outputs for pressure control, one upstream of the plasmafilter (P_{Bi} - Pressure blood inlet), one downstream (P_{Bo} - pressure blood outlet), and another to the side (P_{UF} - Pressure ultra

filtrated). They allow controlling possible problems of plasmafilter clogging. The total volume of the circuit is around 25 mL. Since the rat has a blood volume of approximately 15 mL, the device will need to be filled with plasma (or physiological serum) before therapy can begin. Therefore, for the *in vivo* tests, it will be necessary to take into account this "dilution effect" due to plasma (or physiological serum) injection.

After a first attempt at circulating bovine serum, this first generation BAL showed few problems such as the clogging of plasmafilter and of the 0.2 μm filter, the connections between certain elements. Therefore, a second generation was designed. Other objectives of the new design were to reduce the total volume of the device, and to simplify the filling of the circuit.

3.3. Second generation of the small-scaled BAL

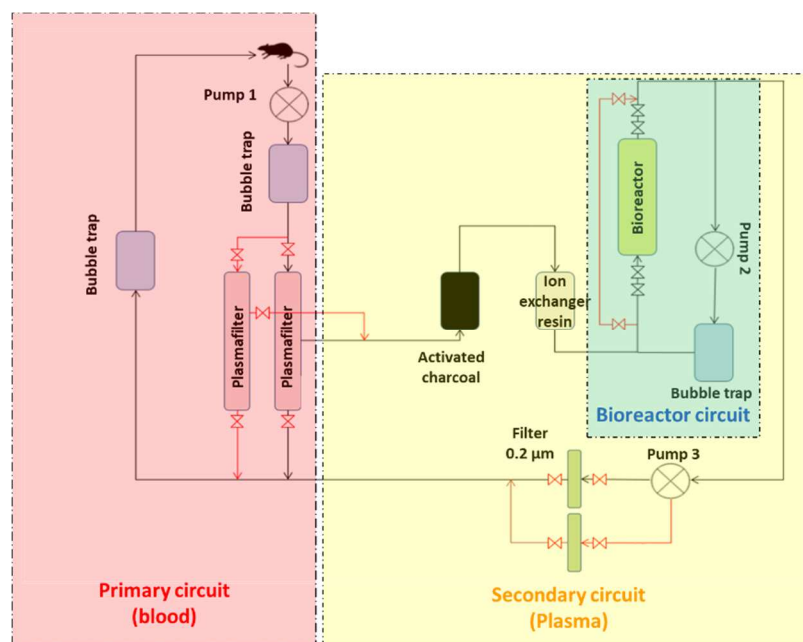


Fig. 83: Second generation BAL design

The engineering students Juliette Delhaye and Guillaume Godefroy realized the second generation prototype. Two modifications of the first circuit were realized, adding a deviation for a second plasmafilter and a second 0.2 μm filter. Moreover, another deviation for a second bioreactor was added to ensure the functioning of the biomass in case of failure of the first one. The new design is presented in figure 83. This is the circuit in its current state. For a better understanding, the extracorporeal circuit is divided into 3 sections: primary circuit (blood), secondary circuit (plasma), bioreactor circuit, each highlighted with different colours (respectively red, yellow and blue). After the final optimization of encapsulated cells with PLL coating, we were not able to perform tests in fluidized bed bioreactor (Chapter 4, §2.3).

3.4. Third generation of the small-scaled BAL

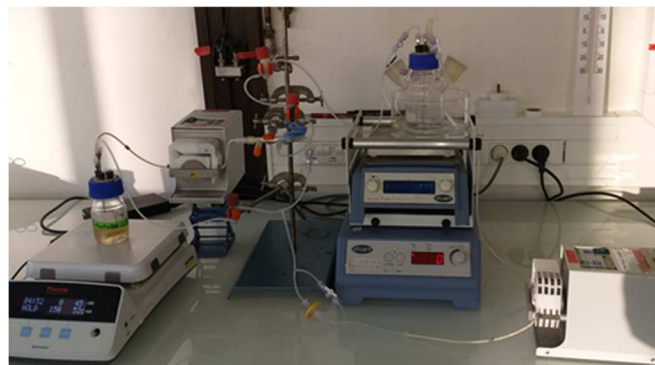
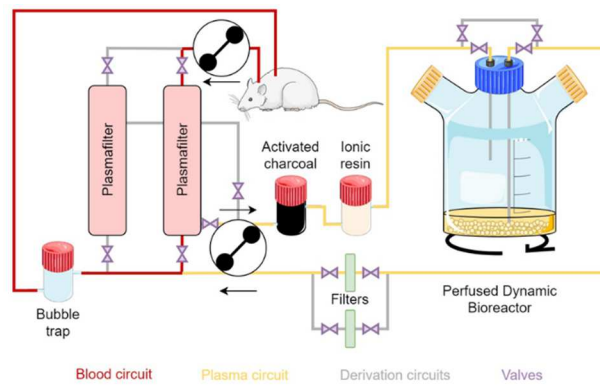


Fig. 84: BAL circuit (top) implementing the PDB bioreactor. BAL device (down)

Given the encouraging results obtained during the *in vitro* cell characterization in PDB, we realized the BAL circuit with this type of bioreactor (Figure 84). There are several advantages in using the PDB instead of fluidized bed bioreactor:

- The whole cell culture process can be carried out in this bioreactor, from the day of encapsulation of the biomass to its clinical use
- Since we do not need fluidization, glass microparticles can be avoided, simplifying the process of encapsulation
- Preliminary experiments on PDB demonstrated very high capacity of detoxification of ammonia and clearance of lactate by the biomass
- The bioreactor can be easily warmed up, through a regular hot plate
- The double arms of the bioreactor allow easy manipulation (addition and removal of culture medium and biomass)
- The high surface exchange between liquid and gas phases guarantees an improved oxygenation of the medium, therefore, an external oxygenator might not be necessary
- The double arms of the bioreactor can be dedicated to an inlet for an external oxygenator, if necessary
- Simplification of the BAL circuit: removal of the pump 2 (dedicated to the FB in an isolated loop), reduction in volume (from 25 to 18 mL)

Through preliminary studies, we observed that 10 mL of fluid was sufficient to submerge all the biomass (5 mL of alginate beads containing the 50 million cells), while the fluidized bed bioreactor needed about 20 mL of fluid. Therefore, using the PDB, we were able to reduce the volume of the whole circuit to about 18 mL.

4. Effects of the artificial elements of the BAL on a model of pathological ALF human plasma

In parallel, we found important to investigate the effect of the artificial elements of our BAL in the removal of specific physiological and ALF markers. The terms "artificial elements" describes here the activated charcoal and the ionic exchanger resin. Indeed, during a BAL therapy, the plasma of the patient will enter in contact with those elements that on one hand could remove ALF toxins (such as ammonia), but on the other hand also elements important for the physiology of the body (such as glucose).

The markers analysed are glucose, calcium, ammonia, lactate, contained in the pathological plasma medium already used for the experiments in cells. They were chosen because glucose and calcium are vital elements for the physiological behaviour of cells and body, while ammonia and lactate are typical molecules of ALF (chapter 1, §3.2). Therefore, it was desirable to not alter glucose and calcium levels, while removing ammonia and lactate.

4.1. Effect of activated charcoal and ionic resin on perfusion medium content

These tests were realized in closed circuits including a media reservoir, a glass container with the artificial elements, and a peristaltic pump to allow medium circulation (see chapter 2, §15), inspired from experiments conducted by Morimoto et al. 1989²⁴¹.

The circuits presented in figure 85 allow testing all the possible configurations of the artificial elements: ionic exchanger resin alone, activated charcoal alone, charcoal and resin in series, and resin and charcoal in series. Importantly, according to the manufacturer (MARS), the activated charcoal had to be washed with a 5% w/v dextrose solution in physiologic serum while the resin only in physiologic serum, both for 30 minutes at flow rate of 1.5 mL/min. Once washed, the different combinations of artificial elements were put in contact with 35 mL of equivalent plasma (HepaRG medium + 70 g/L BSA) for 2 hours at a flow rate of 0.4 mL/min, and then with 35 mL pathological plasma model (HepaRG medium + 70 g/L BSA + 1.5 mM ammonium chloride + 2 mM L-Lactate) for 6 hours at the same flow rate. In the latter medium, we measured the concentration of the selected markers (glucose, calcium, ammonia, lactate) by taking aliquots from the reservoir immediately after the first complete recirculation, and at each hour. In order to eliminate artefacts and measuring a net activity of the artificial elements, empty circuits were also realized as controls. All experiments were conducted in a humidified environment at 37°C, as it will be for a BAL therapy on animals.

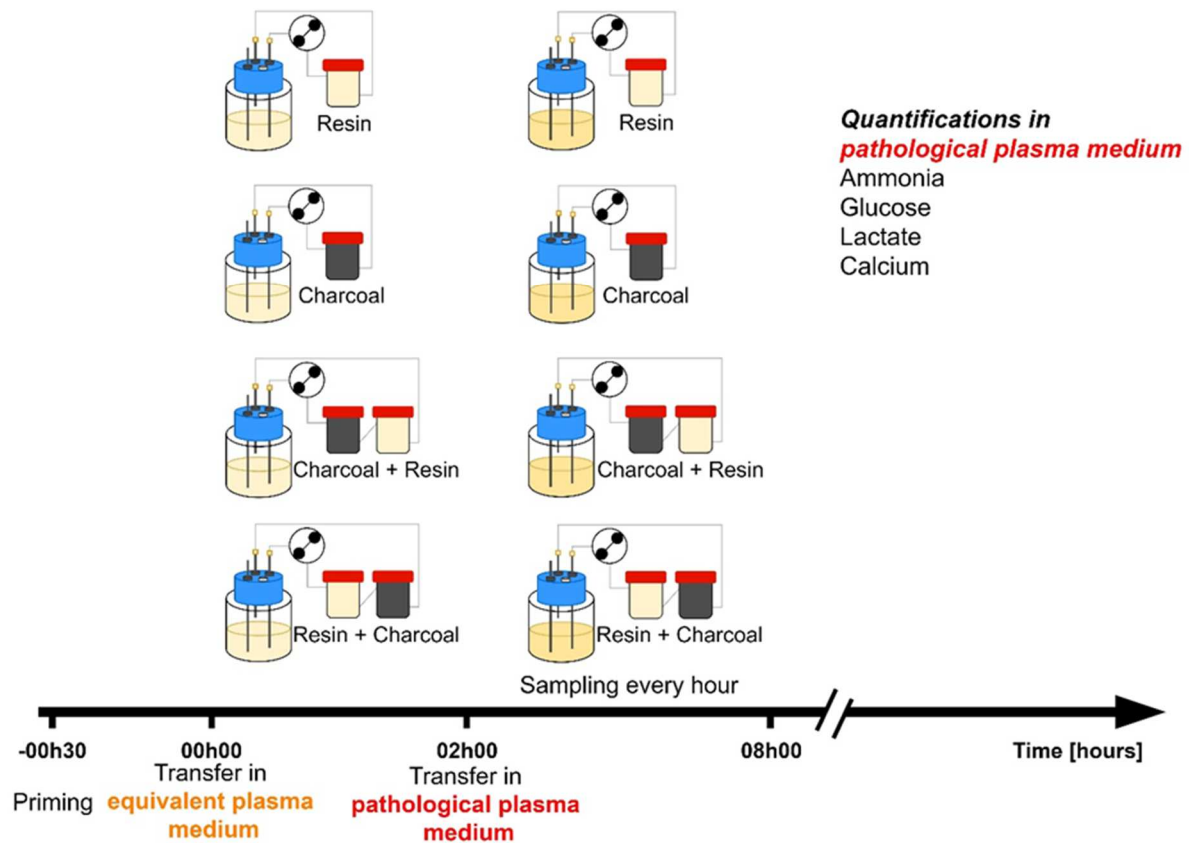


Fig. 85: Closed circuits for testing the artificial elements. Experimental setup. N = 2

The expectations of these tests are:

- No variation in concentration for calcium and glucose
- Reduction in concentration for ammonia and lactate

Preliminary studies showed that the best performance (considering the aforementioned expectations) is obtained when the activated charcoal is connected in series with the ionic resin. Therefore, only these results will be presented and discussed.

The results (Figure 86) show that there was no effect (no removal) on ammonia while calcium and lactate concentrations decreased after 6 hours of recirculation. Instead, glucose concentration increased.

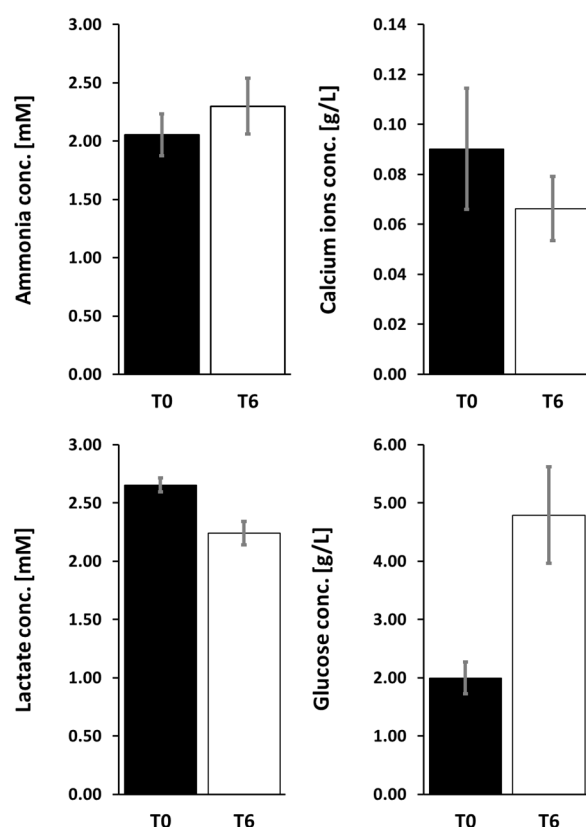


Fig. 86: Effect of charcoal and ionic resin (connected in series) on specific markers contained in pathological medium. Y-axis represents the concentration of the marker while X-axis the time-point of sampling (T0, time zero, means sampling after a complete pathological medium recirculation in the circuit while T6 is the sampling after 6 hours of medium recirculation in the circuit). N = 3

According to these results, for ammonia elimination, our BAL will thus rely only on the detoxification activity of the biomass. The removal of calcium is very slight and we suppose that it will not represent a problem in clinical context. Instead, the removal of lactate with the artificial elements could represent an important added value for our device.

The glucose concentration importantly increased over time. This is very probably due to the priming of activated charcoal with 5% glucose solution. In fact, during that phase, glucose is adsorbed in the charcoal and then released after the 6 hours recirculation. We do not know if the rise in glucose concentration (to about 30 mM in our experiments) represents a problem for next clinical application. At the cellular level, it was observed that primary human hepatocytes, in the presence of high glucose concentrations (about 25 mM), still remained functional ²⁴², even if lipid droplets formation and reduction in insulin sensitivity were observed. In the clinical context, blood glucose concentration can be managed by insulin (or glucose if needed) injection. Therefore, we think that at clinical level, this phenomenon should not have a strong negative impact on the outcome of therapy.

Morimoto et al. ²⁴¹ realized similar *in vitro* experiments demonstrating that a combination in series of resin/charcoal favoured a strong removal of bilirubin and aromatic amino acids (implicated in hepatic encephalopathy). The authors also treated patients in ALF with an extracorporeal circulation system containing charcoal and resin, showing a reduction in bilirubin and aromatic amino acids

levels, improving their clinical conditions. Although the long prognosis was not satisfactory in all cases, the authors believed that the palliative improvement of clinical conditions and the prolongation of life were realized by this treatment. However, they pointed out that also biologically essential substances needed for metabolism could be removed while the patient' plasma was treated with those sorbents.

Overall, all of our observations and those made in the literature encouraged us to use these sorbents in our BAL device, but further investigations are needed, such as the removal of bilirubin and bile acids contained in rat plasma.

4.2. Effect of the whole artificial components in series on the perfusion medium content

Since after the final optimization of encapsulated cells with PLL coating, we were not able to perform tests in fluidized bed bioreactor (Chapter 4, §2.3), the circuit here presented integrates the perfused dynamic bioreactor (PDB). We tested the effect of the whole artificial component of the device on the pathological model, connecting charcoal, resin, and PDB in series, as they will be placed in the final whole setup.

The PDB contained 5 mL of empty 1.5% alginate beads coated, at day 1, with 0.1% PLL. The beads were then kept in shaken culture in the incubator until day 14, when the test was realized, in order to be comparable with the experiments with cells.

The experimental design is shown in figure 87. After resin and charcoal washing (respectively in physiologic and 5% dextrose in physiologic serum for 30 minutes), the whole setup was assembled. The peristaltic pump controlled the flow rate of the medium and worked at 0.4 mL/min. The whole setup was put in contact with 40 mL of equivalent plasma for 2 hours and, after that, with 37.5 mL of pathological plasma model for 6 hours. The PDB constantly contained 10 mL of medium, as it will be in a real therapy. In pathological plasma medium, we measured the initial and final concentrations of the selected markers (glucose, ammonia, lactate, and total proteins) by taking aliquots of medium from the reservoir immediately after the first complete recirculation, and after 6 hours. The whole experiments was conducted at 37°C, mimicking a future BAL therapy.

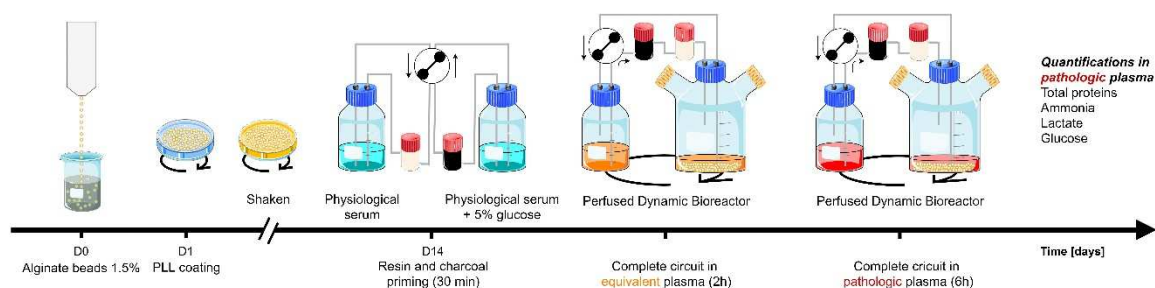


Fig. 87: Experimental plan with all the artificial elements connected in series. N = 1

In this experience we also included total proteins among the markers, to study possible adsorption phenomena. The results in table 22 show that there was an effect of removal only for lactate and

total proteins concentrations, after 6 hours of recirculation in the pathological plasma. Ammonia and glucose concentration instead remained stable.

| Marker | Expectation | Pathological plasma | |
|-----------------------|-------------|---------------------|------|
| | | t0 | t6 |
| Ammonia (mM) | Adsorbed | 15 | 16 |
| Lactate (mM) | Adsorbed | 15 | 12 |
| Glucose (g/L) | Stable | 1.7 | 1.5 |
| Proteins (g/L) | Stable | 99.9 | 77.1 |

Tab. 22: Summary of the activities analysed on artificial elements connected in series

In parallel, we tested a circuit containing only the PDB with the empty beads, and no effect on removal of ammonia and lactate was detected. Therefore, the slight removal of lactate observed was due to its adsorption by charcoal and resin.

While the activities on ammonia and lactate are in the same direction in comparison with the previous experiments conducted on charcoal and resin connected in series, glucose showed a different behaviour, since here its concentration remained quite stable. Indeed, when we analysed the glucose concentration by hour (data not shown), we noticed a constant increasing over time in its concentration, and between time 5 and 6 hours, it was re-adsorbed, turning back at the initial concentration value. It is difficult to link this observation with the presence of empty beads. Indeed, more investigations are needed. We noticed also a decrease in proteins concentration. This could be due to adsorption in the artificial elements and in the alginate beads. A similar effect on protein adsorption was reported by Kumar et al. using activated charcoal ²³⁵.

Overall, this setup showed positive outcome for lactate removal (even if slight), positive observation for BAL application.

In perspective, we will test this same experimental setup but with a biomass present in the PDB. This will allow us to investigate the cellular behaviour, after the culture medium recirculated through charcoal and resin, which could also retain molecules necessary for cell viability. A preliminary experience in this direction is given in the next paragraph.

4.3. Effect of the recirculated medium on cell viability

Here, we tested the indirect cell viability using the media recirculated during the previous experiment, in 2D cell culture. The experiment was carried out in a 12 multi-well culture plate on day 14 post-seeding. All wells were treated in the same way in terms of washings and changing of the medium, in order to avoid artefacts in the viability due to these passages.

We compared 3 conditions:

- "CTRL +" of viability: HepaRG cells cultivated in HepaRG proliferation media (considered as 100% viability)
- "Pathological plasma model": cells treated for 2 hours with equivalent plasma and 6 hours with the pathological plasma model not recirculated through the artificial elements

- "Pathological plasma model after 6 hours recirculation through the artificial elements": cells treated for 2 hours with equivalent plasma and 6 hours with the pathological plasma model recirculated through the artificial elements for 6 hours (to imitate a complete therapy as for the bioreactor)

After exposure, we studied the cell viability through MTS colorimetric testing. The results (Figure 88) showed that cell viability was significantly affected when treated with the pathological plasma recirculated through the artificial elements. It should be noted that the activated charcoal used could have released particulate matter that could affect cell viability. At the moment, it remains difficult to confirm whether the cell viability is affected by the recirculated media rather than by this particulate matter. However, the MARS system (from which our activated charcoal comes) integrates a particle filter capable of blocking these charcoal residues. We have therefore proposed to use this type of filter also in our BAL, to be inserted immediately after the activated carbon (in progress).

Nonetheless, we think that cell viability (around 90%) is not compromised to such an extent that carbon and resin should be excluded from our device.

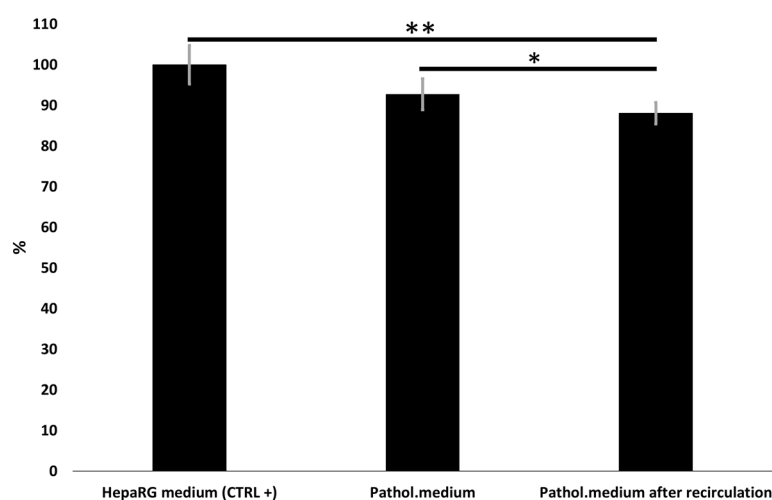


Fig. 88: Cell viability (expressed in %) in relation to the control: cells treated with HepaRG medium. Significance analysed by Mann-Whitney test.

Overall, the effects registered in terms of variation of concentrations of some components of the medium and on cell viability, will find better answers with *in vivo* tests.

5. Setting the safety analysis on healthy rats

In this section, we describe the initial steps for studying the safety of our BAL. The set of these steps will allow us to understand if the BAL therapy will negatively affect the physiological state of healthy rats.

5.1. Preliminary steps for animal testing

Filling the APAFiS legal form to get clearance for conducting the safety investigations of our system was performed together with Baptiste Hirsinger (MS student) and Dr. Ulysse Pereira, in charge of animal facility at UTC.

The preparation of these trials (shown on Fig. 84) raised some issues about the housing conditions of the animals. Indeed, it required connecting the rats via two catheters (jugular/carotid) to our device for 8h (estimated time of therapy) while keeping the animals alert and conscious. This is important to follow some physiological parameters during the therapy, such as the stress/suffering of the animal.

A solution had to be found to avoid the animals biting and ripping off their catheters or tangling themselves in it. Therefore, we contacted a company in the USA specialized in tethering apparatus for rodents (SAI Infusion, 278 Park Ave, Lake Villa, IL 60046, United States). The apparatus described on Fig. 89 allows the free movement of the animal in its cage and easy vascular access. Jugular/carotid catheterized rats were purchased from Janvier Labs (Le Genest-Saint-Isle, France).

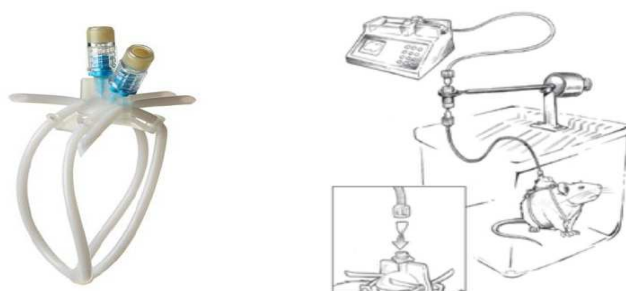


Fig. 89: Catheter harness and tethering mount

5.2. Optimization of the sterilization process of the plasmafilter

The plasmafilter used for our experiments were manufactured by 3M, Science applied to life, United States. It has the following characteristics:

- Material: polyethersulfone
- Number of internal fibres: 74
- Diameter of fibres (μm): 300
- Pore size (μm): 0.2
- Length: (cm): 5
- Surface (cm^2): 34
- Internal volume (cm^3): 1.5
- Dead volume (mL): 20 mL
- Blood flow rate (mL/min): 1
- Ultrafiltration flow rate (mL/min): 0.3

It was important to investigate the best method to sterilize the plasmafilter, the component of the BAL which allows the plasma to be separated from the formed elements of the blood.

Chemical and thermic methods were examined. The integrity of the plasmafilter was analysed by the visual aspect and by measuring the hydraulic permeability of the internal membrane. This technique involves the measurement of the transmembrane pressure (TMP) and the ultrafiltration flow rate.

For the chemical method (disinfection), 2 washes with alcohol at 70°C were carried out (recirculation for 30 minutes). With this method, the internal membrane became very permeable and the plasmafilter was therefore no longer usable.

The thermic method included laboratory autoclave sterilization. It was observed that the internal fibres yellowed at their extremities and the glue, used to assemble the external structure of the plasma filter, was ruined. In addition, one of the plasma filters tested broken during handling. This method increased the membrane permeability ($L_p = 182.15$ and 206.74 mL/min/mmHg respectively before and after autoclaving).

Caution should be taken with these results as the plasmafilters were old. Moreover, we could not use the manufacturer's recommendation for sterilisation because it did not comply with the sterilization hospital standards (15 min at 121°C is not long enough). They also propose a sterilization with gamma rays that we could not be try in our laboratory.

In perspective, we planned to try a disinfection technique based on subsequent washing of the plasmafilter with antibacterial and antifungal solutions.

5.3. *In vivo* testing: feasibility of the plasmapheresis step

In order to study the practical feasibility of therapy and the efficacy of the plasmafilter, preliminary tests were performed in which healthy catheterized rats were anaesthetized with isoflurane and connected to the primary circuit of BAL. Based on the experimental setup (Figure 90), the blood was taken from the carotid artery of the rat through a peristaltic pump at flow rate of 1 mL/min (pump in). This value was chosen based on the observation by Yorimitsu et al.²⁴³ who noticed lowering of blood pressure and hemolysis on rats at higher perfusion rates. The whole blood passes through the plasmafilter where the plasma was separated by the formed element of the blood. The plasma flowed through the secondary circuit (plasma) via a second pump at flow rate of 0.4 mL/min (Pump UF = ultrafiltration). In this way, the 25% of the fluid circulating in the plasmafilter passes to the plasma circuit. This value should prevent clogging problems inside the plasmafilter due to excessive transmembrane pressure (TMP) increasing. Subsequently, the plasma mixed with the formed elements and returned to the rat. Pressure sensors were present before (P_{IN}) and after (P_{UF} in the plasma circuit) the plasmafilter, in order to monitor possible pressure changes due to plasmafilter clogging. In addition, the circuit has outlets for taking plasma and total blood samples, as well as a trap for air bubbles that must not enter the patient.

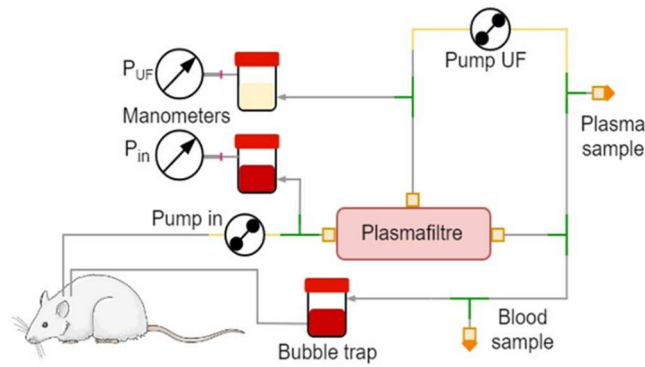


Fig. 90: Extracorporeal circulation setup

Using this setup, we realized two experiments using catheterized healthy rats. The latter experience showed that a larger plasmafilter (twice of three times larger in surface) was needed as it clogged a few minutes after the beginning of the extracorporeal circulation. In addition, the venous access to return the blood was clogged, just after the beginning of the experiment. As a result, the animals were sacrificed shortly after the start of therapy. New experiments with a new plasmafilter design are ongoing.

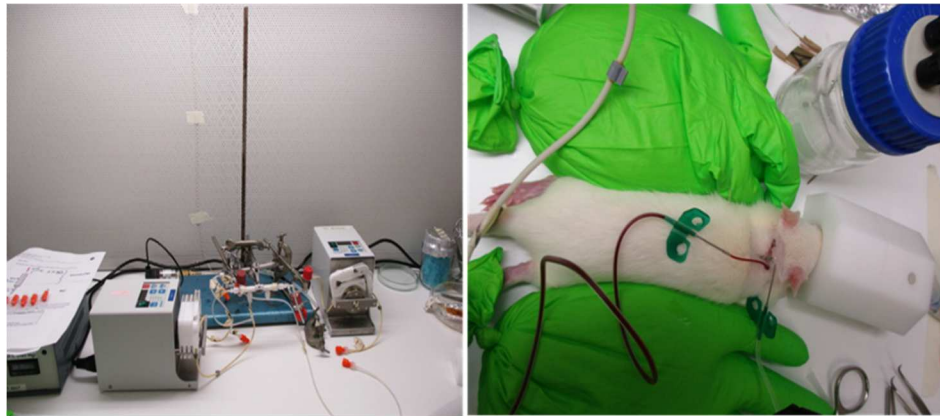


Fig. 91: *In vivo* experiments

The set of these steps will allow us to understand if the BAL therapy will improve the physiological and biochemical parameters, and the survival of the chosen pathological animal model. To date, we realized the APAFiS legal form for testing the effectiveness of the device on pathologic rats, with all the technical details and procedures. We already received some minor corrections. Other answers from animal research authorities are awaited.

6. Conclusions

In this chapter, we presented the animal model that we will use for BAL therapy, highlighting the scientific, economic and experimental advantages. With the assistance of the engineers, we have carried out the scaling-down of the pre-existing human-sized device. The third generation prototype is ready to be used for safety testing on healthy rats. Then, we carried out a series of experiments to analyse the effects on the pathological plasma medium (already used for experiments on cells), when it recirculates through charcoal and resin, in terms of removal of

selected markers. These experiments allowed us to understand that the most convenient disposition is charcoal and resin in series. We then highlighted the effects on the same culture medium, when all the artificial elements are present (charcoal, resin and PDB containing empty beads). These preliminary studies were important to predict what is removed (or modified) from the medium before the whole device will be used for animal therapy. Apparently, these artificial elements contributed to lactate removal, and we believe that this is a beneficial element for BAL therapy. The effect on other markers involved in ALF, such as bilirubin and bile salts, are in progress.

New experiments will be conducted on rats in a few months in our laboratory. Once at this stage, it will be necessary to test firstly (1) the safety of the device and (2) the effectiveness of the BAL therapy, on pathological rats.

7. Key points of phase III

- Wistar rats chosen as animal model for our study
- ALF induction method: chemical induction by single intraperitoneal injection of D-galactosamine at 1.2 g/kg
- We realized a miniaturization of the device to rat scale
- The device implements a perfused dynamic bioreactor to host the biomass. Our fluidized bed bioreactor showed problems during fluidization and needs a better design before implementation in this BAL
- Activated charcoal and ionic resin placed in series showed better performance on the removal of specific markers according to our endpoints
- Charcoal and resin removed lactate, an important marker of ALF prognosis. This represents an added value to our device
- Cells exposed to a medium that recirculated through charcoal and resin, showed reduced (but acceptable) viability
- Better characterization of the artificial elements is in progress. Experiments on rat plasma and effect of the artificial elements on bilirubin and bile acids will be performed
- The small-scaled BAL device is ready for preclinical stage.

General conclusions and perspectives

In this research work, the main objective was initially to validate the extracorporeal bioartificial liver, previously developed in our laboratory with collaborators, in preclinical testing based on a small animal model, the rat. To achieve this goal, we mainly investigated on two researches axis, with a bioengineering approach:

- The optimization of the cell culture method for BAL application
- The development of the device and its characterization

The first part of the thesis regarded the optimization of the biomass for its use in BAL compatible bioreactors, in the treatment of ALF.

Based on studies conducted by other research groups, mostly for toxicology applications, we selected HepaRG as cell model while other teams on the Ilite consortium have worked in parallel on the conception of liver organoids using pluripotent stem cells.

Preliminary investigations conducted in chapter 3 demonstrated that, after 14 days of shaken culture, encapsulated HepaRG cells were able to self-assemble into spheroids, adequately differentiated, and presented a wide range of functions (protein synthesis, enzymatic activities and biotransformation of toxins) in the range or above those presented in other BAL studies. From a logistical point of view, this culture method has advantages in terms of cost and timing. The fact that cells aggregate autonomously into the beads to spheroids does not require additional handling that makes GMP production more complex and not cost-effective. Importantly, this setup can easily be scaled-up and adapted to clinical BAL device to treat acute liver failure. These data had an important relevance in the field of liver tissue engineering and were valorised with a paper published in February 2020 (DOI: 10.1089/ten.TEA.2019.0262).

Once our gold standard culture procedure established, we needed to better optimize the culture protocol to adapt the biomass to a fluidized bed bioreactor, a technology used in our laboratory on a human-scale BAL previously developed. To be closer to a clinical context, some assays were performed with a perfusion medium mimicking ALF-human plasma. The switch to this medium highlighted a problem of severe beads deterioration that could be expected also in a clinical context.

In chapter 4, we investigated solutions to enhance the mechanical stability of the alginate beads and preserve the biomass. After beads' PLL coating, HepaRG, in the new microenvironment, showed once again their potential in terms of metabolic performance. Unfortunately, fluidization with these novel solid phase was difficult to perform in the small scale bioreactors that were planned to be employed in the small animal extracorporeal set-up. Therefore, we developed a perfused dynamic bioreactor that presented biological and logistical advantages, and that is easy to scale-up (and down). While waiting for a functioning fluidized bed bioreactor, *in vivo* testing will be conducted using this new setup, which demonstrated high *in vitro* performance on the optimized biomass.

The second task regarded the choice of the animal model to mimic acute liver failure, the miniaturization of the human-scale BAL previously developed at the lab, the characterization of the artificial elements, and the safety studies. These investigations were presented in chapter 5. It involved engineers and clinicians of the iLite programme.

About the animal model, we chose the rat because it respected the construct validity criterion. The pathological model selected was the D-galactosamine induced rat, since it respected the predictive and face validity criteria and also the criteria proposed by Terblanche and Hickman for ALF. The miniaturization of the BAL at rat scale was successfully achieved starting from our human-scale BAL. The same methodology can be used to adapt the device, in a second phase, to larger animal models. Since in the device there are cartridges of activated charcoal and ionic resins, we found important to investigate their role as detoxifier elements. We found that those elements contributed in the removal of lactate, an important marker of ALF prognosis, without severely affecting the viability of cells. We conclude that the synergic action of these artificial elements together with the biomass activity, create a hybrid-bioartificial system with high potential in the treatment of ALF.

In conclusion, this Ph.D. work followed a path that allowed the optimization of an extracorporeal liver supply system, starting from the cell level and arriving at the complete device, ready for its preclinical use.

There are many perspectives which can be organised in short, medium and long term.

- Short term perspectives:
 - Optimization of the small scaled fluidized bed bioreactor design adapted to our BAL (presence of flow dividers and system that does not allow the blocking, if the beads accumulate at the inlet or outlet)
 - Characterization of PDB in hydrodynamic (through the mathematical models), mass transfer and *in vitro* activity
 - Optimization (plasmafilter, connectors, etc) of the third generation BAL before animal testing
 - Evaluation of encapsulated iPSCs or ESCs with the PDB. Such encapsulation and analysis are currently performed in the team of Dr. Anne Dubart-Kupperschmitt at Inserm U1193, in link for the ESCs cells with the company GoLiver
- Medium term:
 - Investigate if the artificial elements block certain toxins such as bilirubin and bile acids (tests on rat plasma are planned)
 - *In vivo* testing on the safety of the BAL
 - *In vivo* testing on the effectiveness of the device
- Long term:
 - Scale-up of the perfused bed bioreactor (if the human size columns already designed due not operate correctly the fluidization of the PLL coated beads)

- Preclinical tests on large animal models (safety on pig models)
- Clinical evaluation

In addition, cells also have yet to demonstrate other key functions of a bioartificial liver such as production of coagulation factors, the metabolism of bile salts and bilirubin, or even the influence of cells on cytokines that play a key role in the evolution of acute liver failure and liver regeneration. The first preclinical tests will take place in our laboratory in the coming months and all the problems, doubts and hypotheses that emerged during this work will probably find answers.

References

1. Figaro, S. *et al.* SUPPLIVER: Bioartificial supply for liver failure. *Irbm* **36**, 101–109 (2015).
2. Keeffe, E. B. Acute liver failure. *Rev. Gastroenterol. México* **70**, 56–62 (2005).
3. Bernal, W. & Wendon, J. Acute Liver Failure. *N. Engl. J. Med.* **369**, 2525–2534 (2013).
4. Bantel, H. Mechanisms of cell death in acute liver failure. *Front. Physiol.* **3**, 79 (2012).
5. Trey, C. and Davidson, C. S. The management of fulminant hepatic failure. *Prog. Liver Dis.* **3**, 282–298 (1970).
6. Syndromes, A. liver failure : redefining the. Acute liver failure : redefining the syndromes. *Lancet* **342**, 273–275 (1993).
7. Guidelines, C. P. European Association for the Study of the Liver. EASL 2017 Clinical Practice Guidelines on the management of acute (fulminant) liver failure. *J Hepatol* **66**, 81 (2017).
8. O’Grady, J. G., Alexander, G. J. M., Hayllar, K. M. & Williams, R. Early indicators of prognosis in fulminant hepatic failure. *Gastroenterology* **97**, 439–445 (1989).
9. Mishra, A. & Rustgi, V. Prognostic Models in Acute Liver Failure. *Clin. Liver Dis.* **22**, 375–388 (2018).
10. Pazzi, P. *et al.* Serum bile acids in patients with liver failure supported with a bioartificial liver. *Aliment. Pharmacol. Ther.* **16**, 1547–1554 (2002).
11. Woolbright, B. L. & Jaeschke, H. Review Role of the inflammasome in acetaminophen-induced liver injury and acute liver failure. *J. Hepatol.* **66**, 836–848 (2017).
12. Sekiyama, K. D., Yoshiba, M. & Thomson, A. W. Circulating proinflammatory cytokines (IL-1 beta, TNF-alpha, and IL-6) and IL-1 receptor antagonist (IL-1Ra) in fulminant hepatic failure and acute hepatitis. *Clin. Exp. Immunol.* **98**, 71–7 (1994).
13. Vaquero, J., Chung, C., Cahill, M. E., & Blei, A. T. *Pathogenesis of hepatic encephalopathy in acute liver failure. Seminars in liver disease* **23**, (2003).
14. Butterworth, R. F. Pathogenesis of Hepatic Encephalopathy and Brain Edema in Acute Liver Failure. *J. Clin. Exp. Hepatol.* **5**, S96–S103 (2015).
15. Scott, T. R., Kronsten, V. T., Hughes, R. D., & Shawcross, D. L. Pathophysiology of cerebral oedema in acute liver failure. *World J. Gastroenterol.* **19**, 9240–9255 (2013).
16. Wendon, J., Cordoba, J., Dhawan, A., Larsen, F. S., Manns, M., Nevens, F., ... & Bernardi, M. EASL clinical practical guidelines on the management of acute (fulminant) liver failure. *J. Hepatol.* **66**, 1047–1081 (2017).
17. Flamm, S. L., Yang, Y. X., Singh, S., Falck-Ytter, Y. T., Lim, J. K., Rubenstein, J. H., ... & Weinberg, D. S. American Gastroenterological Association Institute guidelines for the diagnosis and management of acute liver failure. **52**, 644–647 (2017).
18. Plauth, M., Cabre, E., Riggio, O., Assis-Camilo, M., Pirlich, M., Kondrup, J., ... & Nolte, W. ESPEN guidelines on enteral nutrition: liver disease. **252**, 285–294 (2006).
19. Starokozhko, V. & Groothuis, G. M. M. Challenges on the road to a multicellular bioartificial liver. *J. Tissue Eng. Regen. Med.* **12**, e227–e236 (2018).
20. Mendizabal, M., Silva, M. O., Mendizabal, M. & Silva, M. O. Liver transplantation in acute liver failure: A challenging scenario. **22**, 1523 (2016).
21. Olivo, R., Guarrera, J. V., & Pyrsopoulos, N. T. Liver transplantation for acute liver failure. **22**, 409–417 (2018).

22. Benhamou, J. P. Fulminant and subfulminant liver failure: definitions and causes. *Semin. Liver Dis.* **6**, 97–106 (1986).
23. Mochida, S., Nakayama, N., Matsui, A., Nagoshi, S., & Fujiwara, K. Re-evaluation of the Guideline published by the Acute Liver Failure Study Group of Japan in 1996 to determine the indications of liver transplantation in patients with fulminant hepatitis: Analysis of 698 patients seen between 1998 and 2003 enrolled in th. *Hepatol. Res.* **38**, 970–979 (2008).
24. Cardoso, L. M. D. F., Moreira, L. F. P., Pinto, M. A., Henriques-Pons, A., & Alves, L. A. Domino hepatocyte transplantation: a therapeutic alternative for the treatment of acute liver failure. *Can. J. Gastroenterol. Hepatol.* **2018**, (2018).
25. Raia, S. Liver transplantation from live donors. *Lancet* **2**, 497–498 (1989).
26. Rauchfuss, F., Bauschke, A., Bärthel, E., Scheuerlein, H., Schüle, S., Malessa, C., & Settmacher, U. Lebertransplantation mit Lebendspende—Historie und Gegenwart. *Thorax-und Gefäßchirurgie* **141**, 559–564 (2016).
27. Pomfret, E. A., Pomposelli, J. J., & Jenkins, R. L. Live donor liver transplantation. *J. Hepatol.* **34**, 613–624 (2001).
28. Florman, S., & Miller, C. M. Live Donor Liver Transplantation. *Liver Transplant.* **12**, 499–510 (2006).
29. Brown Jr, R. S. Live Donors in Liver Transplantation. *Gastroenterology* **134**, 1802–1813 (2008).
30. Song, A. T. W., Avelino-Silva, V. I., Pecora, R. A. A., Pugliese, V., D’Albuquerque, L. A. C., & Abdala, E. Liver transplantation : Fifty years of experience. *World J. Gastroenterol. WJG* **20**, 5363 (2014).
31. Emre, S. & Umman, V. Split Liver Transplantation : An Overview. *TPS* **43**, 884–887 (2011).
32. Lee, S. A complete treatment of adult living donor liver transplantation: a review of surgical technique and current challenges to expand indication of patients. *Am. J. Transplant.* **15**, 17–38 (2015).
33. Wilczek, H. E., Larsson, M., Yamamoto, S., & Ericzon, B. G. Domino liver transplantation. *J. Hepatobiliary. Pancreat. Surg.* **15**, 139–148 (2008).
34. Furtado, A. L., Tome, L., Oliveira, F. J., Furtado, E., Viana, J. S., & Perdigoto, R. Sequential Liver Transplantation. *Transpl. Proc.* **29**, 467–8 (1997).
35. Baccarani, U., Sainz-Barriga, M., Adani, G. L., Risaliti, A., Bresadola, F., Donini, A., & Sanna, A. (. Human hepatocyte isolation for liver cell therapy: Whole marginal livers or healthy segments from splitting?. *Transplantation.* **79**, 249 (2005).
36. Baccarani, U., Sainz-Barriga, M., Adani, G. L., Risaliti, A., Bresadola, F., Donini, A., & Sanna, A. (. Human hepatocyte isolation for liver cell therapy: Whole marginal livers or healthy segments from splitting?. *Transplantation.* **79**, 248–260 (2005).
37. Strom, S. C., Fisher, R. A., Rubinstein, W. S., Barranger, J. A., Towbin, R. B., Charron, M., ... & Reyes, J. Transplantation of Human Hepatocytes. *Transplant. Proc.* **29**, 2103–2106 (1997).
38. Badell, I. R., Hanish, S. I., Hughes, C. B., Hewitt, W. R., Chung, R. T., Spivey, J. R., & Knechtle, S. J. Domino liver transplantation in maple syrup urine disease: a case report and review of the literature. *Transplant. Proc.* **45**, 806–809 (2013).
39. Stéphenne, X., Debray, F. G., Smets, F., Jazouli, N., Sana, G., Tondreau, T., ... & Gersting, S. W. Hepatocyte transplantation using the domino concept in a child with tetrabioprotein nonresponsive phenylketonuria. *Cell Transplant.* **21**, 2765–2770 (2012).
40. Karvellas, C. J., & Subramanian, R. M. Current evidence for extracorporeal liver support systems in acute liver failure and acute-on-chronic liver failure. *Crit. Care Clin.* **32**, 439–451 (2016).
41. Lee, K. C. L., Stadlbauer, V. & Jalan, R. Extracorporeal liver support devices for listed patients. *Liver Transplant.* **22**, 839–848 (2016).

42. Joseph, N. A. & Kumar, L. K. Liver Support Devices : Bridge to Transplant or Recovery. *Indian J. Respir. Care* **6**, 807 (2017).
43. Hernaez, R., Solà, E., Moreau, R., & Ginès, P. Acute-on-chronic liver failure: an update. *Gut* **66**, 541–553 (2017).
44. Moreau, R. *et al.* Acute-on-Chronic Liver Failure Is a Distinct Syndrome That Develops in Patients With Acute Decompensation of Cirrhosis. *YGASt* **144**, 1426–1437.e9 (2013).
45. Jalan, R. *et al.* Development and validation of a prognostic score to predict mortality in patients with acute-on-chronic liver failure. *J. Hepatol.* **61**, 1038–1047 (2014).
46. Azzena, G., & Morsiani, E. Extracorporeal liver support systems. *Ann. Ital. Chir.* **70**, 647 (1999).
47. Carpentier, B., Gautier, A. & Legallais, C. Artificial and bioartificial liver devices: Present and future. *Gut* **58**, 1690–1702 (2009).
48. Court, F. G., Wemyss-Holden, S. A., Dennison, A. R., & Maddern, G. J. Bioartificial liver support devices: historical perspectives. *ANZ J. Surgery*, **73**, 739–748 (2003).
49. Annesini, M. C., Piemonte, V. & Turchetti, L. Removal of albumin-bound toxins from albumin-containing solutions: Tryptophan fixed-bed adsorption on activated carbon. *Chem. Eng. Res. Des.* **88**, 1018–1023 (2010).
50. Figaro, S., Legallais, C., Vantard, G. & D., P. Intégration d'un bioréacteur à lit fluidisé dans un circuit extracorporel monitoré. (University of technology of Compiègne, 2015).
51. Drukker, W., Parsons, F. M., & Maher, J. F. *Replacement of renal function by dialysis: a textbook of dialysis*. (Springer Science & Business Media., 2012).
52. Chirito, E., Reiter, B., Lister, C. & Chang, T. M. S. Artificial Liver: The Effect of ACAC Microencapsulated Charcoal Hemoperfusion on Fulminant Hepatic Failure. *Artif. Organs* **1**, 76–83 (1977).
53. Demetriou, A. A. *et al.* Prospective, Randomized, Multicenter, Controlled Trial of a Bioartificial Liver in Treating Acute Liver Failure. *Ann. Surg.* **239**, 660–670 (2004).
54. Mullon, C. & Pitkin, Z. The HepatAssist® Bioartificial Liver Support System: clinical study and pig hepatocyte process. *Expert Opin. Investig. Drugs* **8**, 229–235 (1999).
55. Shi, X. L. *et al.* Evaluation of a novel hybrid bioartificial liver based on a multi-layer flat-plate bioreactor. *World J. Gastroenterol.* **18**, 3752–3760 (2012).
56. Han, B., Shi, X. L., Zhang, Y., Gu, Z. Z., Yuan, X. W., Ren, H. Z., ... & Ding, Y. T. No transmission of porcine endogenous retrovirus in an acute liver failure model treated by a novel hybrid bioartificial liver containing porcine hepatocytes. *Artif. Organs* **14**, 492–501 (2015).
57. Ton, H. Y., Hughes, R. D., Silk, D. B. A. & Williams, R. Albumin-Coated Amberlite XAD-7 Resin for Hemoperfusion in Acute Liver Failure: Part I: Adsorption Studies. *Artif. Organs* **3**, 20–22 (1979).
58. Lösger, H. *Absorption therapy in acute liver failure: a critical resume*. *Artificial Liver Support* (Springer, 1992).
59. Kandiah, P. A. & Subramanian, R. M. Extracorporeal devices. *Crit. Care Clin.* **35**, 135–150 (2019).
60. Alshamsi, F. *et al.* Extracorporeal liver support in patients with liver failure: a systematic review and meta-analysis of randomized trials. *Intensive Care Med.* **46**, 1–16 (2020).
61. Martínez, J. J. G., & Bendjelid, K. Artificial liver support systems: what is new over the last decade? *Ann. Intensive Care* **8**, 109 (2018).
62. Seige, M. *et al.* Long term treatment of patients with acute exacerbation of chronic liver failure by albumin dialysis. *Transplant. Proc.* **31**, 1371–1375 (1999).
63. Lee, K. C., Stadlbauer, V., & Jalan, R. Extracorporeal liver support devices for listed patients. *Liver*

- Transplant.* **22**, 839–848 (2016).
64. Sakiyama, R., Blau, B. J. & Miki, T. Clinical translation of bioartificial liver support systems with human pluripotent stem cell-derived hepatic cells. *World J. Gastroenterol.* **23**, 1974–1979 (2017).
 65. Patzer, J. F., Campbell, B. & Miller, R. Plasma versus whole blood perfusion in a bioartificial liver assist device. *ASAIO J.* **48**, 226–233 (2002).
 66. Legallais, C. *et al.* Bioengineering Organs for Blood Detoxification. *Adv. Healthc. Mater.* **1800430**, 1–32 (2018).
 67. Gebhardt, R. & Matz-Soja, M. Liver zonation: Novel aspects of its regulation and its impact on homeostasis. *World J. Gastroenterol.* **20**, 8491–8504 (2014).
 68. van Grunsven, L. A. 3D in vitro models of liver fibrosis. *Adv. Drug Deliv. Rev.* **121**, 133–146 (2017).
 69. Allen, J. W., Hassanein, T. & Bhatia, S. N. Advances in bioartificial liver devices. *Hepatology* **34**, 447–455 (2001).
 70. Van Wenum, M. *et al.* Bioartificial livers in vitro and in vivo: Tailoring biocomponents to the expanding variety of applications. *Expert Opin. Biol. Ther.* **14**, 1745–1760 (2014).
 71. Adeva, M. M., Souto, G., Blanco, N. & Donapetry, C. Ammonium metabolism in humans. *Metabolism.* **61**, 1495–1511 (2012).
 72. Nyberg, S. L. *et al.* Primary Hepatocytes Outperform Hep G2 Cells as the Source of Biotransformation Functions in a Bioartificial Liver. *Ann. surgery*, **220**, 59–67 (1994).
 73. Brusilow, S. W., Koehler, R. C., Traystman, R. J., & Cooper, A. J. Astrocyte glutamine synthetase: importance in hyperammonemic syndromes and potential target for therapy. *Neurotherapeutics* **7**, 452–470 (2010).
 74. Andersen, L. W., Mackenhauer, J., Roberts, J. C., Berg, K. M., Cocchi, M. N., & Donnino, M. W. Etiology and therapeutic approach to elevated lactate levels. *Mayo Clin. Proc.* **88**, 1127–1140 (2013).
 75. Tofteng, F., Jorgensen, L., Hansen, B. A., Ott, P., Kondrup, J., & Larsen, F. S. Cerebral microdialysis in patients with fulminant hepatic failure. *Hepatology* **36**, 1333–1340 (2002).
 76. Kalakonda A, Jenkins BA, J. S. *Physiology, Bilirubin*. (StatPearls Publishin, 2002).
 77. Good, W. V. & Hou, C. Visuocortical bilirubin-induced neurological dysfunction. *Semin. Fetal Neonatal Med.* **20**, 37–41 (2015).
 78. Patel, J., Walayat, S., Kalva, N., Palmer-Hill, S. & Dhillon, S. Bile cast nephropathy: A case report and review of the literature. *World J. Gastroenterol.* **22**, 6328–6334 (2016).
 79. Wong, R. J., Bhutani, V. K., Abrams, S. A., & Kim, M. S. Unconjugated hyperbilirubinemia in term and late preterm infants: Epidemiology and clinical manifestations. *UpToDate (online)* (2009).
 80. Martinez-Diez, M. C., Serrano, M. A., Monte, M. J., & Marin, J. J. Comparison of the effects of bile acids on cell viability and DNA synthesis by rat hepatocytes in primary culture. *Biochim. Biophys. Acta - Mol. Basis Dis.* **1500**, 153–160 (2000).
 81. Ben-Moshe, S. *et al.* Spatial sorting enables comprehensive characterization of liver zonation. *Nat. Metab.* **1**, 899–911 (2019).
 82. Atogo-Asse, F. E., Vincent, R. P., Hughes, S. A., Auzinger, G., Le Roux, C. W., Wendon, J., & Bernal, W. High density lipoprotein in patients with liver failure; Relation to sepsis, adrenal function and outcome of illness. *Liver Int.* **32**, 128–136 (2012).
 83. Wang, N., Tsuruoka, S., Yamamoto, H., Enosawa, S., Omasa, T., Sata, N., ... & Fujimura, A. The bioreactor with CYP3A4-and glutamine synthetase-introduced HepG2 cells: treatment of hepatic failure dog with diazepam overdose. *Artif. Organs* **29**, 681–684 (2005).

84. Döring, B. & Petzinger, E. Phase 0 and phase III transport in various organs: Combined concept of phases in xenobiotic transport and metabolism. *Drug Metab. Rev.* **46**, 261–282 (2014).
85. Ahboucha, S. & Butterworth, R. F. Role of endogenous benzodiazepine ligands and their GABA-A-associated receptors in hepatic encephalopathy. *Metab. Brain Dis.* **20**, 425–437 (2005).
86. Suh, K. S. *et al.* Bioartificial liver treatment in rats with fulminant hepatic failure: Effect on DNA-binding activity of liver-enriched and growth-associated transcription factors. *J. Surg. Res.* **85**, 243–250 (1999).
87. Tsiaoussis, J., Newsome, P. N., Nelson, L. J., Hayes, P. C. & Plevris, J. N. Which hepatocyte will it be? hepatocyte choice for bioartificial liver support systems. *Liver Transplant.* **7**, 2–10 (2001).
88. Chamuleau, R. a F. M., Poyck, P. P. C. & van de Kerkhove, M.-P. Bioartificial liver: its pros and cons. *Ther. Apher. Dial.* **10**, 168–174 (2006).
89. Pless, G. Artificial and bioartificial liver support. *Organogenesis* **3**, 20–4 (2007).
90. Zeilinger, K., Freyer, N., Damm, G., Seehofer, D. & Knöspel, F. Cell sources for in vitro human liver cell culture models. *Exp. Biol. Med.* **241**, 1684–1698 (2016).
91. Nelson, L. J. *et al.* Human Hepatic HepaRG Cells Maintain an Organotypic Phenotype with High Intrinsic CYP450 Activity/Metabolism and Significantly Outperform Standard HepG2/C3A Cells for Pharmaceutical and Therapeutic Applications. *Basic Clin. Pharmacol. Toxicol.* **120**, 30–37 (2017).
92. Nibourg, G. A., Chamuleau, R. A., van Gulik, T. M. & Hoekstra, R. Proliferative human cell sources applied as biocomponent in bioartificial livers: a review. *Expert Opin. Biol. Ther.* **12**, 905–921 (2012).
93. Sauer, I. M. *et al.* Primary human liver cells as source for modular extracorporeal liver support - A preliminary report. *Int. J. Artif. Organs* **25**, 1001–1005 (2002).
94. Mazariegos, G. V *et al.* First Clinical Use of a Novel Bioartificial Liver Support System (BLSS)†. *Am. J. Transplant.* **2**, 260–266 (2002).
95. Mundt, A. *et al.* A method to assess biochemical activity of liver cells during clinical application of extracorporeal hybrid liver support. *Int. J. Artif. Organs* **25**, 542–548 (2008).
96. Van De Kerkhove, M. P. *et al.* Phase I clinical trial with the AMC-bioartificial liver. *Int. J. Artif. Organs* **25**, 950–959 (2002).
97. Yang, Q. *et al.* Fluidized-bed bioartificial liver assist devices (BLADs) based on microencapsulated primary porcine hepatocytes have risk of porcine endogenous retroviruses transmission. *Hepatol. Int.* **4**, 757–761 (2010).
98. Te Velde, A. A., Flendrig, L. M., Ladiges, N. C. J. J. & Chamuleau, R. A. F. M. Immunological Consequences of the use of Xenogeneic Hepatocytes in a Bioartificial Liver for Acute Liver Failure. *Int. J. Artif. Organs* **20**, 229–233 (1997).
99. Van De Kerkhove, M. P. *et al.* Liver support therapy: An overview of the AMC-bioartificial liver research. *Dig. Surg.* **22**, 254–264 (2005).
100. Andersson, T. B., Kanebratt, K. P. & Kenna, J. G. The HepaRG cell line: a unique in vitro tool for understanding drug metabolism and toxicology in human. *Expert Opin. Drug Metab. Toxicol.* **8**, 909–920 (2012).
101. Gripon, P. *et al.* Nonlinear partial differential equations and applications: Infection of a human hepatoma cell line by hepatitis B virus. *Proc. Natl. Acad. Sci.* **99**, 15655–15660 (2002).
102. Hart, S. N. *et al.* A comparison of whole genome gene expression profiles of HepaRG cells and HepG2 cells to primary human hepatocytes and human liver tissues. *Drug Metab. Dispos.* **38**, 988–994 (2010).
103. Turpeinen, M. *et al.* Functional expression, inhibition and induction of CYP enzymes in HepaRG cells. *Toxicol. Vitro.* **23**, 748–753 (2009).
104. Aninat, C., Piton, A., Glaise, D., Le Charpentier, T., Langouët, S., Morel, F., ... & Guillouzo, A. Expression of

- cytochromes P450, conjugating enzymes and nuclear receptors in human hepatoma HepaRG cells. *rug Metab. Dispos.* **34**, 75–83 (2006).
105. Cerec, V. *et al.* Transdifferentiation of hepatocyte-like cells from the human hepatoma hepaRG cell line through bipotent progenitor. *Hepatology* **45**, 957–967 (2007).
106. Nibourg, G. A. A. *et al.* Liver progenitor cell line HepaRG differentiated in a bioartificial liver effectively supplies liver support to rats with acute liver failure. *PLoS One* **7**, 1–8 (2012).
107. Hoekstra, R. *et al.* The HepaRG cell line is suitable for bioartificial liver application. *Int. J. Biochem. Cell Biol.* **43**, 1483–1489 (2011).
108. Tabibian, J. H., Masyuk, A. I., Masyuk, T. V., O'Hara, S. P. & LaRusso, N. F. Physiology of cholangiocytes. *Compr. Physiol.* **3**, 541–565 (2013).
109. Hoekstra, R., Nibourg, G. A., van der Hoeven, T. V., Plomer, G., Seppen, J., Ackermans, M. T., ... & Chamuleau, R. A. Phase 1 and phase 2 drug metabolism and bile acid production of HepaRG cells in a bioartificial liver in absence of dimethyl sulfoxide. *Drug Metab. Dispos.* **41**, 562–567 (2013).
110. Sharanek, A. *et al.* Cellular accumulation and toxic effects of bile acids in cyclosporine a-treated hepaRG hepatocytes. *Toxicol. Sci.* **147**, 573–587 (2015).
111. Vazin, T., & Freed, W. J. Human embryonic stem cells: derivation, culture, and differentiation: a review. *Neurol Neurosciences* **28**, 589–603 (2010).
112. Donato, M. T. & Tolosa, L. Stem-cell derived hepatocyte-like cells for the assessment of drug-induced liver injury. *Differentiation* **106**, 15–22 (2019).
113. Choi, D., Lee, S. Y. & Kim, H. J. Cell Sources, Liver Support Systems and Liver Tissue Engineering: Alternatives to Liver Transplantation. *Int. J. Stem Cells* **8**, 36–47 (2015).
114. Ben-David, U. & Benvenisty, N. The tumorigenicity of human embryonic and induced pluripotent stem cells. *Nat. Rev. Cancer* **11**, 268–277 (2011).
115. Mizumoto, H. *et al.* Evaluation of a hybrid artificial liver module based on a spheroid culture system of embryonic stem cell-derived hepatic cells. *Cell Transplant.* **21**, 421–428 (2012).
116. Si-Tayeb, K., Noto, F. K., Nagaoka, M., Li, J., Battle, M. A., Duris, C., ... & Duncan, S. A. In vitro and ex vivo functional evaluation of a hollow fiber-type bioartificial liver module containing ES cell-derived hepatocyte-like cells. *Adv. Biomed. Eng.* **7**, 18–27 (2018).
117. Song, Z. *et al.* Efficient generation of hepatocyte-like cells from human induced pluripotent stem cells. *Cell Res.* **19**, 1233–1242 (2009).
118. Al Tanoury Z, Piskunov A, R.-E. C. *et al.* Highly efficient generation of human hepatocyte-like cells from induced pluripotent stem cells. *Hepatology* **51**, 297–305 (2010).
119. Hannoun, Z., Steichen, C., Dianat, N., Weber, A. & Dubart-Kupperschmitt, A. The potential of induced pluripotent stem cell derived hepatocytes. *J. Hepatol.* **65**, 182–199 (2016).
120. Ren, S., Irudayam, J. I., Contreras, D., Sareen, D., Talavera-Adame, D., Svendsen, C. N., & Arumugaswami, V. Bioartificial Liver Device Based on Induced Pluripotent Stem Cell-Derived Hepatocytes. *J. Stem Cell Res. Ther.* **5**, 2 (2015).
121. Shi, X.-L. *et al.* Improved survival of porcine acute liver failure by a bioartificial liver device implanted with induced human functional hepatocytes. *Cell Res.* **26**, 1–11 (2016).
122. Catapano, G., Gerlach, J. C. *Bioreactors for liver tissue engineering. Topics in tissue engineering* (Oulu University, 2007).
123. Fremond, B. *et al.* Correction of bilirubin conjugation in the Gunn rat using hepatocytes immobilized in alginate gel beads as an extracorporeal bioartificial liver. *Cell Transplant.* **2**, 453–460 (1993).
124. Kusano, T. *et al.* Microencapsule technique protects hepatocytes from cryoinjury. *Hepatol. Res.* **38**, 593–

- 600 (2008).
125. Hang, H. *et al.* In vitro analysis of cryopreserved alginate-poly-L-lysine-alginate-microencapsulated human hepatocytes. *Liver Int.* **30**, 611–622 (2010).
 126. Selden, C. *et al.* A clinical-scale BioArtificial Liver, developed for GMP, improved clinical parameters of liver function in porcine liver failure. *Sci. Rep.* **7**, 1–19 (2017).
 127. Coward, S. M. *et al.* Alginate-encapsulated HepG2 cells in a fluidized bed bioreactor maintain function in human liver failure plasma. *Artif. Organs* **33**, 1117–1126 (2009).
 128. Doré, E. & Legallais, C. A new concept of bioartificial liver based on a fluidized bed bioreactor. *Ther. Apher.* **3**, 264–267 (1999).
 129. David, B., Dufresne, M., Nagel, M. D. & Legallais, C. In vitro assessment of encapsulated C3A hepatocytes functions in a fluidized bed bioreactor. *Biotechnol. Prog.* **20**, 1204–1212 (2004).
 130. Gautier, A. *et al.* Impact of alginate type and bead diameter on mass transfers and the metabolic activities of encapsulated c3a cells in bioartificial liver applications. *Eur. Cells Mater.* **21**, 94–106 (2011).
 131. Draget, K. I. & Taylor, C. Chemical, physical and biological properties of alginates and their biomedical implications. *Food Hydrocoll.* **25**, 251–256 (2011).
 132. Lim, F., & Sun, A. M. Microencapsulated islets as bioartificial endocrine pancreas. *Science.* **210**, 908–910 (1980).
 133. Andersen, T., Auk-Emblem, P. & Dornish, M. 3D Cell Culture in Alginate Hydrogels. *Microarrays* **4**, 133–161 (2015).
 134. Sergeeva, A., Vikulina, A. S. & Volodkin, D. Porous alginate scaffolds assembled using vaterite CaCO₃ crystals. *Micromachines* **10**, 1–21 (2019).
 135. Lee, B. B., Ravindra, P. & Chan, E. S. Size and shape of calcium alginate beads produced by extrusion dripping. *Chem. Eng. Technol.* **36**, 1627–1642 (2013).
 136. Guimarães, C. F., Gasperini, L., Marques, A. P. & Reis, R. L. The stiffness of living tissues and its implications for tissue engineering. *Nat. Rev. Mater.* 1–20 (2020).
 137. Pasqua, M. *et al.* HepaRG Self-Assembled Spheroids in Alginate Beads Meet the Clinical Needs for Bioartificial Liver. *Tissue Eng. Part A* **ahead of p**, 1–33 (2020).
 138. Capone, S. H. *et al.* Impact of Alginate Composition: From Bead Mechanical Properties to Encapsulated HepG2/C3A Cell Activities for In Vivo Implantation. *PLoS One* **8**, (2013).
 139. Kinasiwicz, A. *et al.* Three-dimensional growth of human hepatoma C3A cells within alginate beads for fluidized bioartificial liver. *Int. J. Artif. Organs* **31**, 340–347 (2008).
 140. Tran, N. M. *et al.* An appropriate selection of a 3D alginate culture model for hepatic Huh-7 cell line encapsulation intended for viral studies. *Tissue Eng. Part A* **19**, 103–113 (2013).
 141. Tostões, R. M. *et al.* Human liver cell spheroids in extended perfusion bioreactor culture for repeated-dose drug testing. *Hepatology* **55**, 1227–1236 (2012).
 142. Elkayam, T., Amitay-Shaprut, S., Dvir-Ginzberg, M., Harel, T. & Cohen, S. Enhancing the drug metabolism activities of C3A -a human hepatocyte cell line- by tissue engineering within alginate scaffolds. *Tissue Eng.* **12**, 1357–1368 (2006).
 143. Takayama, K. *et al.* 3D spheroid culture of hESC/hiPSC-derived hepatocyte-like cells for drug toxicity testing. *Biomaterials* **34**, 1781–1789 (2013).
 144. Rowley, J. A., Madlambayan, G. & Mooney, D. J. Alginate hydrogels as synthetic extracellular matrix materials. *Biomaterials* **20**, 45–53 (1999).
 145. Genes, N. G., Rowley, J. A., Mooney, D. J. & Bonassar, L. J. Effect of substrate mechanics on chondrocyte

- adhesion to modified alginate surfaces. *Arch. Biochem. Biophys.* **422**, 161–167 (2004).
146. LeCluyse, E. L., Witek, R. P., Andersen, M. E. & Powers, M. J. Organotypic liver culture models: Meeting current challenges in toxicity testing. *Crit. Rev. Toxicol.* **42**, 501–548 (2012).
147. Rebelo, S. P. *et al.* HepaRG microencapsulated spheroids in DMSO-free culture: novel culturing approaches for enhanced xenobiotic and biosynthetic metabolism. *Arch. Toxicol.* **89**, 1347–1358 (2015).
148. Sgroi, A. *et al.* Transplantation of encapsulated hepatocytes during acute liver failure improves survival without stimulating native liver regeneration. *Cell Transplant.* **20**, 1791–1803 (2011).
149. Figaro, S. *et al.* Development and validation of a bioartificial liver device with fluidized bed bioreactors hosting alginate-encapsulated hepatocyte spheroids. *Proc. Annu. Int. Conf. IEEE Eng. Med. Biol. Soc. EMBS* 1335–1338 (2015).
150. Hau, J. *Animal Models for Human Diseases. Source Book of Models for Biomedical Research* (Humana Press, 2008).
151. San-Miguel, B. *et al.* Melatonin modulates the autophagic response in acute liver failure induced by the rabbit hemorrhagic disease virus. *J. Pineal Res.* **56**, 313–321 (2014).
152. Tuñón, M. J., Alvarez, M., Culebras, J. M. & González-Gallego, J. An overview of animal models for investigating the pathogenesis and therapeutic strategies in acute hepatic failure. *World J. Gastroenterol.* **15**, 3086–3098 (2009).
153. He Y, Zhou J, Dou KF, C. Y. A rat model for acute hepatic failure. *Hepatobiliary Pancreat Dis Int.* **2**, 423–5 (2003).
154. Gao, Y., Mu, N., Xu, X. P. & Wang, Y. Porcine acute liver failure model established by two-phase surgery and treated with hollow fiber bioartificial liver support system. *World J. Gastroenterol.* **11**, 5468–5474 (2005).
155. Frühauf, N. R., Oldhafer, K. J., Westermann, S., Sotiropoulos, G. C. & Kaiser, G. M. Acute hepatic failure in swine: Hepatectomy versus vascular occlusion. *J. Invest. Surg.* **17**, 163–171 (2004).
156. Newsome, P. N., Plevris, J. N., Nelson, L. J. & Hayes, P. C. Animal models of fulminant hepatic failure: a critical evaluation. *Liver Transpl.* **6**, 21–31 (2000).
157. Keppler, D., Lesch, R., Reutter, W. & Decker, K. Experimental hepatitis induced by d-galactosamine. *Exp. Mol. Pathol.* **9**, 279–290 (1968).
158. Kalpana, K., Ong, H. S., Soo, K. C., Tan, S. Y. & Raj, J. P. An improved model of galactosamine-induced fulminant hepatic failure in the pig. *J. Surg. Res.* **82**, 121–130 (1999).
159. Shinoda, M. *et al.* A bioartificial liver device secreting interleukin-1 receptor antagonist for the treatment of hepatic failure in rats. *J. Surg. Res.* **137**, 130–40 (2007).
160. Satoshi Yamamoto, Jeffery L. Steers, Robert E. Wharen J, Christopher B. Eckman, and J. H. N. Cerebrospinal fluid drainage and cranial decompression prolong survival in rats with fulminant hepatic failure. *Transpl Int* **1219**, 675–682 (2006).
161. Terblanche, J., & Hickman, R. Animal models of fulminant hepatic failure. *Dig. Dis. Sci.* **36**, 770–774 (1991).
162. Fourneau, I., Pirenne, J., Roskams, T. & Yap, S. H. An improved model of acute liver failure based on transient ischemia of the liver. *Arch. Surg.* **135**, 1183–1189 (2000).
163. Khanna, O., Larson, J. C., Moya, M. L., Opara, E. C., & Brey, E. M. Generation of alginate microspheres for biomedical applications. *JoVE (Journal Vis. Exp.)* 1–5 (2012).
164. Gabriel, E. *et al.* Differentiation and Selection of Hepatocyte Precursors in Suspension Spheroid Culture of Transgenic Murine Embryonic Stem Cells. *PLoS One* **7**, (2012).
165. Graaf, W. De *et al.* Transporters involved in the hepatic uptake of and indocyanine green Tc-mebrofenin.

- J. Hepatol.* **54**, 738–745 (2011).
166. Cusin, F., Fernandes Azevedo, L., Bonnaventure, P., Desmeules, J., Daali, Y., & Pastor, C. M. Hepatocyte concentrations of indocyanine green reflect transfer rates across membrane transporters. *Basic Clin. Pharmacol. Toxicol.* **120**, 171–178 (2017).
167. Sakai, Y., Tanaka, T., Fukuda, J. & Nakazawa, K. Alkoxyresorufin O-dealkylase assay using a rat hepatocyte spheroid microarray. *J. Biosci. Bioeng.* **109**, 395–399 (2010).
168. Li, Y., Yang, G. & Mei, Z. Spectroscopic and dynamic light scattering studies of the interaction between pterodonic acid and bovine serum albumin. *Acta Pharm. Sin. B* **2**, 53–59 (2012).
169. Wang, N., Adams, G., Buttery, L., Falcone, F. H. & Stolnik, S. Alginate encapsulation technology supports embryonic stem cells differentiation into insulin-producing cells. *J. Biotechnol.* **144**, 304–312 (2009).
170. Gagnon, P., Nian, R., Leong, D. & Hoi, A. Transient conformational modification of immunoglobulin G during purification by protein A affinity chromatography. *J. Chromatogr. A* **1395**, 136–142 (2015).
171. Tran, N. M. *et al.* Alginate hydrogel protects encapsulated hepatic HuH-7 cells against hepatitis C virus and other viral infections. *PLoS One* **9**, 16–17 (2014).
172. Figaro, S. *et al.* Optimizing the fluidized bed bioreactor as an external bioartificial liver. *Int. J. Artif. Organs* **40**, 196–203 (2017).
173. Zhou, P. *et al.* Efficacy of Fluidized Bed Bioartificial Liver in Treating Fulminant Hepatic Failure in Pigs: A Metabolomics Study. *Sci. Rep.* **6**, 1–9 (2016).
174. Chen, C., Soto-Gutierrez, A., Baptista, P. M. & Spee, B. Biotechnology Challenges to In Vitro Maturation of Hepatic Stem Cells. *Gastroenterology* **154**, 1258–1272 (2018).
175. Mehta, G., Hsiao, A. Y., Ingram, M., Luker, G. D. & Takayama, S. Opportunities and challenges for use of tumor spheroids as models to test drug delivery and efficacy. *J. Control. Release* **164**, 192–204 (2012).
176. Chen, A. A., Khetani, S. R., Lee, S., Bhatia, S. N. & Van Vliet, K. J. Modulation of hepatocyte phenotype in vitro via chemomechanical tuning of polyelectrolyte multilayers. *Biomaterials* **30**, 1113–1120 (2009).
177. You, J. *et al.* Characterizing the effects of heparin gel stiffness on function of primary hepatocytes. *Tissue Eng. - Part A* **19**, 2655–2663 (2013).
178. Nemir, S. & West, J. L. Synthetic materials in the study of cell response to substrate rigidity. *Ann. Biomed. Eng.* **38**, 2–20 (2010).
179. Chui, C. Y., Bonilla-Brunner, A., Seifert, J., Contera, S. & Ye, H. Atomic force microscopy-indentation demonstrates that alginate beads are mechanically stable under cell culture conditions. *J. Mech. Behav. Biomed. Mater.* **93**, 61–69 (2019).
180. Simó, G., Fernández-Fernández, E., Vila-Crespo, J., Ruipérez, V. & Rodríguez-Nogales, J. M. Research progress in coating techniques of alginate gel polymer for cell encapsulation. *Carbohydr. Polym.* **170**, 1–14 (2017).
181. Glicklis, R., Shapiro, L., Agbaria, R., Merchuk, J. C. & Cohen, S. Hepatocyte behavior within three-dimensional porous alginate scaffolds. *Biotechnol. Bioeng.* **67**, 344–353 (2000).
182. Dianat, N. *et al.* Generation of functional cholangiocyte-like cells from human pluripotent stem cells and HepaRG cells. *Hepatology* **60**, 700–714 (2014).
183. Jitraruch, S. *et al.* Alginate microencapsulated hepatocytes optimised for transplantation in acute liver failure. *PLoS One* **9**, 1–23 (2014).
184. Legallais, C., Doré, E. & Paullier, P. Design of a fluidized bed bioartificial liver. *Artif. Organs* **24**, 519–525 (2000).
185. Leedale, J., Colley, H. E., Gaskell, H., Williams, D. P., Bearon, R. N., Chadwick, A. E., ... & Webb, S. D. In silico-guided optimisation of oxygen gradients in hepatic spheroids. *Comput. Toxicol.* **12**, 100093 (2019).

186. Hansen, L. K. *et al.* Enhanced morphology and function in hepatocyte spheroids: A model of tissue self-assembly. *Tissue Eng.* **4**, 65–74 (1998).
187. Wu, F. J., Peshwa, M. V., Cerra, F. B. & Hu, W. S. Entrapment of Hepatocyte Spheroids in a Hollow Fiber Bioreactor as a Potential Bioartificial Liver. *Tissue Eng.* **1**, 29–40 (1995).
188. Adam, A. A. A. *et al.* A practice-changing culture method relying on shaking substantially increases mitochondrial energy metabolism and functionality of human liver cell lines. *PLoS One* **13**, 1–19 (2018).
189. Nibourg, G. A. A. *et al.* Increased hepatic functionality of the human hepatoma cell line HepaRG cultured in the AMC bioreactor. *Int. J. Biochem. Cell Biol.* **45**, 1860–1868 (2013).
190. Poyck, P. P. C. *et al.* Functional and morphological comparison of three primary liver cell types cultured in the AMC bioartificial liver. *Liver Transplant.* **13**, 589–598 (2007).
191. Lübberstedt, M. *et al.* HepaRG human hepatic cell line utility as a surrogate for primary human hepatocytes in drug metabolism assessment in vitro. *J. Pharmacol. Toxicol. Methods* **63**, 59–68 (2011).
192. Gunness, P. *et al.* 3D organotypic cultures of human HepaRG cells: A tool for in vitro toxicity studies. *Toxicol. Sci.* **133**, 67–78 (2013).
193. Hoffmann, S. A., Müller-Vieira, U., Biemel, K., Knobloch, D., Heydel, S., Lübberstedt, M., ... & Zeilinger, K. Analysis of Drug Metabolism Activities in a Miniaturized Liver Cell Bioreactor for Use in Pharmacological Studies. *Biotechnol. Bioeng.* **109**, 3172–3181 (2012).
194. Hengstler, J. G. *et al.* Cryopreserved primary hepatocytes as a constantly available in vitro model for the evaluation of human and animal drug metabolism and enzyme induction. *Drug Metab. Rev.* **32**, 81–118 (2000).
195. Acikgöz, A., Giri, S., Cho, M. G. & Bader, A. Morphological and functional analysis of hepatocyte spheroids generated on poly-HEMA-treated surfaces under the influence of fetal calf serum and nonparenchymal cells. *Biomolecules* **3**, 242–269 (2013).
196. Gebhardt, R. *et al.* New hepatocyte in vitro systems for drug metabolism: Metabolic capacity and recommendations for application in basic research and drug development, standard operation procedures. *Drug Metab. Rev.* **35**, 145–213 (2003).
197. Gomez-Lechon, M., Donato, M., Lahoz, A. & Castell, J. Cell Lines: A Tool for In Vitro Drug Metabolism Studies. *Curr. Drug Metab.* **9**, 1–11 (2008).
198. Van Wenum, M. *et al.* Scaling-up of a HepaRG progenitor cell based bioartificial liver: Optimization for clinical application and transport. *Biofabrication* **9**, (2017).
199. Wang, Z. Y. *et al.* A DMSO-free hepatocyte maturation medium accelerates hepatic differentiation of HepaRG cells in vitro. *Biomed. Pharmacother.* **116**, 109010 (2019).
200. Ronald, P., Elferink, J. O., & Paulusma, C. C. Function and pathophysiological importance of ABCB4 (MDR3 P-glycoprotein). *Pflügers Arch. J. Physiol.* **453**, 601 (2007).
201. Kawahara, H. & French, S. W. Role of cytoskeleton in canalicular contraction in cultured differentiated hepatocytes. *Am. J. Pathol.* **136**, 521–532 (1990).
202. Blau, B. J. & Miki, T. The role of cellular interactions in the induction of hepatocyte polarity and functional maturation in stem cell-derived hepatic cells. *Differentiation* **106**, 42–48 (2019).
203. van Wenum, M. *et al.* Oxygen drives hepatocyte differentiation and phenotype stability in liver cell lines. *J. Cell Commun. Signal.* **12**, 575–588 (2018).
204. Perkins, J. D. Techniques to ensure adequate portal flow in the presence of splenorenal shunts. *Liver Transplant.* **13**, 767–768 (2007).
205. Hirschhaeuser, F., Sattler, U. G. A. & Mueller-Klieser, W. Lactate: A metabolic key player in cancer. *Cancer Res.* **71**, 6921–6925 (2011).

-
206. De Vos, P., De Haan, B. & Van Schilfgaarde, R. Effect of the alginate composition on the biocompatibility of alginate-polylysine microcapsules. *Biomaterials* **18**, 273–278 (1997).
207. Joly, A. *et al.* Survival, proliferation, and functions of porcine hepatocytes encapsulated in coated alginate beads: a step toward a reliable bioartificial liver. *Transplantation* **63**, 795–803 (1997).
208. Lou, R. *et al.* Fabrication of stable galactosylated alginate microcapsules via covalent coupling onto hydroxyl groups for hepatocytes applications. *Carbohydr. Polym.* **155**, 456–465 (2017).
209. Dusseault, J. *et al.* Microencapsulation of living cells in semi-permeable membranes with covalently cross-linked layers. *Biomaterials* **26**, 1515–1522 (2005).
210. Du, J. & Yarema, K. J. Cell Microencapsulation for Tissue Engineering and Regenerative Medicine. *Micro- and Nanoeng. Cell Surf.* **23**, 215–239 (2014).
211. Bhujbal, S. V., Paredes-Juarez, G. A., Niclou, S. P. & de Vos, P. Factors influencing the mechanical stability of alginate beads applicable for immunoisolation of mammalian cells. *J. Mech. Behav. Biomed. Mater.* **37**, 196–208 (2014).
212. Goosen, M. F. A., O'Shea, G. M., Gharapetian, H. M., Chou, S. & Sun, A. M. Optimization of microencapsulation parameters: Semipermeable microcapsules as a bioartificial pancreas. *Biotechnol. Bioeng.* **27**, 146–150 (1985).
213. Lu, J. *et al.* A New Fluidized Bed Bioreactor Based on Diversion-Type Microcapsule Suspension for Bioartificial Liver Systems. *PLoS One* **11**, 1–18 (2016).
214. Sun, J. & Tan, H. Alginate-based biomaterials for regenerative medicine applications. *Materials (Basel)*. **6**, 1285–1309 (2013).
215. Benson, J. P., Papas, K. K., Constantinidis, I. & Sambanis, A. Towards the development of a bioartificial pancreas: Effects of poly-L-lysine on alginate beads with BTC3 cells. *Cell Transplant.* **6**, 395–402 (1997).
216. Strand, B. L., Coron, A. E. & Skjak-Braek, G. Current and future perspectives on alginate encapsulated pancreatic islet. *Stem Cells Transl. Med.* **6**, 1053–1058 (2017).
217. Strand, B. L. *et al.* Poly-L-lysine induces fibrosis on alginate microcapsules via the induction of cytokines. *Cell Transplant.* **10**, 263–275 (2001).
218. Tam, S. K. *et al.* Biocompatibility and physicochemical characteristics of alginate-polycation microcapsules. *Acta Biomater.* **7**, 1683–1692 (2011).
219. Bratek-Skicki, A., Zeliszewska, P. & Ruso, J. M. Fibrinogen: A journey into biotechnology. *Soft Matter* **12**, 8393–8653 (2016).
220. Wisse, F. B. and E. Structural and functional aspects of liver sinusoidal endothelial cell fenestrae: a review. *Comp Hepatol* **1**, (2002).
221. Bhujbal, S. V., De Haan, B., Niclou, S. P. & De Vos, P. A novel multilayer immunoisolating encapsulation system overcoming protrusion of cells. *Sci. Rep.* **4**, 1–8 (2014).
222. Chen HS., Joo DJ., Shaheen M., Li Y., WangY., Yang J., Nicolas CT., Predmore K., Amiot B., Michalak G., Mounajjed T., Fidler J., Kremers WK., N. S. Randomized Trial of Spheroid Reservoir Bioartificial Liver in Porcine Model of Posthepatectomy Liver Failure. *Hepatology* **69**, 329–342 (2019).
223. McIntosh, M. B., Corner, S. M., Amiot, B. P. & Nyberg, S. L. Engineering analysis and development of the spheroid reservoir bioartificial liver. *Proc. 31st Annu. Int. Conf. IEEE Eng. Med. Biol. Soc. Eng. Futur. Biomed. EMBC* 5985–5988 (2009).
224. Hoekstra, R. *et al.* The Effect of Rat Acute-Liver-Failure Plasma on HepaRG Cells. *Int. J. Artif. Organs* **35**, 1006–1014 (2012).
225. Figaro, S. *et al.* Development and validation of a bioartificial liver device with fluidized bed bioreactors hosting alginate-encapsulated hepatocyte spheroids. *Proc. Annu. Int. Conf. IEEE Eng. Med. Biol. Soc.*

- 1335–1338 (2015).
226. Kogure, K., Ishizaki, M., Nemoto, M., Kuwano, H. & Makuuchi, M. A comparative study of the anatomy of rat and human livers. *J. Hepatobiliary. Pancreat. Surg.* **6**, 171–175 (1999).
227. Kruepunga, N., Hakvoort, T. B. M., Hikspoors, J. P. J. M., Köhler, S. E. & Lamers, W. H. Anatomy of rodent and human livers: What are the differences? *Biochim. Biophys. Acta - Mol. Basis Dis.* **1865**, 869–878 (2019).
228. Nykonenko, A., Vávra, P. & Zonča, P. Anatomic peculiarities of pig and human liver. *Exp. Clin. Transplant.* **15**, 21–26 (2017).
229. Devices, L. A. Comparison of pig , human and rat hepatocytes as a source of liver specific metabolic functions in culture systems - implications for use in bioartificial liver devices. **24**, 392–396 (2001).
230. Kang, Y. B. A., Eo, J., Mert, S., Yarmush, M. L. & Usta, O. B. Metabolic Patterning on a Chip: Towards in vitro Liver Zonation of Primary Rat and Human Hepatocytes. *Sci. Rep.* **8**, 1–13 (2018).
231. Lee, S. W., Kim, S. H., Min, S. O. & Kim, K. S. Ideal Experimental Rat Models for Liver Diseases. *Korean J. hepato-biliary-pancreatic Surg.* **15**, 67–77 (2011).
232. Tuñón, M. J., Alvarez, M., Culebras, J. M. & González-Gallego, J. An overview of animal models for investigating the pathogenesis and therapeutic strategies in acute hepatic failure. *World J. Gastroenterol.* **15**, 3086–3098 (2009).
233. Flendrig, L. M. *et al.* Evaluation of a novel bioartificial liver in rats with complete liver ischemia: Treatment efficacy and species-specific alpha-GST detection to monitor hepatocyte viability. *J. Hepatol.* **30**, 311–320 (1999).
234. Shito, M., Tilles, A. W., Tompkins, R. G., Yarmush, M. L. & Toner, M. Efficacy of an extracorporeal flat-plate bioartificial liver in treating fulminant hepatic failure. *J. Surg. Res.* **111**, 53–62 (2003).
235. Damania, A., Hassan, M., Shirakigawa, N., Mizumoto, H., Kumar, A., Sarin, S. K., ... & Kumar, A. Alleviating liver failure conditions using an integrated hybrid cryogel based cellular bioreactor as a bioartificial liver support. *Sci. Rep.* **7**, 1–11 (2017).
236. Chang, T. M. . *Hemoperfusion*. (Karger, 1982).
237. Saliba, F., Camus, C., Durand, F., Mathurin, P., Letierce, A., Delafosse, B., ... & Samuel, D. (2013). Albumin Dialysis With a Noncell Artificial Liver Support Device in Patients With Acute Liver Failure. *Ann. Intern. Med.* **159**, 522–531 (2013).
238. Sueoka, A. Present status of apheresis technologies, Part 3: Adsorbent. *Ther. Apher.* **1**, 271–283 (1997).
239. Gay, M. *et al.* Proteomic analysis of polypeptides captured from blood during extracorporeal albumin dialysis in patients with cholestasis and resistant pruritus. *PLoS One* **6**, 1–8 (2011).
240. Dominik, A. *et al.* Reduction of Elevated Cytokine Levels in Acute/Acute-on-Chronic Liver Failure Using Super-Large Pore Albumin Dialysis Treatment: An In Vitro Study. *Ther. Apher. Dial.* **18**, 347–352 (2014).
241. Morimoto, T., Matsushima, M., Sowa, N., Ide, K. & Sawanishi, K. Plasma Adsorption Using Bilirubin-Adsorbent Materials as a Treatment for Patients with Hepatic Failure. *Artif. Organs* **13**, 447–452 (1989).
242. Davidson, M. D., Ballinger, K. R. & Khetani, S. R. Long-term exposure to abnormal glucose levels alters drug metabolism pathways and insulin sensitivity in primary human hepatocytes. *Sci. Rep.* **6**, 1–11 (2016).
243. Yorimitsu, D. *et al.* Establishment of a Blood Purification System for Renal Failure Rats Using Small-Size Dialyzer Membranes. *Ther. Apher. Dial.* **16**, 566–572 (2012).
244. Moussard, C. *Biologie moléculaire. Biochimie des communications cellulaires.* (2005).
245. Ashraf, M. N., Asghar, M. W., Rong, Y., Doschak, M. R., & Kiang, T. K. Advanced in vitro HepaRG culture systems for xenobiotic metabolism and toxicity characterization. *Eur. J. Drug Metab. Pharmacokinet.* 1–22 (2019).

-
246. Dallot, C. Perturbation de la fonction thyroïdienne : mise en place d'une stratégie de criblage des produits chimiques. (Sciences agricoles. Université Nice Sophia Antipolis, 2015).
247. Buckley, D. B. & Klaassen, C. D. Induction of mouse UDP-glucuronosyltransferase mRNA expression in liver and intestine by activators of aryl-hydrocarbon receptor, constitutive androstane receptor, pregnane X receptor, peroxisome proliferator-activated receptor α , and nuclear factor eryth. *Drug Metab. Dispos.* **37**, 847–856 (2009).
248. Reddy, A. *et al.* Hypothyroidism: A Possible Risk Factor for Liver Cancer in Patients With No Known Underlying Cause of Liver Disease. *Clin. Gastroenterol. Hepatol.* **5**, 118–123 (2007).
249. Hassan, M. M. *et al.* Association between hypothyroidism and hepatocellular carcinoma: A case-control study in the United States. *Hepatology* **49**, 1563–1570 (2009).
250. Perra, A., Plateroti, M. & Columbano, A. T3/TRs axis in hepatocellular carcinoma: New concepts for an old pair. *Endocr. Relat. Cancer* **23**, R353–R369 (2016).
251. Kowalik, M. A., Columbano, A. & Perra, A. Thyroid hormones, thyromimetics and their metabolites in the treatment of liver disease. *Front. Endocrinol. (Lausanne)*. **9**, 1–11 (2018).
252. Kowalik, M. A. *et al.* TR β is the critical thyroid hormone receptor isoform in T3-induced proliferation of hepatocytes and pancreatic acinar cells. *J. Hepatol.* **53**, 686–692 (2010).
253. Monga, S. P. Triiodothyronine induces hepatocyte proliferation by Protein Kinase A-Dependent β -Catenin Activation in Rodents. **59**, 2309–2320 (2015).
254. Nejak-Bowen, K. N., Thompson, M. D., Singh, S., Bowen Jr, W. C., Dar, M. J., Khillan, J., ... & Monga, S. P. Accelerated liver regeneration and hepatocarcinogenesis in mice overexpressing serine-45 mutant β -catenin. *Hepatology* **51**, 1602–16013 (2010).
255. Vrzal, R., Vrzalova, A., Grycova, A. & Dvorak, Z. Activated thyroid hormone receptor modulates dioxin-inducible aryl hydrocarbon receptor-mediated CYP1A1 induction in human hepatocytes but not in human hepatocarcinoma HepG2 cells. *Toxicol. Lett.* **275**, 77–82 (2017).
256. Moedas, M. F. *et al.* Advances in methods for characterization of hepatic urea cycle enzymatic activity in HepaRG cells using UPLC-MS/MS. *Anal. Biochem.* **535**, 47–55 (2017).
257. Helbing, C. C. & Atkinson, B. G. 3,5,3'-Triiodothyronine-induced carbamyl-phosphate synthetase gene expression is stabilized in the liver of *Rana catesbeiana* tadpoles during heat shock. *J. Biol. Chem.* **269**, 11743–11750 (1994).
258. van Wenum, M. *et al.* Selecting cells for bioartificial liver devices and the importance of a 3D culture environment: A functional comparison between the hepaRG and C3A cell lines. *Int. J. Biol. Sci.* **12**, 964–978 (2016).
259. Miler, E. A., Ríos de Molina, M. del C., Domínguez, G. & Guerra, L. N. Thyroid hormone effect in human hepatocytes. *Redox Rep.* **13**, 185–191 (2008).
260. Leite, S. B. *et al.* Merging bioreactor technology with 3D hepatocyte-fibroblast culturing approaches: Improved in vitro models for toxicological applications. *Toxicol. Vitro.* **25**, 825–832 (2011).
261. Findlay, K. A. B., Kaptein, E., Visser, T. J. & Burchell, B. Characterization of the uridine diphosphate-glucuronosyltransferase-catalyzing thyroid hormone glucuronidation in man. *J. Clin. Endocrinol. Metab.* **85**, 2879–2883 (2000).

Annexes

Annex 1. Influence of the hormone triiodothyronine (t₃) on cell metabolic performance

1. Introduction

During my Ph.D., I supervised several students during their internship period. Among these students, Alexia Provost was included in a preliminary study that allowed investigating the impact of the hormone triiodothyronine on the metabolism of HepaRG cells. In particular, the main interest of this study was to understand if the addition of this hormone to the culture medium could improve the metabolic activities required for the clinical application of bioartificial liver.

1.1. Description of triiodothyronine

Derived from tyrosine, 3,5,3' triiodothyronine (or T₃ hormone) is synthesized and secreted by the thyroid gland. It has no specific target organs: it acts on the cells of all tissues except for certain organs such as the brain, spleen, gonads and thyroid gland. It has effects on cell growth, development and metabolism. In particular, it acts as a "accelerator" of metabolism by promoting the synthesis of many enzymes: it stimulates the metabolic pathways of glycolysis, neoglucogenesis, lipolysis, proteolysis and to a lesser degree increases cholesterol catabolism ²⁴⁴. More specifically, it acts on lipid, carbohydrate and protein metabolism in the liver. This hormone controls cholesterol levels by promoting the synthesis and liver degradation of cholesterol (increased conversion of cholesterol to bile acids and increased expression of LDL receptors). It works to control blood sugar levels by increasing glycogenolysis in the liver. It is also involved in protein metabolism by increasing protein synthesis and catabolism and by stimulating the activity of key enzymes such as ATPase or cytochromes.

Thyroid hormones are uncoupling proteins of the mitochondrial respiratory chain, which leads to activation of respiratory oxidation, without additional ATP synthesis, but with increased heat production. This activation of cellular oxidation leads to the activation of metabolic pathways such as glycolysis and lipolysis.

1.2. Mechanism of action

More specifically, triiodothyronine exerts its biological effects by stimulating or inhibiting the expression of specific genes via specific nuclear receptors (TR thyroid hormone receptors). There are two of them: TR_α which is preferentially expressed in the liver, and TR_β. They behave as transcriptional factors inducible by their ligand. They control positively or negatively the expression of their target genes in the presence or absence of the hormone T₃. To perform this transcriptional activity, like other nuclear receptors, thyroid receptors interact with multiple nuclear cofactors: co-repressors, which inhibit their action in the absence of T₃, and co-activators that stimulate it in its presence (Figure g2).

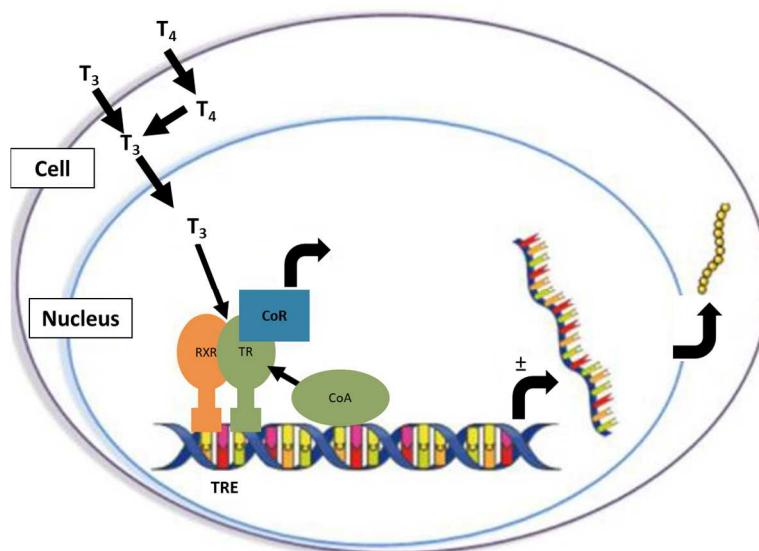


Fig. 92: Mechanism of action of T₃

Legend: CoR = Co-Repressor; CoA = C-activator; RXR = retinoic acid receptor; TR = thyroid hormone receptor; TRE = Thyroid-Responsive Element.

Thyroid hormones must first actively cross the plasma membrane through the specific carriers of amino acids. The best known for hepatocytes are Monocarboxylase Transporters (MCT8, MCT10, expressed in HepaRG ²⁴⁵), Organic Anion-Transporting Polypeptides (OATP1C1 and OATP3A1), Multidrug Resistance Protein (MRP) and Na(+)-Taurocholate Co-transporting Polypeptide (NTCP). Most of them are present and functional in HepaRG cell model.

1.3.Catabolism

The half-life of triiodothyronine is about one day. After conjugation by phase II liver enzymes, it is eliminated by the bile pathway: the hormone T₃ is sulfo-conjugated by sulfotransferases or glucuronoconjugated by UDP-Glucuronosyltransferases (UDP-GT) to facilitate its excretion ²⁴⁶. T₃ can also undergo a transamination and decarboxylation reaction to triiodoacetic (TRIAC) and tetraiodoacetic (TETRAC) acids, which are then desodinated. Iodine is eliminated in the urine or taken up by the thyroid ²⁴⁴. The hormone T₃ increases the activity of hepatic microsomal enzymes and metabolic clearance. Mr. DALLOT, during his thesis work, showed that in rats, xenobiotics induce hepatic UDP-GT activity, which increases the biliary elimination of thyroid hormones ²⁴⁶. Xenobiotics will induce a signal that will increase the transcriptional expression of genes encoding UDP-GT ²⁴⁷.

1.4.Interests in using hormone T3 on HepaRG

In the context bioartificial liver, the main issue is the metabolic activity of the biomass contained in the bioreactor. To this end, we wish to measure the impact of T₃ on the metabolic activity of the cell line HepaRG in conventional (two dimensional) culture in order to determine its interest for the intended clinical application. We chose the T₃ for its stimulating effects on cell growth and metabolism. Some research teams have already investigated the effects of the hormone T₃ on hepatocyte metabolism and its involvement in the development of various liver diseases.

1.4.1. Induction of hepatocyte proliferation

The liver is a major target for thyroid hormones. Cellular alteration of the thyroid signal has been reported to cause several liver diseases such as non-alcoholic fatty liver disease and hepatocellular carcinoma^{248,249,250}. Nevertheless, Kowalik MA et al. 2018²⁵¹ have shown that the hormone T₃ has beneficial effects on the liver. It is capable of lowering cholesterol and triglyceride levels, slowing the development and progression of hepatocarcinoma, and promoting liver regeneration. This same team has previously demonstrated the mitogenic nature of thyroid hormone in rodents. In fact, it induces hepatocyte proliferation by activating the β -catenin signal (TR) ²⁵². This proliferation is dependent on β -catenin²⁵³ and the more β -catenin is expressed, the higher the proliferation of cells after a partial hepatectomy²⁵⁴.

For the reasons given above, it can be assumed that the hormone T₃ will stimulate the proliferation of HepaRG and that this proliferation will be associated with an increase of cell metabolic activity (greater production of proteins such as albumin).

1.4.2. Xenobiotic metabolism

Vrzal et al. 2017²⁵⁵ investigated the impact of T₃ on the basal expression of the cytochrome P450 1A1/2 (CYP1A1/2), involved in xenobiotic detoxification. They used two cell lines: HepG2 and primary human hepatocytes, treated with T₃ concentrations of 0.2 nM, 2 nM, and 20 nM. Although the thyroid receptor is functional in HepG2, the hormone does not affect basal expression of CYP1A1 mRNA, nor the expression level of CYP1A1 proteins nor its catalytic activity, whereas for human hepatocytes, the parameters studied are highly variable. Their hypothesis is that in many hepatocarcinoma, thyroid receptors are mutated (HepG2 is a line from hepatocarcinoma) and that some mutants have decreased binding to the corepressors N-COR and SMRT, which may lead to suppression of the CYP1A1 promoter. However, our study consists in observing the effects of triiodothyronine on the metabolism of the HepaRG lineage, which expresses most of the enzymes implicated in the xenobiotic metabolism as primary human hepatocytes²⁴⁵.

Therefore, it can be hypothesized that the hormone T₃ will improve the xenobiotic metabolism in HepaRG.

1.4.3. Transformation of ammonia by the urea cycle

Ammonia is involved in the progression of certain liver diseases such as hepatic encephalopathy. The excess of this molecule must therefore be eliminated (until normal physiological levels) during BAL therapy. Although Van Wenum M et al. 2017²⁵⁶ showed that HepaRG was able to produce a small amount of urea in conventional (2D) culture, this production is certainly due to the removal of ammonia by glutamine metabolism rather than the urea cycle. Moreover, HepaRG spheroids are not able to produce high levels of urea from ammonia. In fact, it seems that, during their differentiation into hepatocytes-like cells, carbamoylphosphate synthase (key enzyme in the urea cycle) loses part of its functionality. Triiodothyronine has been shown to accelerate the metamorphosis of tadpoles and to initiate the urea cycle by inducing carbamoylphosphate

synthase in amphibians²⁵⁷. Van Wenum M. et al. 2016²⁵⁸ suggested that since the metabolic zonation of the urea cycle is driven by the Wnt signalling pathway, activating this pathway could increase the activity of the urea cycle. The hormone T₃ interacts with this pathway to stimulate it.

Therefore, it can be hypothesized that the addition of the hormone T₃ to the HepaRG culture medium will stimulate the enzymes of the urea cycle and thus increase ammonia removal.

To recapitulate, T₃ stimulates cell growth and metabolism, glycolysis, neoglucogenesis, lipolysis, proteolysis, protein synthesis, and the enzymatic activity of ATPase, cytochromes.

Our hypothesis is that it can:

- Increase albumin production
- Improve the transformation and secretion of xenobiotics
- Increase ammonia detoxification activity

2. Materials and methods

2.1.2D cell culture

HepaRG were cultured in a 24-wells plate for cell culture at a density of 0.055×10^6 cells/well in proliferation culture medium (500 μ L/well). The latter was changed every two days. On day 14, cells were exposed to T₃ (conditions presented in the next paragraph) and, between day 14 and 15, metabolic characterization was performed.

2.2.Material

3,3,5-Triiodo-L-thyronine (T2877) was purchased by Sigma-Aldrich and prepared following the manufacturer instructions. In particular, T₃ solution was prepared at 1 mg T₃/mL of NaOH 1M. Then, this solution was diluted 50 times in proliferation media (mother solution) with a concentration of $2.9 \cdot 10^{-5}$ mole/L. The mother solution was then diluted in proliferation medium, in order to obtain a final concentration of 2 and 20 nM for the subsequent tests.

2.3.Conditions tested

During this experiment, four conditions were compared. The experiment was performed in 3 wells for each condition.

- No stimulation (\emptyset stimulation): no metabolic tests performed, condition used to assess maximum cell viability
- \emptyset T₃: vehicle control (T₃ substituted with an equivalent quantity of HepaRG proliferation medium)
- 2 nM T₃
- 20 nM T₃

According to Miler et al. 2008²⁵⁹, a concentration of 2 nM of T₃ hormone corresponds to a physiological condition and a concentration of 20 nM is similar to hyperthyroidism.

2.4.Experimental design

On day 14, cells were exposed to their respective doses of molecule and incubated for 24 hours. The following metabolic tests were performed on day 15: albumin and urea synthesis, ammonia detoxification, Uridine Diphosphate Glucuronoltransferase (UGT) activity, cell viability via MTS assay. Total DNA quantification was realized for data normalization (Figure 93).

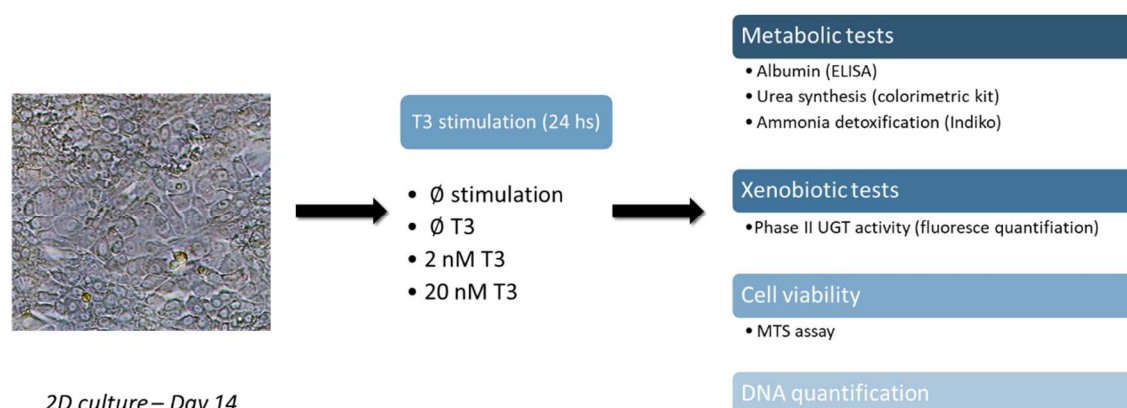


Fig. 93: Experimental method

In particular, on day 14 cells were stimulated with T₃. 8 hours after the first stimulation, the medium was changed with fresh medium at the same conditions (according to a half-life of about 24 hours of the molecule). During the remaining 16 hours of incubation, aliquots of supernatant were taken (time point 0 and time point 16 hours) in order to determine the synthesis rate of albumin and urea, considered as parameters of quality of the cells in culture. On day 15, cells were washed 3 times in DPBS (PAN biotech) and incubated with BAL function test medium for two hours, in order to determine the rate of albumin and urea synthesis, and the detoxification rate of ammonia and lactate. After that, cells were washed 3 times in DPBS and tested for UGT activity for 2 hours (see protocol later). Finally, cells were washed 3 times in DPBS and subjected to MTS assay for determining cell viability. At the end of the experiments, cells were lysed and total DNA were determined. The experimental design is presented in figure 94.

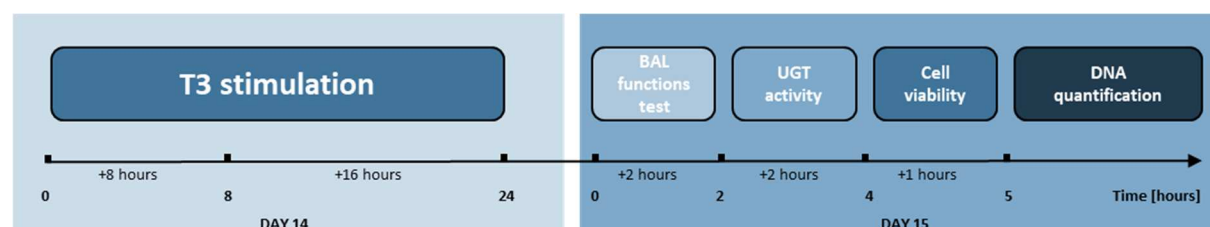


Fig. 94: Experimental design

2.4.1. Uridine Diphosphate Glucuronoltransferase (UGT) activity

UGT activity was assayed according to previous defined procedure²⁶⁰. In short, beads were incubated in 100 µM of 4-Methylumbelliferone (4-MU), prepared DPBS, for 1 hours at 37°C.

Supernatant was saved and used to measure the fluorescence (excitation wavelength of 320 nm and emission wavelength of 450 nm). The 4-MU remaining concentration was deduced from the fluorescence measurements based on a linear standard curve generated in DPBS.

2.4.2. Cell viability

Cell viability was tested by CellTiter 96® AQueous One Solution Cell Proliferation Assay (MTS) following the manufacturer instructions. The condition "Ø stimulation" (No stimulation) was considered as 100% viability and the viability values of the remaining conditions were compared to it.

3. Results

3.1. Metabolic tests

The production rate of albumin and urea was evaluated in two different time intervals:

- In an overnight (basal production) between day 14 and 15, under the stimulation of T3, for a total incubation time of 16 hours (control of the quality of the hepatocytes before the metabolic tests on day 15)
- On day 15, in 2 hours of incubation in BAL function tests medium, containing 1.5 mM ammonium chloride and 2 mM L-Lactate

In all the cases, the results were normalised by the quantity of marker produced (or consumed)/hour of incubation/well (or quantity of cell counted).

Table 23 presents the results obtained for albumin secretion rate in overnight (basal production). In terms of production of albumin per well, it seems that the presence of T3 do not influence this activity, even if a slightly higher production is registered for the condition 20 nM. Instead, when normalizing by the number of cells counted by DNA quantification, it seems that the condition 2 nM is stronger than the other conditions. However, given the large standard deviations, those differences are not significant. No urea was detected in both days.

| Experimental condition | Ø T3 | 2 nM T3 | 20 nM T3 |
|---|--------------|---------------|---------------|
| Albumin synthesis rate ng/h/well | 14.66 ± 1.79 | 14.08 ± 1.39 | 18.11 ± 3.00 |
| Albumin synthesis rate ng/h/10 ⁶ (counted cells) | 35.93 ± 7.50 | 66.80 ± 24.24 | 49.15 ± 13.50 |

Tab. 23: Basal production of albumin in ng/h/well and in ng/h/10⁶ (cell counted by DNA quantification). N = 3. Results are expressed in mean ± standard deviation

Regarding the metabolic performance on day 15 in BAL function tests medium, the results of albumin production rate and ammonia detoxification are summarized in table 24. Albumin secretion rate is not influenced by the presence of T3, compared with the vehicle. The activity of ammonia detoxification is stronger when cells were stimulated with T3 (no significant differences between the condition 2 nM and 20 nM), both if results are normalised by well and by counted cells. We concluded that the hormone T3 has a stimulatory effect on ammonia detoxification activity.

Importantly, since no urea production was detected, it is supposed that the ammonia detoxified is reversibly incorporated rather into amino acids. Unfortunately, we did not have enough supernatant to dose the lactate.

| Experimental condition | Ø T3 | 2 nM T3 | 20 nM T3 |
|---|---------------|---------------|----------------|
| Albumin synthesis rate ng/h/well | 0.126 ± 0.001 | 0.116 ± 0.003 | 0.130 ± 0.004 |
| Albumin synthesis rate ng/h/10 ⁶ (counted cells) | 0.324 ± 0.014 | 0.505 ± 0.252 | 0.334 ± 0.064 |
| Ammonia detox rate nmol/h/well | 26 ± 2.36 | 50.90 ± 5.56 | 50.90 ± 13.97 |
| Ammonia detox rate nmol/h/10 ⁶ (counted cells) | 66.64 ± 2.66 | 216.92 ± 92 | 132.93 ± 56.88 |

Tab. 24: Metabolic activity on day 15 in BAL function tests medium, during 2 hours of incubation. N = 3. Results are expressed in mean ± standard deviation

3.2.Xenobiotic tests

Still with the aim of improving the performance of biomass to be used in the bioreactor in the context of a bioartificial liver, it is relevant to focus on the effects of triiodothyronine on this detoxification activity. The cells were therefore put in contact for one hour with the fluorescent 4-MU (compound to be detoxified) and the remaining 4-MU were quantified by spectrometry in order to measure the activity of UGT enzyme. The results are presented in table 25. When results are normalised by wells, no significant differences are visible between the three conditions. When normalizing by the number of cells counted, the condition 2 nM T3 shows a 2X decreased activity in comparison with the others. We can conclude that the hormone has an inhibitory effect at 2 nM on the UGT activity, while this effect is not observed at stronger T3 concentration (20 nM).

| Experimental condition | Ø T3 | 2 nM T3 | 20 nM T3 |
|---|----------------|---------------|----------------|
| UGT activity µg/h/well | 4.385 ± 0.401 | 3.929 ± 0.730 | 4.854 ± 0.613 |
| UGT activity µg/h/10 ⁶ (counted cells) | 18.887 ± 3.578 | 9.940 ± 0.958 | 17.853 ± 6.721 |

Tab. 25: Effect of T3 on 4-MU biotransformation by UGT enzyme. N = 3. Results are expressed in mean ± standard deviation

3.3.Cell viability

During the whole experiment, cells were exposed for 24 hours to the hormone at different concentrations and then subjected to the metabolic and xenobiotic tests presented. Therefore, at the end of the experiments it was important to evaluate the cell viability. The condition Ø stimulation has not been subjected to the metabolic tests but it received the same stresses as other wells (washing and medium changes). Therefore, it is considered as the reference 100% viability. The results show that cell viability is very high in all the condition tested in comparison with the reference, superior to 95% (Table 26). Therefore, the hormonal treatment and the succession of different tests did not affect cell viability.

| Experimental condition | Ø stimulation | Ø T ₃ | 2 nM T ₃ | 20 nM T ₃ |
|---------------------------|---------------|------------------|---------------------|----------------------|
| mean ± standard deviation | 100% ± 11% | 94% ± 7% | 90% ± 18% | 91% ± 15% |

Tab. 26: Cell viability (%) on the different conditions at the end of the experiment. N = 3. Results are expressed in mean ± standard deviation

4. Discussion

The main aim of this short stage that involved the student Alexia Provost, was to understand if the use of the hormone T₃ could improve the metabolic activities required for the clinical application of bioartificial liver. Those activities included protein secretion (albumin used as marker), ammonia detoxification, and xenobiotic metabolism.

Concerning albumin production, the results showed that triiodothyronine has no significant effect on albumin secretion activity by HepaRG cells, whether grown in a medium enriched with T₃ hormone (tests in overnight incubation) or previously stimulated by triiodothyronine (tests on day 15). In addition, the hormone T₃ has not a stimulating effect on urea production, which possibly remains below 0.08 mg/dL (13 µM), out of the sensitivity of the kit used (QuantiChrome Urea Assay Kit (DIUR-100)). However, it has been reported that these cells, during their differentiation into hepatocyte-like and cholangiocyte-like cells, carbamoylphosphate synthase (key enzyme in the urea cycle) loses part of its functionality²⁵⁶. This enzyme initiates the urea cycle. It is therefore understandable that urea production is minimal if this enzyme is not fully functional.

An interesting observation was the enhancement of ammonia detoxification activity. Indeed, when normalizing by activity per well, the hormonal treatment doubled the detoxification activity of the cells. However, when the results are expressed per million cells counted, the activity studied is significantly doubled for the 2 nM condition (compared to the condition without stimulation). There is therefore a difference in cell activity depending on the normalization of the data. This raises the question of how to present experimental results for clinical application. In our opinion, it would be more relevant to consider the experimental results at the scale of the bioreactor and therefore of the "artificial organ".

However, we have reported that urea production by HepaRG cells is very low. Therefore, we can deduce that the removal of ammonia is done exclusively by reversible fixation into amino acids. It is not possible to say with certainty at what level the hormone T₃ can promote the elimination of ammonia. In tadpoles, this molecule seems to have a stimulating role for the enzyme carbamoylphosphate synthase. To our knowledge, there is no research carried out in this direction on human cells. Since we have not found urea in the samples analysed, it is assumed that T₃ can stimulate the fixation of ammonia into amino acids, but we should investigate these mechanisms in more detail. However, the observation remains very interesting. In any case, even if the hormone T₃ increases this activity, the problem of the irreversible elimination of ammonia by a bioartificial liver using these cells is not solved.

Finally, we evaluated the effects of triiodothyronine on xenobiotic metabolism, studying the activity of the phase II enzyme UGT. Experimental results revealed that the hormone had no impact when normalizing per well. Instead, results change when normalizing per million cells. The enzyme activity drops by 52% for the condition 2 nM T₃ hormone compared to the vehicle while is unchanged for the condition 20 nM. Once again, the way of normalizing data has an impact on the exploitation of the results. Nevertheless, according to the bibliography, these last observations are strange because the hormone T₃ stimulates the UGT enzyme, in particular to induce its own transformation²⁶¹. We therefore expected to observe an increase in the detoxification activity of 4-MU by the phase II enzyme. Vrzal et al. 2017²⁵⁵ also observed an absence of stimulation of xenobiotic pathway enzymes by triiodothyronine. They noted that hepatocarcinoma cells often have mutated thyroid receptors. To be able to affirm that we are in a similar situation, it would have been relevant to evaluate the detoxification activity by phase I enzymes via the EROD (CYP1A1/2) and BROD (CYP3A4) tests.

5. Conclusions

The results of this experimental study show that T₃ has not a stimulating effect on albumin and urea production, and detoxification of the xenobiotic 4-MU. However, it doubles the detoxification activity of ammonia possibly through fixation into amino acids. It is regrettable that this elimination is reversible considering the bioartificial liver application, but the enhancement of this important activity remains interesting. In addition, it would be relevant to complete the study to evaluate the impact of the hormone T₃ on lactate detoxification activity, on carbohydrate metabolism and on the other enzymes of the xenobiotic metabolism.

Annex 2. Overview of proliferative human cell sources applied in bioartificial livers

This annex contains tables that recapitulates the cell sources for BALs already used by investigators in the literature. Those tables are extracted by the review article: "Proliferative human cell sources applied as biocomponent in bioartificial livers: a review" by Nibourg et al. 2012 ⁹².

| Biocomponent | Origin | Bioreactor | Tumorigenicity | Growth potential | IN VITRO functionality | | | | | Animal studies | Clinical studies |
|--------------|--|-------------------------------------|--------------------------------|------------------|---------------------------------|--|----------------------------------|--------------------------------|--|--|--|
| | | | | | Synthesis | Drug-metabolizing activity | Urea production [‡] | NH ₃ elimination | Carbohydrate metabolism | | |
| HepG2 | Hepatoma cells Hepatocellular carcinoma, 15 year old male | Diverse devices | Pos in immunocompromised mice* | Immortal | Pos Alb, AFP, ApoA1, fibrinogen | Neg/low in Phase I and Phase II detoxification | Pos, only due to Arg II activity | Inconsistency between reports | Lactate production and glucose consumption | One animal study (n = 3) in rat with acetaminophen intoxication using a bioreactor based on alginate encapsulated cells: no effect on survival measured, no effect found on ammonia and bilirubin levels | |
| C3A | Clonal derivative of HepG2, selected for strong contact inhibition, high production of albumin and AFP, and growth in glucose-deficient medium | Diverse devices, most often in ELAD | Neg in immunocompromised mice | Immortal | Pos Alb, AFP, transferrin | Detectable 7-ethoxycoumarin metabolism, level inconclusive | Pos, only due to Arg II activity | Detectable, level inconclusive | Glucose consumption | Only in ELAD. Two inconclusive animal studies (n = 3) in anhepatic dogs and dogs with acetaminophen intoxication | Two clinical Phase I studies showing safety. Two randomized controlled clinical trials; the first one not showing positive effects and the second one with unpublished results |
| Huh 7 | Hepatoma | Polyurethane foam/spheroid | Pos in immunocompromised mice | Immortal | Pos Alb | | | | | | |
| FLC | Hepatoma | Radial flow | | Immortal | | | | | | | |
| FLC-4 | Hepatoma | Radial flow | | Immortal | Pos Alb, coagulation factors | Detectable CYP mRNAs, level inconclusive | No CPS and OTC expression | | | One animal study (n = 2 – 3) in pigs with A-amanitin and lipopolysaccharide intoxication. Inconclusive results | |
| FLC-5 | Hepatoma | Radial flow | | Immortal | Pos Alb, coagulation factors | Detectable 6b-hydroxylation, level inconclusive | No CPS and OTC expression | | | | |

Grayscales indicate the potential for BAL application as indicated by in vitro functionality or efficacy in animal studies; white: no data available; lightest graytone: in vitro functionality < 5% of primary hepatocytes, or not effective in animal study; middle graytone: inconclusive; darkest graytone: in vitro functionality > 10% of primary hepatocytes, or proven efficacy in animal study.

*Although the ATCC datasheet states that HepG2 does not form tumors in SCID mice, several investigators use HepG2 cells to induce tumor formation in SCID mice [104,105].

[‡]Ureagenesis can be positive without a functional urea cycle.

AFP: Alpha-fetoprotein; Alb: Albumin; ALF: Acute liver failure; AMC-BAL: Academic Medical Center-BAL; ApoA1: Apolipoprotein A-1; Arg: Arginase; CYP: Cytochrome P450; ELAD: Extracorporeal liver assist device; elim: Elimination; GS: Glutamine synthetase; HE: Hepatic encephalopathy; HNF4: Hepatocyte nuclear factor 4; hTERT: Human telomere reverse transcriptase; IL-1: Interleukin 1; neg: Negative; OTC: Ornithine transcarbamoylase; PH: Primary hepatocyte; pos: Positive; pRb: Retinoblastoma protein; prod: Production; PXR: Pregnane X receptor; revers imm PHH: Reversibly immortalized primary human hepatocytes; SV40: Simian | virus 40.

| Biocomponent | Origin | Bioreactor | Tumorigenicity | Growth potential | IN VITRO functionality | | | | | Animal studies | Clinical studies |
|--------------|---|---|-------------------------------|------------------|------------------------------|---|------------------------------|-----------------------------|--|---|------------------|
| | | | | | Synthesis | Drug-metabolizing activity | Urea production [‡] | NH ₃ elimination | Carbohydrate metabolism | | |
| FLC-7 | Hepatoma | Radial flow | | Immortal | Pos Alb, coagulation factors | Detectable CYP mRNAs, level inconclusive | No CPS and OTC expression | | Glucose consumption | | |
| HepaRG | Hepatoma | AMC-BAL and multi-compartment hollow fiber capillary membrane | Neg in immunocompromised mice | Immortal | Pos ApoA1 | Pos CYP3A4, 6-b hydroxylation testosterone | | | Lactate consumption, stable glucose levels | One animal study (n = 5, 6) in rats with total liver ischemia: positive effect on survival time, HE, bleeding, creatinine, and ammonia levels | |
| HepZ | IN VITRO immortalized cells Hepatocyte cell line immortalized through E2F and cyclin D1 overexpression and suppression of pRB and P53 | Based on microporous gelatin microcarriers | | Immortal | | Detectable lidocaine metabolism, level inconclusive | | Production | Lactate production converting to consumption and glucose consumption | | |
| OUMS-29 | Fetal hepatocyte cell line immortalized through expression of SV40 large and small T antigen | Radial flow | | Immortal | Pos Alb | | | | | | |
| cBAL111 | Fetal hepatocytes immortalized through hTERT overexpression | AMC-BAL | | Immortal | Alb level only 6% | | | | Lactate production and glucose consumption | One animal study (n = 4) in rats with total liver ischemia. No positive effect on survival time | |

Grayscale indicates the potential for BAL application as indicated by in vitro functionality or efficacy in animal studies; white: no data available; lightest graytone: in vitro functionality < 5% of primary hepatocytes, or not effective in animal study; middle graytone: inconclusive; darkest graytone: in vitro functionality > 10% of primary hepatocytes, or proven efficacy in animal study.

*Although the ATCC datasheet states that HepG2 does not form tumors in SCID mice, several investigators use HepG2 cells to induce tumor formation in SCID mice [104,105].

[‡]Ureagenesis can be positive without a functional urea cycle.

AFP: Alpha-fetoprotein; Alb: Albumin; ALF: Acute liver failure; AMC-BAL: Academic Medical Center-BAL; ApoA1: Apolipoprotein A-1; Arg: Arginase; CYP: Cytochrome P450; ELAD: Extracorporeal liver assist device; elim: Elimination; GS: Glutamine synthetase; HE: Hepatic encephalopathy; HNF4: Hepatocyte nuclear factor 4; hTERT: Human telomere reverse transcriptase; IL-1: Interleukin 1; neg: Negative; OTC: Ornithine transcarbamoylase; PH: Primary hepatocyte; pos: Positive; pRb: Retinoblastoma protein; prod: Production; PXR: Pregnane X receptor; revers imm PHH: Reversibly immortalized primary human hepatocytes; SV40: Simian virus 40.

| Biocomponent | Origin | Bioreactor | Tumorigenicity | Growth potential | IN VITRO functionality | | | | | Animal studies | Clinical studies |
|--------------------------------|--|--|----------------|------------------|---|--|--------------------------------------|-----------------------------|---|---|------------------|
| | | | | | Synthesis | Drug-metabolizing activity | Urea production [‡] | NH ₃ elimination | Carbohydrate metabolism | | |
| Kobayashi revers imm hTERT PHH | Hepatocytes reversibly immortalized through hTERT overexpression | Hollow fiber | | Immortal | | | | | | Two animal studies. The first study in monkeys with D-galactosamine intoxication with inconclusive results. The second study in pigs with ALF, ongoing. | |
| Fetal hepatocytes | Fetal cells and stem cells Fetal liver | AMC-BAL and hollow fiber | | Limited | Pos Alb | Lidocaine metabolism | | Production | Lactate production and glucose production converting into consumption | | |
| Small hepatocytes | Liver | Rotary cell culture with cytodex microcarriers | | Limited | Relatively low Alb, and substantial decline in time | CYP3A4 protein expression and metabolism of methadone however, no metabolism of morphine and susceptible to toxins | Pos, but substantial decline in time | | Lactate production and glucose consumption, but both parameters decline substantially in time | | |
| Liver stem cells | Liver | Rotary system | | ? | Pos Alb | Metabolism 7-ethoxy-4-trifluoromethyl coumarin | | | Glucose consumption | | |
| Mesenchymal stem cells | Differentiated bone-marrow cells | Flat plate or with 3D nanofibrous scaffold | | ? | Transferrin, Alb detectable, level inconclusive | Detectable CYP3A4 mRNA, level inconclusive | Detectable, level inconclusive | | | One animal study (n = 7) in rats with D-galactosamine intoxication. Positive effects on survival and on leakage of AST and ALT. | |

Grayscale indicates the potential for BAL application as indicated by in vitro functionality or efficacy in animal studies; white: no data available; lightest graytone: in vitro functionality < 5% of primary hepatocytes, or not effective in animal study; middle graytone: inconclusive; darkest graytone: in vitro functionality > 10% of primary hepatocytes, or proven efficacy in animal study.

*Although the ATCC datasheet states that HepG2 does not form tumors in SCID mice, several investigators use HepG2 cells to induce tumor formation in SCID mice [104,105].

[‡]Ureagenesis can be positive without a functional urea cycle.

AFP: Alpha-fetoprotein; Alb: Albumin; ALF: Acute liver failure; AMC-BAL: Academic Medical Center-BAL; ApoA1: Apolipoprotein A-1; Arg: Arginase; CYP: Cytochrome P450; ELAD: Extracorporeal liver assist device; elim: Elimination; GS: Glutamine synthetase; HE: Hepatic encephalopathy; HNF4: Hepatocyte nuclear factor 4; hTERT: Human telomere reverse transcriptase; IL-1: Interleukin 1; neg: Negative; OTC: Ornithine transcarbamoylase; PH: Primary hepatocyte; pos: Positive; pRb: Retinoblastoma protein; prod: Production; PXR: Pregnane X receptor; revers imm PHH: Reversibly immortalized primary human hepatocytes; SV40: Simian virus 40.

| Biocomponent | Origin | Bioreactor | Tumorigenicity | Growth potential | IN VITRO functionality | | | | | Animal studies | Clinical studies |
|---|--|--|----------------|------------------|------------------------|--|--------------------------------|-----------------------------|-------------------------|--|------------------|
| | | | | | Synthesis | Drug-metabolizing activity | Urea production [‡] | NH ₃ elimination | Carbohydrate metabolism | | |
| Differentiated human embryonic stem cells | Blastocyst | Multi-compartment hollow fiber capillary membrane | | ? | Alb level only < 1% | Detectable CYP3A4 and CYP3A7 mRNA, level inconclusive | Detectable, level inconclusive | | | Lactate production and glucose consumption | |
| HepG2-GS | Genetically modified cells HepG2 with overexpression GS | Radial flow | | Immortal | | | | | | Two animal studies. The first study in pigs with total liver ischemia (n = 8 -- 9): positive effect on survival time. The second study in dogs with total liver ischemia (n = 5 -- 7): no effect on survival time. | |
| HepG2-GS-Cyp3A4 | HepG2 with overexpression GS and Cyp3A4 | Radial flow | | Immortal | | Detectable diazepam metabolism, level inconclusive | | | | One animal study (n = 7 -- 8) in dogs with total liver ischemia: pos effect on survival time and diazepam metabolism | |
| HepG2-DT | HepG2 with overexpression OTC and ArgI | Fluidized bed based on alginate encapsulated cells | | Immortal | Pos Alb | | | | | | |
| cBAL119 | HepG2 with overexpression PXR | AMC-BAL | | Immortal | Pos ApoA1 | Enhanced 6-b hydroxylation testosterone compared with HepG2, but still low | | | | Lactate production and glucose consumption | |
| OUMS-29/H-11 | OUMS-29 with overexpression HNF4 | Radial flow | | Immortal | Pos Alb | CYP3A4 protein present, level inconclusive. Enhanced 6-b hydroxylation testosterone in late culture phase, but still low | | | | | |

Grayscales indicate the potential for BAL application as indicated by in vitro functionality or efficacy in animal studies; white: no data available; lightest graytone: in vitro functionality < 5% of primary hepatocytes, or not effective in animal study; middle graytone: inconclusive; darkest graytone: in vitro functionality > 10% of primary hepatocytes, or proven efficacy in animal study.

*Although the ATCC datasheet states that HepG2 does not form tumors in SCID mice, several investigators use HepG2 cells to induce tumor formation in SCID mice [104,105].

[‡]Ureagenesis can be positive without a functional urea cycle.

AFP: Alpha-fetoprotein; Alb: Albumin; ALF: Acute liver failure; AMC-BAL: Academic Medical Center-BAL; ApoA1: Apolipoprotein A-1; Arg: Arginase; CYP: Cytochrome P450; ELAD: Extracorporeal liver assist device; elim: Elimination; GS: Glutamine synthetase; HE: Hepatic encephalopathy; HNF4: Hepatocyte nuclear factor 4; hTERT: Human telomere reverse transcriptase; IL-1: Interleukin 1; neg: Negative; OTC: Ornithine transcarbamoylase; PH: Primary hepatocyte; pos: Positive; pRb: Retinoblastoma protein; prod: Production; PXR: Pregnane X receptor; revers imm PHH: Reversibly immortalized primary human hepatocytes; SV40: Simian virus 40.

| Biocomponent | Origin | Bioreactor | Tumorigenicity | Growth potential | IN VITRO functionality | | | | | Animal studies | Clinical studies |
|------------------------------|---|---|----------------|------------------|---|----------------------------|------------------------------|-----------------------------|-------------------------|--|------------------|
| | | | | | Synthesis | Drug-metabolizing activity | Urea production [‡] | NH ₃ elimination | Carbohydrate metabolism | | |
| TTNT with AdIL-1Ra | Hepatocytes reversibly immortalized through hTERT overexpression, and further expressing IL-1 receptor antagonist | Flat-plate | | Immortal | | | | | | One animal study (n = 9) in rats with D-galactosamine intoxication. No positive effects on survival. Significant reduction IL-6 levels | |
| FLC-5, M1, and A7 | Combinations of cells Human hepatoma cell line with murine cell lines (endothelial and stellate) | Radial flow | | | Alb production FLC-5 decreased by co-culturing | | No OTC expression | | | | |
| HepG2-GS-CYP3A4 and PCTL-MDR | Modified hepatoma cell line with rabbit renal cell line transduced with MDR | Compartment bioreactor | | | | | | | Lactate production | | |
| HLSC, stellate cells | Human liver stem cells with human stellate cells | Perfusion bioreactor with porous scaffold | | | Pos Alb | | | | | | |

Grayscales indicate the potential for BAL application as indicated by in vitro functionality or efficacy in animal studies; white: no data available; lightest graytone: in vitro functionality < 5% of primary hepatocytes, or not effective in animal study; middle graytone: inconclusive; darkest graytone: in vitro functionality > 10% of primary hepatocytes, or proven efficacy in animal study.

*Although the ATCC datasheet states that HepG2 does not form tumors in SCID mice, several investigators use HepG2 cells to induce tumor formation in SCID mice [104,105].

[‡]Ureagenesis can be positive without a functional urea cycle.

AFP: Alpha-fetoprotein; Alb: Albumin; ALF: Acute liver failure; AMC-BAL: Academic Medical Center-BAL; ApoA1: Apolipoprotein A-1; Arg: Arginase; CYP: Cytochrome P450; ELAD: Extracorporeal liver assist device; elim: Elimination; GS: Glutamine synthetase; HE: Hepatic encephalopathy; HNF4: Hepatocyte nuclear factor 4; hTERT: Human telomere reverse transcriptase; IL-1: Interleukin 1; neg: Negative; OTC: Ornithine transcarbamoylase; PH: Primary hepatocyte; pos: Positive; pRb: Retinoblastoma protein; prod: Production; PXR: Pregnane X receptor; revers imm PHH: Reversibly immortalized primary human hepatocytes; SV40: Simian virus 40.

Tab. 27: Overview of proliferative human cells sources applied in BAL

Annex 3. Other cell densities tested

In the context of microencapsulation for BAL, augmenting the cell density is a way to obtain a higher quantity of biomass. While, during the thesis, most of the characterizations were performed on cell densities of 5-10 M/mL, we also evaluated the effect of other cell densities in cell metabolic performance and viability. The aim was to understand to what extent the cell density of alginate beads can be loaded in cells, in the perspective of a bioreactor that can host as many cells as possible. We performed preliminary tests on different cell densities, testing 1, 5, 10, 20, 40 M/mL. We evaluated the albumin synthesis rate (Figure 95A normalised by the number of cell seeded and 95B by the global quantity of protein produced) and the viability of the cells (Figure 96). It seems that the 5 M/mL condition is the one that most favoured protein production. However, as the amount of cells increased, overall protein production (per bioreactor) increased as well. Cell viability decreased dramatically at the highest concentrations (20 and 40 M/mL), especially in the core of the bead. At 1 M/mL there was cellular mortality higher than the conditions 5 and 10 M/mL. Moreover, at the 40 M/mL, the beads were so full of cells that they broke, causing cell loss (Figure 97). The latter was not observed at lower cell densities.

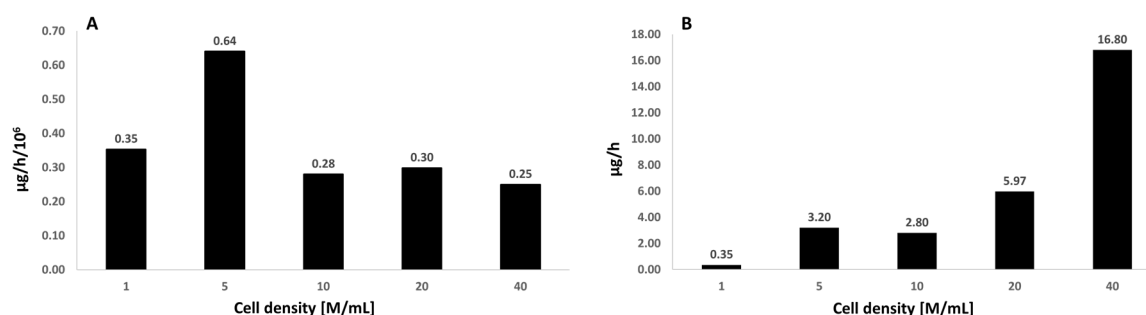


Fig. 95: Albumin synthesis rate normalised by the number of cell seeded (A). Global albumin quantity produced in each condition tested (B)

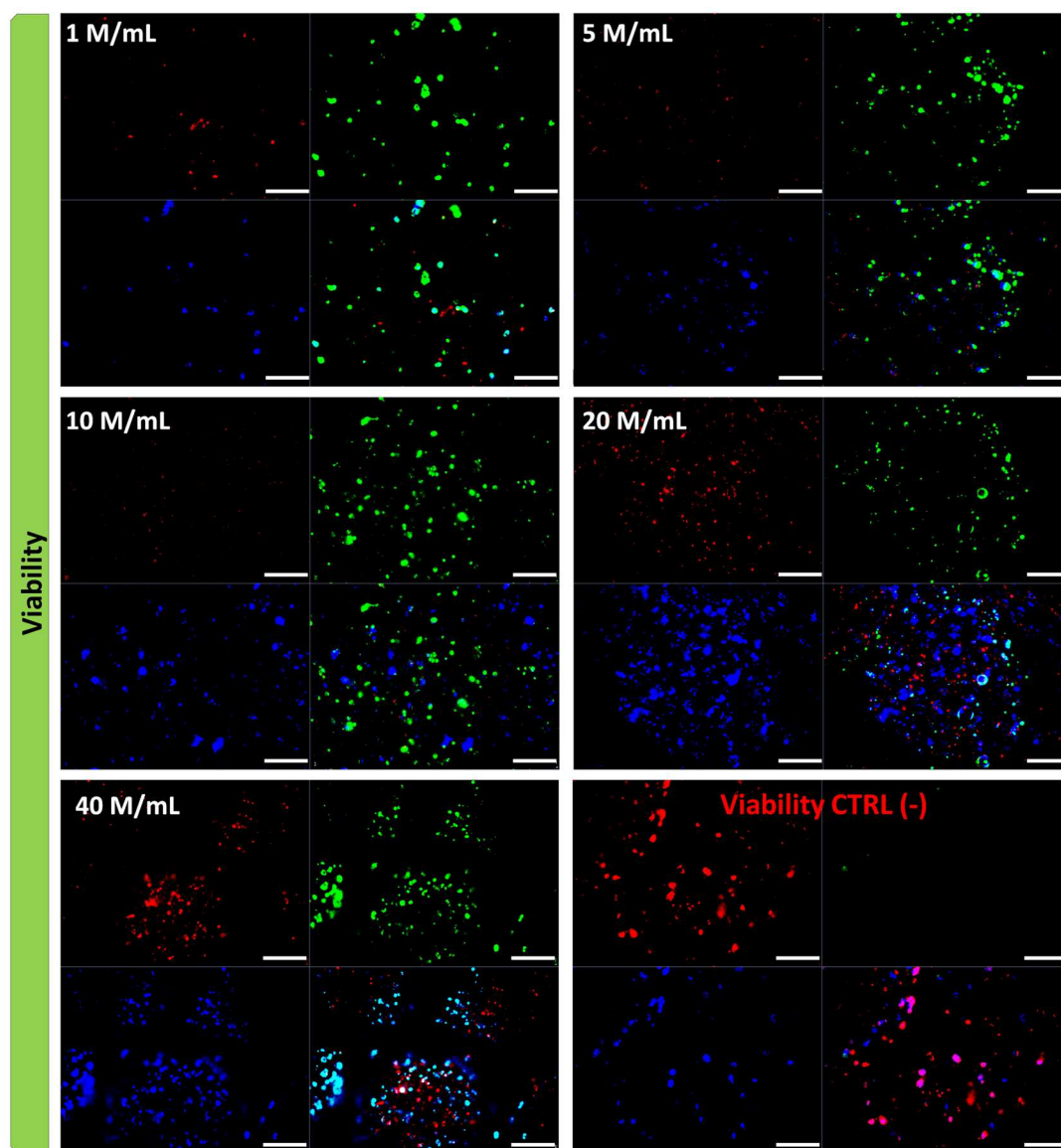


Fig. 96: Cell viability (confocal microscopy) between cell density at 1, 5, 10, 20 and 40 million cells/mL (M/mL) of alginate 1.5% on day 14. In green (Calcein AM): viable cells, in red (ethidium homodimer-1): dead cells, in blue (Hoechst 33342 dye): cell nuclei. Scale bar: 250 μ m

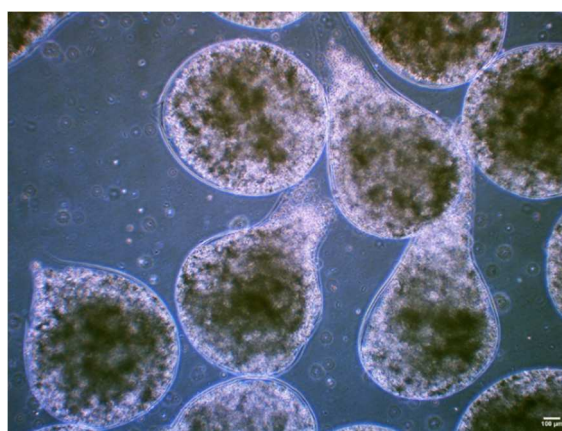


Fig. 97: Condition 40 M/mL (bright field microscopy)

Importantly, we have also tried to understand to what extent the cell density of alginate beads could be loaded, in the perspective of a bioreactor that can host as many cells as possible.

Unfortunately, for this experiment only albumin secretion rate was evaluated. When results are normalised by the number of cells seeded, it appears that the condition 5 M/mL is the most functional condition while, when normalizing by the quantity of albumin produced per hour, the condition 40 M/mL appears to be the best (clearly because of a higher number of cells). At the same time, at 40 M/mL, beads are excessively loaded, they start to leak cells and cell viability is affected. A good compromise would be then 20 M/mL but further metabolic characterization must be performed in order to analyse the other functions required for BAL.

Annex 4. Summary of the metabolic activities measured during this thesis

The following table 28 summarizes all the results concerning the metabolic performance of cells in the different setups and media. For the results concerning the pathological plasma model, since the metabolic performance was evaluated during 6 hours incubation in the medium, the results in this table were normalized by hour of activity (dividing our results by 6) to be comparable to the other conditions.

The results are presented in a chronological manner, following the passages from phase I to phase II.

| Phase | Biomass (Cell density, mL alginate) | Culture condition | Culture medium | Albumin synthesis rate ($\mu\text{g}/\text{h}/10^6$) | ICG clearance rate ($\mu\text{g}/\text{h}/10^6$) | CYP 1A1/2 activity ($\text{pmol}/\text{h}/10^6$) | CYP 3A4 activity ($\text{pmol}/\text{h}/10^6$) | Ammonia detox. rate ($\text{nmol}/\text{h}/10^6$) | Lactate clearance rate ($\text{nmol}/\text{h}/10^6$) |
|-------|--|--------------------------------|-----------------------------------|---|---|---|--|---|--|
| I | 1.5% alginate beads, SPHs (5M/mL, 1 mL) | Shaken condition, day 7 | HepaRG proliferation medium | 0.19 ± 0.09 | 24.11 ± 12.32 | - | - | - | - |
| | 1.5% alginate beads, DCs (5M/mL, 1 mL) | Shaken condition, day 7 | HepaRG proliferation medium | 0.48 ± 0.11 | 35.15 ± 1.73 | ND (not induced) 25.95 ± 8.47 (induced) | 0.72 ± 0.05 | - | - |
| | | | BAL test medium | 0.33 ± 0.09 | - | - | - | 93.03 ± 4.92 | 111.75 ± 28.62 |
| | 1% Alginate beads, DCs (5M/mL, 1 mL) | Shaken condition, day 7 | HepaRG proliferation medium | 0.23 ± 0.09 | 32.45 ± 17.07 | - | - | - | - |
| | 1.5% alginate beads, DCs (5M/mL, 1 mL) | Shaken condition, day 14 | HepaRG proliferation medium | 0.64 ± 0.21 | 32.83 ± 16.02 | 0.65 ± 0.44 (not induced) 36.45 ± 5.74 (induced) | 1.35 ± 0.12 | - | - |
| | | | BAL test medium | 0.51 ± 0.08 | - | - | - | 118.75 ± 23.06 | 166.75 ± 23.66 |
| | 1.5% alginate beads + 1.25% GM, DCs (5M/mL, 1 mL) | Shaken condition, day 14 | HepaRG proliferation medium | 1.03 ± 0.57 | 45.27 ± 6.91 | 6.46 ± 1.90 | - | - | - |
| | | | BAL test medium | 0.43 ± 0.19 | - | - | - | 143 ± 140.93 | 144.64 ± 100.99 |
| | 1.5% alginate beads, DCs (10M/mL, 1 mL) | Shaken condition, day 14 | HepaRG proliferation medium | 0.28 ± 0.09 | 46.30 ± 2.63 | 3.62 ± 1.60 | - | - | - |
| | | | BAL test medium | 0.35 ± 0.15 | - | - | - | 69.55 ± 21.89 | 53.75 ± 64.37 |
| | 1.5% alginate beads, DCs (1M/mL, 1 mL) | Shaken condition, day 14 | HepaRG proliferation medium | 0.35 (N=1) | - | - | - | - | - |
| | 1.5% alginate beads, DCs (20M/mL, 1 mL) | | | 0.3 (N=1) | - | - | - | - | - |
| | 1.5% alginate beads, DCs (40M/mL, 1 mL) | | | 0.25 (N=1) | - | - | - | - | - |
| II | 1.5% alginate beads + 1.25% GM, DCs (10M/mL, 1 mL) | Shaken condition, day 14 | Pathological plasma model | 0.26 ± 0.10 | - | - | - | 4.25 ± 1.81 | -67.35 ± 32.15 |
| | 1.5% alginate beads + 1.25% GM, DCs (10M/mL, 5 mL) | FB day 14 | Pathological plasma model | 0.30 ± 0.15 | - | - | - | 4.89 ± 0.92 | 20.26 ± 19.95 |
| | 1.5% alginate beads no PLL coating (5M/mL, 1 mL) | Shaken condition, day 14 | HepaRG proliferation medium | 0.85 ± 0.42 | 45.3 ± 6.9 | 6.5 ± 1.9 | - | - | - |
| | | | BAL test medium | 0.43 ± 0.19 | - | - | - | 90.4 ± 61.0 | 111.8 ± 68.3 |

| | | | | | | | | |
|--|------------------------------|-----------------------------------|-------------|------------|-----------|---|-------------|-------------|
| 15% alginate beads + 0.1% PLL coating (5M/mL, 1 mL) | Shaken culture, day 14 | HepaRG proliferation medium | 0.62 ± 0.22 | 20.9 ± 7.8 | 1.8 ± 1.0 | - | - | - |
| | | BAL test medium | 0.56 ± 0.24 | - | - | - | 73.7 ± 28.4 | 95.6 ± 50.4 |
| | | Pathological plasma model | 0.20 ± 0.04 | - | - | - | 30.8 ± 7.8 | 17.3 ± 10.3 |
| 15% alginate beads + 0.1% PLL coating (10M/mL, 1 mL) | Shaken culture, day 14 | Pathological plasma model | 0.71 ± 0.26 | - | - | - | 13.91 ± 1.1 | 11.52 (N=1) |
| 15% alginate beads + 0.1% PLL coating (10M/mL, 5 mL) | PDB, day 14 | Pathological plasma model | 0.11 ± 0.05 | - | - | - | 66.2 ± 5.9 | 76.7 ± 5.2 |

Tab. 28: Summary of the metabolic activities measured in all conditions tested. N ≥ 3 if not differently specified

Legend: / indicates the HepaRG proliferation medium. SPHs: pre-formed spheroids. DCs: dissociated cells. ND: not detectable, -: not measured. GM: glass microparticles. FB: fluidized bed bioreactor. PDB: perfused dynamic bioreactor

Remerciements

Je tiens tout d'abord à remercier ma directrice de thèse Cécile Legallais de m'avoir accueilli dans son laboratoire et de m'avoir donné la possibilité de faire une thèse. Merci beaucoup pour la façon dont tu m'as encadré et pour toute l'attention que tu as accordée à ma formation doctorale.

Ensuite, je tiens à remercier mon co-directeur de thèse, Ulysse Pereira. Merci beaucoup de m'avoir si bien formé, tant sur le plan pratique que théorique. Grâce à mes deux directeurs de thèse, j'ai pu développer un esprit scientifique et critique de haut niveau, ce qui est essentiel pour ma future carrière scientifique. Je vous remercie du fond du cœur d'avoir consacré votre temps et votre énergie à mon projet et à ma formation.

Merci également à mon équipe de recherche, Claire, Jonathan, Baptiste, Marwa et à toutes les personnes qui ont contribué à mon travail de thèse. Les mérites de ces années sont aussi les vôtres.

Un remerciement particulier est adressé à tout le personnel du laboratoire. Grâce à chacun d'entre vous, mon expérience ici dans notre laboratoire a été formidable. J'ai adoré l'ambiance de travail, et en même temps de divertissement, qui a été établie. Merci à toutes les personnes qui m'ont consacré leur temps quand j'en avais besoin, tant sur le plan professionnel que personnel. J'aurai toujours un très beau souvenir de chacun d'entre vous.

Merci également à nos collègues-amis de Paris, Anne Dubart, Antonietta Messina, Marwa Hussein et les autres aimables collègues. Merci beaucoup pour les conseils, les expériences, les réunions toujours agréables, les échanges scientifiques. J'ai beaucoup apprécié de travailler avec vous.

Et enfin, un grand merci à mes collègues, qui sont en fait des amis importants. J'ai eu la chance de passer près de quatre belles années ici en France, surtout grâce à vous. Nous avons partagé beaucoup de choses, des moments les plus joyeux aux plus difficiles... Mais vous le savez, la thèse est aussi faite de moments compliqués. Et quand c'était le cas, nous nous sommes réunis pour nous renforcer et nous battre ensemble. Chaque fois que je penserai à la France, mes pensées seront vers vous et toutes les belles expériences que nous avons vécues ensemble. Je souhaite à chacun de vous le meilleur, une brillante carrière et une merveilleuse vie personnelle. Je vous adore.

Per concludere, un grande ringraziamento importante va alla mia famiglia. Se oggi sono quello che sono è grazie a voi che mi avete sempre spinto verso la migliore direzione. E anche alla mia bellissima ragazza Francesca che mi ha supportato costantemente ogni giorno in maniera incondizionata. Arrivo !

Je peux maintenant me lancer dans un nouveau voyage, une nouvelle aventure, avec un sac plein de connaissances et de beaux souvenirs. Je porterai toujours ce sac avec moi. Ciao.

Titre : Etudes précliniques sur un foie extracorporel bioartificiel

Mots-clés : Insuffisance hépatique aiguë, HepaRG, billes d'alginate, encapsulation de cellules hépatiques, foie bioartificiel, culture 3D, sphéroïdes, différenciation cellulaires, bioréacteurs, activités métaboliques.

Résumé : Pour tous les patients souffrant d'une insuffisance hépatique aiguë, il existe un besoin urgent de solutions alternatives à la transplantation du foie. En raison de divers facteurs, ces patients n'ont pas toujours accès à un organe et meurent dans l'attente d'une greffe. Il est donc impératif de trouver des alternatives viables à la transplantation du foie.

Parmi les différentes alternatives apparues ces dernières années, notre groupe a principalement étudié le concept de foie bioartificiel. Il s'agit d'un dispositif de circulation extracorporelle équipé d'éléments artificiels (charbon actif et résine ionique) et d'éléments biologiques (biomasse hépatique) capables de soutenir l'organe défaillant. Ce dispositif a pour rôle de fournir les fonctions hépatiques, perdues à cause de la maladie, afin d'aider le patient à rester en vie jusqu'à ce qu'un organe soit disponible ou de favoriser la régénération naturelle du foie.

Cette thèse retrace l'évolution de ces dispositifs au cours du temps, en décrivant leur principe de fonctionnement et les principaux résultats proposés par la littérature. Un accent est ensuite mis sur le développement de notre dispositif de suppléance hépatique et sur la voie scientifique qui a permis d'optimiser au mieux la biomasse hépatique. Ce travail a conduit à la mise au point d'un dispositif BAL prêt à l'emploi sur des modèles de petits animaux en insuffisance hépatique aiguë.

Title: Preclinical studies on an extracorporeal bioartificial liver

Keywords: Acute liver failure, HepaRG, alginate beads, hepatic cell encapsulation, bioartificial liver, 3D culture, spheroids, cell differentiation, bioreactors, metabolic activities.

Summary: For all patients suffering of acute liver failure, there is an urgent need of alternatives to liver transplantation. Due to a variety of factors, those patients do not always have easy access to an available organ and die waiting for a transplant. Therefore, it is imperative to find viable alternatives to liver transplantation.

Among the various alternatives that emerged in recent years, our group has mainly investigated the concept of bioartificial liver. It is an extracorporeal circulation device equipped with artificial elements (activated charcoal and ionic resin) and a biological element (hepatic biomass) capable of supporting the failing organ. This device has the role of providing hepatic functions, lost due to the disease, helping the patient to remain alive until an organ is available or, otherwise, capable of promoting natural liver regeneration.

This thesis retraces the evolution of these devices over time, describing their principle of operation and the main results proposed by the literature. The focus is then moved on the development of our liver supply device and the scientific path that allowed optimizing the hepatic biomass at best. This thesis work led to the development of a ready-to-use BAL device on animal models of acute liver failure.